PB86-210960

Research Study on Pillar Design for Vertical Crater Retreat (VCR) Mining

Utah Univ., Salt Lake City

Prepared for

Bureau of Mines, Washington, DC

Oct 85

BuMines OFR 44-86

PB86-210960

A mining research contract report
OCTOBER 1985

RESEARCH STUDY ON PILLAR DESIGN FOR VERTICAL CRATER RETREAT (VCR) MINING

Contract J0215043
University of Utah

BuMines Open File Report 44-86

BUREAU OF MINES
UNITED STATES DEPARTMENT OF THE INTERIOR

The views and conclusions contained in this report are those of the author and should not be interpreted as necessarily representing the official policies or recommendations of the Interior Department's Bureau of Mines, the U. S. Government, Anaconda Minerals Company or the Homestake Mining Company.

REPORT DOCUMENTATION PAGE	1. REPORT NO. BuMines OFR 44-86	2.	3. Recipient's Accession No. PB86 210960/AS
4. Title and Subtitle: Research Study on Pillar Design for Vertical Crater Retreat (VCR) Mining			5. Report Date: Oct. 1985
7. Author(s): William G. Pariseau			8. Performing Organization Rept. No.
9. Performing Organization Name and Address: Department of Mining Engineering, University of Utah, Salt Lake City, UT 84112-1183			10. Project/Task/Work Unit No.
			11. Contract(C) or Grant(G) No. (C) J0215043 (G)
12. Sponsoring Organization Name and Address: Office of Assistant Director--Mining Research, Bureau of Mines, U.S. Department of the Interior, Washington, DC 20241			13. Type of Report & Period Covered: Contract research, 7-31-81--5-31-85
			14.

15. Supplementary Notes

Approved for release May 5, 1986.

16. Abstract

A 4-year study was conducted of the rock mechanics aspects of two underground hard-rock mine study stopes: (1) Anaconda Minerals Co.'s Carr Fork Mine near Tooele, UT, and (2) Homestake Mining Co.'s Homestake Mine in Lead, SD. Large-diameter (6 1/2 in.) blastholes were an integral part of the stoping method at each mine. A true vertical crater retreat (VCR) method was used at the Homestake Mine, while a vertical bench mining method (VBM) was used at the Carr Fork Mine. Since there are no personnel in a VCR or VBM stope, all ground control including dimensioning of stopes and pillars and the layout of cable bolt assays or other artificial support must be done in advance of production blasting. Accordingly, the objective of the research study was the establishment of a procedure for optimizing stope and pillar sizes. The approach taken in each case was a combination of mine measurements of the study stope response to mining, laboratory testing for rock properties and in situ stress measurements of the premining stress field, and theoretical calculations of the study stope response to mining. All calculations were done with the UTAH-II finite element computer program. Simulation of the blasting sequence gave a correlation of 0.88 between measured and calculated extensometer readings (incremental relative displacements) at the Carr Fork Mine where over 30 instrumentation boreholes were used to monitor the test stope response. A correlation of 0.84 was obtained at the Homestake Mine where 19 instrumented boreholes were used for monitoring purposes. These high correlations validated the computer model and calibrated it for rock mass properties. The calibrated model was then used in parametric studies of alternative design layouts.

17. Document Analysis a. Descriptors

b. Identifiers/Open-Ended Terms

c. COSATI Field/Group

18. Availability Statement	19. Security Class (This Report)	21. No. of Pages
Release unlimited by NTIS.	Unclassified	234
	20. Security Class (This Page) Unclassified	22. Price

FORWARD

The research reported here concerns two geomechanics case studies of underground hardrock stopes that were mined with large diameter (6 1/2 in.) blastholes. Two mines were involved, the Carr Fork Mine of the Anaconda Minerals Company and the Homestake Mine of the Homestake Mining Company. Bighole stoping methods offer significant gains in safety, productivity and recovery over more traditional methods. However, the new technology also brings with it new engineering questions including those having to do with ground control. This report specifically addresses the traditional mine design questions of stope and pillar size as posed in new form by bighole stopes. The approach taken is also traditional, but technologically current and based on computer modeling of the mining sequence.

The work is a four year combined effort of personnel from the Anaconda Company, the Homestake Mining Company, the Spokane Research Center of the Bureau of Mines and the Department of Mining Engineering at the University of Utah. A large number of individuals contributed directly and indirectly to the research.

We especially thank Dan Rovig, Bill Thompson, Chani Sra, Bob Franz, Irwin Sass, Bob Archibald, Ross Wayment, Khush Hal Singh and Rico Ramos of the Anaconda Minerals Company for their support during the Carr Fork Mine test stope project.

We also are most appreciative of the support of Al Winters, Carl Schmuck, Mike Cepak and Paul Sterk of the Homestake Mining Company during the study stope work at the Homestake Mine.

The in situ stress measurements and instrumentation efforts of Ted Williams, Mike King, Mike Jenkins and Bob McKibbin of the Spokane Research Center are gratefully acknowledged.

A number of students at the University of Utah have contributed to the research. In this regard, the efforts of Matt Fowler, Jeff Johnson, Kevin Donovan, Fei Duan and Mark Larson are appreciated. The project has supported three M.S. theses. Several technical papers have been presented on the work. The University of Utah also contributed financially to the project via cost sharing.

The research was done under contract J0215043 between the Bureau of Mines and the University of Utah. The contract was under the technical direction of Ernie Corp and Mel Poad of the Spokane Research Center. D. J. Askins and L. Rock administered the contract. Their encouragement and cooperation are greatly appreciated.

TABLE OF CONTENTS

Page

PART 2. - GEOMECHANICS OF THE HOMESTAKE MINE STUDY STOPE

APPENDIX

LIST OF FIGURES

LIST OF TABLES

EXECUTIVE SUMMARY

The research reported here concerns a four year study of the geomechanics aspects of two underground hardrock mine stopes. The first study was conducted at the Carr Fork Mine near Tooele, Utah. The Carr Fork Mine is owned by Anaconda Mineral Company. The second study was conducted at the Homestake Mine near Lead, South Dakota. The Homestake Mine is owned by the Homestake Mining Company. Both studies were cooperative efforts with mine personnel, the Spokane Research Center of the Bureau of Mines and the rock mechanics group at the University of Utah. Large diameter (6 1/2 inch) blastholes were an integral part of the stoping method at each mine.

The introduction of large diameter blastholes to underground hardrock mining in combination with spherical charge technology led to the development in the mid-1970's of a new stoping method known as vertical crater retreat (VCR). The method proved highly successful in reducing costs and controlling dilution and is now used in many parts of the world. In true VCR stoping the blastholes are loaded with spherical charges near the hole bottoms. Blasting brings down a horizontal slice usually about 12 ft thick. Subsequent blasts result in an upward retreat from extraction to drill level.

An important departure from true VCR stoping is vertical bench mining (VBM) in which holes are loaded only once and retreat is horizontal. VBM is essentially blasthole stoping. However, blasthole stoping with large diameter holes has considerable advantages over conventional blasthole stopes, especially in development costs, because of the much greater level interval possible. The relative advantages and disadvantages of VCR and VBM stopes have been discussed recently by Singh, Rao and Ramos (1985).

The new technology has brought with it new questions and the need for a more sophisticated level of engineering. There are no personnel in a VCR or VBM stope proper. This is a considerable safety advantage, but it also requires careful stope and pillar dimensioning for stability and the engineering and installation of any artificial support, for example, cable bolt systems, well in advance of slash rounds, ring rounds and production blasting. The objective of the research reported here is the development of a procedure for optimizing stope and pillar sizes in order to maximize productivity and resource recovery without sacrifice in safety.

The approach taken consists of mine measurements of study stope response to mining, laboratory tests for rock properties and in situ stress measurements, and theoretical calculations of the study stope response to mining. A direct comparison between theory and practice is then made through regression analysis of calculated on measured multi-anchor borehole extensometer readings (relative incremental displacements). A high correlation coefficient validates and calibrates the elastic component of the theoretical model. A match between calculated and observed slough zones calibrates the inelastic component of the model. All calculations were done using the finite element method as implemented in the UTAH-II and UTAH-III computer programs. The first is

a two-dimensional program (plane stress, plane strain, axial symmetry) and was used for the bulk of the calculations. Both are elastic-plastic programs that use associated flow rules and a nonlinear Drucker-Prager yield criterion for anisotropic geologic media. UTAH-II has been used extensively for rock mechanics analyses.

The Carr Fork Mine study was done first. The study stope region is in the Steep Highland Boy ore body at a depth of 4200 ft. Dip of the ore zone is vertical in the test stope region. Eight rock types were recognized, sampled and tested for rock mechanics properties. In situ stress measurements defined a near hydrostatic stress field in the vicinity of the study stope. Some 36 holes were drilled for instrumentation purposes. Installation of extensometers, load cells, vibrating wire stress gages and so forth began in June and was completed in August 1982 in advance of the first production blast. Widening of the slot raise began in late September; the last production blast was in October 1982. The test stope produced approximately 30,000 tons of ore and was mined by the VBM method in a transverse layout that involved horizontal retreat from footwall to hanging wall. Correlations of 0.88 and 0.89 between calculated and measured displacements were obtained in two separate vertical sections through the test stope. Comparison between observed and calculated slough or yield zones were also quite satisfactory. The finite element representations of the test stope were thus validated. Application of the model to questions of stope size, pillar size, extraction ratio and so forth indicate that at 50% extraction, stope width could be doubled without sacrifice of stability or safety.

Installation of instrumentation at the Homestake Mine began October and was completed in November 1983. Three panels in a study stope region between the 6950 and 7100 levels were instrumented. Some 19 holes were used. Most were collared in a hanging wall cable drift that provided a unique opportunity to measure hanging wall motion during mining of the steeply dipping central panel. Mining was by a true VCR technique. Ring blasting began in March 1984, VCR blasting began in June. The first crown pillar blast was completed in October 1984. During this time rock properties testing and in situ stress data were gathered, study stope geology defined, and an initial finite element calculation made against extensometer measurements in the hanging wall of a nearby stope that had been mined earlier.

The optimism that followed from the highly successful Carr Fork Mine study was dashed by the poor correlation obtained from the initial calculations. Great care to approximate physical reality was exercised in all subsequent phases of activity concerned with the study stope at hand. Additional laboratory rock properties tests were conducted at the University of Utah in order to check the main data set obtained at the South Dakota School of Mines and Technology. Definition of anisotropic shear moduli and strengths were of particular importance. Additional in situ stress measurements were made by the Spokane Research Center. Study stope geology through the center of the panel to be mined was incorporated into a new finite element mesh with node points located at all extensometer anchors within the section. Blasting records were consulted in order to specify the mining sequence to be followed by the computer, including an update to allow for two crown pillar blasts.

During mining care was taken to read all instrumentation before and after each blast and between blasts when time and ventilation permitted. The attention to detail proved worthwhile. Finite element calculations using UTAH-II resulted in a correlation coefficient of 0.84 between calculated and measured extensometer readings in the immediate hanging wall. Following the same validation and calibration procedure, but using data specific to the Homestake Mine study stope, led to scaling factors of 0.36 and 0.80 for elastic moduli and strengths. All independent dimensional elastic (18) and strength (27) properties for the rock mass were obtained by multiplication of the corresponding laboratory values. A re-analysis using scaled elastic moduli and strengths produced a correlation of 0.80 and good agreement between calculated yield zone extent and that inferred from extensometer anchor loss in the immediate hanging wall. Parameter studies of dip influence, stope width and length, pillar length and extraction indicate that stope lengths between two and four times width (as seen in plan view where length is measured along strike) are possible at an extraction of 50%. A greater initial extraction may be feasible, but at 75% pillar stability is lost. These guidelines are specific to study stope conditions.

The model could be fine tuned in order to improve the correlation. For example, the computer mining sequence could be done in a one to one correspondence with each VCR blast instead of combining several blasts in a single cut. This would require a more refined finite element mesh and a greater computational effort. However, the benefits of an even higher correlation for appearance's sake outweighed the costs. No attempt was made to fine tune the model.

The results of the two geomechanics case studies summarized here demonstrate that what is possible in principle is also possible in practice. The achievement of high correlations between calculated and measured displacements and yield zone extents in two very different geologic settings, in situ stress states, mining depths, ore body dips and stoping methods through application of the same basic procedure cannot be fortuitous but instead must reflect an approximation to physical reality that is adequate for engineering purposes. Although the numerical details are specific to the study stope regions, the objective of establishing a procedure for optimizing stope and pillar sizes in VCR type stopes has been achieved.

The cooperation between industry, government and university personnel was excellent throughout the work. Both study stopes had features that greatly facilitated installation of borehole instrumentation at critical points in the vicinity of the mined areas. The combination contributed enormously to the success of the research, as did the dedication of the graduate students in the rock mechanics group at the University of Utah. Hopefully the education they obtained is just compensation for their efforts and will serve them well in future years.

There is more to be done. Two of the three instrumented panels at the Homestake Mine study site should be maintained and monitored through stope completion and backfilling. The data suggest a possible short- and long-term dependency that should be investigated to gain a better

understanding of time dependent rock mass behavior. There is also a question of two- and three-dimensional effects that influence scaling factors. An intensive three-dimensional modeling effort is justified on a research basis in order to obtain a factual basis for understanding such effects and to distinguish them from those associated with the issue that pervades so much of rock mechanics, the relationship between laboratory rock properties and the properties of rock masses. The fact that only two scale factors, one for elastic moduli and one for strength, were needed in both cases is itself puzzling when one considers the large number of independent properties that were present. In this regard, the inverse or identification problem could be a potentially beneficial line of investigation for the development of guidelines for economical and efficient instrumentation layouts. Beyond such research questions is the problem of incorporating research results into the design process at operating mines. A simple answer is, of course, to place a rock mechanics person on the engineering staff. Although such may be a step in the right direction, the question could also be beneficially addressed by considering what changes or efficiencies need to be brought about in the "tools" of the rock mechanics engineer that are available at operating mines. What has been done here on a research basis should be done in a streamlined manner and on a routine basis at the mine. The more that research is brought to bear on productivity, resource recovery and safety, the more competitive will be our domestic mining industry.

INTRODUCTION

A combination of large diameter blastholes and spherical charges has led to a new method of underground hardrock mining known as vertical crater retreat (VCR). Ground control in VCR and other bighole stopes always involves the natural support action of the adjacent rock mass and quite frequently the support action of cable bolts.

This report discusses the potential for a rational rock mechanics approach to ground control in VCR stopes against a background of two recent case studies. The first study was done at the Carr Fork Mine, Utah, with the broad geomechanics objective of developing a design procedure for optimizing stope and pillar widths. The second study was done at the Homestake Mine, South Dakota, where additional complexities of schistosity and cable bolting of the hanging wall were present. The studies are cooperative efforts with Anaconda Minerals Company, Homestake Mining Company, the Spokane Research Center of the Bureau of Mines, and the Department of Mining Engineering at the University of Utah.

Unstable walls lead to dilution, the bane of underground hardrock mining. There are two distinct ways to combat the situation:

(i) increase productivity so that a lower grade of ore can be handled while still mining at a profit,

(ii) support the stope walls, especially the hanging wall, with properly sized pillars and cable bolts to minimize dilution.

The combination of large diameter blastholes and spherical charge technology that led to the VCR method follows the first avenue of attack. The second avenue of attack is a combination of the traditional mining engineering problem of optimizing pillar size for safety and resource recovery and of the more recent and still evolving technology of cable bolting. Of course, the two approaches are closely related and are often combined in VCR and bighole stopes.

Development of the VCR Method

In 1971 the International Nickel Company of Canada conducted a series of underground tests at the Copper Cliff North Mine using blastholes 6 3/4 to 11 inches in diameter (White, 1975). The success of these tests led to an examination of drilling technology with a view towards further adaptation of surface drill rigs to underground conditions (Barsotti and Kitchner, 1981; White, 1984). Improvements followed and large diameter blasthole mining became almost routine by 1975.

In 1973 experimentation with a novel pillar recovery technique began at Inco's Levack Mine. The technique involved placement of short charges near the bottom of 6 1/2-inch diameter blastholes that were drilled from level to level. Blasting then resulted in the removal of a horizontal slice. Holes were subsequently reloaded and an additional slice blasted down. The short charges were considered "spherical"

because their length to diameter ratio was less than six. Results were excellent with mining rates of 36 tons per man shift compared with the regular average then of 17 t/ms using undercut and fill for pillar recovery (Anderson, 1977). The method became known as "vertical crater retreat" or VCR and was patented by Canadian Industries Ltd. (Lang, 1976).

Lang, Roach and Osoko (1977) present the data in Table 1 to illustrate the powder factor advantage of spherical over cylindrical charges.

TABLE 1. - Comparison of spherical and cylindrical charges

Diameter/Length	Spherical	Cylindrical
Explosive	C2	C2
Weight	10 lbs	10 lbs
Hole Diameter	4 1/2 in.	2 5/8 in.
Hole Depth	4 ft	4 ft
Diameter/Length	1/2.7	1/15.
Crater Radius	5.7 ft	4.8 ft
Crater Volume	155 cu ft	38.6 cu ft

Use of the new technology has spread quite rapidly throughout the world. In many mines it is the primary stoping method. During this time, a number of modifications have been introduced in response to local conditions. In some instances the changes have resulted in entirely different stoping methods. Significant increases in productivity and decreases in dilution have been achieved. A number of mines that have adopted big hole stoping methods and their experiences are given in Table 2. The overview of VCR developments summarized in Table 2 points to significant increases in productivity and decreases in dilution with VCR stoping but greater efficiency with large diameter blasthole stoping.

TABLE 2. - Examples of VCR and big hole stopes

	Mine	Comments	References
1.	Levack, Canada, Ni	Tons per man shift more than doubled, 17 to 36 t/ms, pillar recovery operations, 90% recovery, 10% dilution	Lang, 1976 Anderson, 1977
2.	Centennial*, Canada, Cu,Zn	Much less development and secondary blasting, tried longhole stoping without success	Crocker, 1979

*True VCR

	Mine	Comments	References
3.	Birchtree*, Canada, Ni	2 1/2 times more t/ms, 34% of cost of standard cut and fill, well sized, 80% less than 6 inches, 96% recovery, 23% dilution	Brooks and Myers, 1979
4.	Rubiales*, Spain, Pb,Zn	New mine, first 100% VCR, some secondary blasting because of slabbing	Mining Mag., 1980
5.	Mufulira, Zambia, Cu	40% reduction in development, 30% savings in cost, quick preparation time, better ventilation	World Min., 1980 Mabson and Russell, 1981
6.	East Mine, Canada	400% increase in t/ms to 28 from 6 t/ms, tried VCR and benching, benching more efficient but VCR better dilution control	Singh and Rajala, 1981
7.	Radiore No. 2*, Canada, Cu,Zn	Narrow vein 5-20 ft, shallow, developed from surface.	Goodier, 1982
8.	Whitehorse, Canada, Cu	Tried longhole stoping, weak footwall, large reduction in powder factor to 0.61 lb/ton	Jannssen and Percival, 1981 White, 1981
9.	Cherokee, Tenn., Cu	Reduced secondary blasting, will obtain 50 t/ms	Zimmerman and Verner, 1981
10.	Fabian, Sweden, Fe	Caving method abandoned after 40% of reserve mined, first time use of large holes underground in Sweden	Holmberg and others, 1982

*True VCR

	Mine	Comments	References
11.	El Mochito, Honduras, Ag,Pb,Zn	Weak hanging wall, transverse stopes, 12 m wide by 35 m high, 45 m across, 50% extraction on first mining.	Paddock, 1981
12.	Escalante, Utah, Ag	Blasthole end slice, VCR drop raises, plugged holes a problem with true VCR	Burger, 1984
13.	16 to 1 Nevada, Ag,Au	Drop raise, blasthole stope, dilution of concern, 10% goal	E/MJ, 1984
14.	Carr Fork, Utah, Cu	Tried true VCR, experienced difficulties and excessive dilution, changed to blasthole stoping, successful full-scale test stope	Crackel, Heisel and Ramos, 1981; Pariseau and others, 1984; Singh, Rao and Ramos, 1985
15.	Homestake*, S.Dakota, Au	Double t/ms compared with cut and fill, and almost 50% more than blasthole stopes, dilution a concern	Mitchell, 1980; Orr, 1983

*True VCR

Further advances are expected. Lang (1982) reports that three underground mines (tin) in Australia were testing the VCR approach in conjunction with blasting research by the Swedish Detonic Research Foundation. Additional research is also being conducted at the Luossavaara Research Mine near Kiruna, Sweden. Lang also notes that the first mine in Central America to use VCR is the El Mochito Mine, Honduras, where 64% of the production is expected from VCR stoping in 1983, up from the 35% of the 1,500 tpd obtained in 1982. Kossatz (1983) states that 50% of the production from Inco's Ontario Division in Sudbury is expected to be from "vertical retreat mining (VRM)" in 1983, up from about 33% in 1982. According to Kossatz, "The adaptation of the cratering technique to a mining method, termed VRM at Inco, provides the efficiency of a bulk mining method while still maintaining the inherent ground control, dilution and recovery qualities of the tried and true incremental fill methods."

True VCR stoping at the present time involves drilling large diameter blastholes, usually 6 1/2-inch diameter holes, from the topsill or drill level to the bottom sill or extraction level and the placement of spherical charges near the hole bottoms. When blasted, the charges link

to form overlapping inverse craters that bring down a horizontal section of ore. Holes are then reloaded. Successive lifts are taken down as the stope retreats vertically towards the topsill. The topsill or crown pillar is usually brought down with the last blast that is larger than the regular production blasts, while muck in the stope is generally handled as if it were in a conventional shrinkage stope. However, there are no miners in a VCR stope proper.

The main advantages of VCR stoping according to Jorgenson (1981) are:

- Improved fragmentation.
- Increased safety.
- Reduced overbreak and vibration.
- Reduced dilution.
- Less development.
- Higher productivity.

Careful planning and execution of drilling and blasting operations is essential to the success of the VCR method. The main disadvantage of VCR stoping is that miscalculation tends to involve the entire stope.

Development of Cable Bolting Systems

Support requirements must be engineered and installed in advance of production blasting. Because there are no miners in the stope proper, there is little opportunity for the installation of additional support once stoping commences. The same is true of large diameter blasthole stopes. In this regard, control of the hanging wall is of particular importance in steeply dipping VCR stopes because of the potential for caving and dilution, the bane of underground mining.

Cable bolting is the most common form of ground control in primary VCR stopes. Of course, fill is of great importance in secondary stopes and pillar recovery operations. Cable bolting is also of great importance to other stoping methods. Clifford (1974) reports the first use of cable bolts as crown pillar support at New Broken Hill Consolidated (NBHC). Palmer, Bailey and Fuller (1976) describe the details of the evolution of pre-placed bolting at Cobar, N.S.W., and the considerable economic advantages achieved, but note that little is known of the relative effects of altering the spacing of bolts on their reinforcement action. However, the practical success of the technique was undeniable and led to a number of investigations of bolt rock interaction and load transfer mechanisms (e.g., Fuller and Cox, 1975, 1977; Jeremic and Delaire, 1983; Goris, 1984).

Matthews, Tillman and Worotnicki (1983) at NRHC describe a full-scale field test of a new load transfer mechanism designed to more efficiently utilize the support capacity of the steel in crown pillar support. Jeremic and Delaire (1983) report on a similar concept.

Cassidy (1979) describes implementation of cable bolting at the Con Mine of Cominco Ltd. Bolting practice at the Homestake Mine and the variety of purposes it serves including reduction of hanging wall dilution is described by Schmuck (1979). Stheeman (1982) describes in detail a practical approach to cable bolt system design based on mine observations at the Tsumeb Mine, Namibia, and states, "The determination of the mass of the rock to be supported is the most important and also the most difficult parameter to be solved for the design of the cable bolt system." In essence, his approach to estimating bolt load (in contrast to bolt capacity) is a deadweight load approach. The bolt load is simply calculated as the weight of a potential rock fall from the stope back. Estimating the volume of the potential fall is the real problem.

Lappalainen and Pulkkinen (1983) give a detailed account of extensive study of cable bolting at Outokumpu Oy Mines, Finland, and point out that finite element and boundary element analysis provide guides to installation patterns but still do not directly model the influence of bolting on ground control. Bharti, Lebl and Cornett (1983) point out the role of finite element analysis in defining zones of high stress concentration and of monitoring for cable bolt support effectiveness while converting from post pillar cut and fill to blasthole stoping at the Strathcona Mine, Canada. Another full-scale field study involving numerical analysis, laboratory testing and mine observations at the King Island Mine, Australia, is described by Cullum (1984).

Fuller (1984) in a keynote address during an international symposium on rock bolting summarizes much of the Australian experience with cable bolts underground, while Bywater and Fuller (1984) describe in some detail open stope cable bolting of hanging walls at Mount Isa Mines. Lappalainen and others (1984) in the same symposium further describe experience with steel strand and cable bolts in Finland. Sellden (1984) reports observations of a cable reinforced footwall in the Fabian orebody in Northern Sweden, while Stillborg (1984) outlines cable bolting research at the Swedish Mining Research Foundation.

Thus it appears that although much is being learned about the properties of cable bolting steel, grout properties, bonding at interfaces and practical uses of cable bolts, much less is known about the engineering design of cable bolt systems. Brawner and Haugen (1983) in their review state, "Because of our inability to develop an accurate structural geological, stress and strain relief model, the design of pre-reinforcement is still more of an art than a science." The main difficulty is in estimating bolt loads. The problem is complex. Indeed, state of the art computer codes for stress analysis are deficient with respect to cable bolt action for reasons that are not clear. In this regard, Warburton (1977) considers the finite element approach to modeling progressive mining through a cable bolted region of pre-placed support and concludes, ". . . that the rock is virtually

unaffected by the presence of the cable bolts" and that a much more sophisticated model is needed. In fact, this is a common experience in finite element modeling of a great variety of underground support systems. The reason for this is simple enough: In the elastic range, the stiffness of support elements is small relative to the stiffness of adjacent rock elements and thus support makes an insignificant contribution to the overall stiffness of the system.

REFERENCES

Alexander, L. G., D. J. Maconochie, S. M. Matthews, V. H. Tillman, 1981, "Observations and Analysis of Rock Deformation Around Some Open Stopes," Design and Operation of Caving and Sublevel Stoping Mines, D. R. Stewart, editor, SME/AIME, N.Y., 1981, pp. 483-498.

Anderson, D. E., 1977, "Vertical Crater Retreat Mining at Inco's Levack Mine," CIM Underground Operators Conference, Winnipeg.

Anon., 1980, "Rubiales," Mining Magazine, pp. 318-325.

Anon., 1980, "Large Diameter Blasthole Open Stoping," World Mining, pp. 58-60.

Anon, 1984, "Sunshine's New Sixteen to One Mine," Engineering and Mining Journal, May, Vol. 185, pp. 46-52.

Barsotti, C., and L. C. Kitchner, 1981, "The Development of 'in-the-Hole' Drilling and Remote Control Equipment at Inco Metals Co.," Design and Operation of Caving and Sublevel Stoping Mines, D. R. Stewart, Editor, SME/AIME, NY, 1981, pp. 643-652.

Bharti, S., J. Lebl, and D. J. Cornett, 1983, "Conversion from 'Post' Pillar Cut and Fill Mining to Blasthole--A Case Study at Falconbridge," CIM Bulletin, Vol. 76, pp. 61-68.

Brawner, D. C., and M. Haugen, 1983, "Pre-reinforcement to Improve Underground Stability," Mini-Symp. Rock Reinforcement, SME/AIME Annual Meeting, Atlanta, pp. 63-70.

Brooks, R. H., and R. E. Myers, 1979, "Blasthole Stoping at Inco's Birchtree Mine," CIM Bulletin, Vol. 72, pp. 68-76.

Burger, J. R., 1984, "Ranchers End-Slices Escalante Silver Deposit," Engineering and Mining Journal, Jan., Vol 185, pp. 48-53.

Bywater, S., and P. G. Fuller, 1984, "Cable Support of Lead Open Stope Walls of Mount Isa Mines Limited," Proceedings International Symposium on Rock Bolting, O. Stepnansson, editor, A. A. Balkema, pp. 539-555.

Cassidy, K., 1980, "The Implementation of a Cable Bolting Program at the Con Mine," CIM Bulletin, Vol. 73, pp. 67-72.

Clifford, R. L., 1974, "Long Rockbolt Support at New Broken Hill Consolidated," Proc. Aus. Inst. Min. Met., No. 251, pp. 21-26.

Crackel, D., Jr., M. Heisel, and G. G. Ramos, 1981, "Stope Blasting Design and Experience at the Carr Fork Mine," Design and Operation of Caving and Sublevel Stoping Mines, D. R. Stewart, editor, SME/AIME, N.Y., 1981, pp. 529-538.

Crocker, C. S., 1979, "Vertical Crater Retreat Mining at the Centennial Mine," Mining Congress Journal, June, Vol. 65, p. 31.

Cullum, A. G., 1984, "King Island Scheelite Mine: Open Stoping Under a Major Shear Zone," Engineering and Mining Journal, July, Vol. 185, pp. 34-43.

Desai, C. S., M. M. Zaman, J. G. Lightner and H. J. Siriwaradane, 1984, "Thin Layer Elements for Interfaces and Joints," Int. J. Numer. Anal. Methods Geomech., Vol. 8, pp 19-43.

Donovan, K., and W. G. Pariseau, 1984, "Finite Element Approach to Cable Bolting in Steeply Dipping VCR Stopes," Geomechanics Applications in Underground Hardrock Mining, SME/AIME, N.Y., pp. 65-90.

Fuller, P. G., 1984, "Cable Support in Mining," Proceedings International Symposium on Rock Bolting, O. Stephansson, editor, A. A. Balkema, pp. 511-522

Fuller, P. G. and R. H. T. Cox, 1975, "Mechanics of Load Transfer from Steel Tendons to Cement Based Grout," Proc. Fifth Australian Conference on the Mechanics of Structures and Materials, Melbourne, pp. 189-203.

Goodier, A., 1982, "Mining Narrow Veins by Vertical Crater Retreat at the Radiore No. 2 Mine," CIM Bulletin, Vol. 75, p. 65.

Goris, J., 1984, personal communication.

Heuze, F., and R. E. Goodman, 1973, "Finite Element and Physical Model Studies of Tunnel Reinforcement in Rock," Proc. 15th U. S. Symp. Rock Mech., ASCE, N.Y., pp. 37-67.

Holmberg, R., T. Naarttijauri, and L. Nisson, 1982, "LKAB Introduces Large Hole Diameter Stoping at the Fabian Mine," Mining Engineering, Vol. 34, pp. 268-271.

Janssens, J. J. and P. W. Percival, 1981, "A Practical Approach to Vertical Crater Retreat Mining in Soft Ground at Whitehorse Copper," CIM Bulletin, Vol. 74, pp. 72-78.

Jeremic, M. L., and G. J. P. Delaire, 1983, "Failure Mechanics of Cable Bolt Systems," CIM Bulletin, Vol. 76, pp. 66-71.

Jorgenson, G. K., 1981, "A Review of Vertical Crater Retreat Mining," Mining Congress Journal, July, Vol. 67, p. 48.

Kossatz, E., 1983, "Inco Boosts Productivity Using Bulk Mining Methods," Canadian Mining Journal, Vol. 104, p. 23.

Lang, L. C., 1976, "The Application of Spherical Charge Technology in Stope and Pillar Mining," Engineering and Mining Journal, May, Vol. 177, pp. 318-325.

Lang, L. C., R. J. Roach and M. N. Osoko, 1977, "Vertical Crater Retreat: An Important New Mining Method," Canadian Mining Journal, Vol. 98, p. 69.

Lang, L. C., 1983, "VCR Method Improves Fragmentation, Lowers Costs," Canadian Mining Journal, Vol. 104, p. 8.

Lappalainen, P., and J. Pulkkinen, 1983, "Pre-reinforcement by Cable Bolting at Outokumpu Oy Mines,"Stability in Underground Mining, L. O. Brouner, editor, SME/AIME, N.Y., pp. 962-977.

Lappalainen, P., J. Pulkkinen, and J. Kuparinen, 1984, "Use of Steel Strands in Cable Bolting and Rock Bolting," Proceedings International Symposium on Rock Bolting, O. Stephansson, editor, A. A. Balkema, pp. 557-562.

Mabson, L. R., and F. M. Russell, 1981, "Application of Sublevel Open Stoping on the RCM Limited Mines of the Zambian Copper Belt," Design and Operation of Caving and Sublevel Stoping Mines, D. R. Stewart, editor, SME/AIME, N.Y., 1981, pp. 585-607.

Matthews, S. M., V. H. Tillman, and G. Worotnicki, 1983, "A Modified Cable Bolt System for the Support of Underground Openings," The Aus. I.M.M. Conference, Broken Hill, N.S.W., pp. 243-255.

Mitchell, S. T., 1980, "Vertical Crater Retreat Stoping Proves Successful at Homestake Mine," Mining Engineering, Vol. 32, pp. 1581-1586.

Orr, S. A., 1983, "Refinement of Vertical Crater Retreat Stoping at the Homestake Mine," Homestake Mining Company Report.

Paddock, R. C., 1981, "Mining the San Juan Ore Body, El Mochito, Honduras, Central America," Design and Operation of Caving and Sublevel Stoping Mines, D. R. Stewart, editor, SME/AIME, N.Y., 1981, pp. 75-84.

Palmer, W. T., S. G. Bailey, and P. G. Fuller, 1976, "Experience with Pre-placed Supports in Timber and Cut and Fill Stopes," Proc. AMIRA Tech. Meeting, Wollongong, pp. 45-71.

Pariseau, W. G., M. E. Fowler, J. C. Johnson, M. Poad, and E. L. Corp, 1984, "Geomechanics of the Carr Fork Mine Test Stope," Geomechanics Applications in Underground Hardrock Mining, SME/AIME, N.Y., pp. 3-38.

Pariseau, W. G., and F. Duan, 1984, "Numerical Assessment of the Influence of Anisotropy on Steeply Dipping VCR Stopes," Geomechanics Applications in Underground Hardrock Mining, SME/AIME, N.Y., pp. 39-63.

St. John, C. M., and D. E. VanDillen, 1983, "Rockbolts: A New Numerical Representation and its Application in Tunnel Design," Proc. 24th U. S. Symp. Rock Mech., Texas A&M Univ., pp. 13-25.

Schmuck, C. H., 1979, "Cable Bolting at the Homestake Gold Mine," Mining Engineering, Vol. 31, pp. 1677-1681.

Sellden, H., 1984, "Cable Bolting in Fabian Ore Body, Malmberget," Proceedings International Symposium on Rock Bolting, O. Stephansson, editor, A. A. Balkema, pp. 563-569.

Singh, K. H., and L. H. Rajala, 1981, "Falconbridge Introduces Advanced Technology to Deep Mining," CIM Bulletin, Vol. 74, pp. 75-83.

Singh, K. H., G. G. Ramos, and T. V. Rao, 1985, "Evaluation of Blasthole Stoping Alternatives," SME-AIME Preprint 85-84.

Stheeman, W. H., 1982, "A Practical Solution to Cable Bolting Problems at the Tsumeb Mine," CIM Bulletin, Vol. 75, p. 65.

Stillborg, B., 1984, "Research Carried Out Within the Swedish Mining Research Foundation in Relation to Cables and Cable Bolting," Proceedings International Symposium on Rock Bolting, O. Stephansson, editor, A. A. Balkema, pp. 571-573.

Warburton, P. M., 1977, "Modelling Considerations in Finite-Element Analysis of Progressive Mining Through Cable Bolts," CSIRO Div. of Geomechanics Tech. Rpt. No. 54, p. 21.

White, L., 1975, "Open-pit Concepts Boost Inco Productivity Underground," Engineering and Mining Journal, May, Vol. 176, pp. 101-104.

White, L., 1984, "In-the-Hole Drills," Engineering and Mining Journal, September, Vol. 185, pp. 52-57.

White, R. L., 1981, "Whitehorse Copper Applies Vertical Crater Retreat in Soft Ground," Engineering and Mining Journal, Vol. 182, pp. 231-233.

Zimmerman, C. L., and M. E. Verner, 1981, "Large Hole Rotary Sublevel Stoping," Mining Congress Journal, Vol. 67, p. 20.

PART 1.

GEOMECHANICS OF THE CARR FORK MINE TEST STOPE

ABSTRACT

This section describes a comprehensive geomechanics case study of a full-scale 30,000 ton test stope at the Carr Fork Mine. The mine is owned by Anaconda Minerals Company and is located near Tooele, Utah. The ore occurs in the Steep Highland Boy ore body, a skarn deposit with chalcopyrite as the chief ore mineral. Test stope depth is 4200 ft. Large diameter blast holes were used in a new method known as blast hole post-fill (BHPF). The new design proved highly successful in contrast with earlier experience with vertical crater retreat (VCR) stopes. The main geomechanics objective was the establishment of a design procedure for optimizing stope and pillar dimensions with respect to productivity and recovery. An integrated three-part approach consisting of mine measurements, laboratory testing and finite element calculations was taken. Measurements were made in more than 30 instrumentation boreholes up to 100 ft in length and include in situ stress determinations before and after stoping, vibrating wire stress gage change measurements during mining and multi-anchor borehole extensometer measurements before, during and after mining. Several hundred laboratory tests were conducted in order to determine the elastic and strength properties of the nine rock types identified for geomechanics purposes.

Independent correlations of 0.88 and 0.89 between calculated and measured displacements and between estimated and observed yield zones substantiate the finite element design approach using UTAH-II. Yielding was limited to a small zone in the fractured footwall quartzite as expected. The high correlations substantiate the form of the elastic-plastic material model used and allow for the determination of scale factors for extrapolating laboratory rock properties to rock mass values. Simulation of the mining sequence using rock mass properties then produces calculated displacements and yield zones then can be compared directly on a one to one basis with the mine measurements for final validation of the procedure. Subsequent stope and pillar design analyses using the calibrated finite element model indicate that doubling of the original stope width at 50% extraction is quite possible without sacrifice of safety or stability. Other alternative designs and mining sequences including stope on stope layouts can be considered quite inexpensively compared with full-scale trials.

INTRODUCTION

The Carr Fork Mine is an underground copper mine located near Tooele, Utah, about 70 km (40 miles) southwest of Salt Lake City as shown in Figure 1. Design capacity of the mine is 9,000 tonnes per day (10,000 stpd). Ore mineralization is the skarn type; chalcopyrite is the principal ore mineral. The test stope is located in the Steep Highland Boy orebody, one of several on the property, and is well beyond the influence of previously mined areas. Vertical shafts, ramps, and horizontal crosscuts provide primary access; main haulage is by rail. Figure 2 is a composite longitudinal section that shows the general development of the mine.

Original VCR Stope

The original method of mining implemented in the upper levels of the Steep Highland Boy orebody was vertical crater retreat. Figure 3 shows the original VCR stope layout. As mining proceeded, difficulties with caving ground, high dilution, poor fragmentation, and low productivity developed. The method eventually proved less than successful despite its early promise. From the rock mechanics view, contributing factors include unanticipated blasting effects, drillhole deviation, proximity to old workings and a relatively large amount of exposed ground. Production ceased in October 1981, while development work continued and alternative mining methods were considered. These included sublevel caving, mechanized cut and fill, and blasthole stoping. Blasthole stoping with post fill (BHPF) was selected for full-scale field testing.

BHPF Stope

Development for the blasthole post-fill stopes begins by driving an extraction drift parallel to the ore zone as shown in Figure 4. Panel drifts are then driven from the extraction drift across the orebody. The panel drifts are subsequently widened to form an undercut. The back of the undercut is arched. Similar development occurs over the top of the stope. The overcut provides access for production drilling. After development of the undercut, a slot raise is driven to the overcut and enlarged the full width of the stope. A down-the-hole machine is used to drill 16.5 cm (6.5 in.) diameter blastholes. Production blasting begins with the first row of holes blasted to the slot.

The new stope design greatly reduces the amount of exposed ground. Not only are stope dimensions less, but the initial extraction ratio is also reduced. The mining sequence associated with the new layout requires secondary stopes adjacent to previously mined and filled stopes. Progress is upwards from lower to higher levels in the mine. The method is flexible and allows adaptation of stope and pillar dimensions to the assay hanging wall and other local geologic conditions.

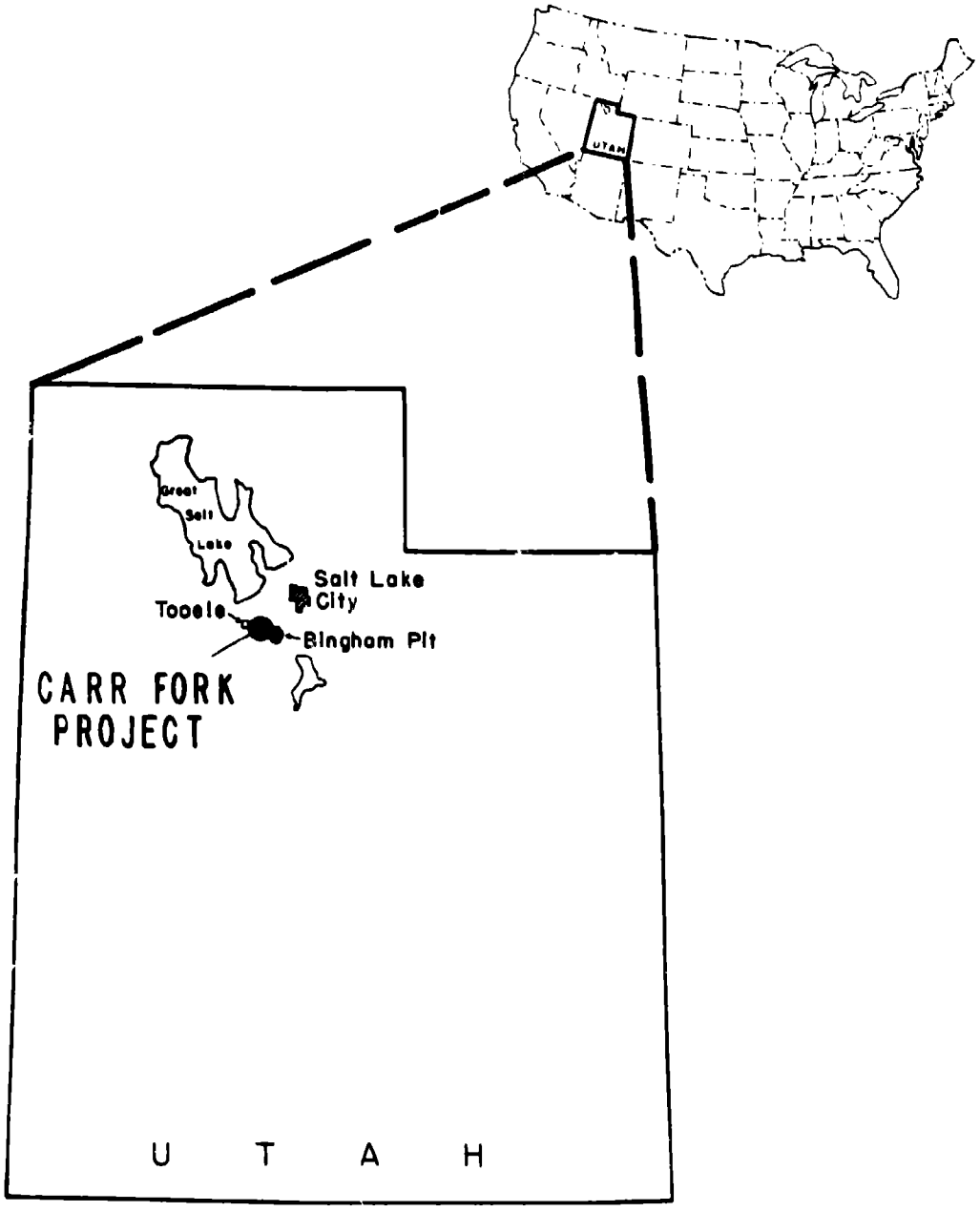

Location of the Carr Fork Mine.

Figure 1. - Location of the Carr Fork Mine.

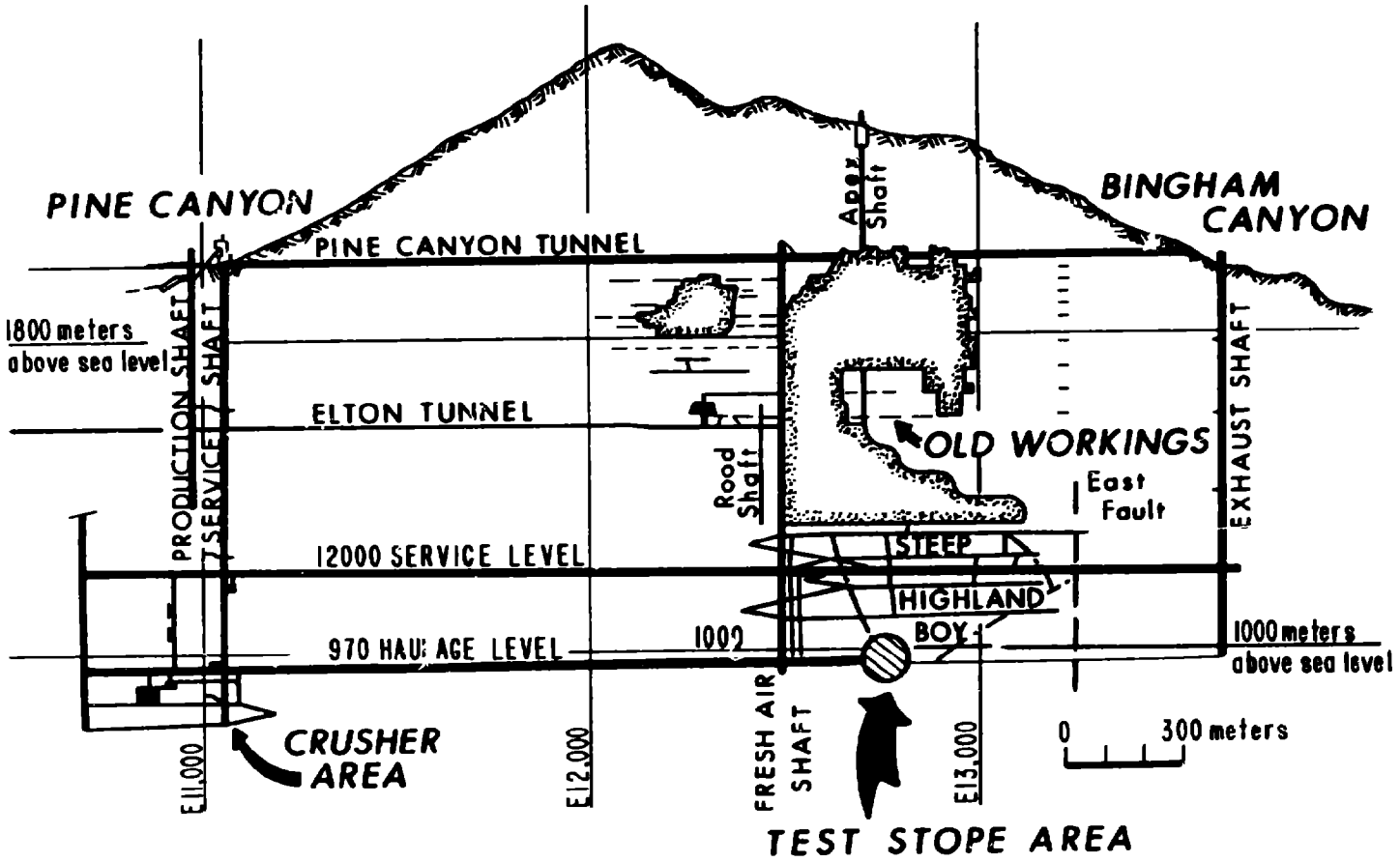

CARR FORK MINE

LONGITUDINAL COMPOSITE SECTION

LOOKING NORTH

Figure 2. - General mine development and location of the test stope.

Original VCR Stope Schematic.

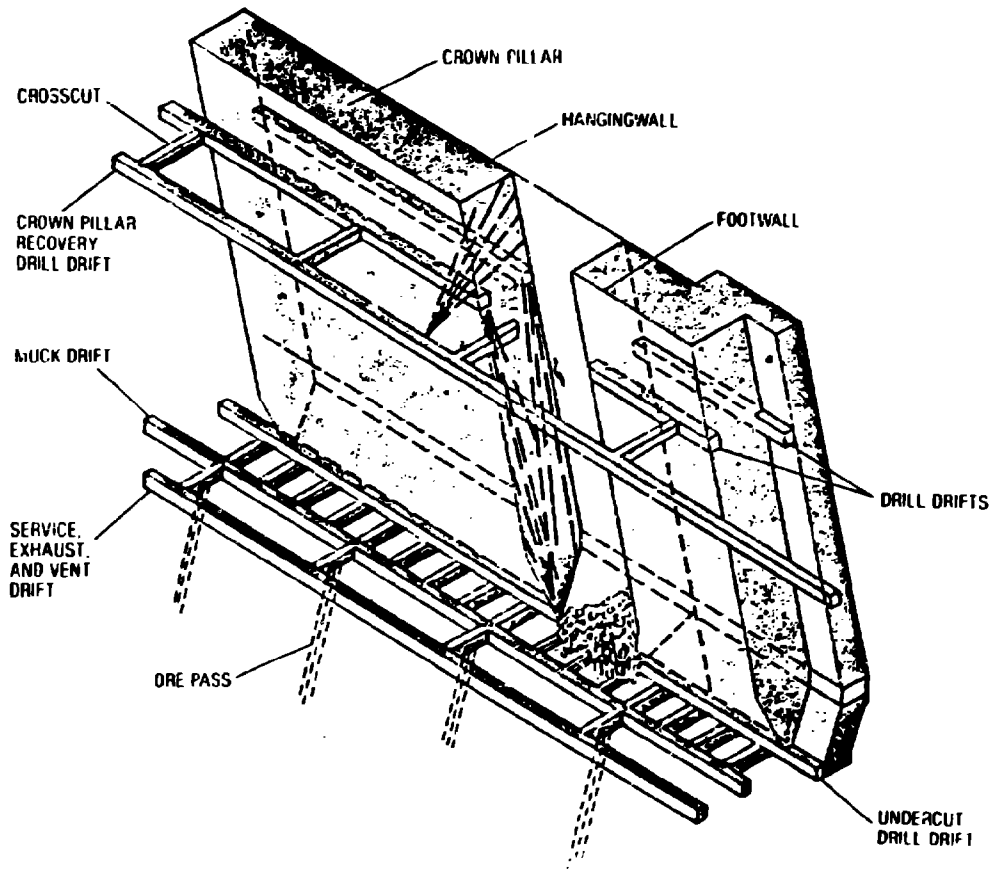

Figure 3. - Original VCR stope schematic.

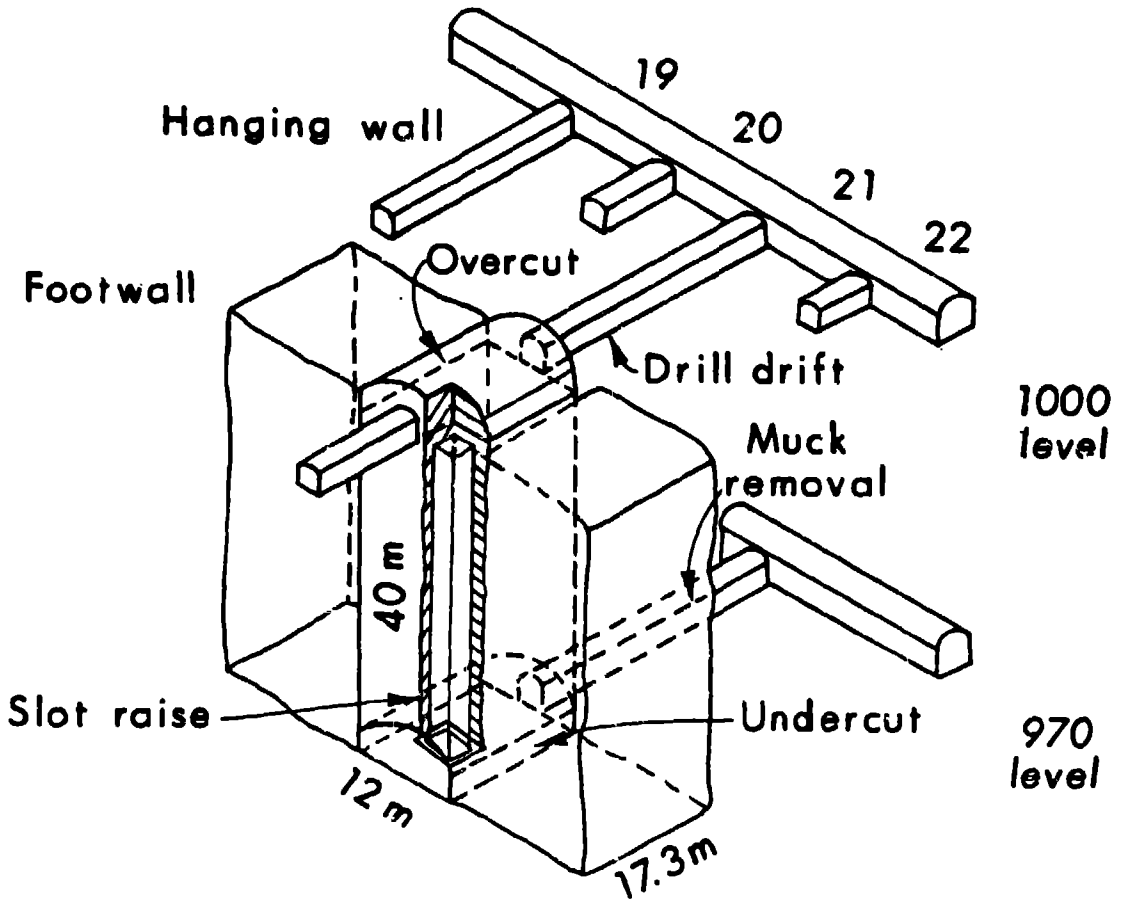

Test Stope (BHPF) Schematic.

Figure 4. - Test stope (BHPF) schematic.

Geology

The Steep Highland Boy ore zone, one of several on the property, is localized in the Highland Boy limestone of the Bingham Syncline. The mineralized portion of the Steep Highland Boy is a garnetized limestone (garnetite) approximately 30 m (100 ft) thick on average. The ore zone is gradational and trends west-northwest and generally dips 75° to 80° to the north. Occasionally it is vertical to slightly overturned. Hornfels, hornfelsy quartzites, and quartzites overlie the Highland Boy limestone. A persistent but weakly garnetized bed also appears in the hanging wall formations. The footwall consists of a highly fractured quartzite.

The Steep Highland Boy is slightly overturned in the vicinity of the test stope where a quartz latite porphyry dike 1 to 2 m (3 to 6 ft) wide is present in the hanging wall. Small quartz monzonite dikes are present in the footwall. Figure 5 shows the test stope geology. In this regard, the Steep Highland Boy is generally quite competent but can be soft where clay alteration is present or where highly mineralized or faulted. In addition to garnet, varying amounts of diopside, quartz, calcite, magnetite, pyrite, and pyrrhotite are present in the Steep Highland Boy. Chalcopyrite is the principal ore mineral. Minor faults and shear zones also occur in the foot and hanging walls of the test stope as shown in Figure 5.

Objective and Approach

The general objective of the test stope study is to optimize mine productivity and resource recovery. A number of specific goals are associated with the general study. These include determination of the feasibility of remote controlled scoop-tram operation, blasting practice definition, ground control optimization and so forth. The rock mechanics study relates to the general test stope goals in the area of ground control.

The specific objective of the rock mechanics investigation is to establish a design procedure for calculating in advance of actual mining, stope and pillar dimensions that are favorable to productivity and resource recovery and that have an acceptable margin of safety. In this regard, there is a trade-off between opening stability and mining productivity. Relatively small, widely spaced openings favor stability; while large, closely spaced openings favor productivity and recovery. The optimum size and spacing of openings is a compromise.

The approach to the rock mechanics study consists of three major activities:

(i) mine measurements,
(ii) laboratory tests, and
(iii) analyses.

Mine measurements serve two purposes. They provide a portion of the input data needed for design analysis and calculations. But most

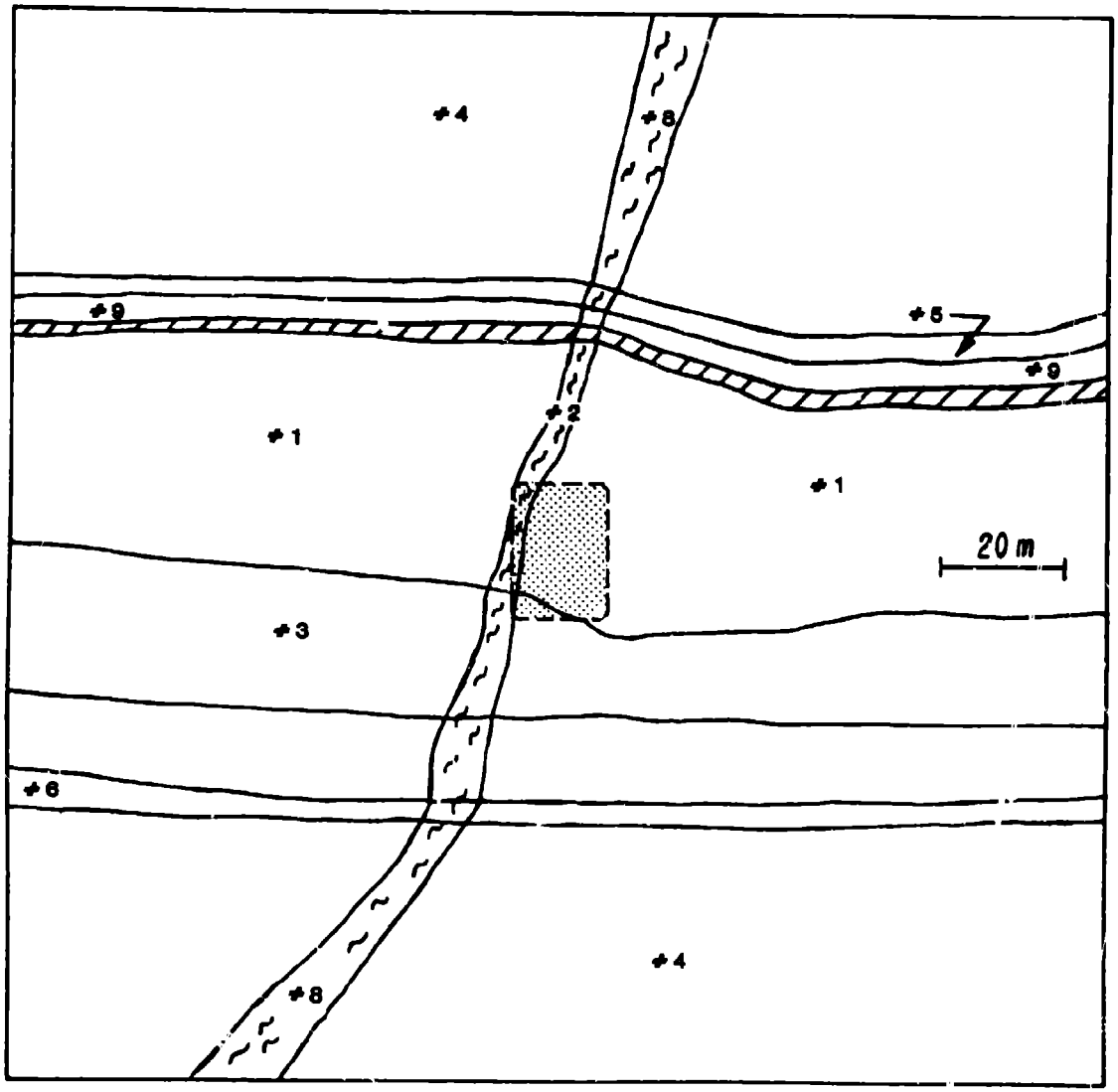

Plan Section Geology

Figure 5. - Test stope geology. (a) Plan. North at top of page. Numbers correspond to rock type in Table 7.

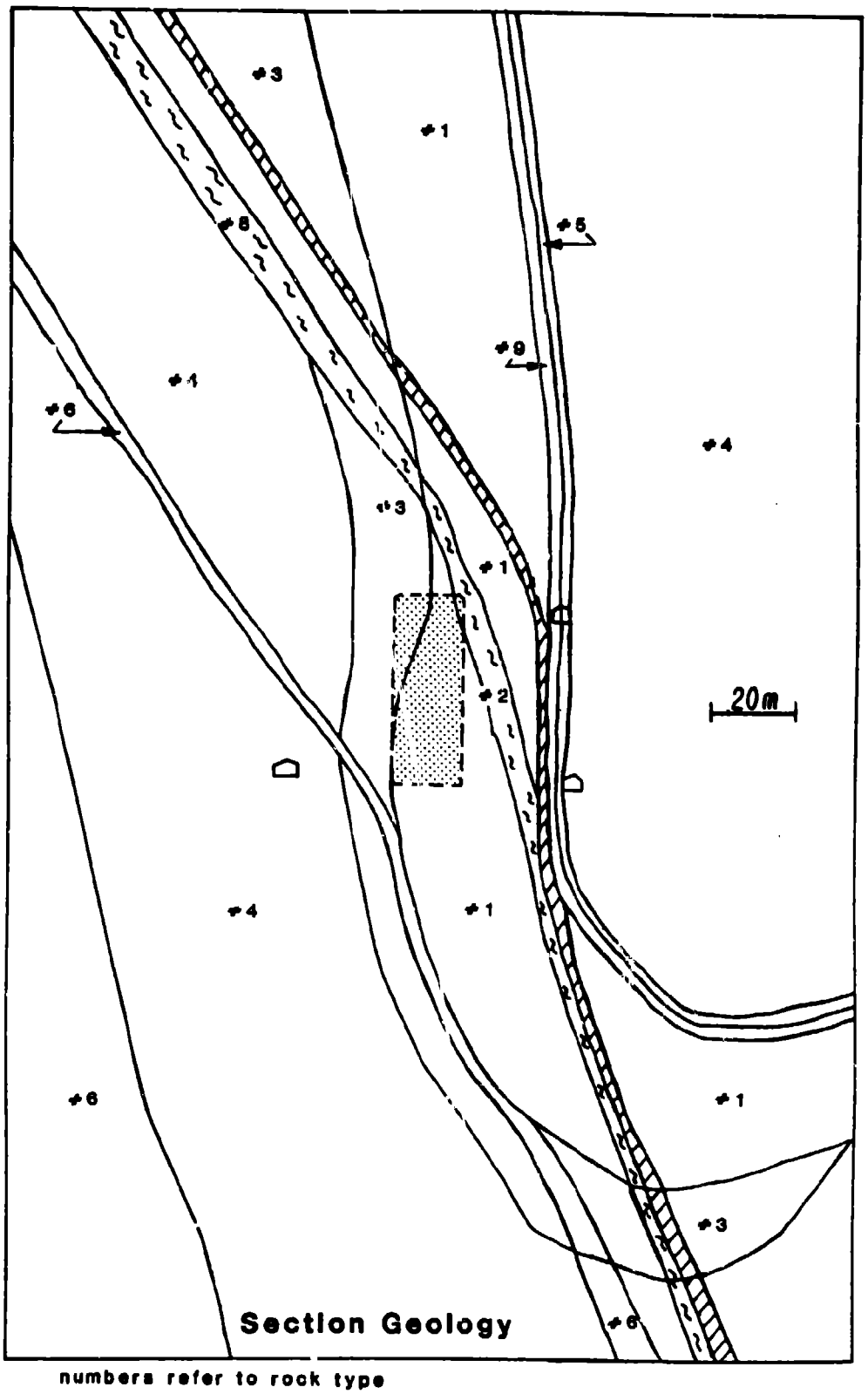

Figure 5. - Test stope geology. Looking West. (b) Section perpendicular to strike. Numbers correspond to rock type in Table 7.

importantly, they provide the experimental data essential to the validation of the design procedure itself. Laboratory testing is needed for calibration of instrumentation used in the mine and for the determination of rock properties needed in design analyses and calculations. Calculations, in turn, provide a quantitative link between theory and practice, that is, between design hypotheses and mine measurements.

FIELD INSTRUMENTATION AND MINE MEASUREMENTS

The objectives of the field instrumentation and mine measurements program were to determine the test stope response to mining. Eight types of monitoring instrumentation were used in the study. Table 3 lists the instrumentation types and their purpose.

Some 36 holes were drilled for monitoring purposes. The majority of holes are for 3-anchor extensometers and are 5.1 cm (2 in.) diameter holes. All instrumentation holes are percussion machine drill holes, while in situ stress and modulus measurement holes are diamond drill holes. The use of percussion drill holes for monitoring instrumentation is a considerable economy because most such holes can be drilled with a machine such as a fan drill that is already mobilized and working in the area. Approximately 610 m (2,000 ft) of hole was drilled for instrumentation and measurement purposes.

TABLE 3. - Field instrumentation type and purpose

Type	Purpose
1. Borehole extensometer (rod type--EXT)	Measure relative displacement: H-1,4,9,13,16,18,22,24,25,28,30-35.
2. Sonic probe (SPB)	Measure relative displacement: H-6.
3. Vibrating wire stress-meter (VSM)	Measure stress change: H-2,5,7,10,12,17,20,21,C,D,F.
4. Borehole deformation gage (BDG)	Measure stress change: H-B,D.
5. Rock bolt load cell (RBC)	Measure rock bolt load: H-19,29.
6. Instrumented rock bolt (IRB)	Measure rock bolt load: H-23,A.
7. Slough meter (SLM)	Measure extent of overbreak: H-3,8.
8. Closure points (CLP)	Measure opening closure.

Instrumentation Layout

Figures 6, 7, and 8 show the instrumentation layout in plan and vertical sections. The test stope is in Panel 21, as shown in Figure 4. The instrumentation plan is best understood by hole groups: (i) ribs, (ii) backs and brows, (iii) foot and hanging walls.

Ribs

Panel 19 and 23 development crosscuts on the 1000 Level provided access for instrumentation Holes 1-10, 33, D, and E. Holes 1 and 4 are 3-point rod extensometer holes collared in Panel 19 at the third points along the stope as shown in Figure 6 (plan view). These extensometers are fitted with potentiometric heads for electrical readout. Anchors in Holes 1 and 4 farthest downhole are positioned near the west rib at mid-height of the future test stope as shown in Figure 7. The other two anchors in Holes 1 and 4 are positioned approximately one-half and three-fourths the distance to hole bottom.

Holes 6 and 9 drilled from Panel 23 access the east side of the test stope and are similar to Holes 1 and 4. However, Hole 6 contains a "sonic probe" extensometer which is also read by electrical means but with special equipment.

Hole 33 in Panel 23 is a single point extensometer that extends away from the test stope for the purpose of assessing the extent of the zone of influence of the fully mined test stope.

Holes 2 and 5 in Panel 19 and Holes 7 and 10 in Panel 23 contain arrays of vibrating wire stress gages. There are three gages in each hole. These holes are collared near Holes 1, 4, 6, and 9 but bottom at a lower elevation near the future stope walls as shown in Figure 7. The three-gage arrays in principle allow determination of changes in the secondary principal stresses and in the Cartesian components of stress in planes normal to the drill holes.

Holes 3 and 8 shown in Figures 6 and 7 are slough meter holes located midway between foot and hanging walls. The slough meters are intended to indicate the extent of any overbreak or slabbing of the stope walls. They are read electrically. In this regard, mining of the test stope proceeds towards the hanging wall access drift from the footwall.

Holes D and E in Panel 19 crosscut on the 1000 Level are short, horizontal holes that contained vibrating wire stress meters and a borehole deformation gage, respectively. Their purpose was to obtain data for a comparison of stress changes indicated by the two devices.

Holes B and C in the Panel 20 stub drift on the 1000 Level constituted a similar comparison test.

The remainder of the instrumentation holes, Holes A, 11-32, 34, and F are best seen in Figure 8. Mining progresses from left to right in Figure 8.

Instrumentation Layout--Plan View.

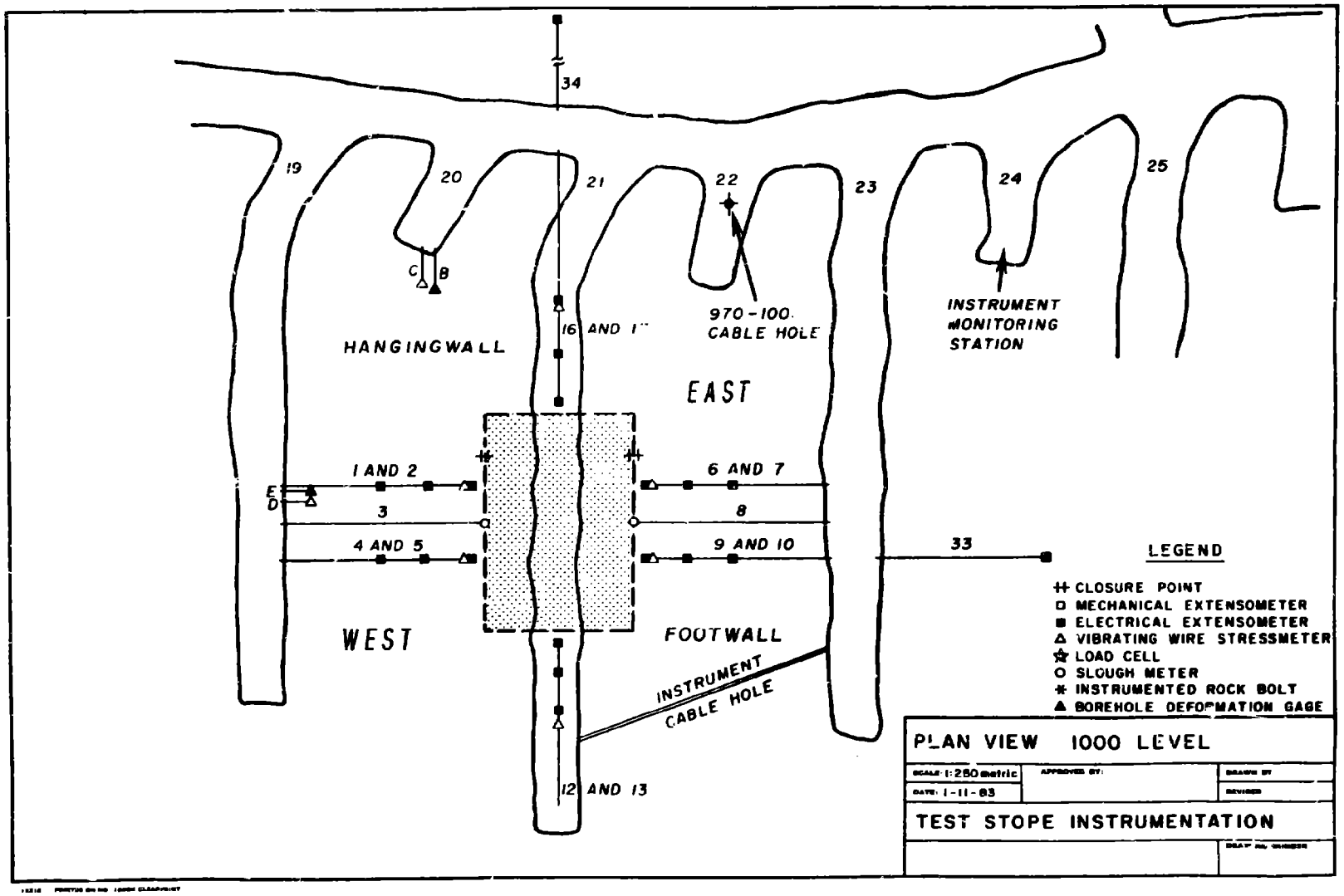

Figure 6. - Instrumentation layout--plan view.

Instrumentation Layout--Parallel to Strike.

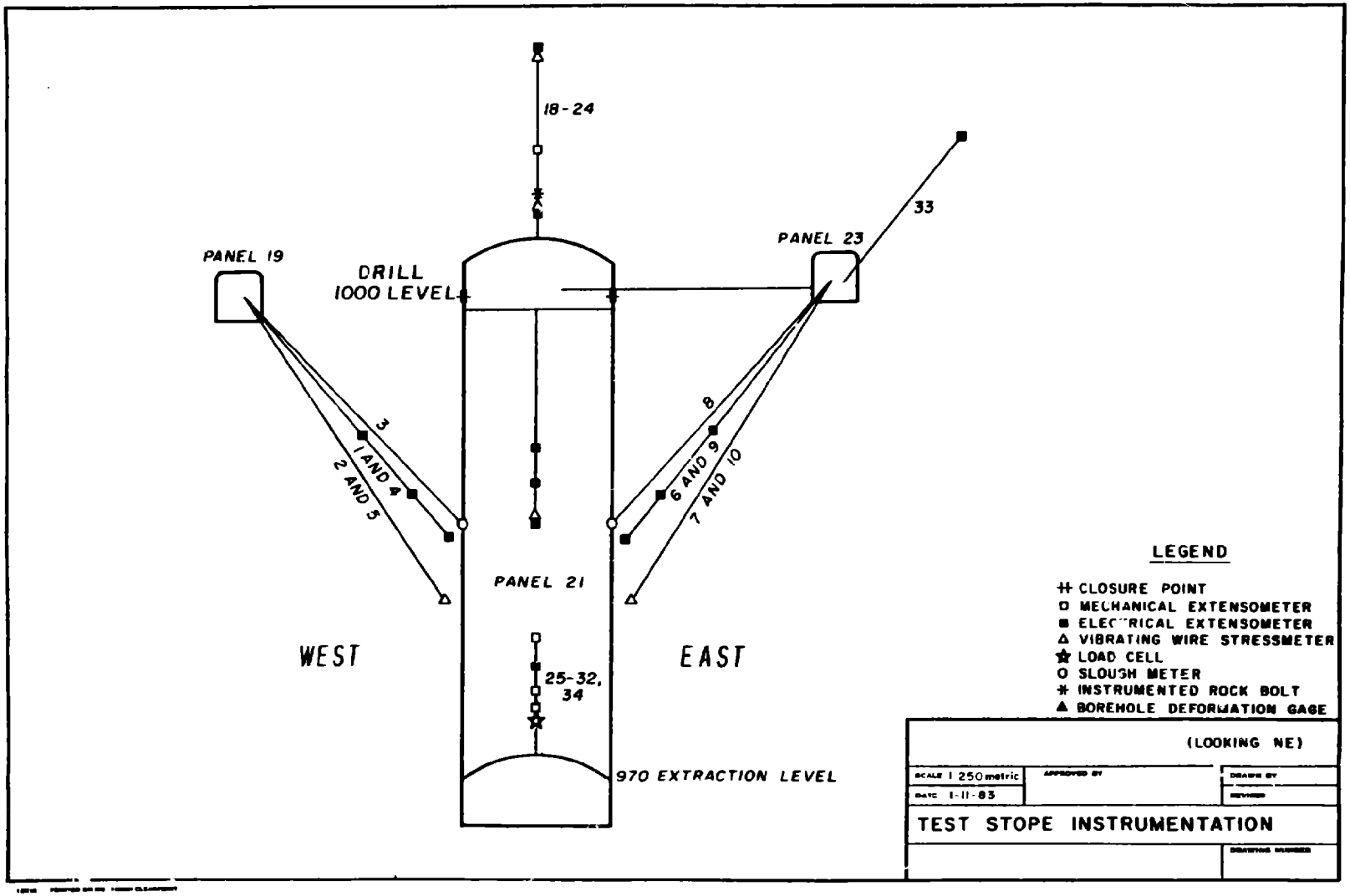

Figure 7. - Instrumentation layout--section parallel to strike.

Instrumentation Layout--Perpendicular to Strike.

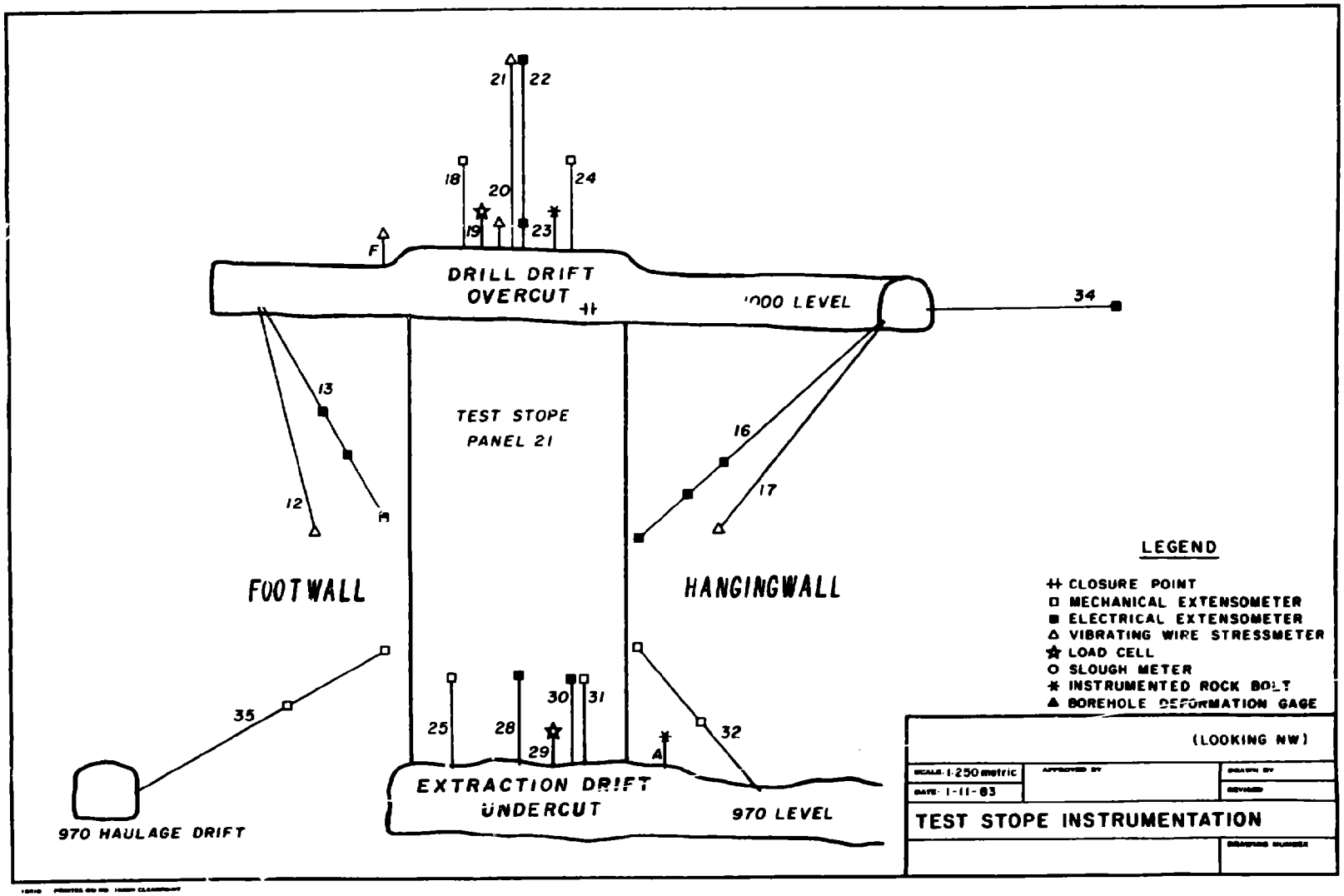

Figure 8. - Instrumentation layout--section perpendicular to strike.

Backs and Brows

Holes 18 through 24 contain instrumentation for monitoring displacements, rock stress changes and rock bolt loading in the back of the overcut. Two types of rock bolt load measurements were made. One type (Hole 19) is a Bureau of Mines rock bolt load cell fitted to the bolt head and read with a conventional strain indicator calibrated in units of force. The other type (Hole 23) is an "instrumented rock bolt" read with vibrating wire equipment.

Hole F monitors rock stress change in the shoulder of the overcut. The overcut is higher than the top drift in order to provide head room.

Holes 25, 28-31, and A shown in Figure 8 measure similar quantities in the back and brow of the undercut on the 970 Level. Stability of the brows over the extraction crosscuts is, of course, important to the safe and reliable flow of muck from the stope. Hole A contains an instrumented rock bolt.

Protection from blast damage was provided for instrumentation in the back of the overcut. Life of the undercut instrumentation was necessarily limited to the time between installation and the production blast that encompassed any particular instrumentation hole.

Foot and Hanging Walls

Holes 16, 17, 32, and 34 shown in Figure 8 are hanging wall instrumentation holes collared from the test stope panel crosscut (Panel 21) on the 1000 Level. Hole 34 is an extensometer hole intended to assist in the determination of the extent of the zone of influence of the fully mined test stope. Strong protection for these instrument heads was required because of traffic in the hanging wall access drift.

Holes 12, 13, and 35 are footwall holes as seen in Figure 8. The fractured quartzite of the footwall is much less competent than the hanging wall garnetite, so that it was especially important to monitor the footwall. In this regard, the extension of the Panel 21 overcut drift into the footwall was necessary for collaring footwall Holes 12 and 13 and for bolting the footwall. Since access to footwall Holes 12 and 13 would be lost after widening the slot raise to full stope width, remote electrical readout was used via the instrument cable hole between Panels 21 and 23 as shown in Figure 6.

Data Logging

With few exceptions, all instrumentation was monitored remotely by data logging equipment in the instrumentation monitoring station located in the Panel 24 stub drift shown in Figure 6. Extensometers, borehole deformation gages, slough meters and a rock bolt load cell were monitored as DC analog devices. The vibrating wire stress meters were monitored with a separate data logger. The sonic probe and instrumented rock bolts were read with a third unit.

Readings were subsequently entered into computer files that provided rapid retrieval and inspection in the form of readings versus time plots on computer terminal screens. Hardcopy plots and detailed instrumentation histories are also readily obtained.

Chronology

The installation of the test stope instrumentation that began in late June 1982 was essentially complete by mid-August. From one to five holes per day could be instrumented depending on hole length and type of instrumentation. This includes cleaning holes and grouting when required. Grouted rebar anchor extensometer holes were installed with relative ease and speed. The vibrating wire stress meters required the greatest effort because of the close hole tolerances of the gages that make them liable to lodging in the hole. Occasionally a vibrating wire stress gage array could not be installed at the planned downhole orientation of 0-45-90°. This circumstance and the need to proceed with the installation plan in order to avoid the critical path of the test stope project necessitated the development of a new data reduction scheme that allows for arbitrary downhole orientation of gages (Pariseau, 1984).

Measured Test Stope Response

Widening of the slot raise to full stope width began September 25, 1982; the last production blast was October 14. The test stope was subsequently filled with waste rock. Monitoring continued well into 1984. Pre-stope baseline data were thus obtained well in advance of production blasting. Some development rounds were pulled in the interim, but these appeared to have no noticeable effect on the test stope instrumentation. Data logging provided ample data acquisition during the 20 days of actual mining. The continuation of data acquisition since backfilling of the test stope has generated a unique set of data relevant to the long term as well as short term and instantaneous response of the test stope and similar field scale rock masses.

Generally, the relative displacements indicated by the extensometers are the most reliable data. Displacement measurements are considered simple to interpret, but this is not always the case, especially when holes are long and the motion history is complicated by the mining sequence. Vibrating stress gage installations were less reliable. The gages themselves are durable, but the roughness of percussion drill holes and blasting effects combined to produce a high loss rate. The rock bolt strain gage load cells worked well, while the "instrumented rock bolts" produced questionable readings. The slough meters did not respond at all.

The short-term results from installation time to two weeks after the last blast are summarized according to instrumentation group: (i) ribs, (ii) backs and brows, (iii) foot and hanging walls.

Ribs

The maximum displacement indicated by the extensometers immediately after the last blast is of the order of 2.5 cm (1.0 in.). Two weeks after the last blast the readings more than doubled. Higher readings were obtained on occasion, but these are attributed to anchors lost during overbreak. The highest reading on any of the remote anchors (No. 3 anchors, approximately 8 m or 26 ft from stope ribline) immediately after the last blast is 8.4 cm (3.3 in.). Figure 9 shows the extensometer histories of Holes 1, 4, 6, and 9. A high correlation between blasting events and sudden increases in readings is quite evident in Figure 9. Also indicated in Figure 9 is a continued increase in readings between blasts but at a decreasing rate with time.

The maximum tensile stress change indicated by any of the ribline vibrating wire stress meters is 3.8 MPa (550 psi); the maximum compressive stress change is nearly the same. Figure 10 shows a portion of the histories of the three-gage arrays of vibrating wire stress meters in ribline Holes 2, 10, and D. The correlation between sudden change in readings and blasting is quite evident here, too.

Backs and Brows

The back of the 1000 Level overcut proved to be quite stable. Instrumentation readings are in accord with this observation. Only 0.05 cm (0.02 in.) of displacement was observed prior to the first blast at a point 2 m (6.6 ft) into the back on the center of the overcut (Hole 22). Before the last blast, 0.18 cm (0.07 in.) of relative displacement was observed. Two weeks after the last blast, the displacement was 0.25 cm (0.10 in.). In this regard, blasting had considerably less of an effect on readings in the back than in the ribs as the hole histories in Figure 11 show.

Stress changes in the back as indicated by the vibrating wire stress gage array in Hole 20 are also shown in Figure 11. The blank region in Figure 11 was caused by a cut wire that was subsequently repaired.

The rock bolt load cell in the back of the overcut showed a tension of 22.2 kN (5,000 lbs) prior to the first blast. This increased to 27.4 kN (6,150 lbs) before the last blast. Several weeks after the last blast the rock bolt tension reached 45.8 kN (10,300 lbs). Subsequent increases have been quite small.

The brow of the 970 Level undercut stood well. Extensometer Holes 25, 28, 30, and 31 showed little displacement prior to the first blast and approximately 1.3 cm (0.5 in.) prior to the blast that brought them down. Figure 12 illustrates the response of Holes 28, 29, and 30. (The Hole 30 head was lost during the cutout for the operator of the remote controlled scoop-tram.)

The rock bolt load cell in the brow registered 4.4 kN (1,000 lbs) prior to the first blast and 30.7 kN (6,900 lbs) before the blast that brought it down. The instrumented rock bolt showed a 2.8 kN (640 lb)

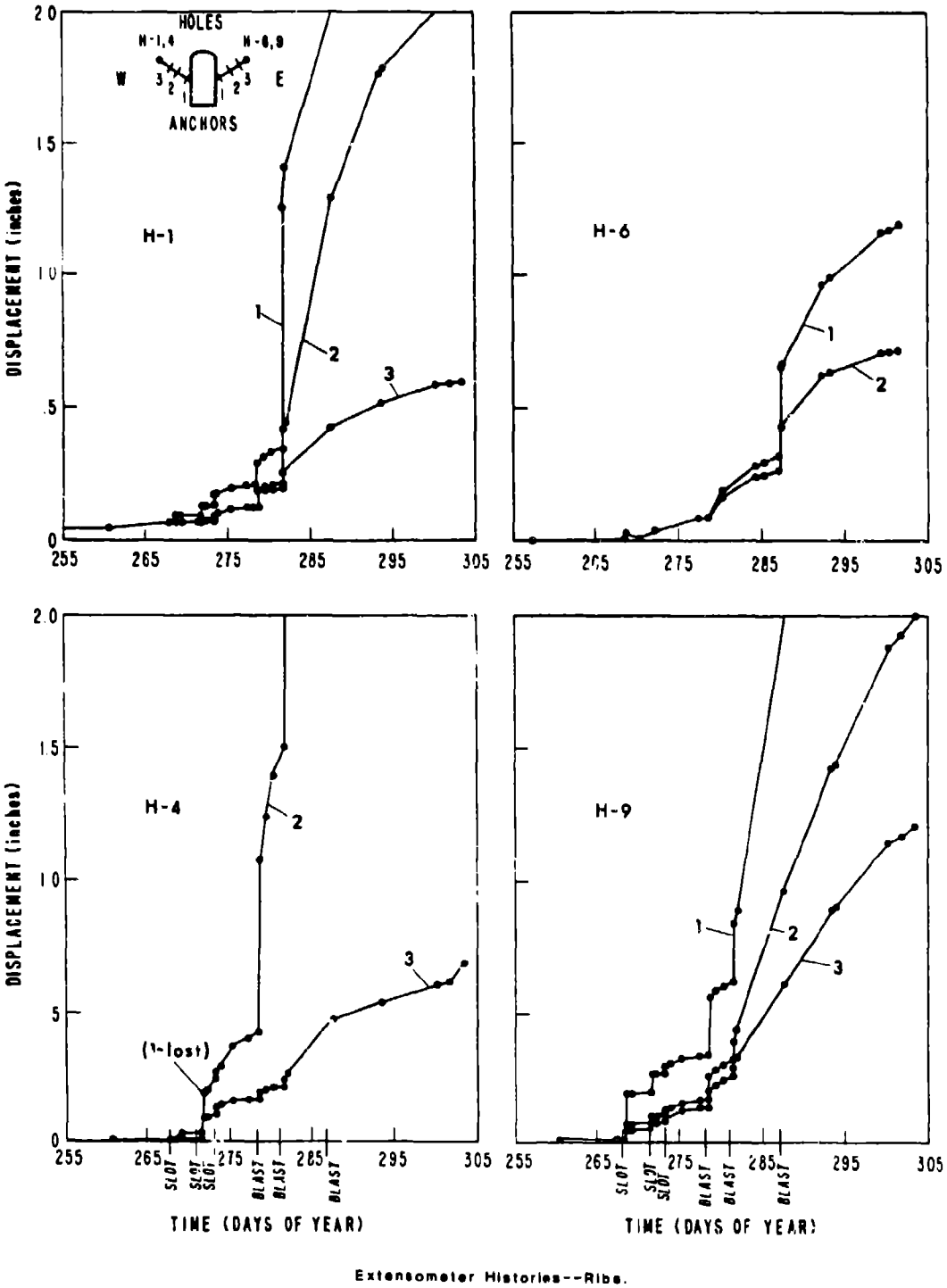

Extensometer Histories--Ribs.

Figure 9. - Extensometer histories--ribs.

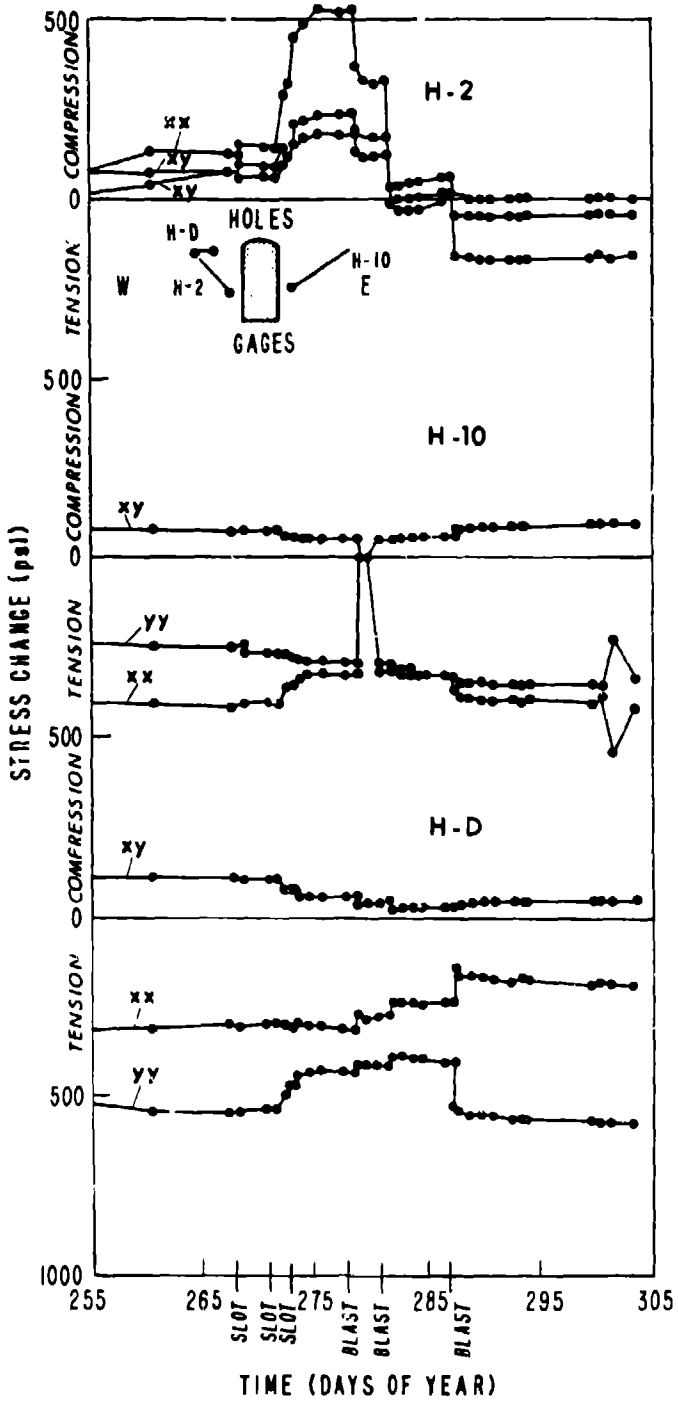

Vibrating Wire Stress Gage Histories--Ribs.

Figure 10. - Vibrating wire stress gage histories--ribs.

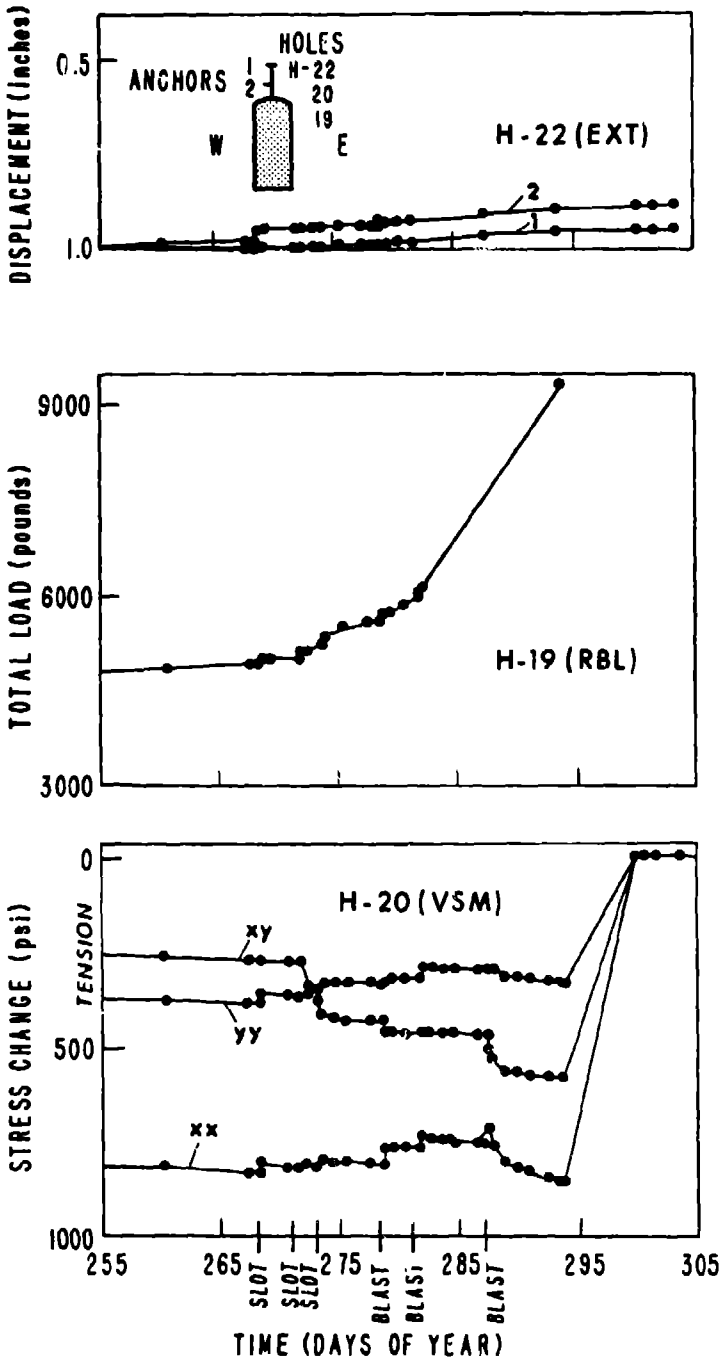

Instrumentation Histories--Overcut Back.

Figure 11. - Instrumentation histories--overcut back.

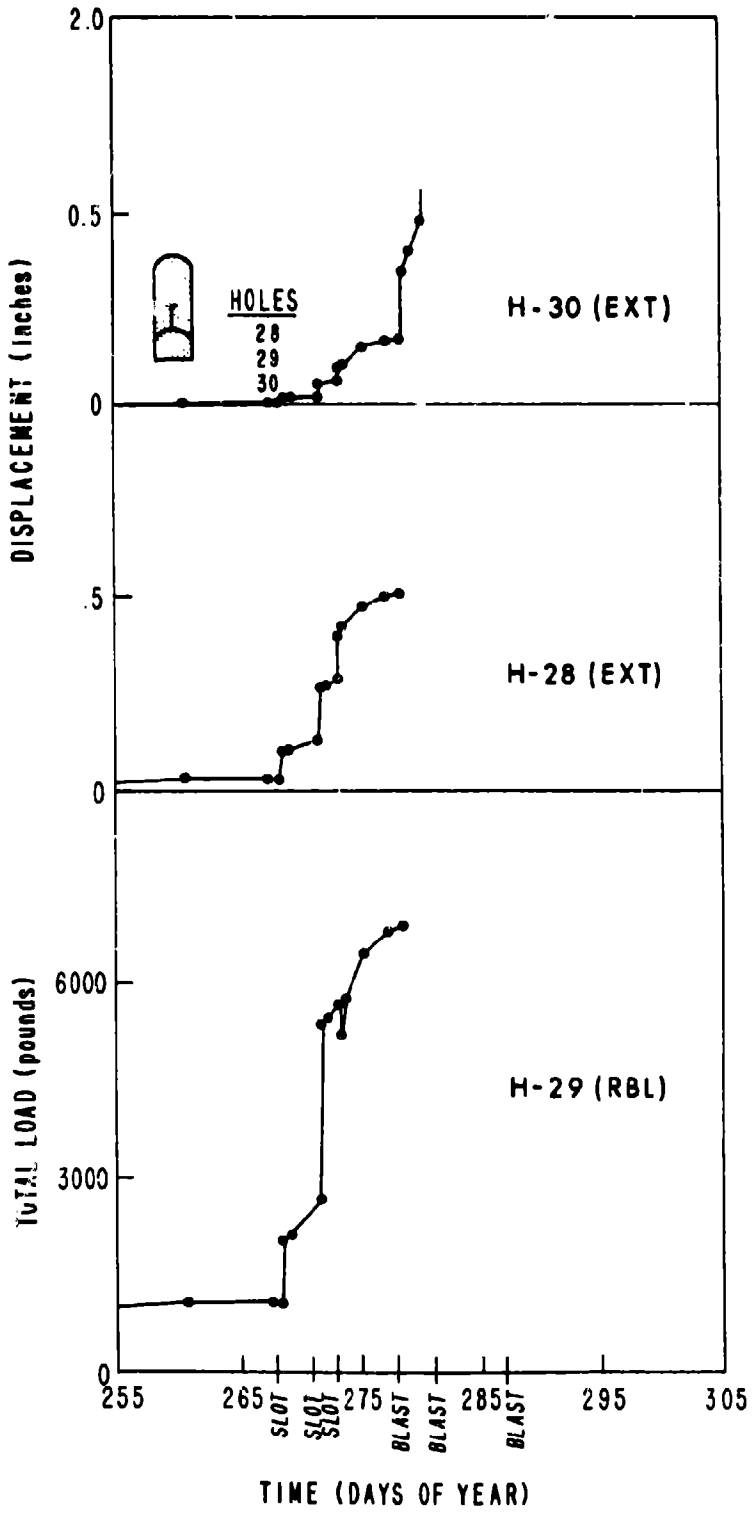

Instrumentation Histories--Undercut Brow.

Figure 12. - Instrumentation histories--undercut brow.

compression before the first blast and a 18.7 kN (4,200 lb) tension after the last blast.

Foot and Hanging Walls

The footwall extensometers, Holes 13 and 35, showed a very small displacement prior to the first blast. Both were affected by overbreak of the footwall. Hole 13 showed 0.25 cm (0.1 in.) prior to the third blast. The deepest anchor nearest the stope was lost after the third blast. The uppermost anchor eventually showed over 8.4 cm (3.3 in.) of movement before being lost. Hole 35 is collared in the 970 footwall haulage drift. This extensometer indicated 0.91 cm (0.36 in.) of relative displacement two weeks after the last blast.

The footwall stress gage array (Hole 12) indicated a change of 2.6 MPa (370 psi) before being lost.

The hanging wall was stable; extensometer Hole 16 indicated a relative displacement of 1.1 cm (0.42 in.) two weeks after the last blast. Hole 34 collared in the 970 extraction drift indicated a displacement of 0.7 cm (0.27 in.) two weeks after the last blast. Hole 34 extends away from the test stope and indicated a slight relative displacement of 0.2 cm (0.08 in.) between collar and a point 15 m (49 ft) into the hanging wall. Although the movement is slight, it is clearly associated with mining of the test stope.

Prior to the first blast, the vibrating wire stress gage array in Hole 17 indicated a stress change of 1.9 MPa (270 psi). Two weeks after the final blast the change was 5.0 MPa (730 psi) as shown in Figure 13.

Summary

The extensometer readings show the test stope response best. These are summarized in Table 4. Qualitatively, the response is what one would expect. The largest displacements occur in the areas of greatest exposure. In this study, these are the test stope ribs. Movement is of the order of 2.5 cm (1.0 in.) at the ribline, and as expected, decreases with distance away from the stope walls. At 27 m (89 ft) away from the east rib and 37 m (128 ft) into the hanging wall, distances of roughly one stope height (33 m or 108 ft), displacements before the final blast although detectable were small, less than 0.23 cm (0.09 in.).

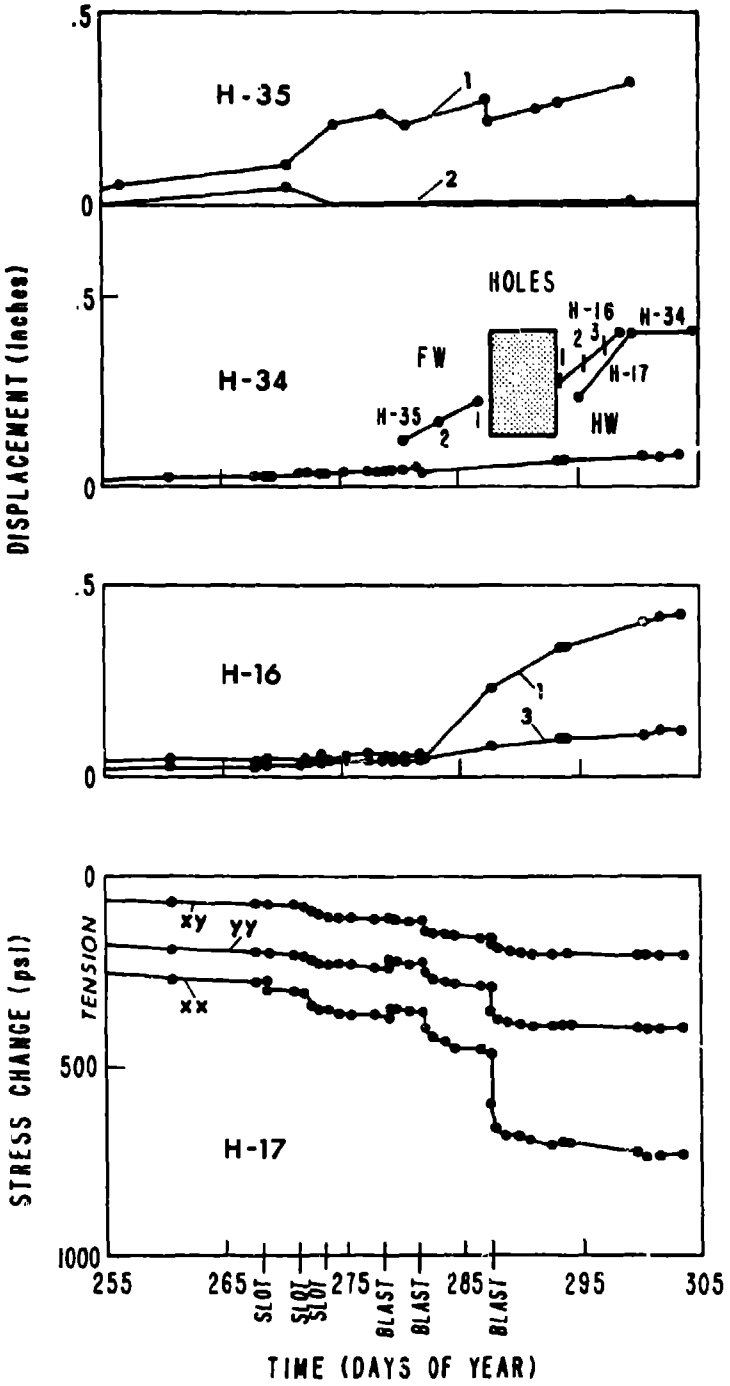

Instrumentation Histories--Foot and Hanging Walls.

Figure 13. - Instrumentation histories--foot and hanging walls.

TABLE 4. - Summary of stope wall displacements

Area	Movement	Remarks
1. East and west ribs	2.5 cm (1.0 in.)	stable
2. Overcut back	0.25 cm (0.1 in.)	very stable
3. Undercut brow	1.3 cm (0.5 in.)	stable until blasted
4. Footwall	1.3 cm (0.5 in.)	some overbreak
5. Hanging wall	1.0 cm (0.4 in.)	stable

The overcut back stood very well; displacements were approximately 0.25 cm (0.1 in.). The brows of the undercut were stable until overtaken by advance of the stope; displacements were 1.3 cm (0.5 in.) just prior to removal.

The hanging wall was also quite stable. Approximately 1.0 cm (0.4 in.) of displacement was measured from the 1000 Level, while less than 0.8 cm (0.3 in.) was measured from the 970 Level. Footwall extensometer readings were less easily interpreted because of the footwall overbreak that developed in the course of mining. However, prior to loss, 1.3 cm (0.5 in.) of displacement was measured from the 1000 Level and 0.9 cm (0.36 in.) from the 970 haulage Level.

Data from the vibrating wire stress gages are erratic; no consistent trend or correlation could be discerned. In this regard, the data suggest that in many instances stress relaxation at the gage site is responsible for much of the indicated stress change rather than mining activity. This seems especially evident when most of the stress change indicated occurs before the first production blast.

IN SITU STRESS MEASUREMENTS AND ROCK PROPERTIES

In situ stress measurements in advance of mining and rock properties tests provide input data essential to design analysis. In principal, stress changes obtained during the monitoring phase of the test stope project when added to the prestope stresses give the post-stope stress state. The post-stope stress state can also be measured in situ. A comparison between the two sets of measurements provides a check on the procedures, equipment, and data reduction formulas. Rock properties are usually determined in the laboratory where both loads and displacements are known. However, the elastic modulus (Young's modulus) is also determined on site in the biaxial chamber in conjunction with the in situ stress measurements. Borehole jacking tests also provide on site measurements for determining the elastic modulus. Borehole tests for shear strength were not done. In this regard, borehole tests have the advantage of involving a volume of rock somewhat larger than conventional laboratory size samples. Their disadvantage lies primarily in data reduction schemes that may be poor approximations to actual borehole conditions. A variety of tests in situ, on site, and in the laboratory would seem desirable, although some difficulties in correlation should perhaps be expected.

In Situ Stress Measurements

Stress measurements were made before and after mining the test stope using the U. S. Bureau of Mines borehole deformation gage, the doorstopper gage, and combinations of the two types of devices. The three-dimensional state of stress in situ was determined on the 1300 Level, the 1200 Level, and the 1000 Level. (Level number refers to elevation above sea level in meters; the 1000 Level is the lower of the three levels.) Table 5 shows the results of the in situ stress measurements on the 1000 Level.

TABLE 5. - Summary of in situ stress measurements

Location	Magnitude (psi)*	Bearing	Dip* (degrees)
1000 Level (USBM-Doorstopper)			
Major	3531	N56°W	+50
Inter.	3052	N48°E	- 2
Minor	2904	S48°E	+52
Vertical	3134	-	-
N-S	3201	-	-
E-W	3152	-	-

*1 psi = 6.9 kPa
+ = down, - = up
Inter. = intermediate

Measurements show that the state of stress varies noticeably over distances of 100 m (300 ft). This is not surprising in view of the geologic variability and the sensitivity of in situ stress measurements to the local value of Young's modulus at each gage setting down hole.

Another set of 1000 Level doorstopper results (not shown in Table 5) proved unreliable. A new, faster setting epoxy was being tested at the time. Subsequent data analysis including the mean normal strain ratio test applicable to the four-gage doorstoppers that were used indicate a general lack of adequate bonding of gage to rock.

On the 1300 Level, the vertical (V) stress is significantly greater than either the North-South (N) or East-West (E) normal stresses which are close to the principal stresses. (The orebody trend is roughly east-west and near vertical in the vicinity of the test stope.) The shear stresses relative to the V, N, E directions are small. The N-S stress tends to increase with depth, while the vertical stress tends to decrease. The E-W stress remains almost constant. The decrease of the vertical stress with depth is somewhat unexpected but not too surprising in this region of high topographic relief and orebody geology.

However, the mean normal stress (first invariant) does increase with depth from the 1300 to the 1000 Level, while the second invariant of deviatoric stress, a mean shear stress, decreases. The in situ stress state thus tends towards a true hydrostatic state of stress with depth. In view of the topography, natural variability, and limited number of measurements, this inference should not be extrapolated very far beyond the region of measurements.

Post-stope stress measurement in the east and west ribs of the test stope overcut (1000 Level) are shown in Figure 14. Also shown in Figure 14 is the extent of overbreak that occurred in the footwall. Figure 15 shows in vertical section the maximum compression measured in the ribs of the test stope after mining and backfilling. Again, there is considerable variability in the stress measurements. However, there is also a trend in that stress concentration is greatest at the edge of the projected overbreak zone below the ribs rather than at the measurement hole collars. The periphery of the overcut is also subject to blast damage during development. Both tend to move the concentration of stress into the rib. Beyond the zone of peak stress concentration, the maximum stress appears to decrease with distance into the rib as expected.

In Situ Modulus Measurements

In situ modulus measurements were attempted in the west rib of the test stope using the Goodman Jack (Hardrock model). A short 4 m (13 ft) NX size hole was drilled for this purpose. Hole location is near and parallel to Hole 2 (west rib) shown in Figures 14 and 15. The test procedure involved advancing the jack in 0.3 m (1 ft) increments down the hole. At each station a test was attempted but aborted if the jack platens exceeded the recommended skew tolerance. A successful test involved three cycles of loading to 55.2 MPa (8,000 psi) and unloading.

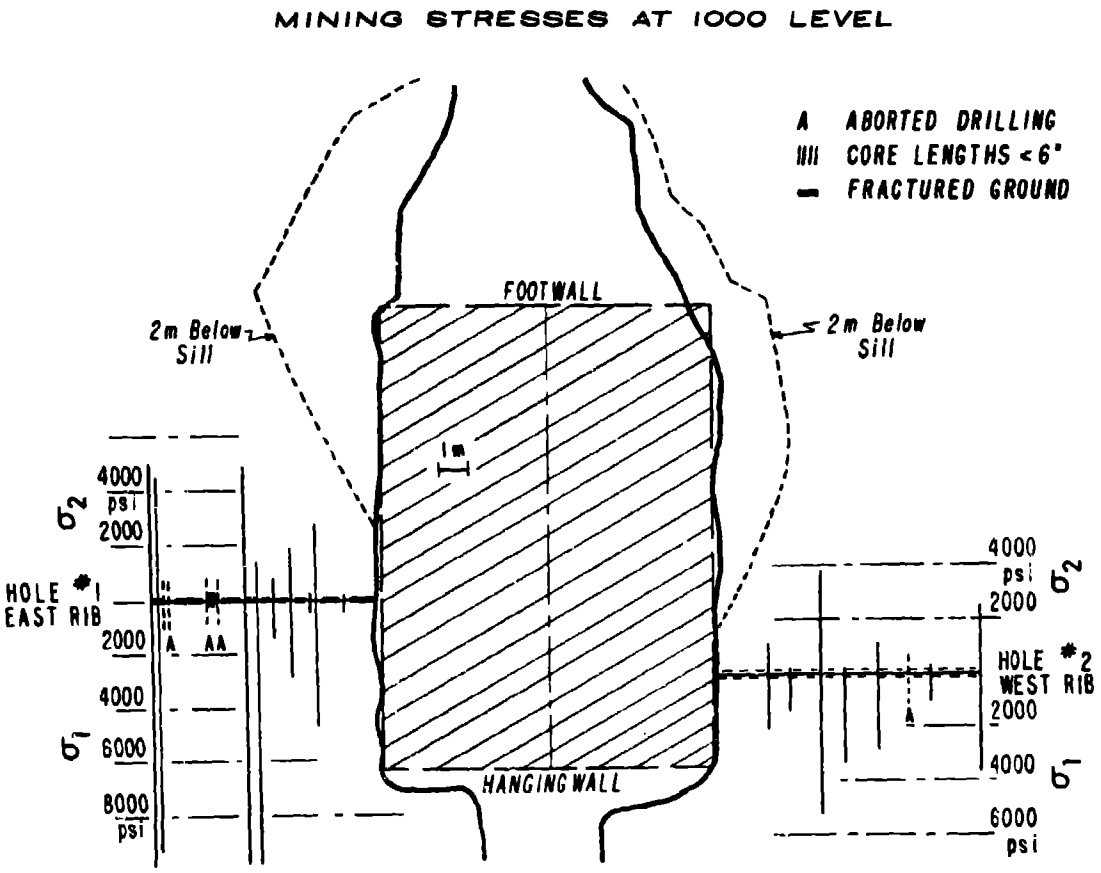

Figure 14. - Principal post-stope stress measurement in the ribs.

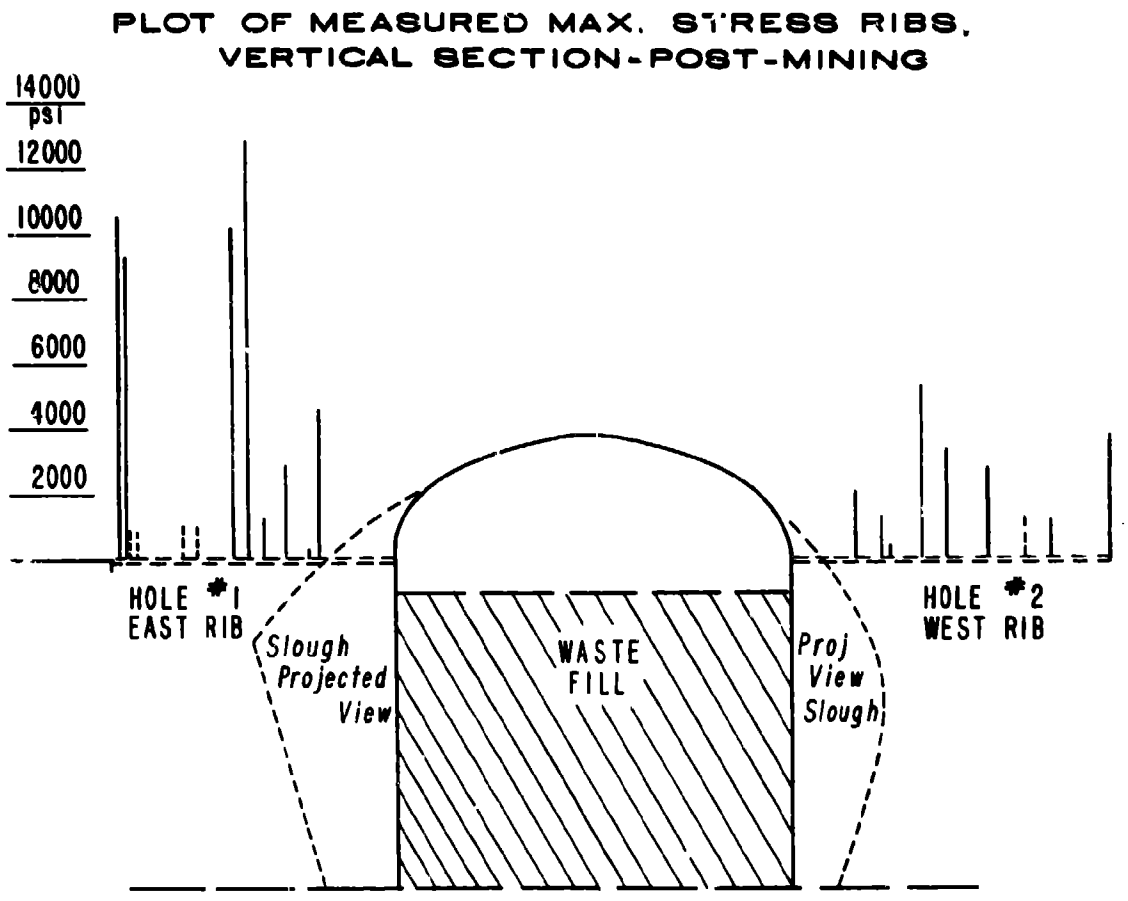

Figure 15. - Vertical section showing maximum post-stope compression measured in the ribs.

Generally, the loading unloading cycles were quite reproducible and linear at loads above 13.8 MPa (2,000 psi) as shown in Figure 16.

The results of the in situ modulus measurements are summarized in Table 6. These results were obtained from the raw data according to the latest data reduction formula described by Heuze and Amadei (1984). The regression statistics in Table 6 show that the data are rather linear. They also show variability; the standard deviation is 36 percent of the mean (coefficient of variation). Although relatively few tests were made from the statistical viewpoint, more tests in a longer hole could well increase the scatter in the data. Indeed, laboratory test data range over an order of magnitude.

TABLE 6. - In situ Young's modulus

(Goodman Jack Test--Heavily Mineralized Ore)

Hole Depth (ft)	Jack Direction	E (10^6 psi)*
7	horizontal	2.04
8	horizontal	0.79
9	horizontal	1.11
10	vertical	1.25
11	horizontal	1.46
12	horizontal	0.87

mean $\bar{x}$ = 1.25

std. dev. s = 0.46

coeff. var. $s/\bar{x}$ = 36%

$$E = (0.86)(0.93)(3.0)(1.46)(\Delta Q_h/\Delta D)$$

0.86 = 3D effect
0.93 = hydraulic efficiency
3.0 = borehole diameter
1.46 = contact angle and Poisson's ratio effect
$(\Delta Q_h/\Delta D)$ = slope of pressure displacement curve
*1 psi = 6.9 kPa.

Reference: Heuze and Amadei, 1984.

Laboratory Rock Properties Tests

Rock properties of greatest importance are the strength properties and elastic moduli. Unconfined compressive strength (Co), tensile strength (To), cohesion (c), angle of internal friction (ϕ), and

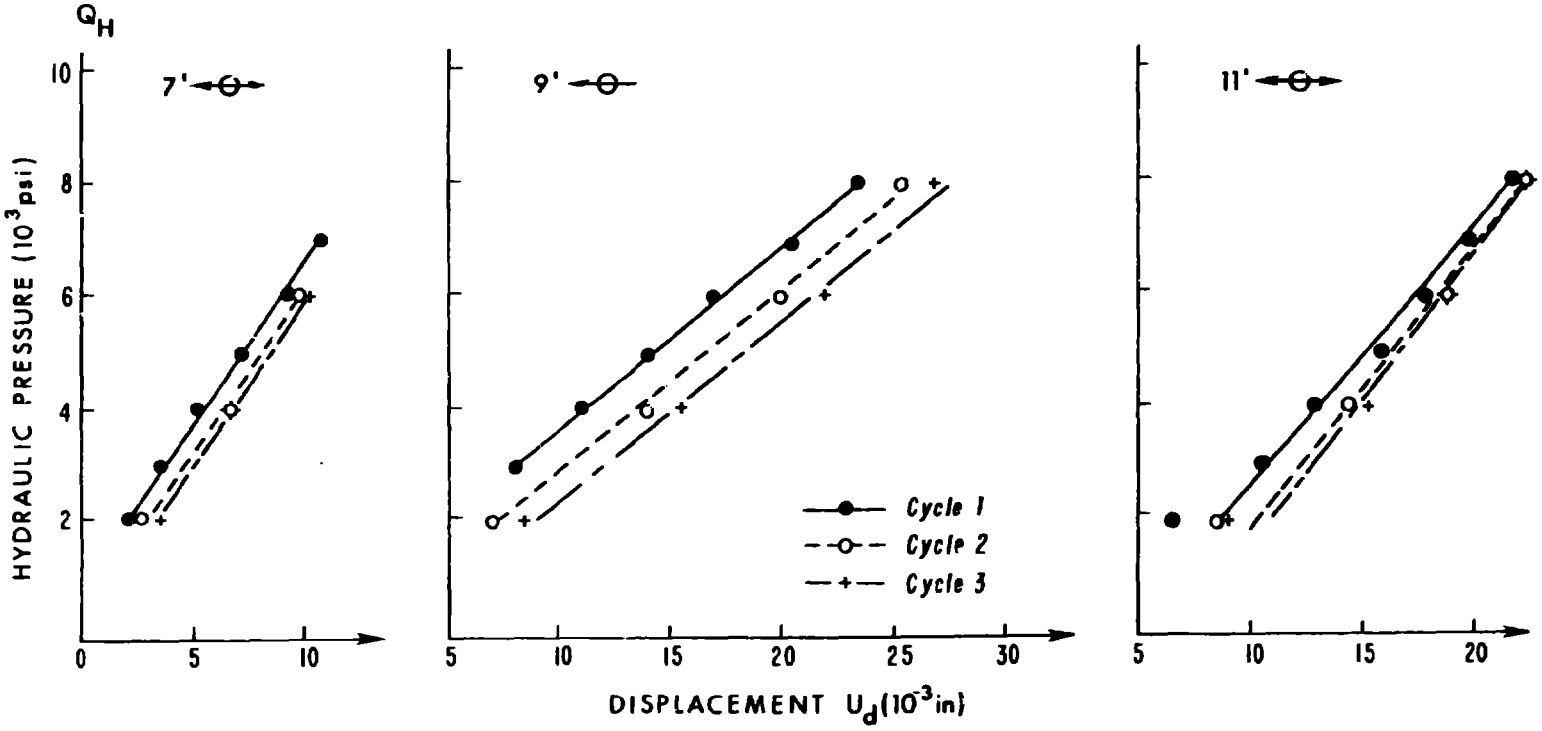

Figure 16. - In situ Young's modulus and Goodman borehole jack loading cycles (about 2,000 psi).

specific weight (γ) for nine rock types are summarized in Table 7. The strength properties in Table 7 are mean values but represent more than 200 tests on samples from the Steep Highland Boy and other ore zones at the Carr Fork Mine. They thus represent a broad measure of mine rock.

TABLE 7. - Rock strength properties

Rock Type	γ(pcf)	Co(psi)	To(psi)	c(psi)	$\phi(^0)$
1. Garnetite and lm.	200	11,800	890	3,000	48
2. Faults in gn	200	7,000	-	-	25
3. Gn/qtz-fw	200	3,600	270	3,000	30
4. Qtz. and H-qtz.	171	8,000	720	3,000	35
5. Hornfels	169	9,200	800	4,000	50
6. QMP/ intrusive	162	7,000	580	-	25
7. QLP Dike/ intrusive	162	4,000	200	-	20
8. Faults in quartzite	171	4,000	-	-	25
9. Gn/hornfels contact	200	13,500	360	4,000	40

lm = limestone, gn = garnetite, qtz. = quartzite, H-qtz. = hard quartzite, QMP = quartz monzonite porphyry, QLP = quartz latite porphyry.

γ = specific weight, Co = unconfined compressive strength, To = unconfined tensile strength, c = cohesion, ϕ = angle of internal friction.

pcf = pounds per cubic foot
1 pcf = 157 N/m^3
psi = pounds per square inch
1 psi = 6.9 kPa

A high degree of variability is present in the test data, particularly in the heavily mineralized ore zone. Table 8 presents test statistics for heavily mineralized ore and shows an order of magnitude range of values for Young's modulus as well as strengths. Some of the scatter is no doubt caused by experimental error in the sense that there is variability in sample preparation, test procedure, and so forth.

However, the experimental component of variance would seem small relative to the natural or geologic component in view of the metamorphic nature of the region.

TABLE 8. - Rock properties statistics--ore

1. Young's Modulus E (10^6 psi):

average	E	= 4.81
std. dev.	s	= 2.59
range		0.9 - 11.6
cof. var.	$s/\bar{x}$	= 54%
	$s/\sqrt{n}$	= 0.35
tests	n	= 54

2. Unconfined Compressive Strengtn Co (psi):

average	Co	= 9,363
std. dev.	s	= 4,477
range		1,090 - 17,780 psi
cof. var.	$s/\bar{x}$	= 42%
	$s/\sqrt{n}$	= 895
tests	n	= 25

3. Unconfined Tensile Strength To (psi):

average	To	= 855 psi
std. dev.	s	= 386 psi
range		107 psi - 1,916 psi
cof. var.	$s/\bar{x}$	= 55%
	$s/\sqrt{n}$	= 55

4. Specific weight (γ) :

average = 204 pcf
(scatter is small, 50 tests)

average = sample average, std. dev. = standard deviation, cof. var. = coefficient of variation, tests = number of tests

The standard deviation of the sample mean is $s/\sqrt{n}$.

Tensile strength is determined from Brazil Test data.

Despite the spread of data, there is a correlation between properties within a given rock type as shown in Figure 17 for heavily mineralized ore. In Figure 17, Eo refers to Young's modulus obtained in unconfined tests; Ep refers to values determined in tests under confining pressures to 34.5 MPa (5,000 psi). Figure 18 shows the correlation between Young's modulus and unconfined compressive strength for eight rock types.

A secant modulus is plotted in Figure 18. The use of the secant modulus (Es) rather than a tangent modulus (Et) is an experimental convenience. The difference between the two may be attributed to nonlinear elasticity and the use of displacement transducers attached to testing machine platens. In the case of a linear elastic material, a nearly straight line relationship exists between the secant and tangent moduli. Figure 19 shows the relationship between secant and tangent moduli. The high (0.92) linear correlation coefficient indicates that linear elasticity is a good approximation.

Triaxial test results for compressive strength of ore under confining pressure are presented in Figure 20 in the form of Mohr circles and their envelopes. Again, considerable variability is present, but there is no doubt that strength increases with confining pressure. Figure 21 shows typical force displacement plots obtained in the triaxial tests. The data in Figure 21 indicate that under relatively small confining pressures the inelastic range of deformation is characterized by flow with little strain hardening before reaching peak stress. The flow is macroscopic, of course. Inspection of the test specimens generally reveals some fracturing, although occasionally no visible fractures were in evidence upon removal of the specimen from the pressure cells.

A few tests for strength and modulus were performed on 15 cm (6 in.) core obtained during the in situ stress measurement program. These tests are of interest because they involve a volume of rock that is an order of magnitude greater than the smaller core volume. The results are summarized in Table 9. The number of tests is too few for statistical analyses, but as Figure 22 shows, the response to load of these larger test specimens is similar to the small core response. A reasonably linear elastic range is evident; the inelastic response is plastic flow. The strain softening indicated in Figure 22 cannot be quantitatively assessed because of the complicated changes in stress and structure of the test specimen after large inelastic straining. Indeed, the softening is more apparent than real because of the greatly reduced cross-sectional area of the test specimens.

Biaxial chamber tests on overcore obtained during in situ stress measurements are an additional source of Young's modulus data. Figure 23 shows pressure versus displacement curves obtained on aluminum and ore using a three axis Bureau of Mines borehole deformation gage. In theory, the three curves should be identical, but as Figure 23 shows this is not always the case. The question then is how to interpret such test data. A natural but mistaken impulse is to average the slopes of the three curves, however, The curve showing the greatest displacement yields the best estimate of Young's modulus. Curves showing lesser displacement are caused by a lack of contact between a gage prong and hole

Downhole Association of Properties for Ore.

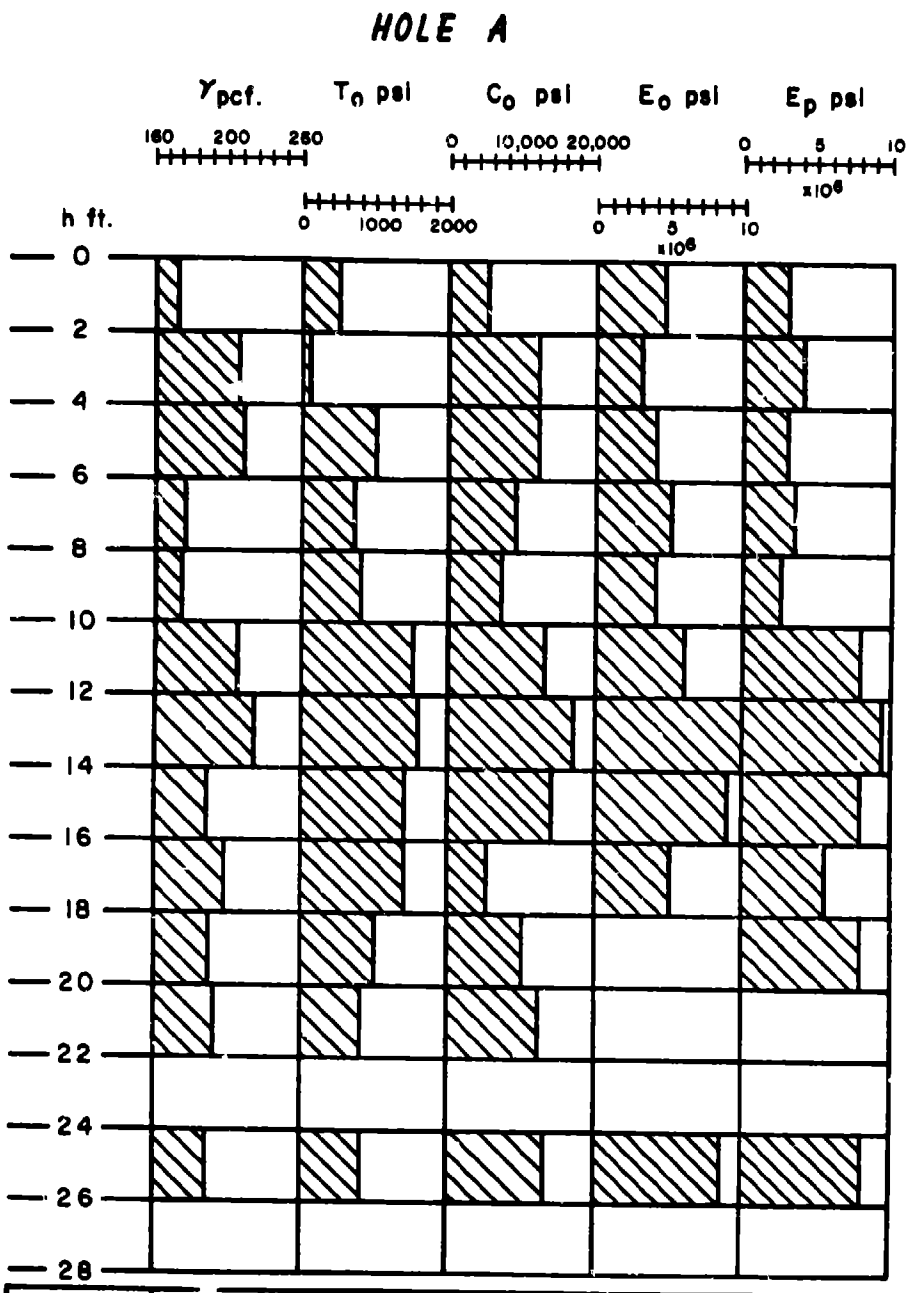

X	201	964	10,740	4.94	4.25
s	17	454	3,800	2.98	2.57
s/X	9%	47%	35%	60%	60%

* 1 psi = 6.9 k Pa, 1 pcf = 157 N/m^3

Figure 17. - Downhole association of properties for ore.

Young's Modulus versus Compressive Strength in All Rock Types.

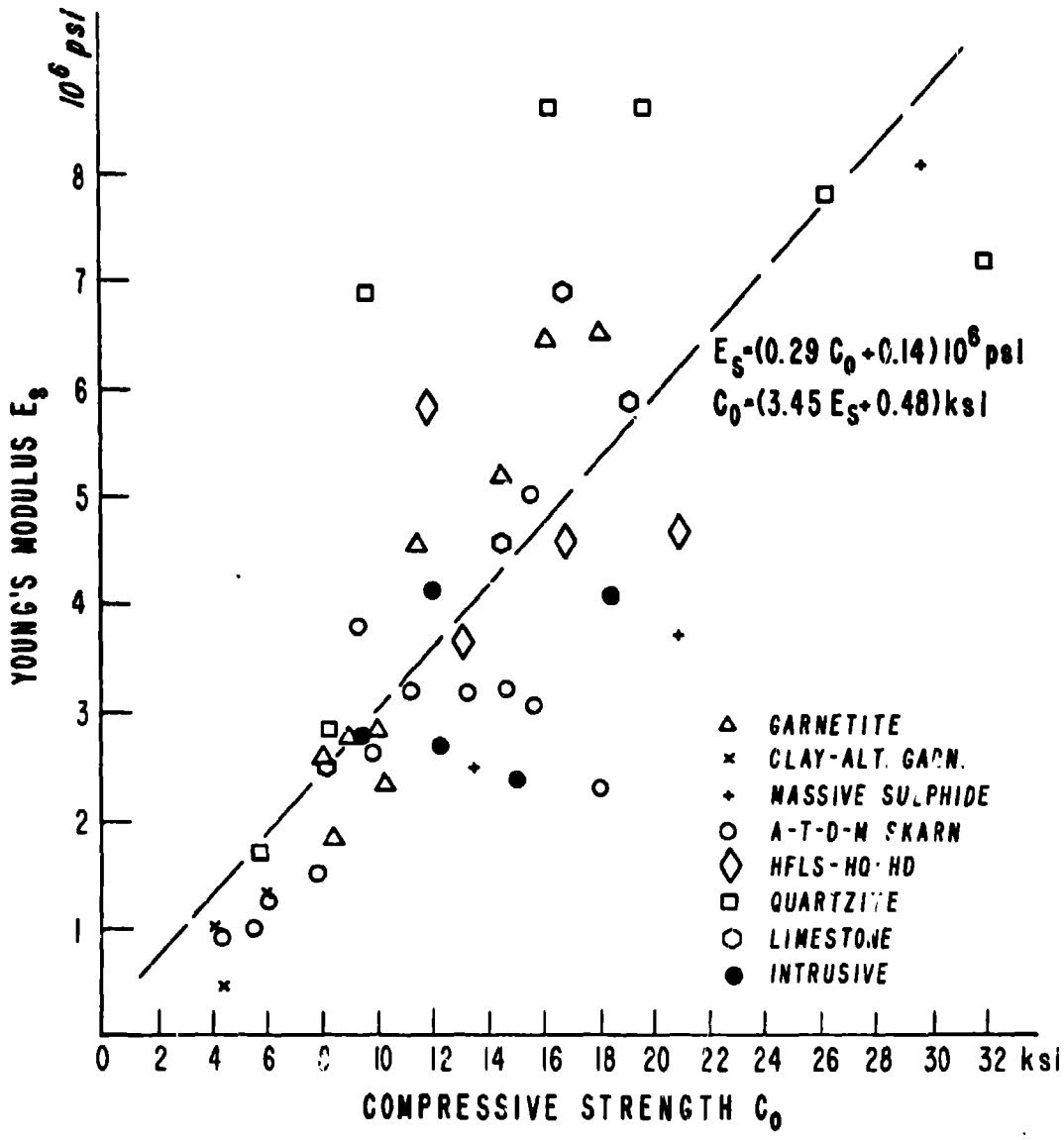

Laboratory Test Data.

Figure 18. - Young's modulus versus compressive strength in all rock types. Laboratory test data.

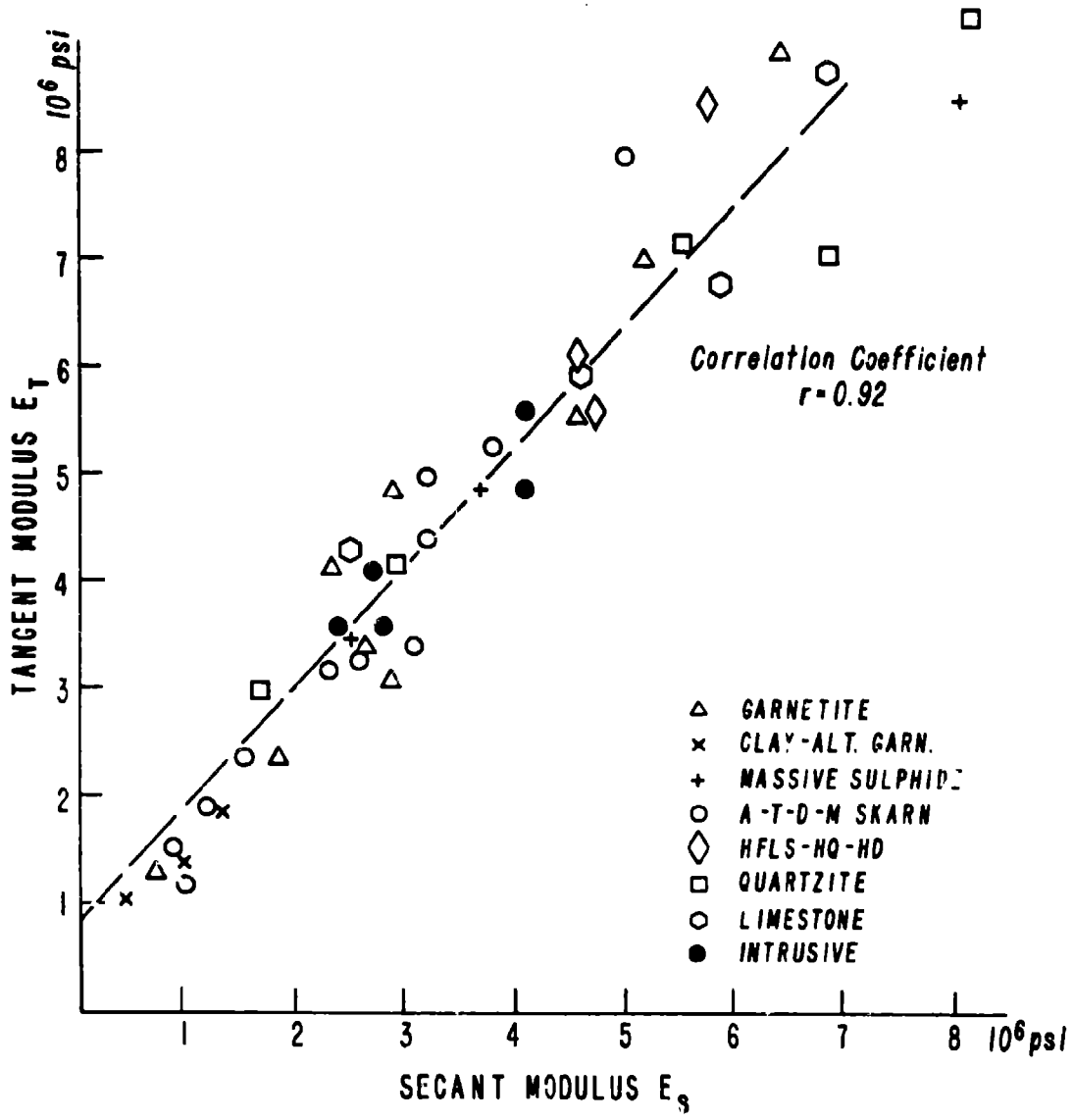

Correlation between Secant and Tangent Young's Moduli.

Figure 19. - Correlation between secant and tangent Young's moduli.

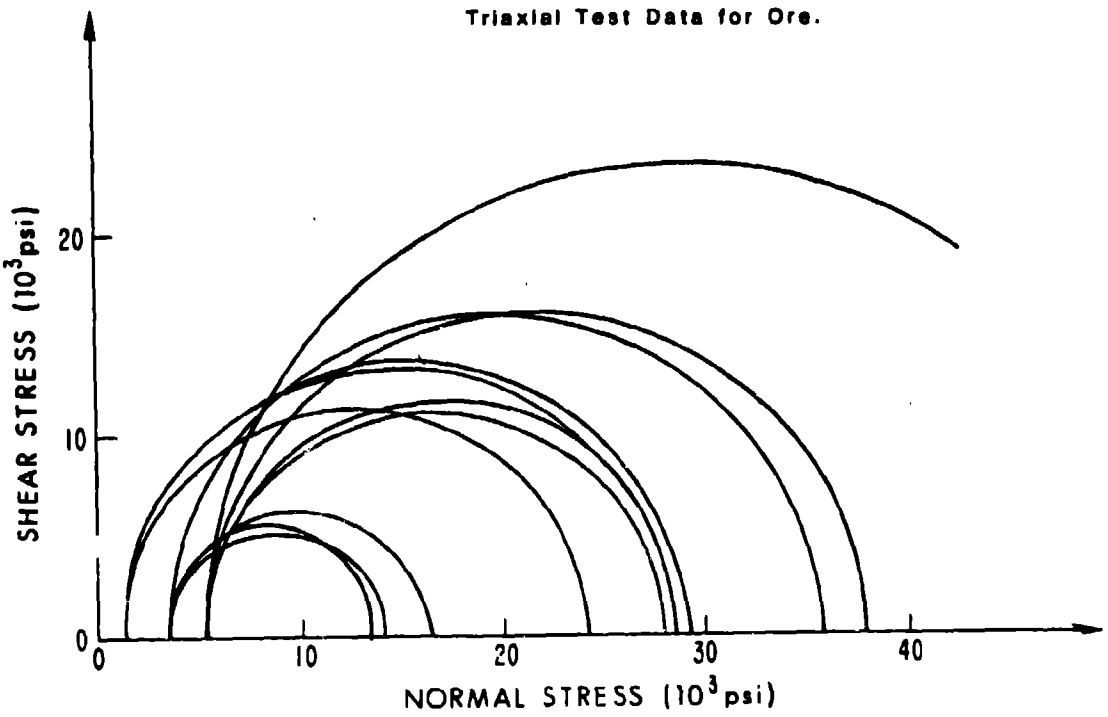

Figure 20. Triaxial test data for ore.

Triaxial Force-Displacement Curves for Ore at Three Confining Pressures.

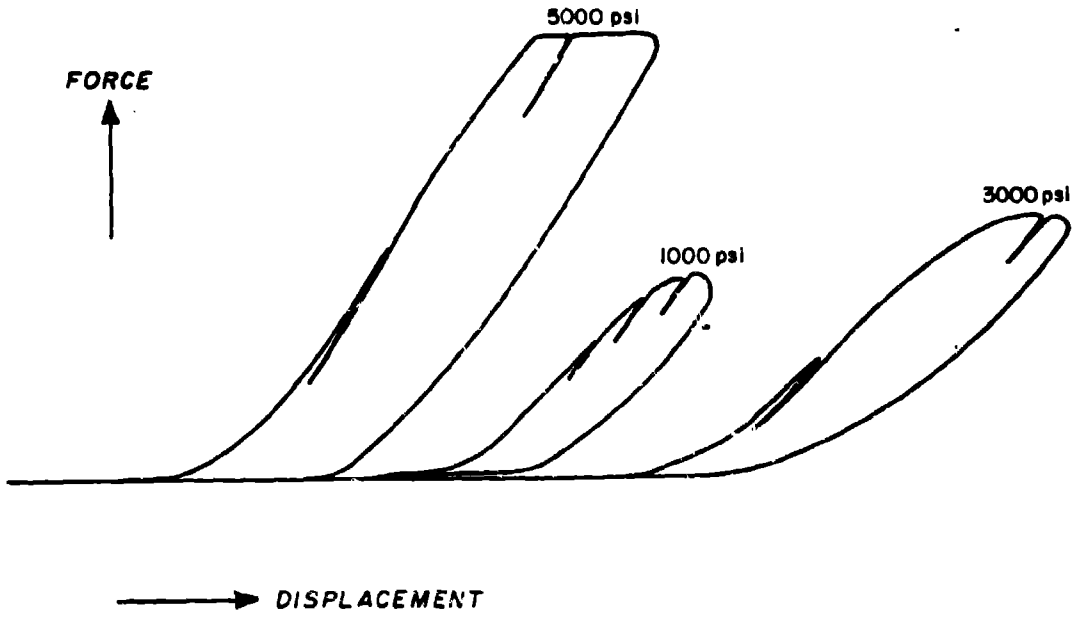

Figure 21. - Triaxial force-displacement curves for ore at three confining pressures.

Uniaxial Stress-Strain Curve for Large Core (6-in. diameter overcore).

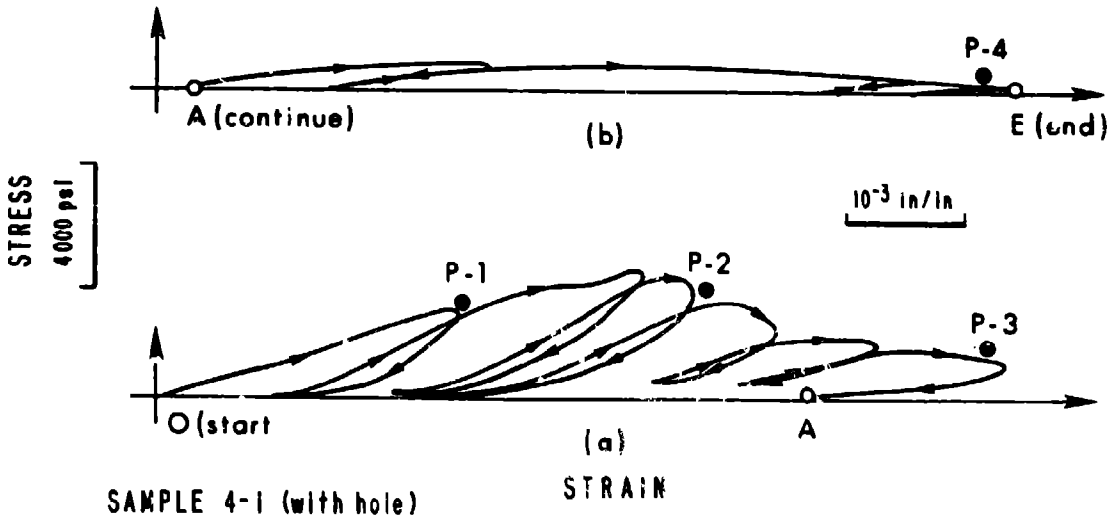

SAMPLE 4-1 (with hole)
D = 5.65 in.
L = 12.67 in
L/D = 2.25 in.

Figure 22. - Uniaxial stress-strain curve for large core (6-in. diameter overcore).

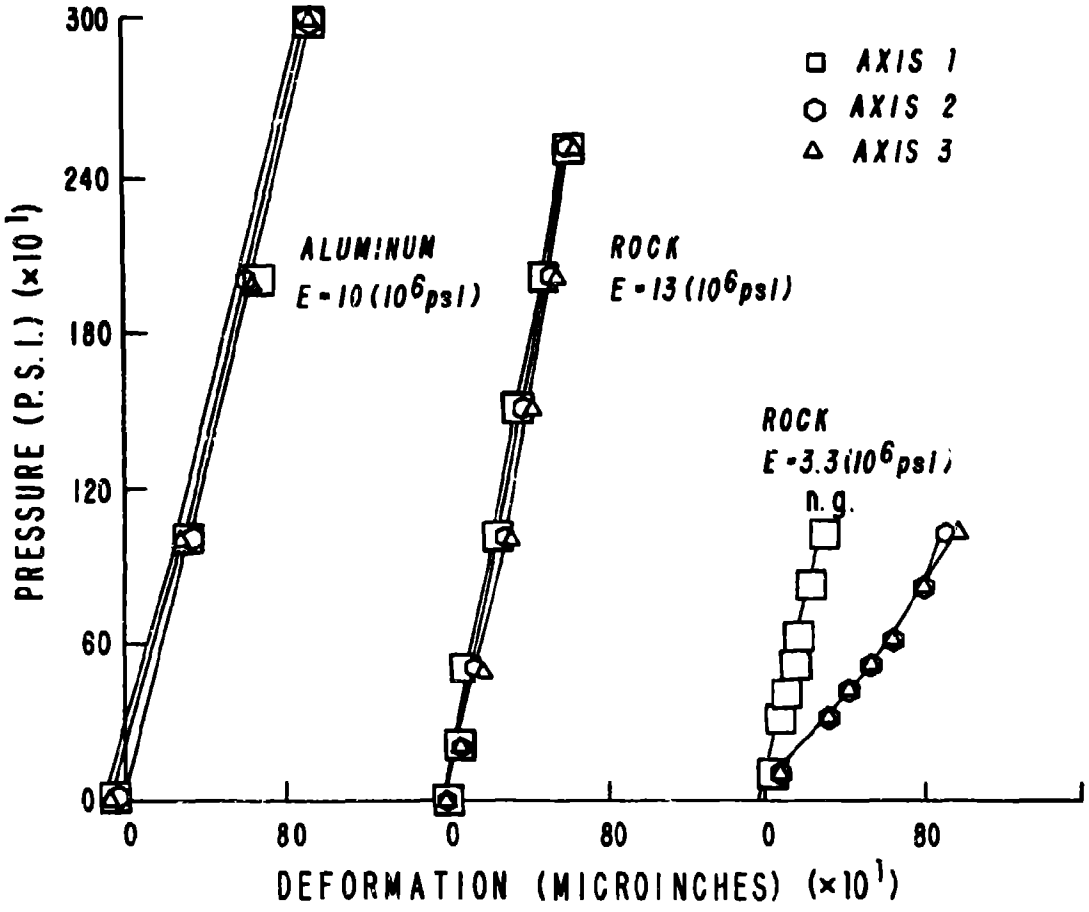

Biaxial Chamber Pressure-Displacement Curves for Aluminum and Rock Core.

Figure 23. - Biaxial chamber pressure-displacement curves for aluminum and rock core.

wall. Consequently, they displace less as the chamber applies pressure to the outer surface of the overcore. The biaxial tests results for Young's modulus are similar to those obtained in the large core uniaxial laboratory tests.

TABLE 9. - Large core strength and modulus

Sample	L/D	Co (psi)*	C (psi)	E (10^6 psi)
4	1.95	3,194	3,184	1.81
5	1.50	5,395	5,188	2.53
4-2	2.39	7,303	7,449	6.27
4-i	2.25	3,971	4,025	2.18
1-4	2.10	4,101	4,125	2.17
1-2	1.19	3,393	3,137	1.33
mean	$\bar{x}$ =	4,560	4,518	2.72
std. dev	s =	1,550	1,620	1.78
coeff. variation	$s/\bar{x}$ =	34%	36%	66%
number of tests	n =	6	6	6

E = Young's modulus
C = test result
C_o = uniaxial strength of L/D = 2
C_o = C (0.88 + 0.24 D/L)

*1 psi = 6.9 kPa

Summary

The in situ stress measurements indicate that the pre-mining stress state changes over distances of 100 m (300 ft) and that the stress state before mining the test stope was approximately hydrostatic. Post-stope measurements in the east and west ribs of the stope show a peak stress concentration not at the periphery of the stope but into the ribs past the projected overbreak zone over the solid.

Rock properties tests on the nine rock types in the vicinity of the test stope reflect the gradational metamorphism and geologic variability expected in orebodies of metamorphic origin. Correlation between Young's modulus and compressive strength is evident within rock types including heavily mineralized ore. Stress strain curves show reasonable linearity within a well-defined elastic range up to confining pressures of 34.5 MPa (5,000 psi), the maximum used in the confining pressure tests. Inelastic behavior is characterized by macroscopic flow with little strain hardening or softening. This is especially evident in the few large diameter 15 cm (6 in.) overcores tested. A linearly elastic perfectly plastic material model with pressure dependent yielding is thus justified.

COMPARISONS BETWEEN FINITE ELEMENT CALCULATIONS AND MINE MEASUREMENTS

Comparisons between theoretical calculations of the test stope response to mining and measurements made during actual mining of the test stope provide quantitative links between theory and practice. The establishment of rock mass properties is of particular importance to the process of establishing a reliable design procedure. Once established, design refinements and alternative layouts can be studied numerically at a very small fraction of the cost of full-scale mine trials. With the aid of the computer, the influence of stope widths, pillar widths, extraction sequences, post-fill properties and other design variables on stability can then be considered.

The rock mass properties of primary importance are: (i) the elastic moduli which play a predominant role in the deformation aspects of the test stope response, and (ii) the strength properties which are critical to stability. In this regard, a high correlation coefficient *and* a one-to-one relationship between calculated and actual extensometer readings within the elastic range establishes Young's moduli for the test stope rock types. Comparisons between calculated and observed overbreak zones aid in establishing strength values. The Utah-II and Utah-III finite element programs were used for these tasks and subsequent analyses.

Calculated Test Stope Response

Three two-dimensional finite element representations of the test stope were analyzed:

(i) a vertical section parallel to the strike, Section A,

(ii) a vertical section perpendicular to strike, Section B, and

(iii) a plan view (horizontal section) at stope mid-height, Section C.

Figure 24 shows the test stope geometry in plan and section. Section A allows study of the development crosscuts, the east and west ribs, the overcut back, and most importantly, the effect of stope and pillar widths. Section B allows study of the foot and hanging walls, the overcut back and undercut brow, the blasting sequence, and progressive enlargement of the test stope. The plan view, Section C, is complementary to the two vertical sections. The mining sequence is also seen in this section. Sections A and B thus allow for rather direct comparisons between actual and calculated extensometer readings, while sections B and C show the extent of the footwall overbreak zones.

The sequence of test stope analyses is thus:

(i) establish the rock mass Young's modulus E for ore using Section A displacements and then reduce the laboratory Young's modulus for all other rock types in the same ratio of rock mass E to laboratory E as for ore,

Test Stope Geometry and Finite Element Mesh Dimensions.

(a) Section A, Parallel to Strike.

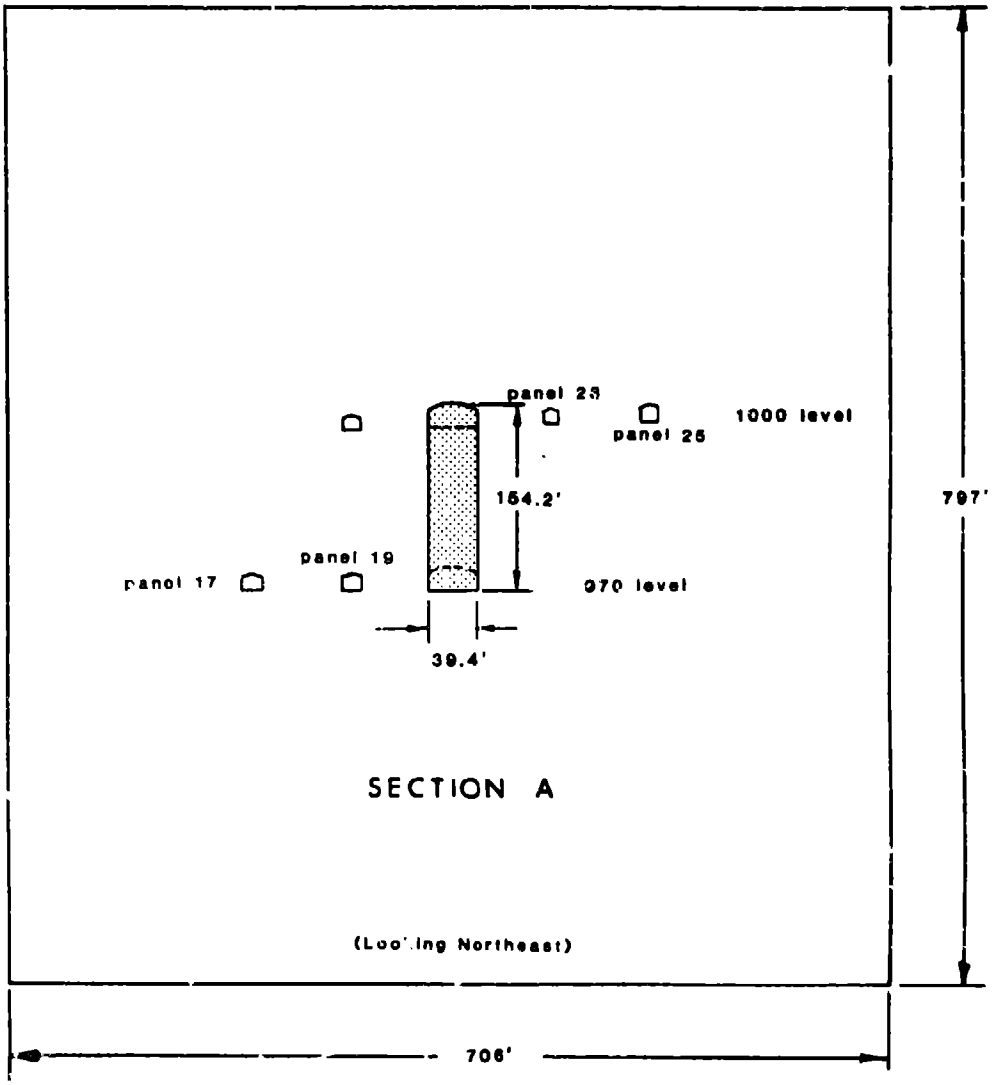

Figure 24. - Test stope geometry and finite element mesh dimensions.
(a) Section A, parallel to strike.

(b) Section B, Perpendicular to Strike.

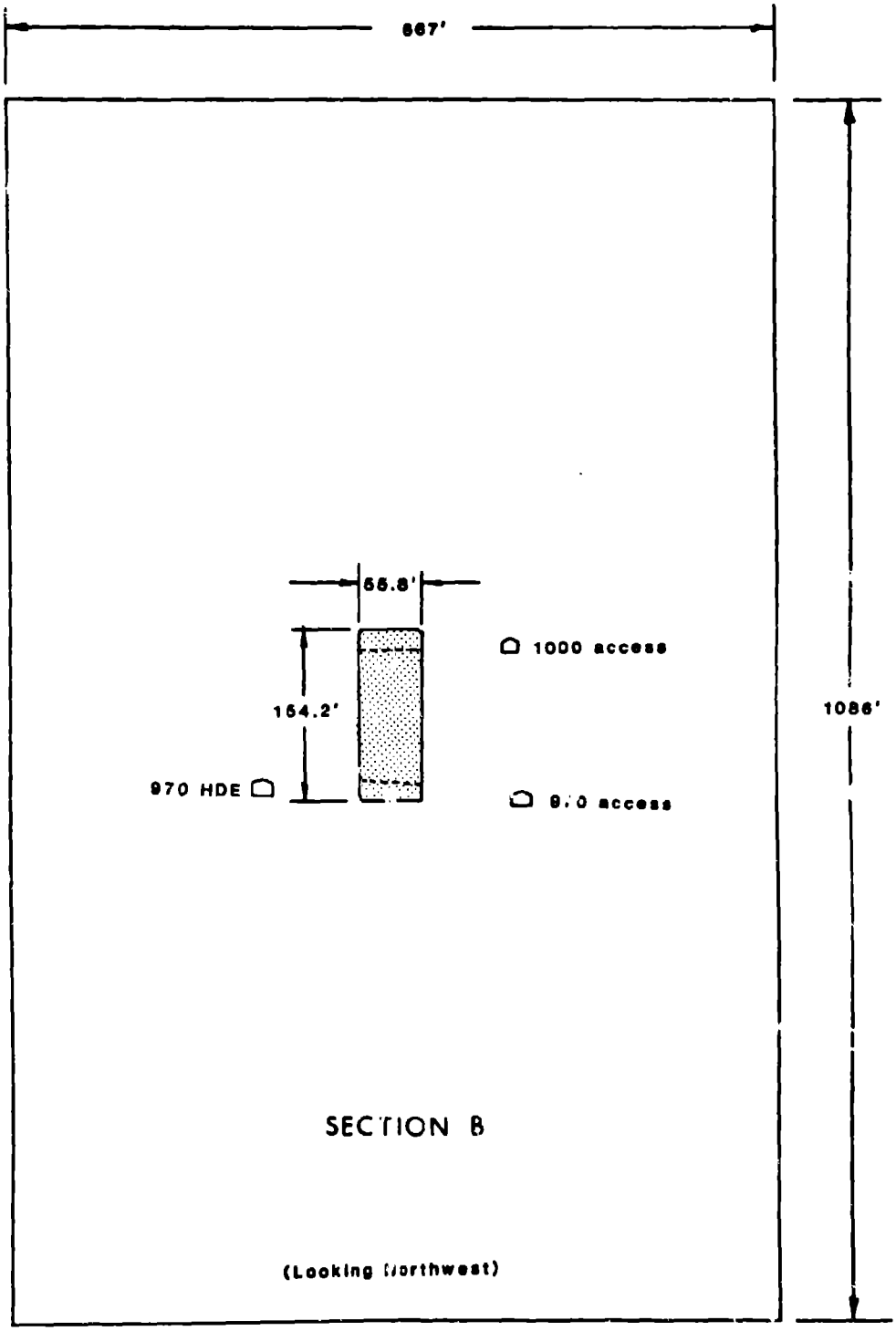

Figure 24. - Test stope geometry and finite element mesh dimensions. (b) Section B, perpendicular to strike.

(c) Section C, Plan View.

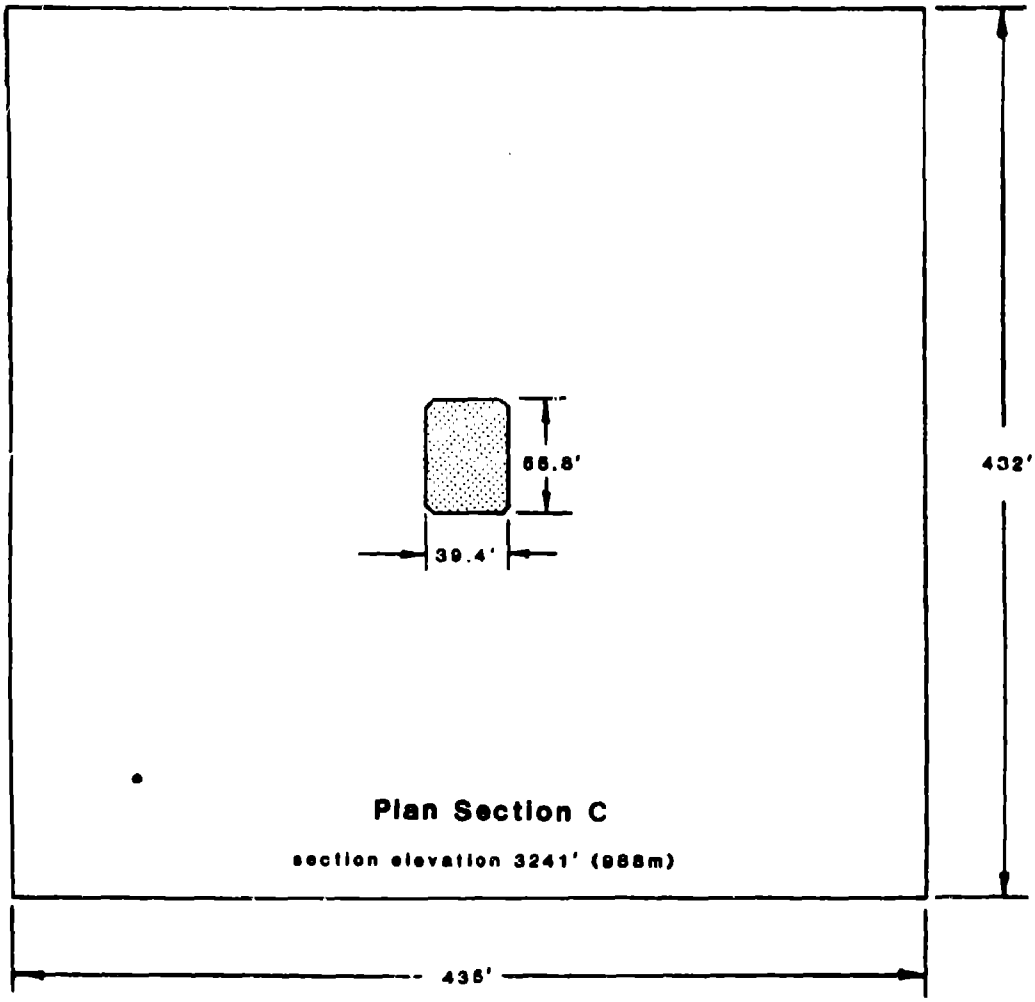

Figure 24. - Test stope geometry and finite element mesh dimensions (c) Section C, plan view.

(ii) verify with Section B instrumentation data the rock mass moduli established oreviously and proceed to the establishment of rock mass strengths through overbreak considerations,

(iii) verify the rock mass reduction factor for strengths found previously by comparing Section C overbreak zone extent with that obtained previously in section B.

Finite Element Preliminaries

Features of importance to the analysis include the finite element geometry, geology, rock properties, mesh refinement, in situ stress states and material law used.

Figure 24 also shows the dimensions of the Section A, B and C finite element meshes. Mesh dimensions are determined by the requirement that the outer boundaries should have a negligible influence on results. Moving the outer boundaries farther from the test stope should not change the results significantly. This is a matter of judgment initially but can always be checked later by examining the stress state near the outer boundaries before and after a computer run. Mesh dimensions approximately five times the greatest stope dimension are usually sufficient to insure that outer boundary stresses are within 10 percent of their starting values.

The test stope geology incorporated into the finite element analyses is shown in Figure 5 in section and plan. The numbers in Figure 5 correspond to the rock types and properties listed in Table 7.

Subdivision of the test stope region into finite element meshes is shown in Figures 25a, 26a, and 27a (which correspond to Figures 24a, b, and c, respectively). Mesh refinement in the immediate vicinity of the test stope is shown in Figures 25b, 26b, and 27b. Mesh refinement is important for two reasons: (i) quality of results and (ii) economy. A relatively high degree of refinement is desirable and indeed necessary for reliable results, but the cost of analysis also increases with the number of elements and nodes used. A satisfactory compromise is to use 10 or so approximately square (constant strain) elements along the least dimension of the stope seen in the considered mesh. Meshes used in the present study satisfy this criterion. Much larger elements in the periphery of an opening are unsatisfactory because of their high average confining pressure that masks potential yielding and its possible propagation.

The in situ state of stress used to calculate the test stope response involved extrapolating the measured state of stress from the 1300 Level at a depth of 1042 m (3420 ft) to the test stope region between the 970 and 1000 Levels at an average depth of 1280 m (4200 ft). The extrapolation was accomplished by equating the vertical normal stress to the product of unit weight of rock times depth, approximately 25 kPa per meter of depth (1.1 psi per ft). The remaining five components of stress were first computed as fractions of the vertical stress on the 1300 Level; these fractions were then used at all other depths.

Section A Finite Element Mesh.

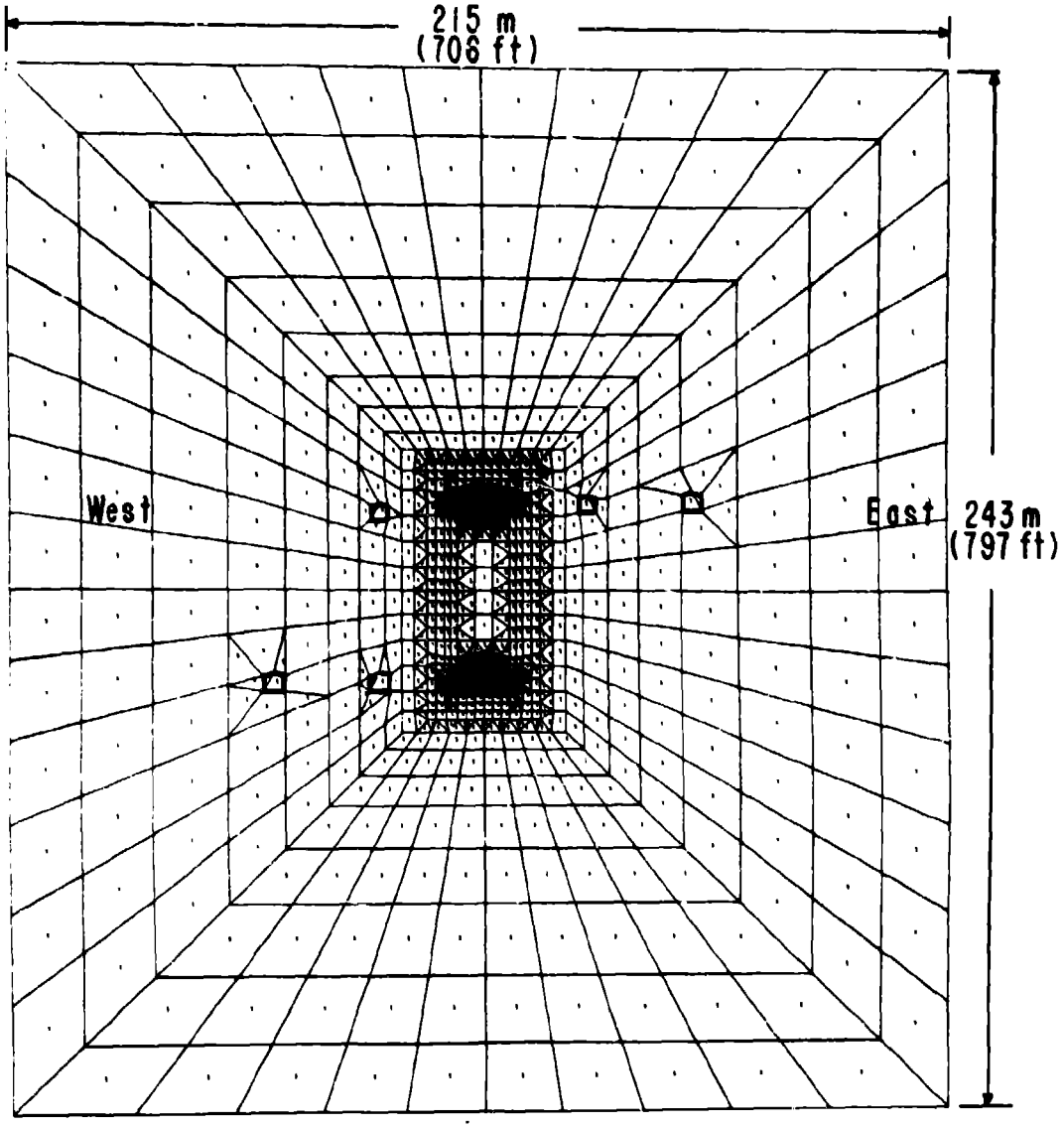

Figure 25. - (a) Section A finite element mesh.

Section A Mesh Refinement Near the Test Stope.

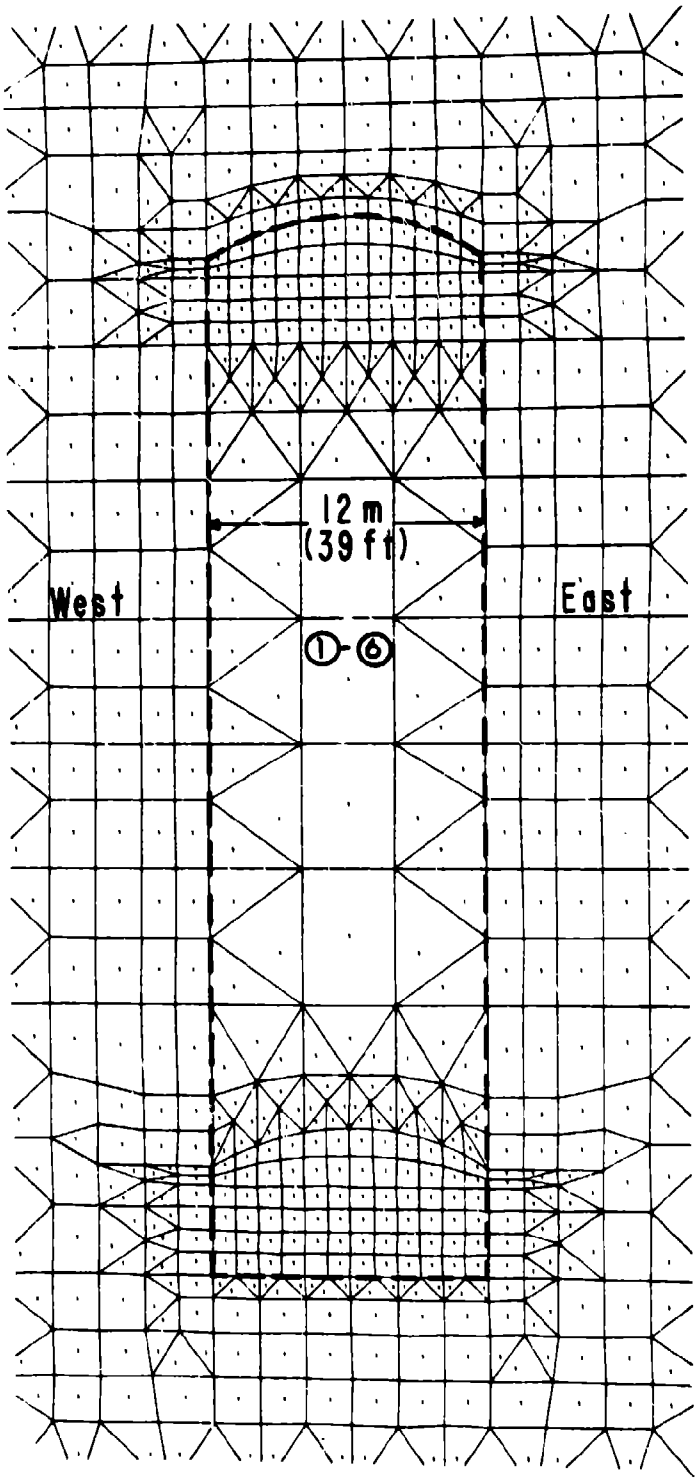

Figure 25. - (b) Mesh refinement near the test stope.

Section B Finite Element Mesh.

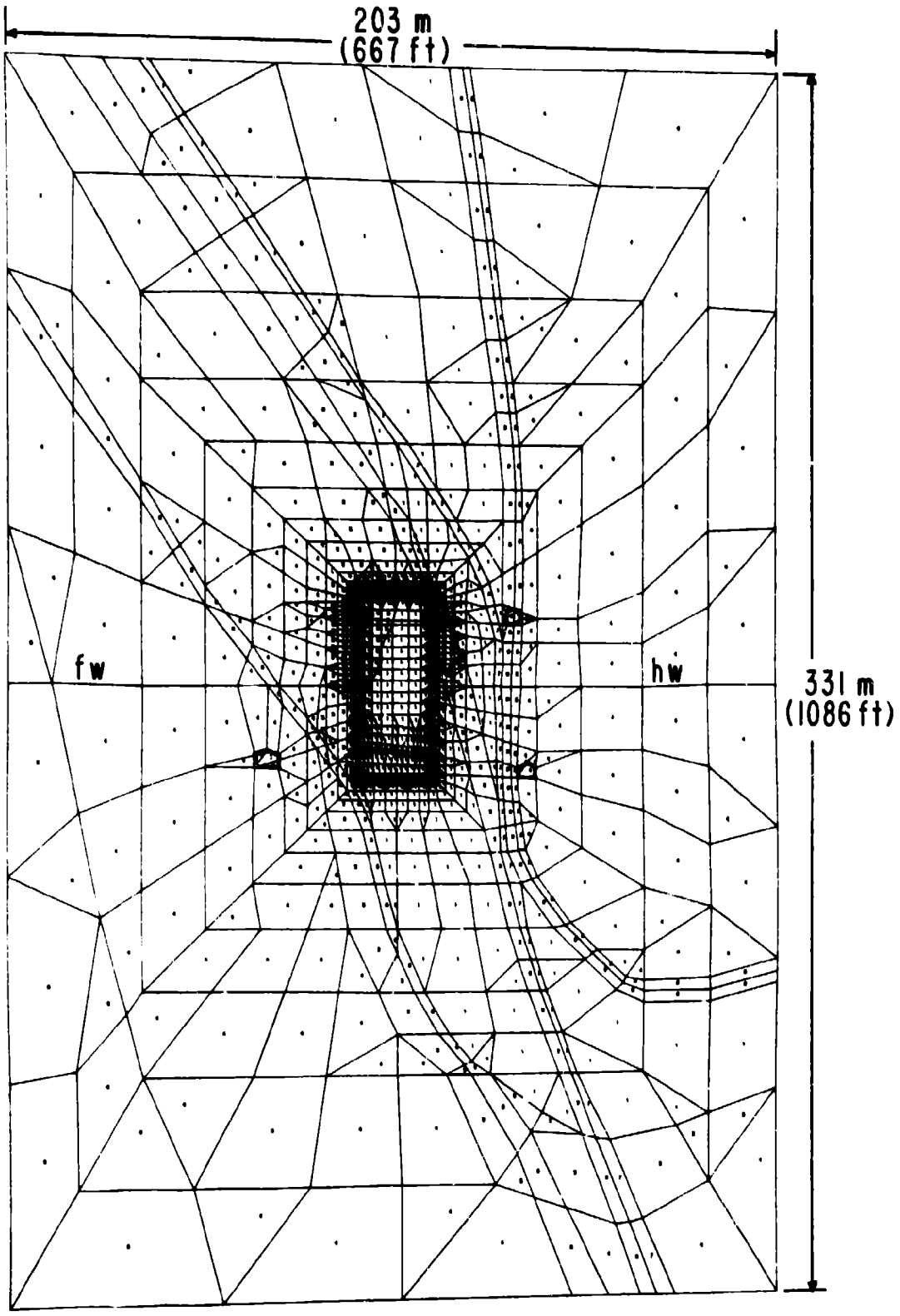

Figure 26. - (a) Section B finite element mesh.

Section B Mesh Refinement Near the Test Stope.

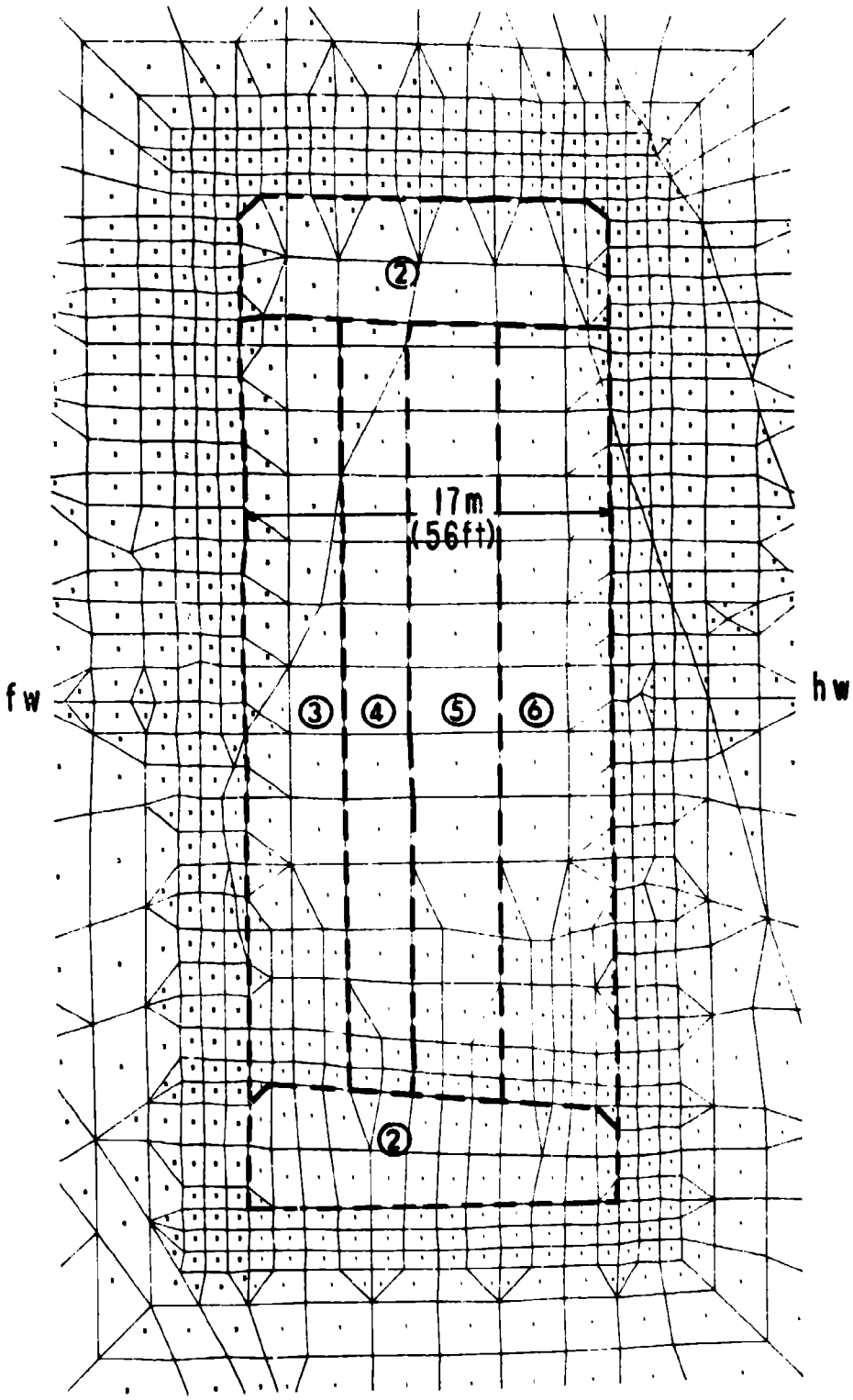

Figure 26. - (b) Mesh refinement near the test stope.

Section C Finite Element Mesh.

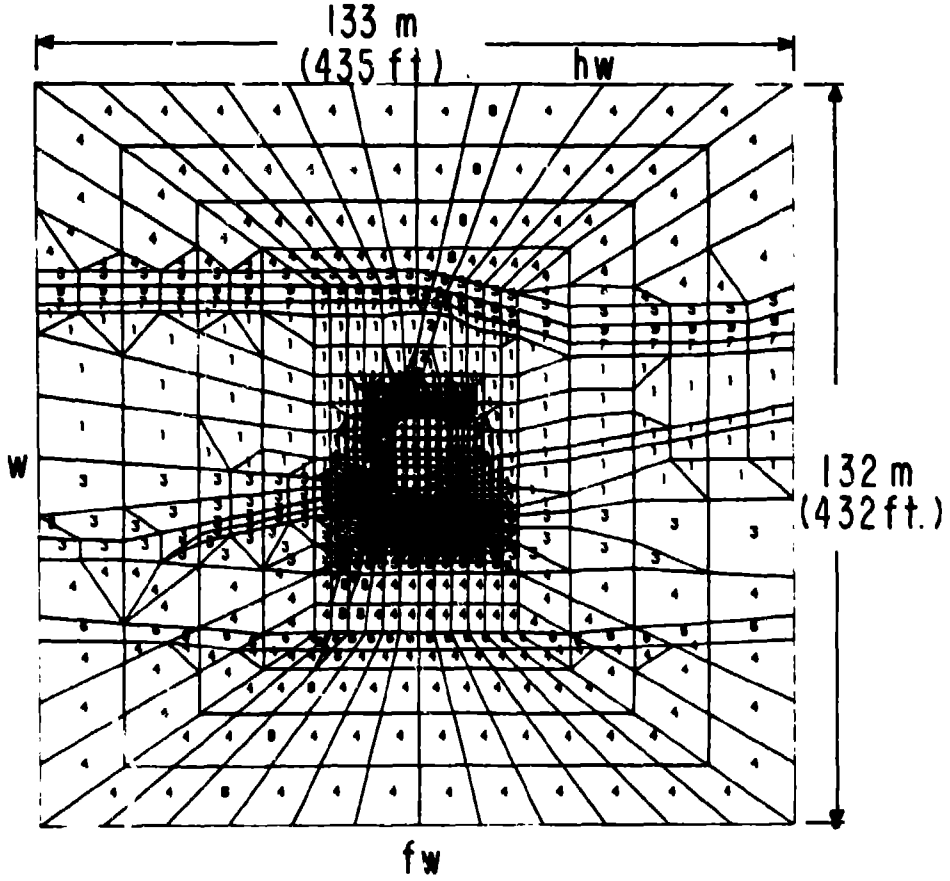

Figure 27. - (a) Section C finite element mesh.

Section C Mesh Refinement Near the Test Stope.

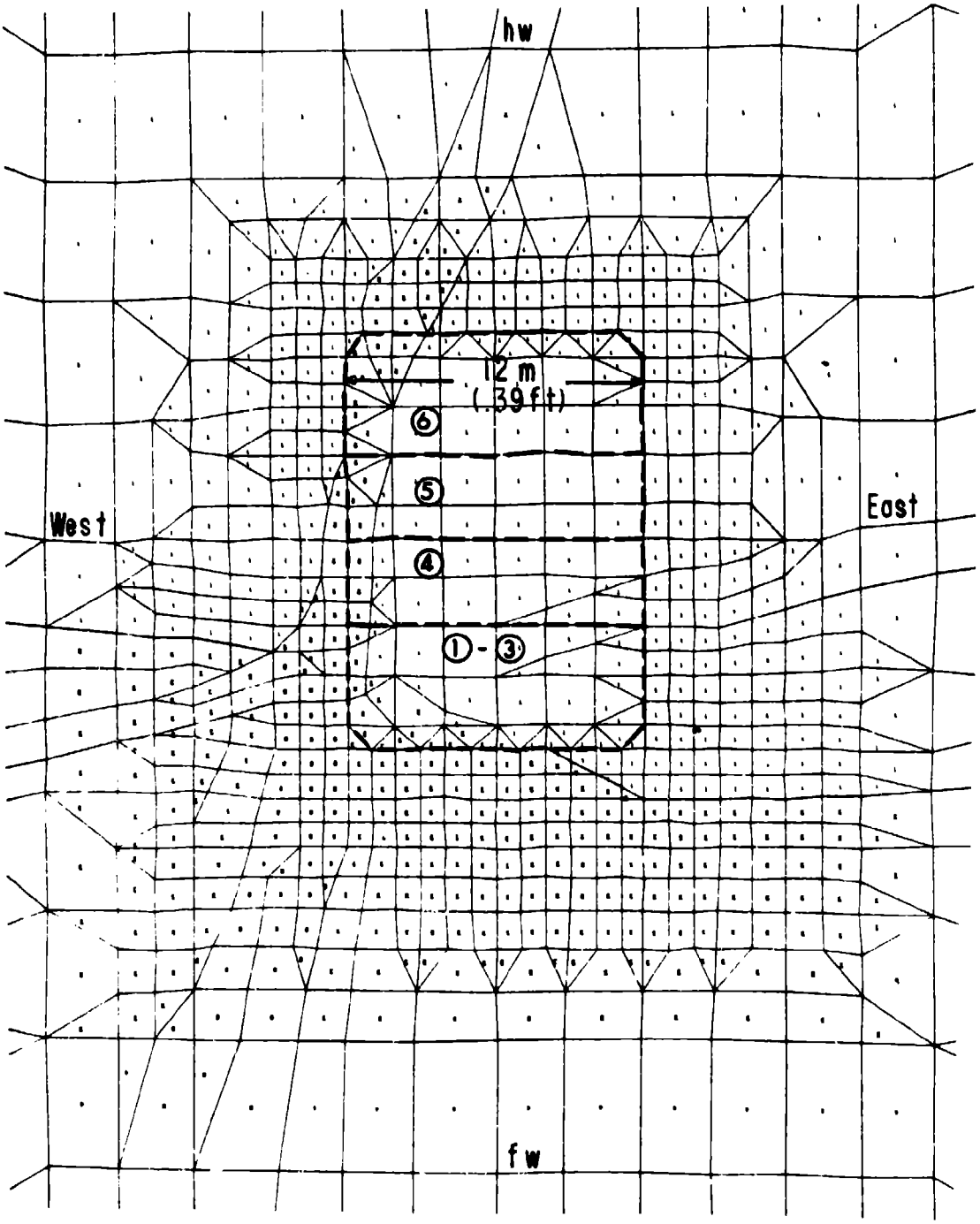

Figure 27. - (b) Mesh refinement near the test stope.

After extrapolating to depth, the premining stress state was referred to a vein system of coordinates oriented parallel and perpendicular to the strike of the ore zone at the test stope. These directions coincide with mesh Sections A, B, and C. The resulting stresses served as the initial stresses for the subsequent test stope analyses.

The shear stresses are small, an order of magnitude less than the normal stresses, so that the latter dominate the test stope response. The ratios of premining horizontal to vertical normal stresses are:

(i) East-West to Vertical - 0.84
(ii) North-South to Vertical - 0.54

The first ratio is the "Ko" value appropriate to mesh Section A in which the stope width is seen. The second value is the "Ko" seen in Section B in which the foot and hanging walls are seen. In this regard, the stope width section sees an almost hydrostatic ("Ko" = 1.) in situ stress state, a state that was confirmed by subsequent measurements.

An elastic perfectly plastic material model based on associated flow rules and a nonlinear, pressure dependent Drucker-Prager type of yield criterion was used in calculating the test stope response. The material thus deforms elastically up to yield point and then flows without increase or loss of strength. The Utah-II program accepts unconfined strengths as basic input and then calculates derived strength parameters necessary to fit the nonlinear (parabolic) form of the yield condition to the experimentally determined rock properties input. All rock types are considered isotropic; there is no evidence that suggests anisotropy is of great importance at the Carr Fork Mine.

The mining sequence implemented on the computer parallels the major stages of extraction underground and consists of:

(1) development drifts and crosscuts,
(2) overcut and undercut slash,
(3-6) production blasting.

The circled numbers in Figures 26b and 27b correspond to these stages. At the completion of each stage of computer mining, the stress field is updated by adding the stress changes to the stresses that were initially present at the beginning of the stage. Each stage is done incrementally in order to allow for inelastic behavior should such occur.

Calculated versus Measured Displacements

Extensometer readings approximate the relative displacement that occurs between anchor and collar from installation time to the present. Corresponding displacements are, in principal, obtained from the finite element output by first subtracting the displacement that occurs during the development stage computer run from the displacement that has occurred after the run that completes mining of the test stope. These differences are the displacements associated with mining the test stope only. Calculated extensometer readings are then computed from these

differences by subtracting the displacement at the finite element mesh point corresponding to the anchor location from the mesh point displacement corresponding to the collar position. (The extensometer hole and assemblage have negligible influences on the test stope response and are not explicitly represented in the finite element mesh.) In fact, the Utah-II program displacements are those caused by the current excavation stage, so that the relative displacement between anchor and collar can be calculated directly from the output displacement components.

Figure 28 shows the correlation between calculated and measured displacements as seen in Section A after the last blast when the test stope is fully mined. The correlation coefficient r is 0.882. Thus, 78 percent of the observed variance is explained by the assumed material model in the finite element analysis. This is an excellent result in view of the many potential complications present in field studies at underground hardrock vein mines. Moreover, since the correlation coefficient is independent of the scales used in the plot of the regression line, a change in Young's modulus has no effect on r.

However, the *slope* of the regression line in Figure 28 does depend on Young's modulus because the calculated displacements depend linearly on the reciprocal of Young's modulus. Figure 29 contains plots of displacements at the back, bottom, and rib centers in Section A as a function of (1/E) and shows that this is indeed the case. (The intercept also depends on Young's modulus.) This feature of the analysis allows one to estimate the value of Young's modulus for the rock mass.

The best rock mass value of Young's modulus results in a regression line slope of 1.0. An increase in E in Figure 28 reduces the slope. Hence, a rock mass Young's modulus for heavily mineralized ore somewhat greater than 20.7 GPa (3.0 million psi) is indicated.

A regression of calculated on measured displacements seen by Section B instrumentation is shown in Figure 30a. The coefficient of linear correlation is 0.886; the correlation is nearly the same as obtained for Section A. The finite element material model is again seen to capture the major features of the test stope response. The rock mass modulus determined by the requirement for a slope of 1.0 is different. In this case, the modulus is 31 GPa (4.6 million psi). However, the difference is within the coefficient of variation of laboratory test data.

A composite regression analysis using all extensometer data is shown in Figure 30b. The result is the same.

Calculated versus Observed Overbreak Zones

Overbreak refers to the difference between the stope dimensions as blasted and the expected or design dimensions. The extent of overbreak is observed after the stope is mucked but before filling begins. The footwall overbreak zone that developed during mining of the test stope is seen in Sections B and C. With sufficient reduction of laboratory strengths, yielding is sure to be induced in the finite element

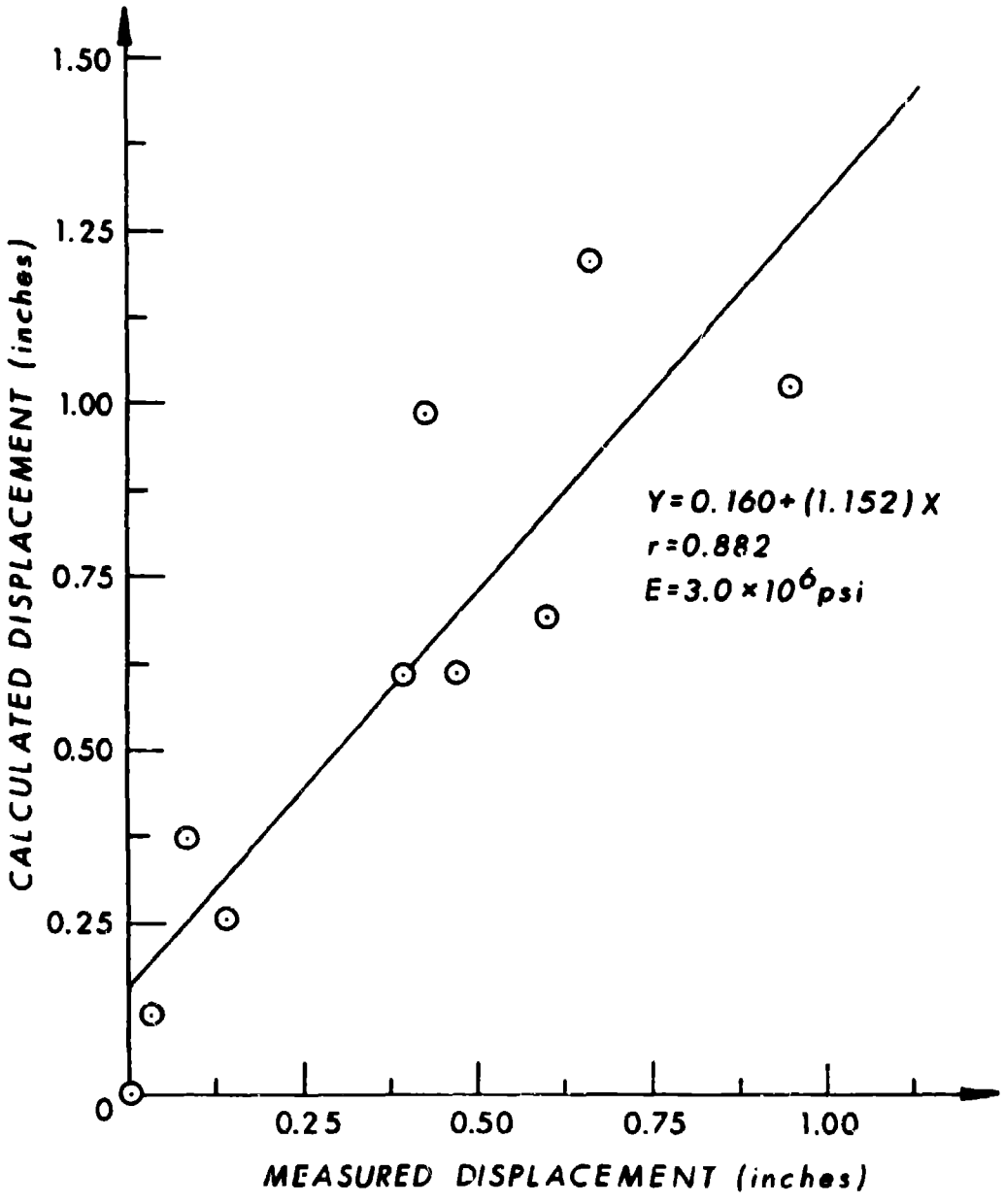

Calculated versus Measured Displacements in Section A.

Figure 28. - Calculated versus measured displacements in section A.

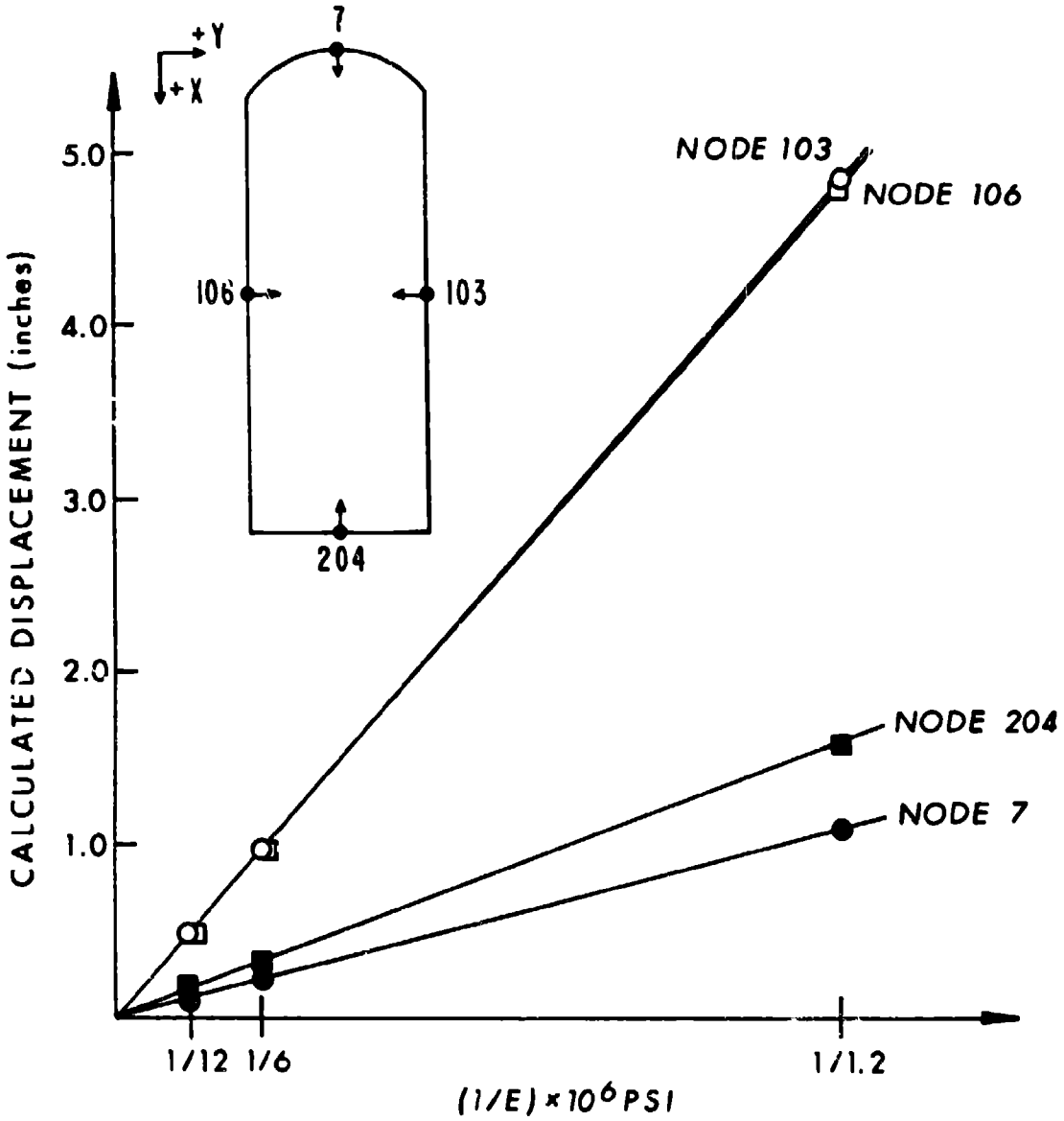

Linearity of Calculated Displacements

in the Reciprocal of Young's Modulus.

Figure 29. - Linearity of calculated displacements in the reciprocal of Young's modulus.

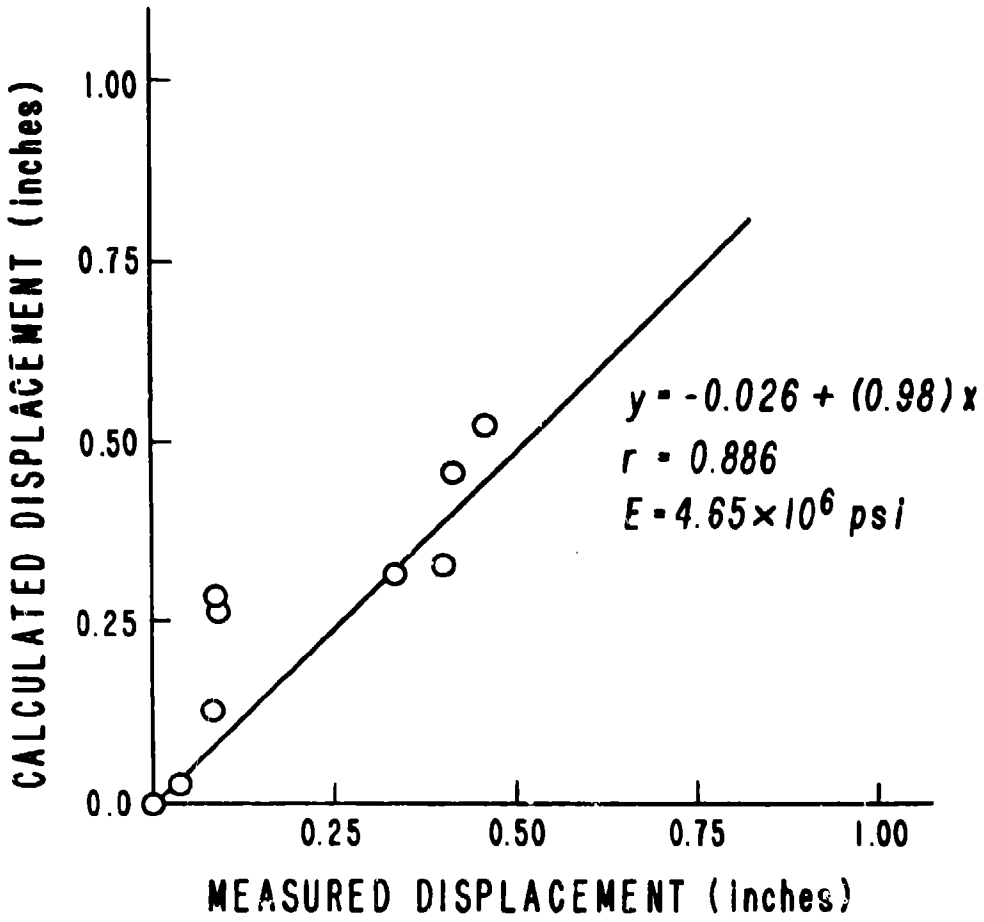

Calculated versus Measured Displacements in Section B.

Figure 30. - (a) Calculated versus measured displacements in section B.

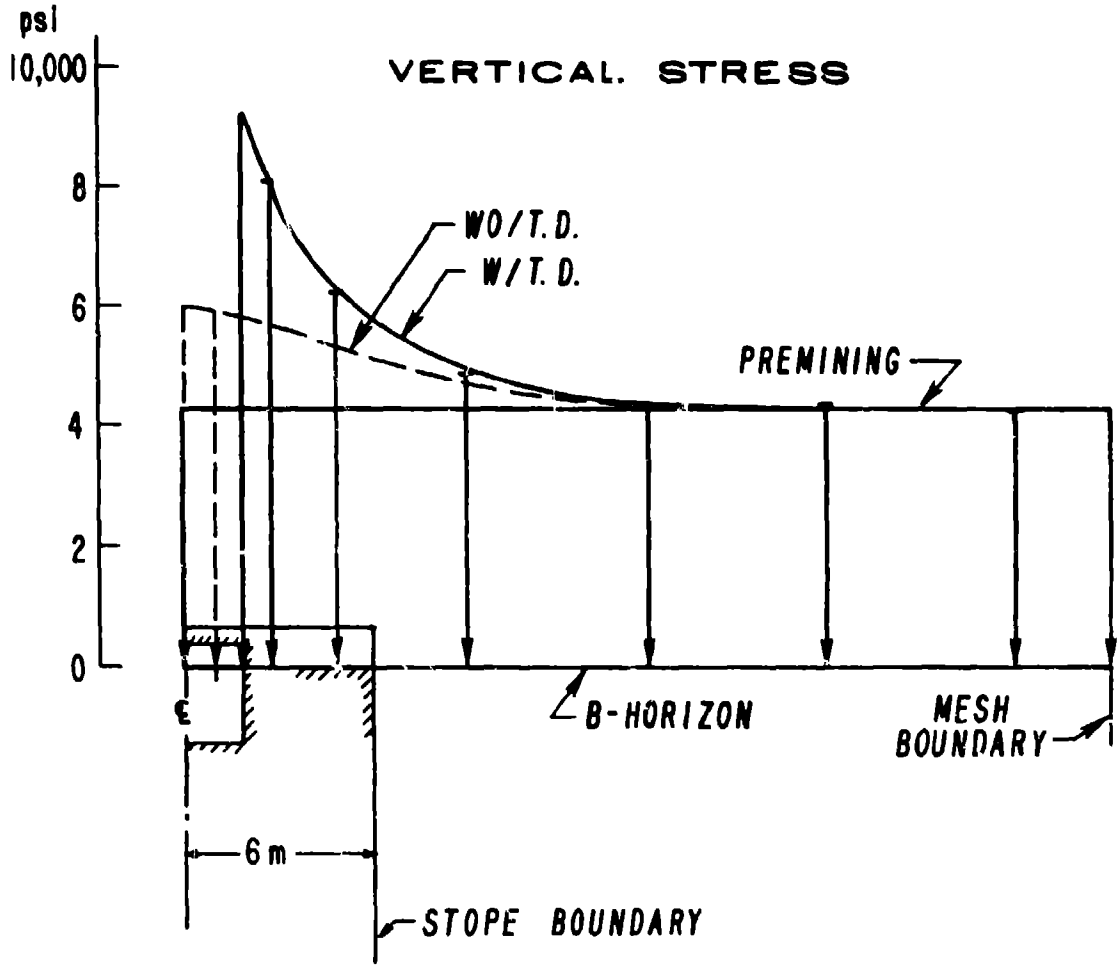

Vertical Stress in the Footwall with and without the Topdrift Extension into the Foctwall. 3D FEM Calculation.

Figure 33. - Vertical stress in the footwall with and without the top-drift extension into the footwall, 3D FEM calculation.

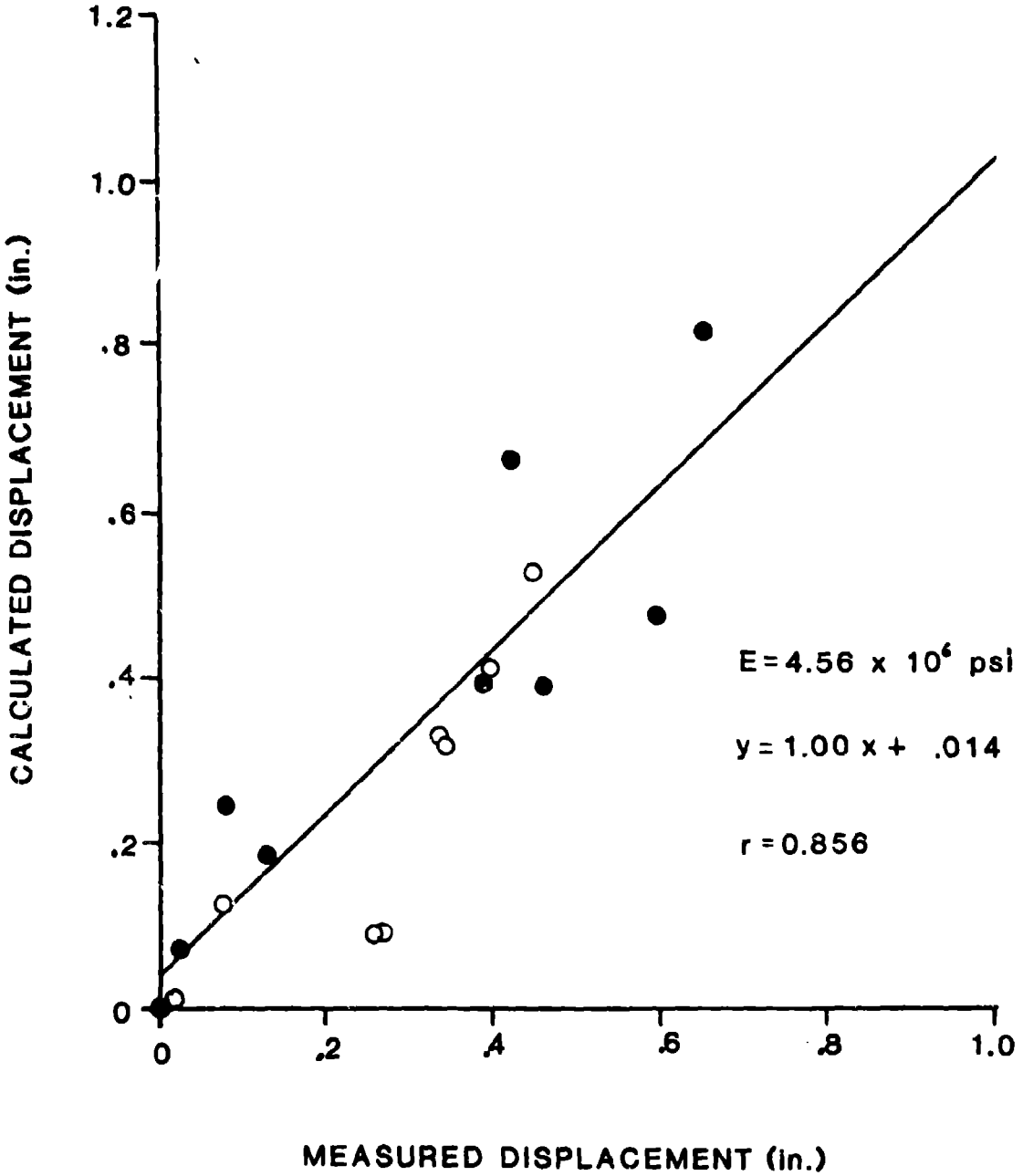

Figure 30. - (b) Calculated versus measured displacements--combined sections A and B.

representation of the test stope. The question that arises is whether the size and location of the resulting yield zones resemble in any way that observed in the footwall of the test stope. There is an infinite variety of strength values that could be assigned to the nine separate rock types in Sections B and C. The probability of matching calculated and observed overbreak zones in an arbitrary way, that is, at random, thus seems quite small, so small that the "fishing" approach of making a large number of runs is impractical. A simple rule that overcomes this difficulty and that has proved useful in the past is to reduce all strengths by the same fraction. This is the same rule applied to Young's modulus, although the same fraction need not be used.

Figure 31 shows the extent of the footwall overbreak zone in Section B achieved at rock mass strengths 75 percent of laboratory values. No yielding occurs in the finite element analysis at full strength, while a very large footwall overbreak occurs at half strength. At 75 percent, the rock mass strengths are within the variability of the laboratory data.

Figure 32 shows the extent of the footwall overbreak zone seen in plan view, Section C, with the previously obtained rock mass Young's moduli and strengths. The extent into the footwall is close to that obtained in Section B and confirms the previous result.

There is a complication in estimating the overbreak zone extent that involves the extension of the topdrift into the footwall. The topdrift extension causes an additional stress concentration in the footwall beyond that of the test stope itself. Unfortunately, the geometry is not amenable to a two-dimensional view. Utah-III was therefore used for a preliminary assessment of the effect of the topdrift extension on footwall stability.

Figure 33 compares the vertical stress at the footwall with and without the topdrift extension. There is clearly a significant increase in stress in the footwall as a result of the topdrift extension. The inference is that overbreak in the footwall would be reduced considerably in the absence of the topdrift extension, that is, in production stopes. This is an important practical point.

Discussion

It seems unlikely that the agreement between theory and experiment obtained in the complex geotechnical environment of the Carr Fork Mine test stope project is fortuitous. The fact that the test stope was successful and stability prevailed no doubt simplified the analysis by virtue of predominantly elastic behavior. Screening of data was still necessary. The procedure was to assume initially that all instrument readings were valid regardless of appearances and expectations. Data were subsequently ignored only for cause such as damage to an extensometer head by scoop tram travel or loss of an anchor to blasting. The high correlations (0.88-0.89) between calculated and measured displacements and the qualitativ agreement in footwall overbreak zone extent obtained in independent views of the test stope therefore support the

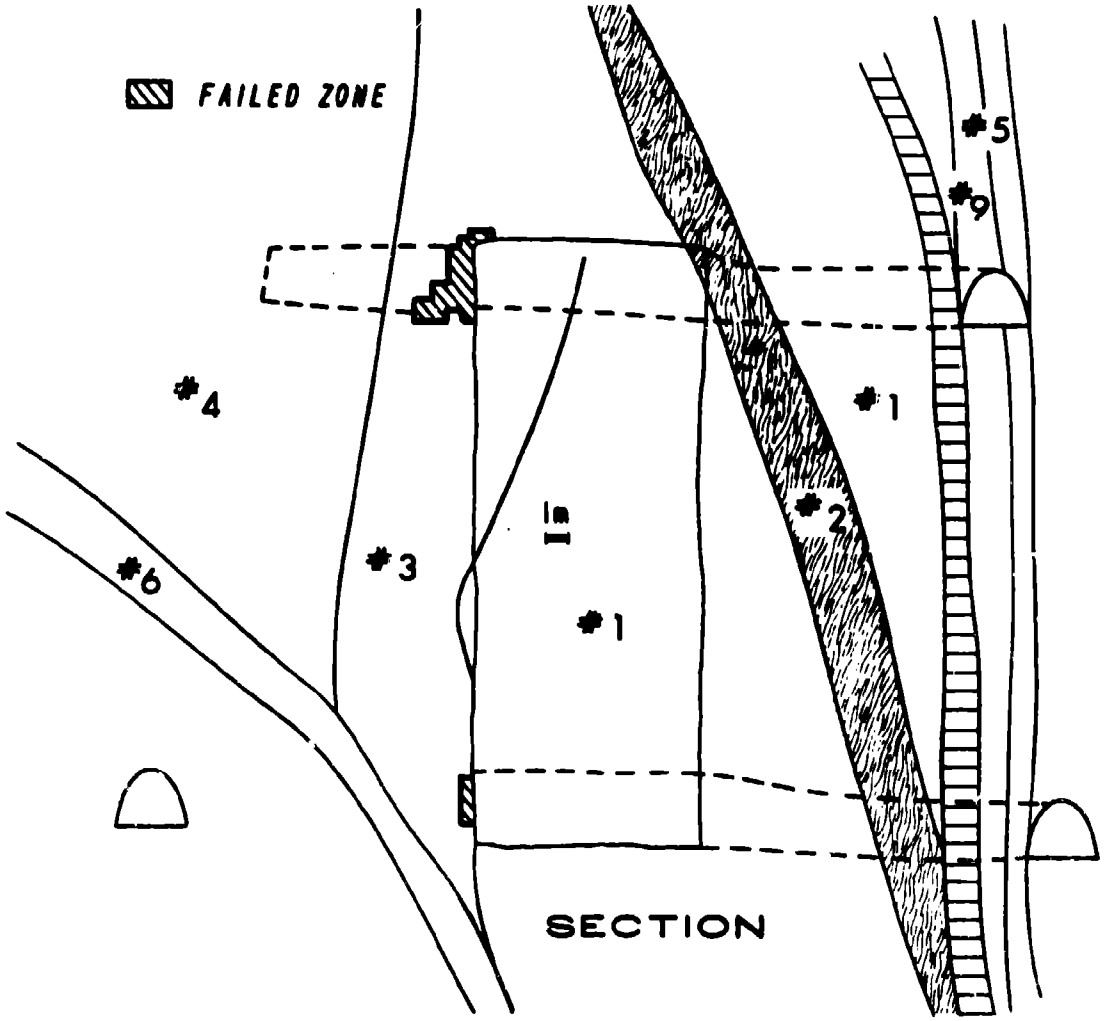

Calculated Footwall Overbreak Zone in Section B.

Figure 31. - Calculated footwall overbreak zone in section B.

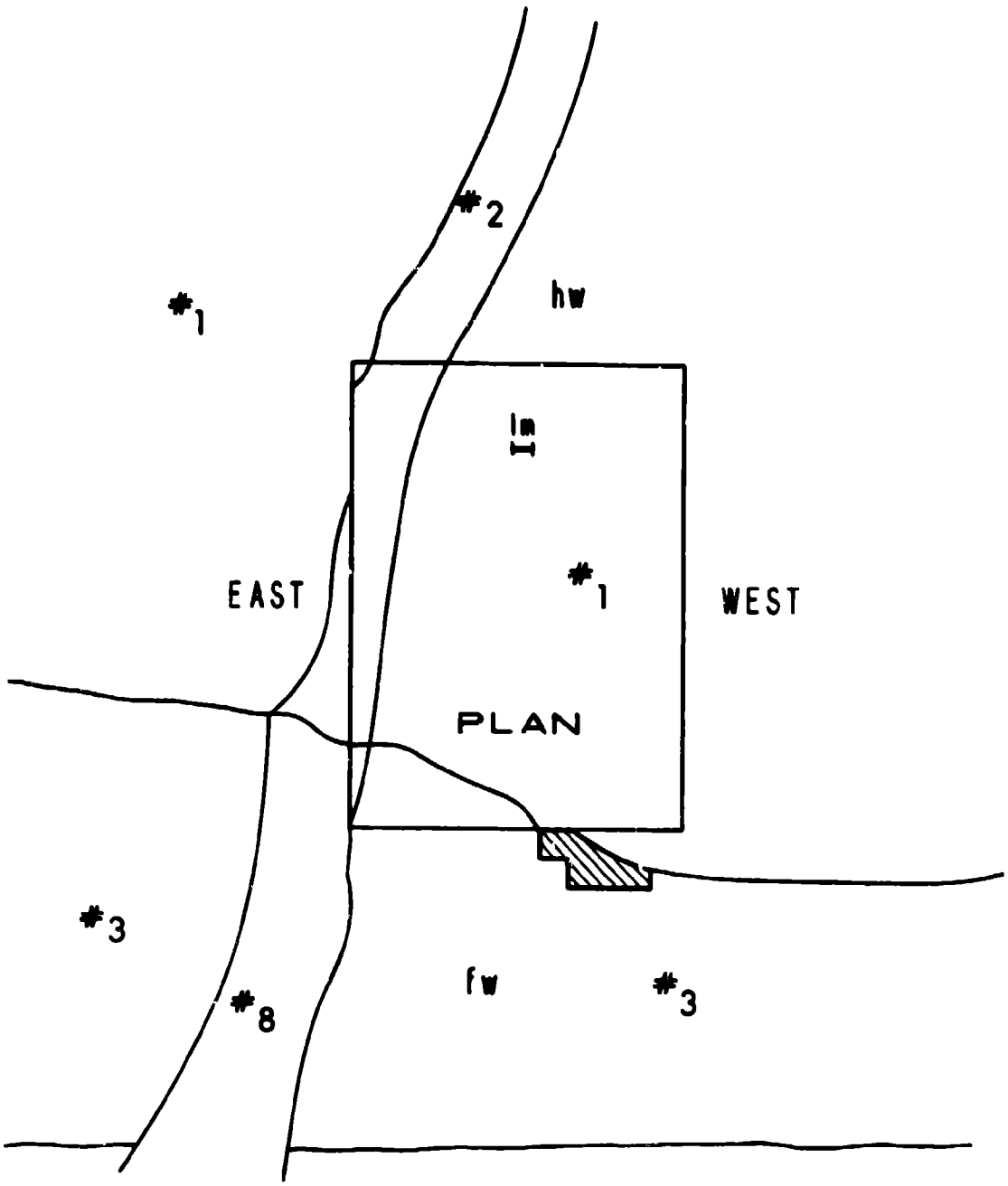

Calculated Footwall Overbreak Zone in Section C.

Figure 32. - Calculated footwall overbreak zone in section C.

conclusion that the finite element representation of the test stope (including geometry, geology, material behavior, rock properties, and in situ stress state) is valid.

In this regard, numerical values of Young's modulus assigned to the various rock types present is of less importance than the fact that linear, isotropic elasticity proved to be a reasonable approximation to the test stope response under initial development and load. However, the elastic range is limited as the subsequent evolution of the footwall overbreak zone shows. Some overbreak was expected, of course.

Inelastic rock mass behavior is less easily quantified than a purely elastic response and yet is of considerably greater importance in most mining applications than the estimation of displacement which is controlled primarily by Young's modulus. The association of rock falls, caving and so forth with rock strength, fracture and flow and hence with safety and stability is inescapable. However, quantitative design requires quantitative estimates of strengths. While considerable theoretical work has been done on estimating the elastic properties of regularly jointed rock masses, especially in the context of surface excavations and foundations, very little has been done on rock mass strengths in mining environments. Back analysis of full scale test stopes remains essential to the task.

Analysis of field scale test data is not as straightforward as it may seem, and there is no guarantee of success even with close adherence to engineering problem solving procedures. This is not primarily due to the usual constraints of time, budget, and personnel, although these are certainly important, but rather because of limitations to existing knowledge and equipment. An example of the first that was encountered during the test stope project concerns interpretation of in situ stress measurement data. Most stress measurements depend upon deformation about a borehole; the in situ stresses are calculated from such. Thus at the measurement site, the in situ stresses are in one-to-one correspondence with in situ strains. The question that arises is simply this: Which should one use? If only one rock type is present, as in Section A, then there is no difference. Subsequent calculations result in identical stress, strain, and displacement fields. However, if different rock types are present, as in Section B, then a noticeable difference in results may occur. Even under the simplifying assumption of a uniform field throughout the region of interest, there appears to be no theoretical way of deciding from the measurements themselves whether to use the in situ stress or in situ strain field. The data reduction procedure itself appears inconsistent, although this is state of the art.

Both in situ stress and strain fields were examined in the Carr Fork Mine test stope project; the conservative approach was adopted. The in situ strain field approach leads to a higher correlation ($r = 0.981$) between measured and calculated displacements and also to a lower rock mass Young's modulus 20.7 GPa (3.0 million psi) than in the in situ stress approach ($r = 0.89$, $E = 31.7$ GPa or 4.6 million psi). Calculated displacements by the two approaches are themselves highly correlated ($r = 0.95$). However, the footwall overbreak zone was much less in the

strain based analysis. The stress-based analysis is therefore conservative with respect to stability and was the one followed. Two other reasons were used in deciding in favor of the stress based analysis. One is "social"; it is "customary". The other is the supposition that the geologic processes responsible for the present spatial relationships between geologic units were accompanied by some slip and shearing between units. This implies nonuniform strain and thus favors a stress-based approach.

A closer study of the extensometer readings shows that there is significant displacement after a blast. In fact, the displacements more than double three weeks after the last blast. There was no other mining activity in progress, so that the increase in displacements after blasting is time dependent. Interestingly, the measured displacements still correlate very well with calculated displacements using a lower Young's modulus. This suggests that a delayed time-dependent elasticity model is appropriate for the short term. Displacement data over a year after the last blast show a slight amount of long-term creep. As a practical matter, the stresses are the same as before, although some time, several weeks, is required before peak values are achieved. In this regard, the footwall overbreak zone was stabilized by the backfill; no overbreak has developed elsewhere. The time question for field scale rock masses is nevertheless of some interest.

Stope and Pillar Width Analyses

A major benefit of a successful case study is the establishment of a reliable design procedure for considering alternative layouts. The ability to estimate ground movement and potential overbreak lends confidence to parameter studies of design alternatives intended to improve productivity and resource recovery. In this regard, stope height is largely determined by drill hole deviation and the need for close control over blasting in VCR and BHPF stopes. Stope length (across the vein) is usually determined by extent of the ore. However, stope width measured along strike is subject to engineering control. Widening a stope has production advantages but can only be done if stability is maintained. Once stope width is specified, stope spacing or equivalently pillar width must be determined.

A practical question to be answered in advance of the stope and pillar width analyses concerns the influence of crosscuts on the test stope. Preparation of finite element meshes can be a time-consuming task, so that it would be a considerable advantage to be able to omit them from parametric studies of the test stope.

Influence of Crosscuts on the Test Stope

One suspects that since the crosscuts are relatively far from and small compared with the mined stope dimensions that their influence on the test stope is also small. The reverse may not be true because the zone of influence of an opening is proportional to the size of the opening. The test stope may influence development openings.

The most direct way to answer the question is to actually carry out analyses with and without the crosscuts and compare them. However, it is not obvious how such a comparison should be made. Criteria for comparing stress, strain, and displacement fields raise rather subtle questions in mechanics, especially where different geometries are involved as they are here. A pragmatic approach is to use the algebraic fact that the difference between two tensors is also a tensor just as the difference between two vectors (rank one tensors) is also a vector. Stress and displacement differences can then be computed from the analyses with and without development openings and plotted for visual as well as quantitative comparison. In addition, the distributions of the local factor of safety can be subtracted and the resulting difference plotted for comparison. Near the development openings, differences in stress, displacement and safety factors should be noticeable. However, if the differences in the vicinity of the test stope are small, then omission of the crosscuts from the test stope width analyses is justifiable.

Figures 34, 35, and 36 show the stress, displacement, and safety factor fields in the vicinity of the test stope with the crosscuts present. Figures 37, 38, and 39 show the difference fields of stress, displacement, and safety factor. The plots are to the same scale, so that a direct visual estimation of the influence of the crosscuts on the test stope can be made. It is obvious from these data that the crosscuts can be omitted from the test stope width studies.

Stope Width

A specific question concerning test stope width asks at what width and where does inelastic behavior first occur as the stope is widened with other parameters held constant.

A second question concerns the growth of inelastic zones with increasing stope width. It may be economically viable to support a limited volume of loose and flowing rock, provided there is no threat to the whole stope.

Parametric studies aid in answering these questions. In this regard, stope width is seen in Section A parallel to strike. Section A is entirely in ore. The in situ stress is characterized by a ratio of horizontal to vertical stress equal to 0.84. As before, the rock is elastic perfectly plastic with a parabolic yield condition. Both rock properties and stope width are varied from their original values.

Figure 40 presents the results of a study of three stope widths for three combinations of strength and modulus; the results are in the form of contours of safety factor and yield zone extent. A safety factor of one means that locally the elastic limit has been reached. High, medium, and low values of strength and modulus are roughly one, one-half, and one-fourth times laboratory values. The reference stope width is the original 12 m (39 ft) width. Figure 40 shows only a portion of the ground in the vicinity of the test stope. An example of a full mesh plot is shown in Figure 41.

Stress Field in Section A with Crosscuts Present.

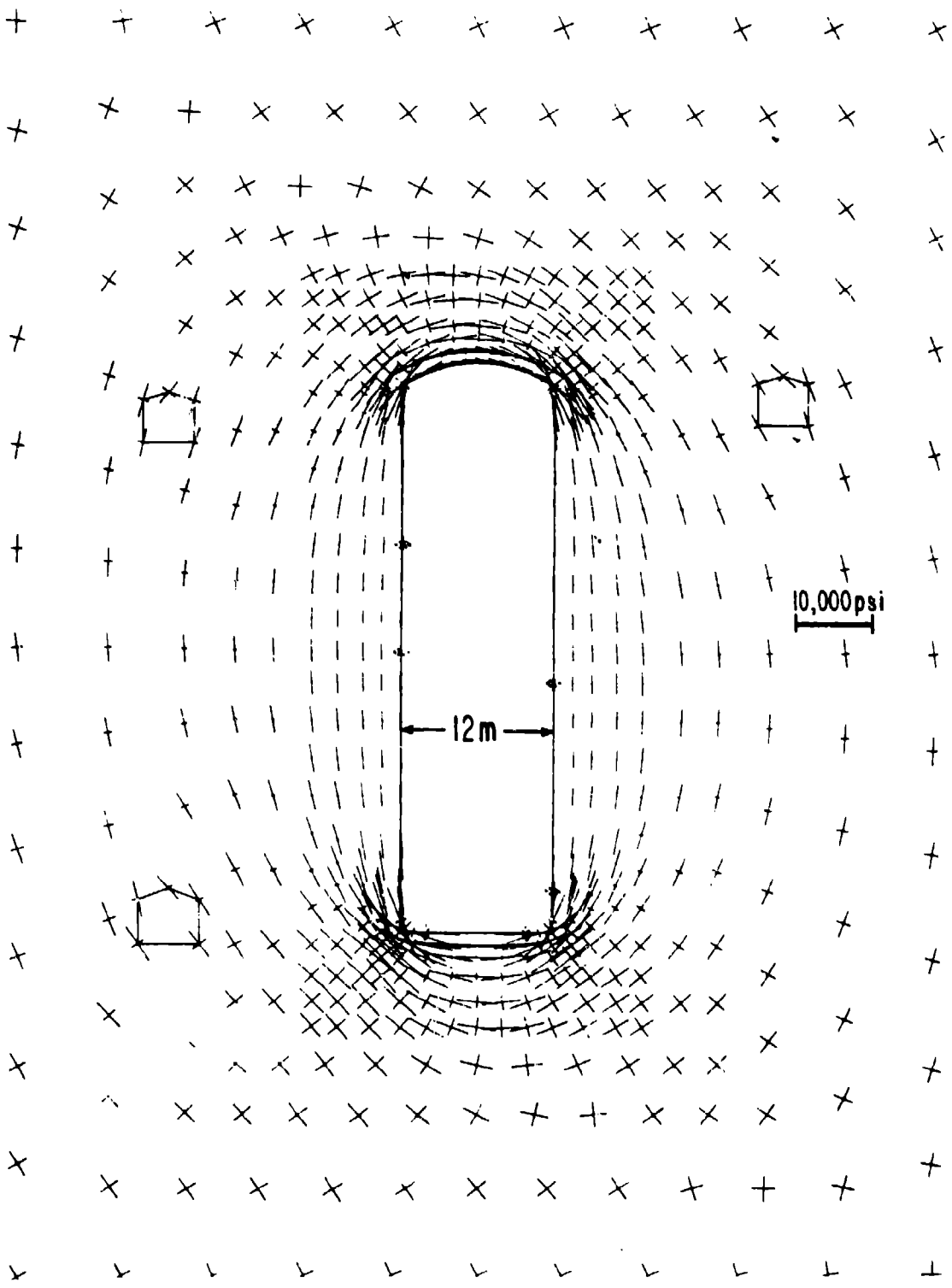

Figure 34. - Stress field in section A with crosscuts present.

Displacement Field in Section A with Crosscuts Present.

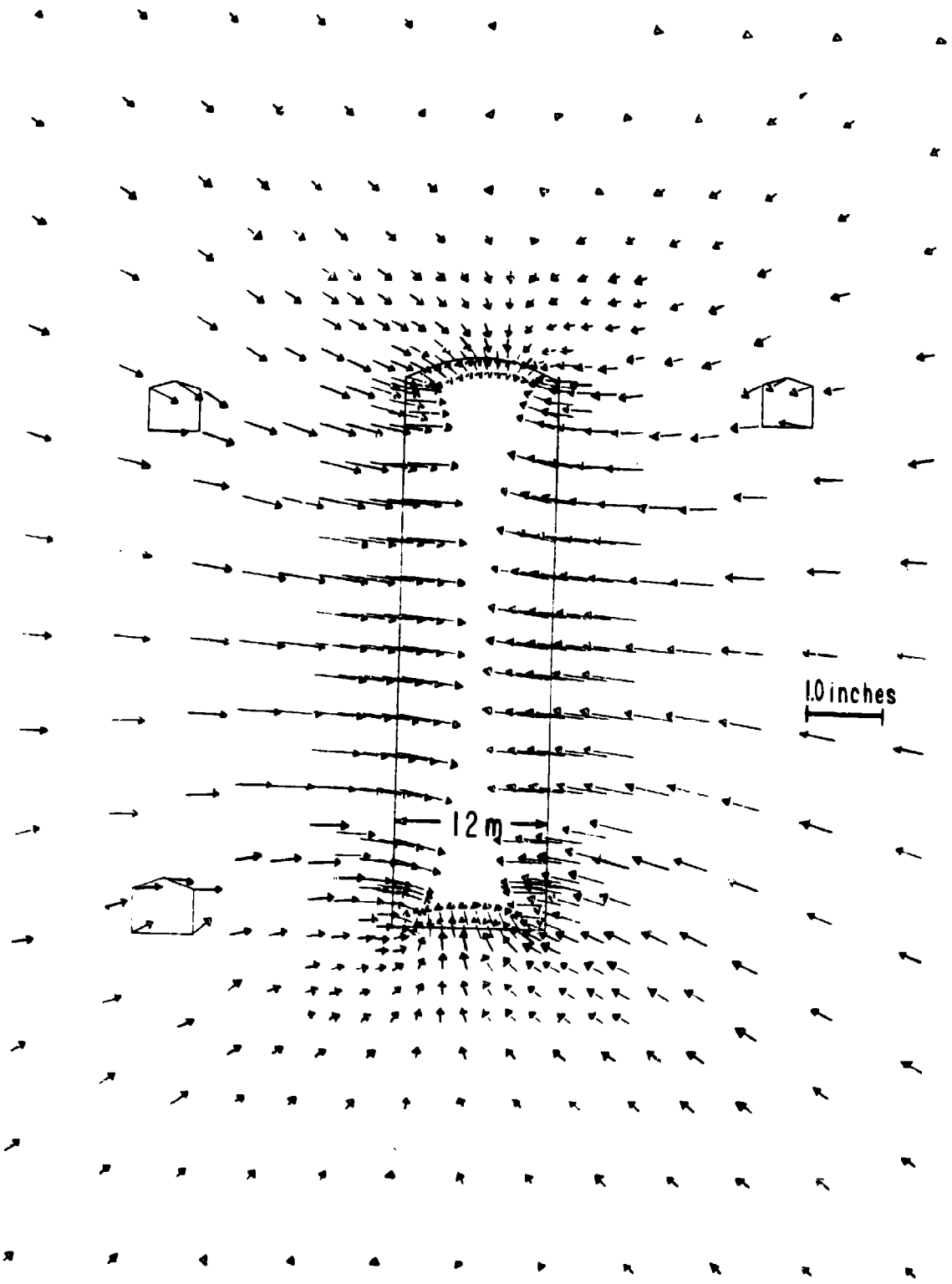

Figure 35. - Displacement field in section A with crosscuts present.


1.0
1.1
1.25
1.4
1.6
2.8
3.2
3.6
4.0
2.5
2.2
2.0
1.8

Safety Factor Distribution in Section A with Crosscuts Present.

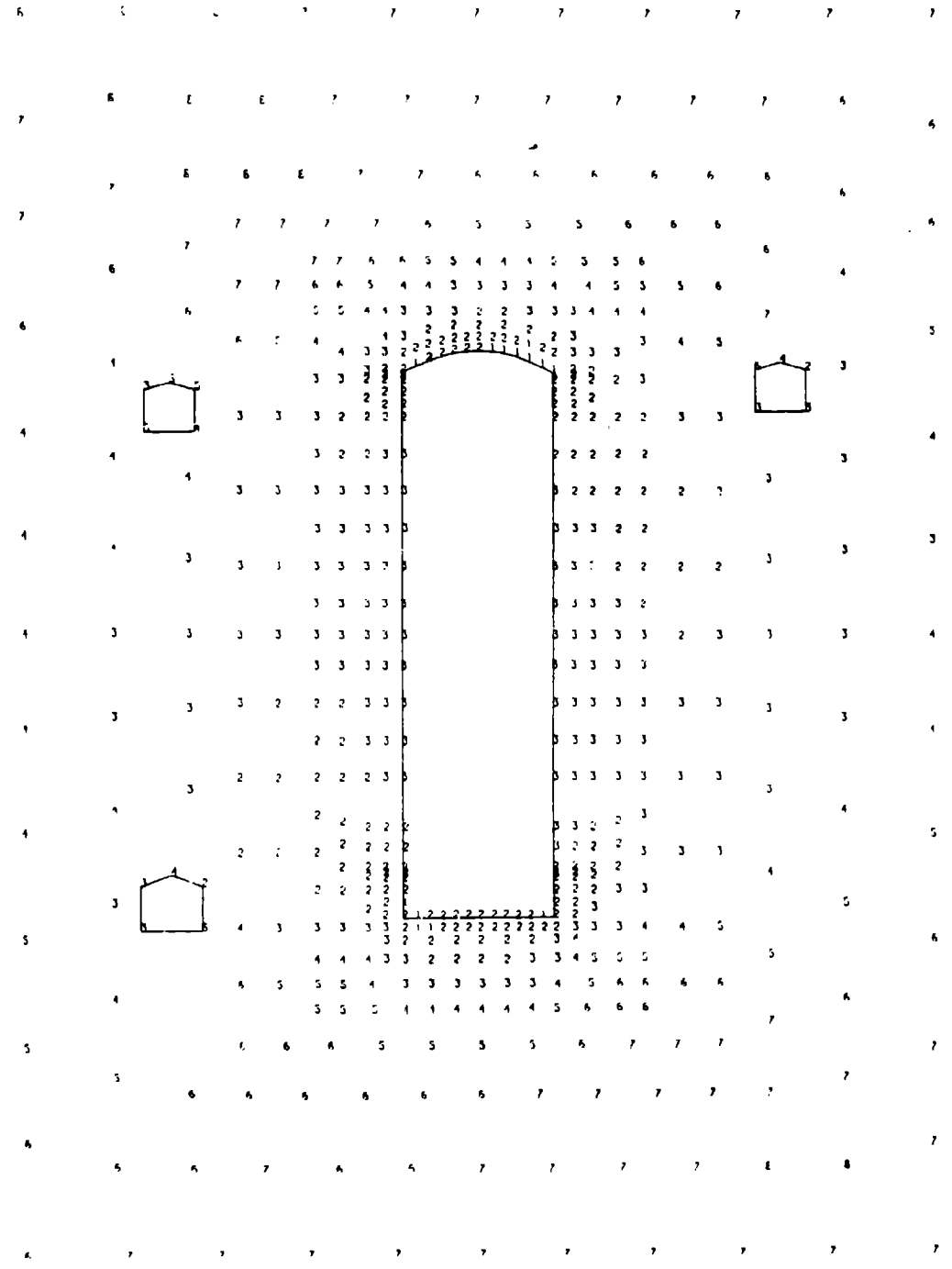

Figure 36. - Safety factor distribution. Section A with crosscuts.

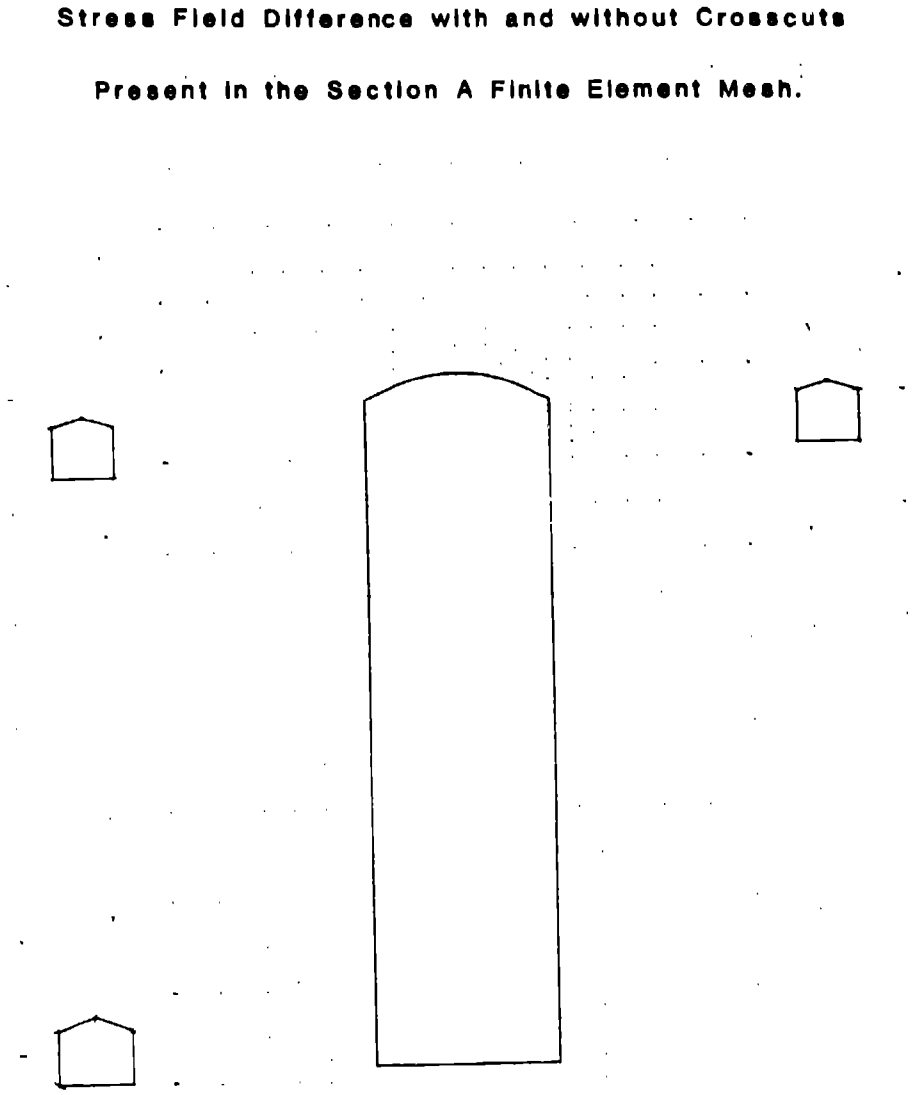

Figure 37. - Stress field difference with and without crosscuts present in the section A finite element mesh. (Scales are the same as in Fig 34.)

Displacement Field Difference with and without Crosscuts Present in Section A.

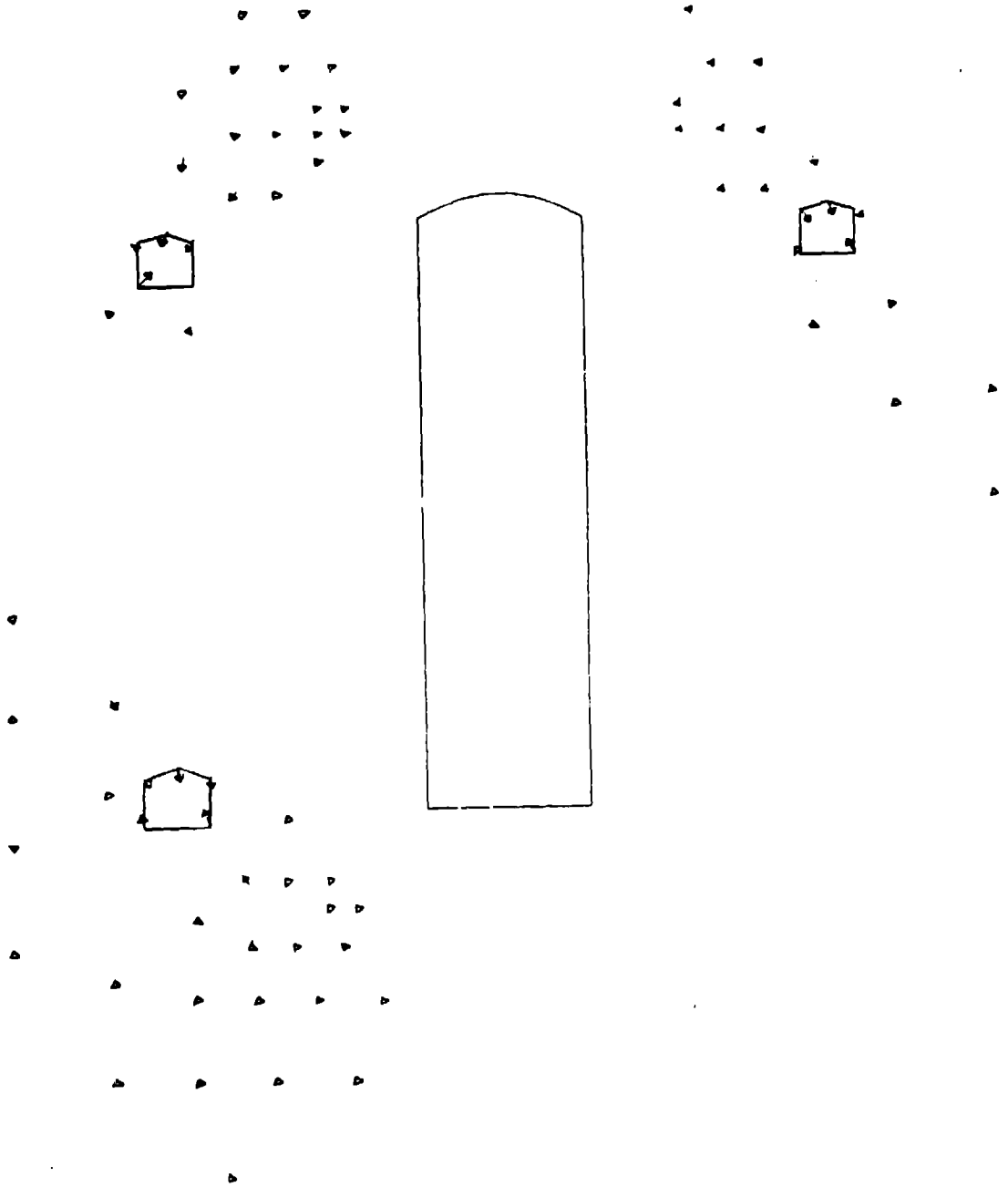

Figure 38. - Displacement field difference with and without crosscuts present in section A. (Scales are the same as in Fig. 35.)

Safety Factor Difference with and without Crosscuts Present in Section A.

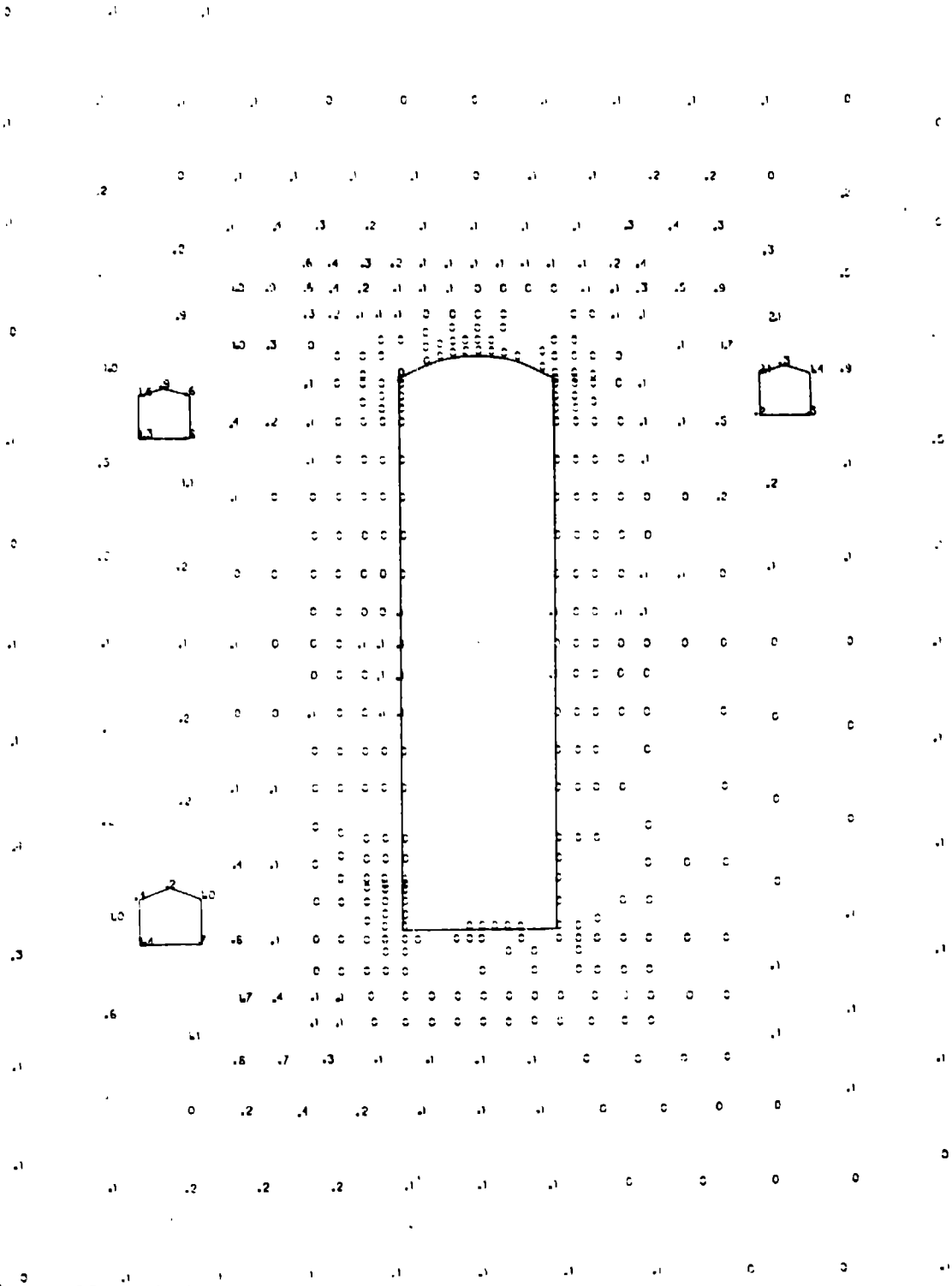

Figure 39. - Safety factor difference with and without crosscuts present in section A. (Scales are the same as in Fig. 36.)

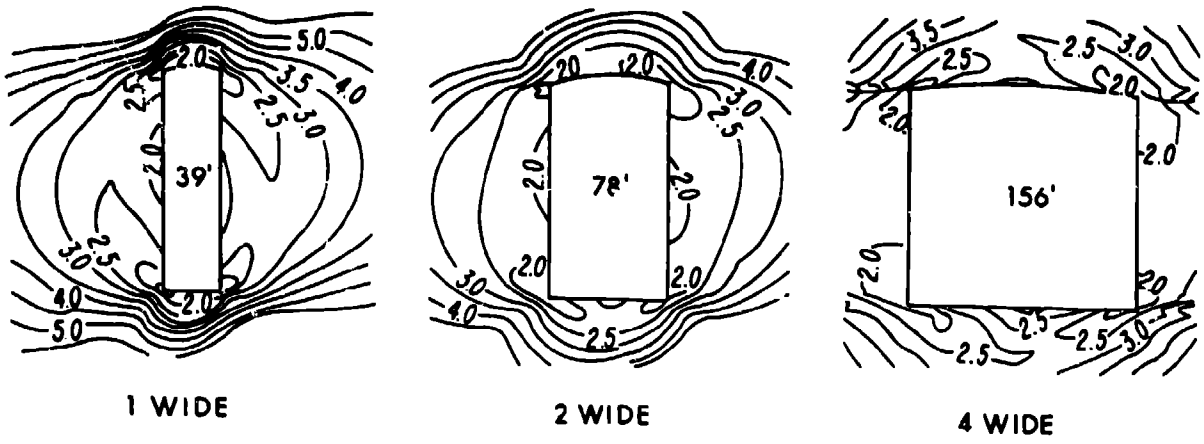

Yield Zone Extent and Safety Factor Distribution as Functions of

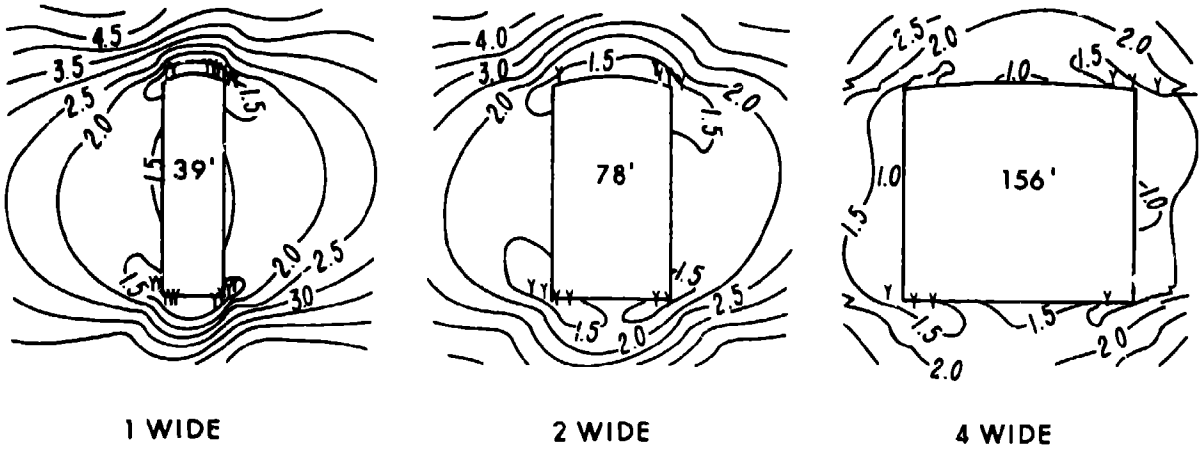

Stope Width at High, Medium, and Low Strength and Modulus Values.

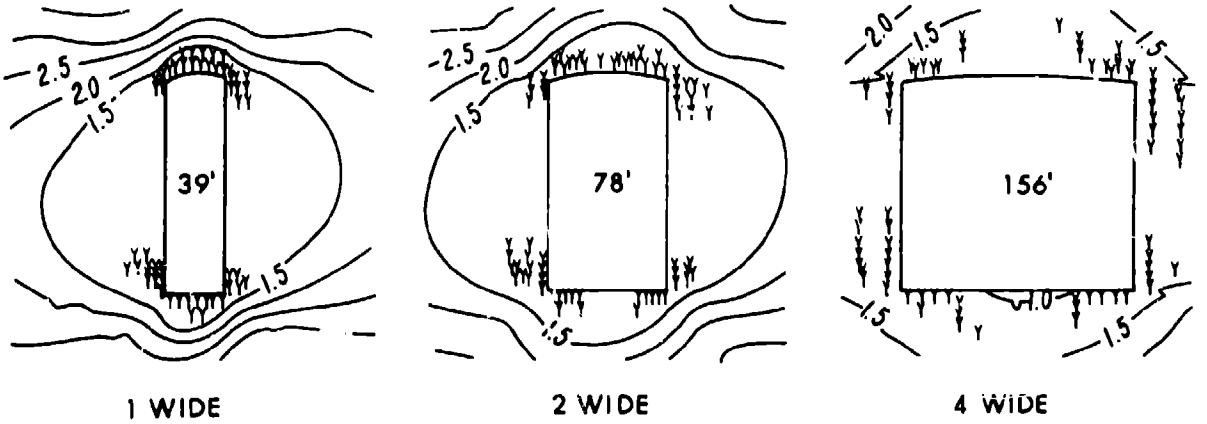

Figure 40. - Yield zone extent and safety factor distribution as functions of stope width at high (top row), medium (middle row) and low (bottom row) strength and modulus values.

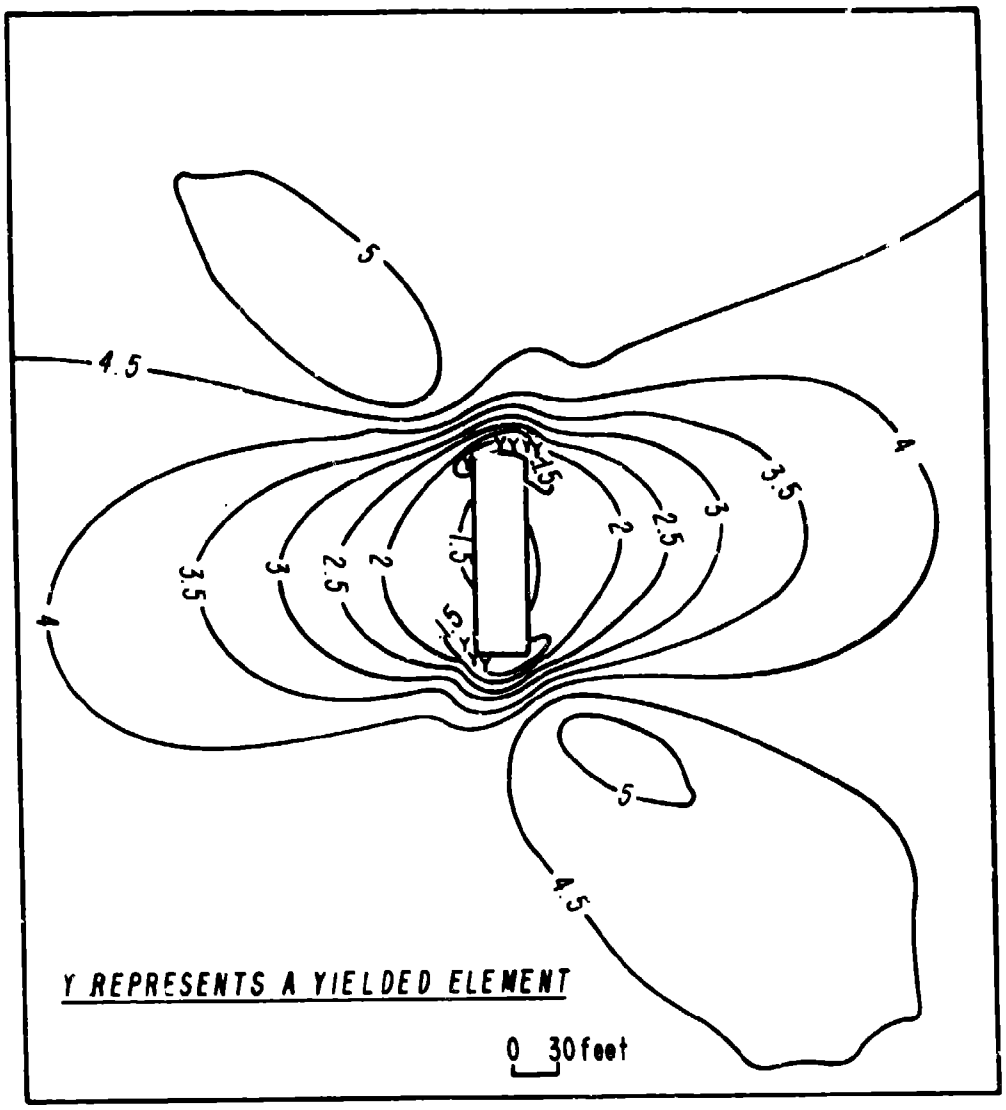

Full Mesh Extent Example, Medium Strength and Modulus Case.

Figure 41. - Full mesh extent example, medium strength and modulus case.

Study of the data in Figure 40 reveals an unexpected result: widening of the test stope has little influence on stability regardless of strength and modulus values. For a given set of rock properties, increasing the width of the test stope up to four times original width actually increases stability. Yielding appears at rock mass properties one-half laboratory values, and spans the stope at one-fourth laboratory values. Yield zones in back and brows were not observed in the test stope, however.

The inference that widening of the test stope posed no threat to stability was contrary to intuition, so that additional evidence was sought. It is known that the peak compressive stress at the periphery of a rectangular opening increases linearly with width to height ratio for widths greater than height and Ko values less than one. For width less than height, the peak stress decreases with an increase in width, although not linearly, for values of Ko greater than about 0.3 as Figure 42 shows. Measured Ko values are greater than 0.5. In either case any tension present tends to be independent of width to height ratio. Figure 42 also shows that the benefits of widening the opening are greatest for the hydrostatic case (Ko = 1.), although peak stress is less for lower Ko values. (A measured Ko of 0.84 was used in the stope width analyses.) This evidence supports the conclusion that widening the test stope, say, to twice original width could be done safely. Only half the number of crosscuts would then be needed.

Pillar Width

The question of stope width cannot be completely answered without considering a stope spacing or equivalently pillar width. One determines the other at a set stope width. Stope and pillar width together fix the initial extraction ratio and therefore recovery on first mining. A rough rule of thumb states that the zone of influence of a single opening is proportional to opening size, so that interaction begins at a pillar width equal to the stope width, that is, at an initial extraction ratio of 50 percent. Another rule of thumb states that pillar stress tends to be uniform and uniaxial in pillars higher than they are wide. The expectation is that in a long row of pillars and stopes on a given level, the pillar stress state is insensitive (i) to stope width increases to less than the stope height at 50 percent extraction and (ii) to pillar width increases to less than stope height at fixed stope width.

However, vein pillars are not isolated columns. Although the rib sides are unconfined before back filling, the foot and hanging wall sides are always confined when mining full vein width. Since strength is confining pressure dependent, the confinement in one direction and not in the other raises a question as to what strength to use, especially in the presence of high horizontal stress. Fortunately, the yield condition used in the analyses allows for varying confinement in different directions, so that the question automatically resolves itself in the finite element calculations. However, an extraction ratio or tributary area calculation could be unreliable in such cases.

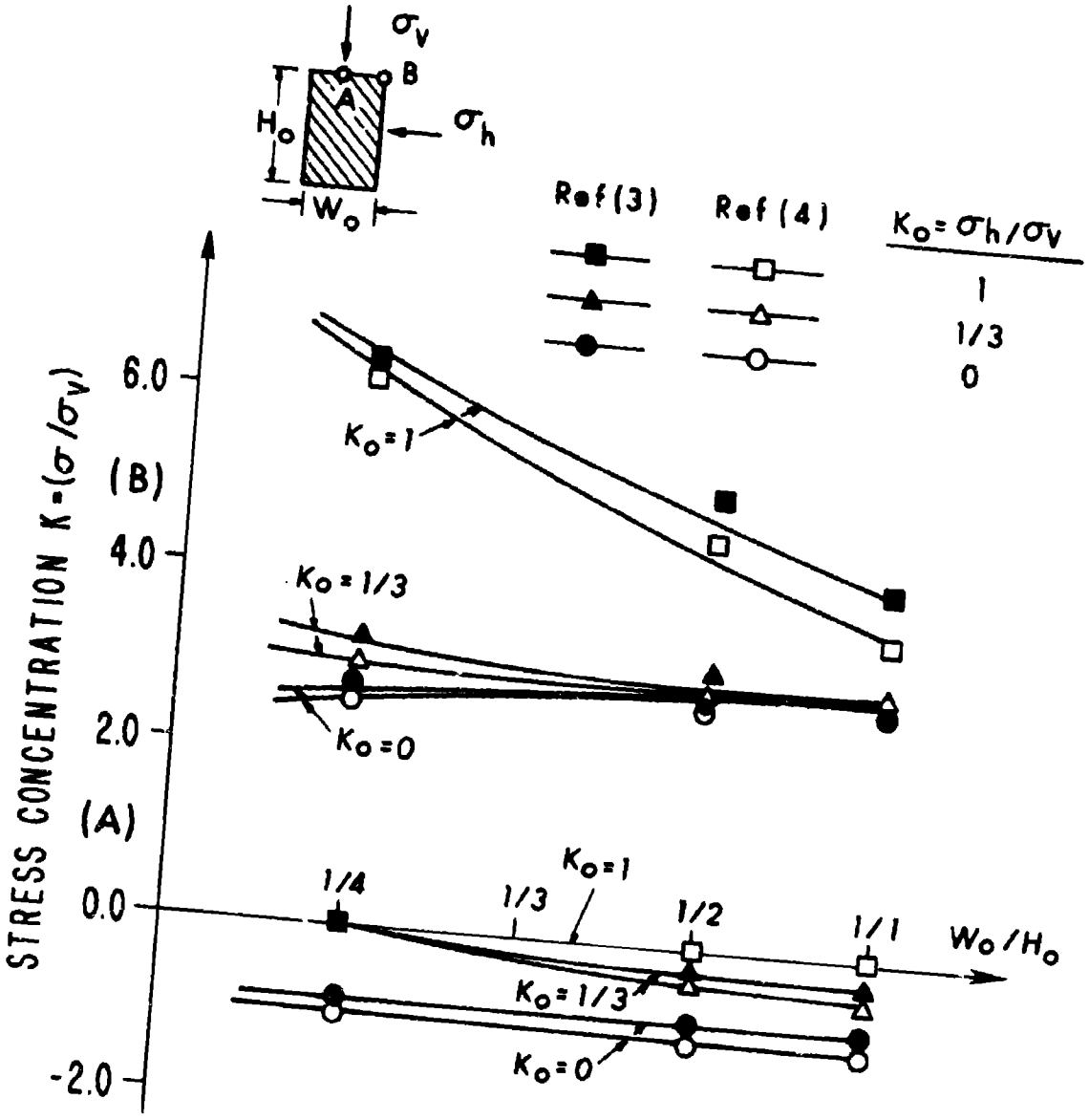

Theoretical Stress Concentration as a Function of Width to Height Ratio and Applied Stress Ratio (Ko).

Figure 42. - Theoretical stress concentration as a function of width to height ratio and applied stress ratio (Ko).

The results of a series of analyses at stope widths Wo of 1, 2, and 4 times the original width (12 m) and at pillar widths Wp of 1, 2, and 4 times the stope width for low and high horizontal stress (2/3 and 3/2 of vertical) are presented in Table 10. The local safety factors presented in Table 10 are at pillar mid-height.

TABLE 10. - Pillar width study results

W_p/W_o	R	W_o	1X (12m) FS		2X (24m) FS		4X (48m) FS	
			Center	Edge	Center	Edge	Center	Edge
1	1/2	L	1.3	1.3	1.3	1.3	1.5	1.4
		H	1.4	1.4	1.3	1.4	1.6	1.5
2	1/3	L	1.5	1.5	1.7	1.6	2.7	1.6
		H	1.5	1.6	1.7	1.7	3.9	1.8
4	1/5	L	1.8	1.8	2.8	1.9	4.6	1.7
		H	1.8	1.8	3.8	1.9	9.0	2.0

W_o = width of opening
W_p = width of pillar
R = extraction ratio
Fs = factor of safety
L = low horizontal stress (2/3 vertical)
H = high horizontal stress (3/2 vertical)
Ho = Hp = height of opening, pillar

These results show that:

(i) the safety factor in the core or center of the pillar is equal to or greater than at the edge or rib of the pillar,

(ii) high horizontal stress tends to increase safety because of greater confinement, but the effect is small, about 10 percent, at the ribline where the safety factor is lowest,

(iii) at fixed pillar to stope width ratio but Wp/Wo > 1 and therefore constant extraction ratio (R > 50%), the ribline safety factor is nearly independent of stope width up to a stope width nearly equal to stope height,

(iv) increasing the pillar width from 1 to 4 times stope width increases the ribline safety factor roughly 20 percent (1.4 to 1.8).

These results show, for example, that doubling the stope width and therefore the pillar width while maintaining the initial extraction ratio at 50 percent is actually somewhat beneficial to stability. Figure 43 shows the double width factor of safety map for the low and high horizontal stress cases. The lowest local safety factor in Figure 43 is 1.6. Contour interval is 1.

An analysis at double stope width (24 m) but at a lesser pillar width (Wp/Wo = 1/2) and an extraction ratio of 67 percent (R = 2/3) shows an extensive plastic zone across the entire section of the pillar and thus global yielding and potential collapse (FS = 1.0). These conditions are similar to the original VCR stopes on the 1300 Level where mining proved difficult. At high horizontal stress, the pillar is marginally stable with localized plastic zones (FS = 1.1).

The BHPF system progresses upwards from level to level as well as along a level. A stope on stope analysis was done to show the capability of the computer program to follow the mining sequence. Stope geometry and mining sequence are shown in Figure 44; properties are given in Table 11. A comparison between a single level of stopes and pillars and a two level stope on stope case with backfill and columnized pillars is shown in Figure 45. The backs of the open stopes are virtually the same, while the lowest factors of safety anywhere in the pillars are also the same (1.3). This is as expected because the pillar is tall at the outset with a height to width ratio near 4. Increasing pillar height thus does not change the pillar stress state.

TABLE 11. - Rock properties for stope on stope analyses

Property / Material	E (psi)	ν (--)	Co (psi)	To (psi)	γ (pcf)
Rock	3.0×10^6	0.2	9,000	700	165
Fill	3.0×10^4	0.2	90	7	100

1 psi = 6.9 kPa, 1 pcf = 157 N/m^3

Double Width Stope Safety Factor Map at 50% Extraction.

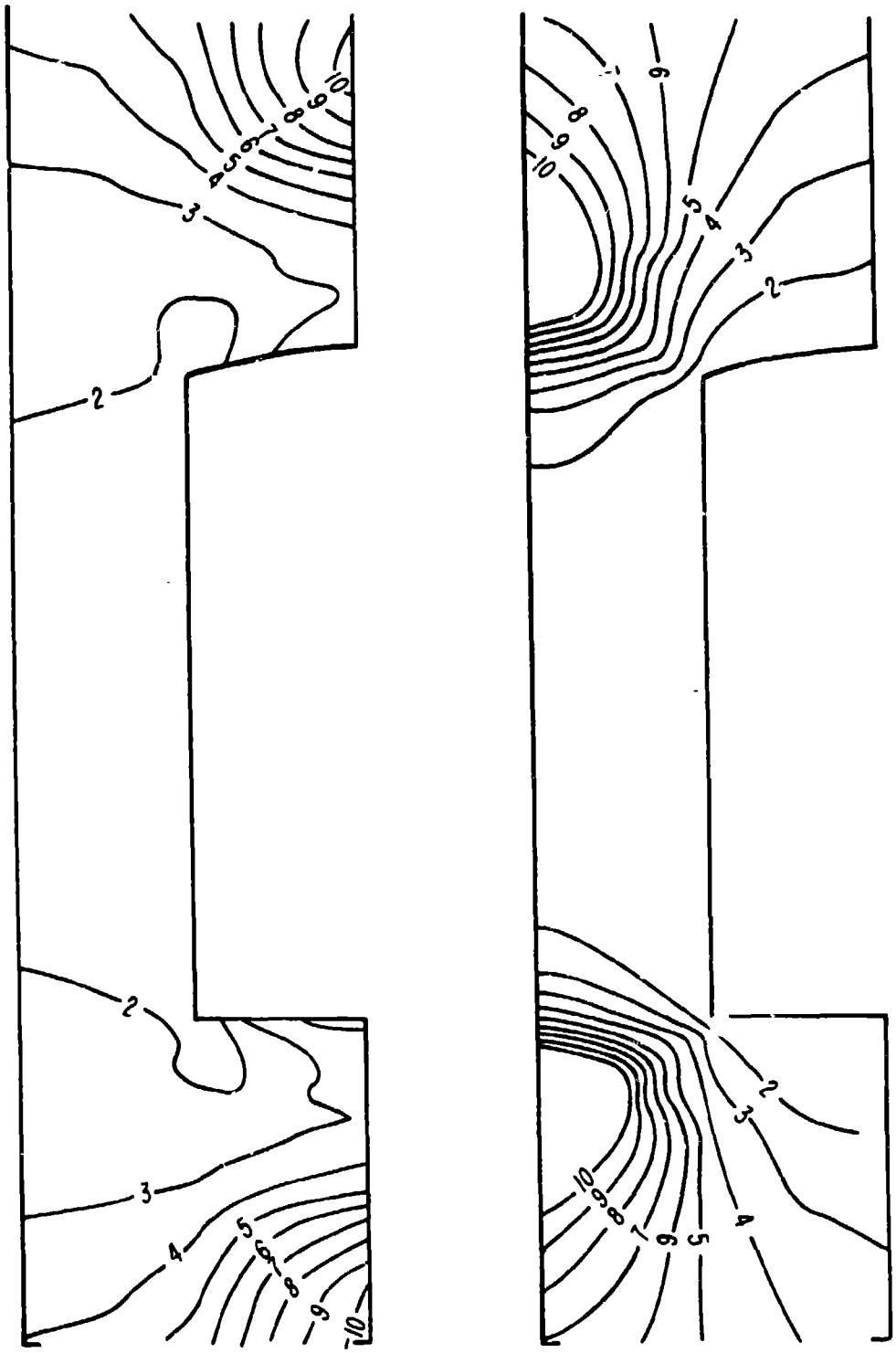

(a) Low Horizontal Stresses. **(b) High Horizontal Stresses.**

Figure 43. - Double width stope safety factor map at 50% extraction. (a) Low horizontal stresses. (b) High horizontal stresses.

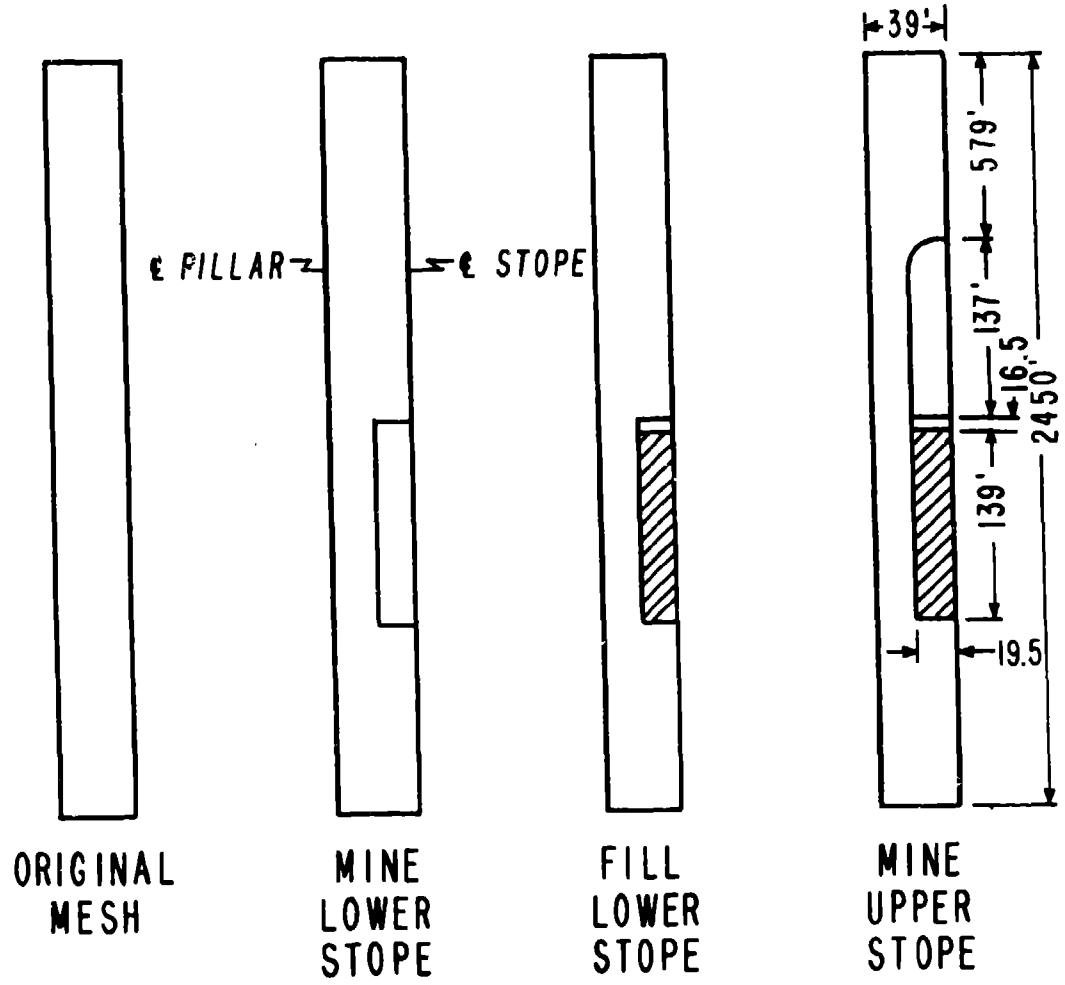

Stope-on-Stope Mining Sequence.

Figure 44. - Stope-on-stope mining sequence.

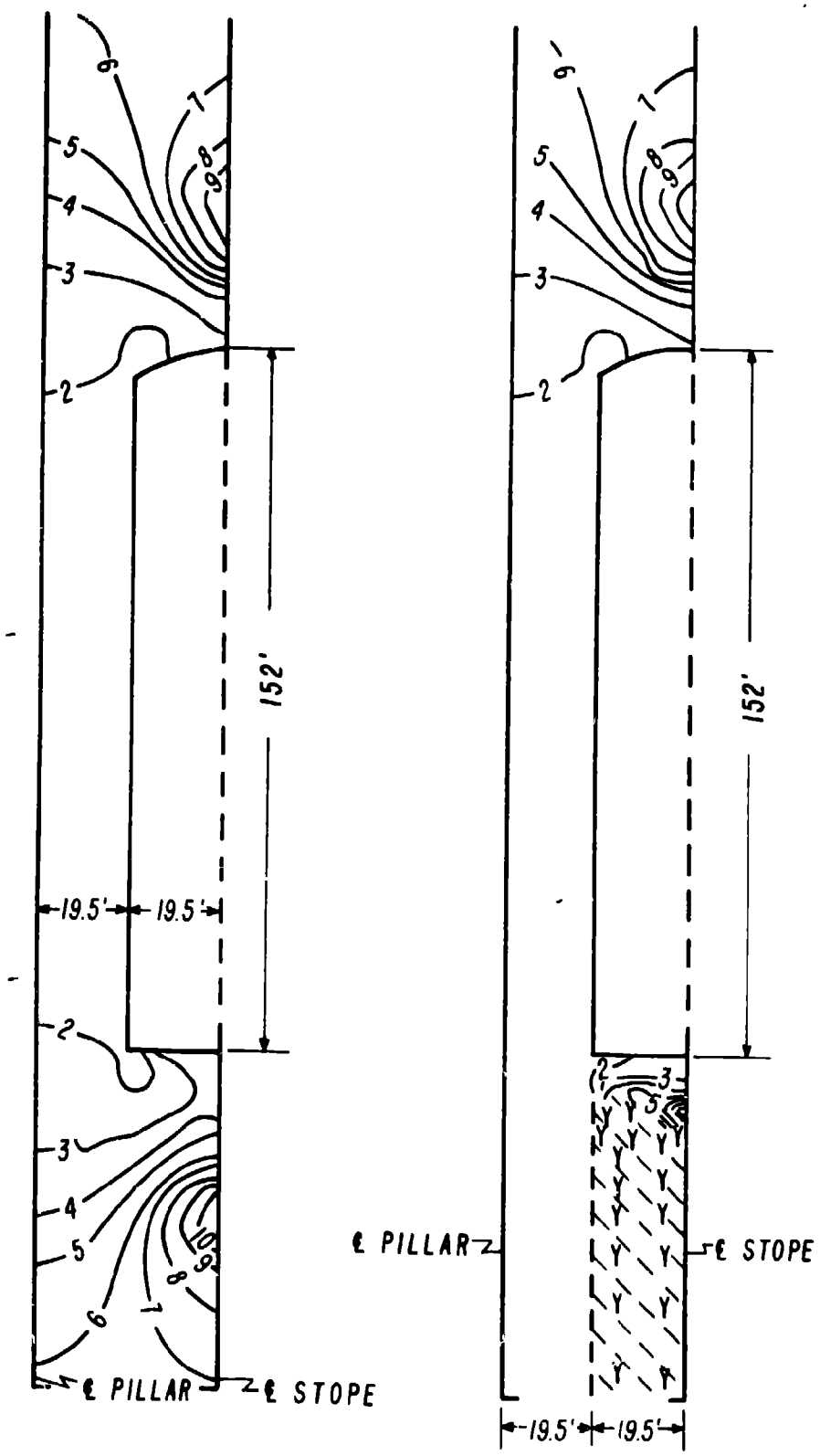

Single Stope Compared with Stope-on-Stope with Backfill.

Figure 45. - Single stope compared with stope-on-stope with backfill.

CONCLUSION

The background, objectives, approach, and results of a geomechanics case study have been presented. The study was a cooperative effort by the Anaconda Minerals Company, the U. S. Bureau of Mines, and the University of Utah. During the course of the study, a full-scale test stope was mined to completion and subsequently backfilled with waste rock. In this regard, the mining method involved large diameter blast holes in a new design known as blast hole post-fill (BHPF) stoping. The main geomechanics objective was to establish a design procedure for optimizing stope and pillar dimensions through a combination of mine measurements, laboratory testing and finite element calculations.

Some 36 drill holes up to 27 m (90 ft) in length were used for monitoring the test response to mining. These holes were strategically located in the ribs of the test stope, in the back of the overcut and the brow of the undercut, and in the foot and hanging walls. Relative displacement measurements obtained from multi-anchor rod extensometers proved to be the most consistent of the various measurements made. The bulk of the data was recorded automatically and semi-continuously by data loggers. Scanning frequency was adjusted according to the blasting schedule and previous instrument activity. As expected, a strong association between production blasts and jumps in instrument readings was observed. Generally, displacements were less than 2.5 cm (1.0 in.) before the loss of an anchor occurred. Instrument losses were "normal" and generally attributable to unit operations. However, some instrument loss also occurred with the development of a foot wall overbreak zone.

Three two-dimensional finite element representations of the test stope that incorporated stope geometry and eight rock types identified in the skarn type Steep Highland Boy ore zone were used in the calculation of stress, strain, and displacement fields associated with the mining sequence. The premining stress field was determined from stress measurements in situ. An elastic-plastic material model was suggested by the combination of laboratory testing and mine observations. Such a model is available in the UTAH-II and UTAH-III finite element computer programs. Both use nonlinear versions of Drucker-Prager yield and associated flow rules appropriate to geologic media.

Regression analyses of calculated on measured displacements gave correlation coefficients of 0.882 and 0.886 in vertical sections parallel and perpendicular to strike, respectively. The correlation coefficient is independent of Young's modulus. However, the slope of the regression line is essentially linear in the reciprocal of Young's modulus. This feature of the analysis allows one to determine Young's moduli for the rock mass about the test stope and thus to "tune" the model for accurate displacement calculations. However, accurate displacement prediction is of less importance than rock mass strengths which are needed for the assessment of safety and stability.

Comparison of observed and calculated footwall overbreak zone extent provided estimates of rock mass strengths. This comparison was complicated by the three-dimensional aspects of the topdrift extension into the footwall. Analysis of the situation with the three-dimensional finite element code UTAH-III indicated a significant increase in stress concentration in the vicinity of the footwall overbreak zone because of the topdrift extension. Overbreak zone extent would be less, perhaps nonexistent, without the topdrift extension. This is an important practical consideration because of the role that dilution plays in the business of underground hardrock mining.

Application of the finite element procedure to the analysis of alternative stope and pillar widths was made in a subsequent series of analyses. The results show that increasing the width of a single stope up to a value equal to the height of the stope is in fact slightly beneficial. Peak stress concentration in the periphery of the stope does not change significantly with an increase in stope width. This inference based on the finite element results was verified independently from other analytic and experimental results.

Multiple stopes and therefore pillars would be necessary in a production setting. In this regard, the combination of stope and pillar width fixes stope spacing and the initial extraction ratio. Analyses results show that at 50% extraction the minimum safety factor in the pillar is 1.3. Doubling of the stope width, say, from 12 m to 24 m at 50% extraction could thus be undertaken with some confidence. Analysis of 24 m wide (by 33 m high) stopes separated by only 12 m wide pillars (67% extraction), however, shows a large plastic zone extending from pillar rib through the core indicating potential instability and collapse. Stopes 24 m wide separated by 12 m wide pillars roughly correspond to the original VCR stope layout that was less than successful.

In conclusion, the excellent agreement observed between measured and calculated displacements and footwall overbreak zone extent substantiated the material model and the accuracy of the finite element representation of test stope geometry, geology, and mining sequence. Parametric studies for the purpose of optimizing stope and pillar sizes in alternative stope layouts were therefore justified. The main geomechanics objective of the test stope study was thus achieved. In fact, the test stope design proved to be highly successful with further improvement possible.

REFERENCES

1. Heller, S. R., Jr., Brock, J. S., and Bart, R., 1958, "The Stresses Around a Rectangular Opening with Rounded Corners in a Uniformly Loaded Plate," trans. 3rd U. S. Congress on Applied Mechanics, pp. 357-368.

2. Heuze, F. E., and Amadel, B., 1984, "The NX-Borehole Jack: A Lesson in Trial-and-Errors," UCRL-90282 Preprint.

3. Obert, L., and Duvall, W. I., 1967, Rock Mechanics and the Design of Structures in Rock, Wiley, N. Y., p. 506.

4. Pariseau, W. G., 1984, "Linearization of In situ Stress Change Data Reduction Formulas for Gages at Arbitrary Down-hole Orientations," in press Int. J. Numer. Anal. Methods Geomech.

PART 2.

GEOMECHANICS OF THE HOMESTAKE MINE STUDY STOPE

ABSTRACT

This section describes a comprehensive geomechanics case study of a full-scale vertical crater retreat (VCR) panel at the Homestake Mine. The mine is owned by the Homestake Mining Company and is located in Lead, South Dakota. The study region lies between the 6950 and 7100 levels (feet below surface). Three panels of the study stope region were instrumented with multi-anchor borehole extensometers and vibrating wire stress gages from a cable bolt drift in the hanging wall and with footwall extensometers installed from the footwall haulage drift on the extraction level. Nineteen instrumentation boreholes, some over 100 ft in length, were used to monitor the study region response before, during and after mining. Laboratory tests for elastic moduli and strengths were conducted on drill core from mutually perpendicular holes in the study region in order to define the mechanical anisotropy of the Poorman, Homestake and Ellison formations. The Poorman formation, in particular, shows a well-developed foliation. In situ stress measurements from several sources including recent hollow inclusion overcoring tests on the 7400 level were used to define the in situ stress state. The center panel produced approximately 65,000 ton of ore and allowed direct comparisons to be made between theoretical and measured displacements. Displacements were greatest in the immediate hanging wall where some instrumentation loss occurred during mining. Anchor by anchor correlation coefficients obtained from regression analyses of calculated on measured displacements were all greater than 0.9. Regression analysis using all data gave a correlation coefficient of 0.84 and fixed the rock mass elastic moduli. Comparisons between inferred and calculated yield zone extent in the hanging wall fixed the rock mass strengths. A total of 54 independent rock mass properties were needed to define the anisotropic elastic-plastic material model (18 for each of the three formations present). All calculations were done with the UTAH-II finite element program.

The calibrated finite element model was subsequently used to assess the influence of dip, stope size, and pillar size on stability. Under study stope conditions, an initial extraction of 50% is quite safe, but 75% is not. At a stope height of 150 ft, widths and strike lengths greater than 50 ft can be accommodated, but length to width ratios (plan view) greater than four show marginal hanging wall stability. Alternative layouts, sequences under different geologies and in situ stresses can be considered using the same procedure without the need for full scale tests. However, some compromise is necessary in this regard because unlike the transverse section that shows the hanging wall response best, plan and longitudinal sections which show pillar size and strike dimensions best are three dimensional when the dip is not near vertical. Three dimensional analyses were beyond the scope of this investigation.

INTRODUCTION

The Homestake Mine is a deep underground gold mine located in the northern Black Hills near Lead, South Dakota, as shown in Figure 46. Mining began at Homestake in 1878. Development currently extends more than 8,000 ft below the surface. A variety of stoping methods have been used in the past. Cut and fill (Waterland and Conolly, 1966) and vertical crater retreat or VCR stopes (Mitchell, 1980) account for the bulk of production at the present. The use of large diameter blast holes and VCR methods is expected to increase (Orr, 1983).

The ore occurs in the steeply dipping and plunging folds of the Precambrian Homestake formation (Slaughter, 1968). The Ellison formation overlies the Homestake; the Poorman formation usually forms the footwall. The Ellison and Poorman formations are also Precambrian. Three well-defined zones of increasing metamorphism have been identified in the region: the biotite, garnet and staurolite zones. Ore deposits occur in the biotite and garnet zones. Phyllites and schists of varying composition are the dominant rock types. The folding is complex. Many world class ore bodies occur in a similar setting of ancient, steeply dipping metasediments. The questions posed here thus have wide applicability.

Control of the hanging wall is an historic task in underground mining. A stable hanging wall is important not only for safety but also for economic reasons. Dilution from a caving hanging wall may reduce the grade of ore below the level of profitability. With VCR stoping methods, hanging wall control must be secured in advance of production blasting. No miners are present in the stope proper, so that direct observation of the hanging wall and the opportunity to add support during the life of the stope is not generally practical. A greater engineering design effort is therefore required for successful VCR stope layouts. Careful control of production drilling and blasting is also essential.

The objectives and approach to the study stope project at the Homestake Mine were similar to those at the Carr Fork Mine. A technically sound and practical technique for sizing stopes and pillars associated with VCR mining was sought. Accordingly, a plan for instrumenting the study region was implemented and measurements of ground movement in response to mining were made. These were subsequently compared with theoretical calculations based on a finite element computer model of the mining sequence. Input data in the form of stope geology, geometry, in situ stress state and rock properties were obtained in advance of mining. The mining sequence was then simulated on the computer. A favorable comparison of calculated with measured displacements justified use of the model for analysis of alternative stope and pillar sizes. The objective is to optimize both for productivity and recovery without sacrifice of safety and stability.

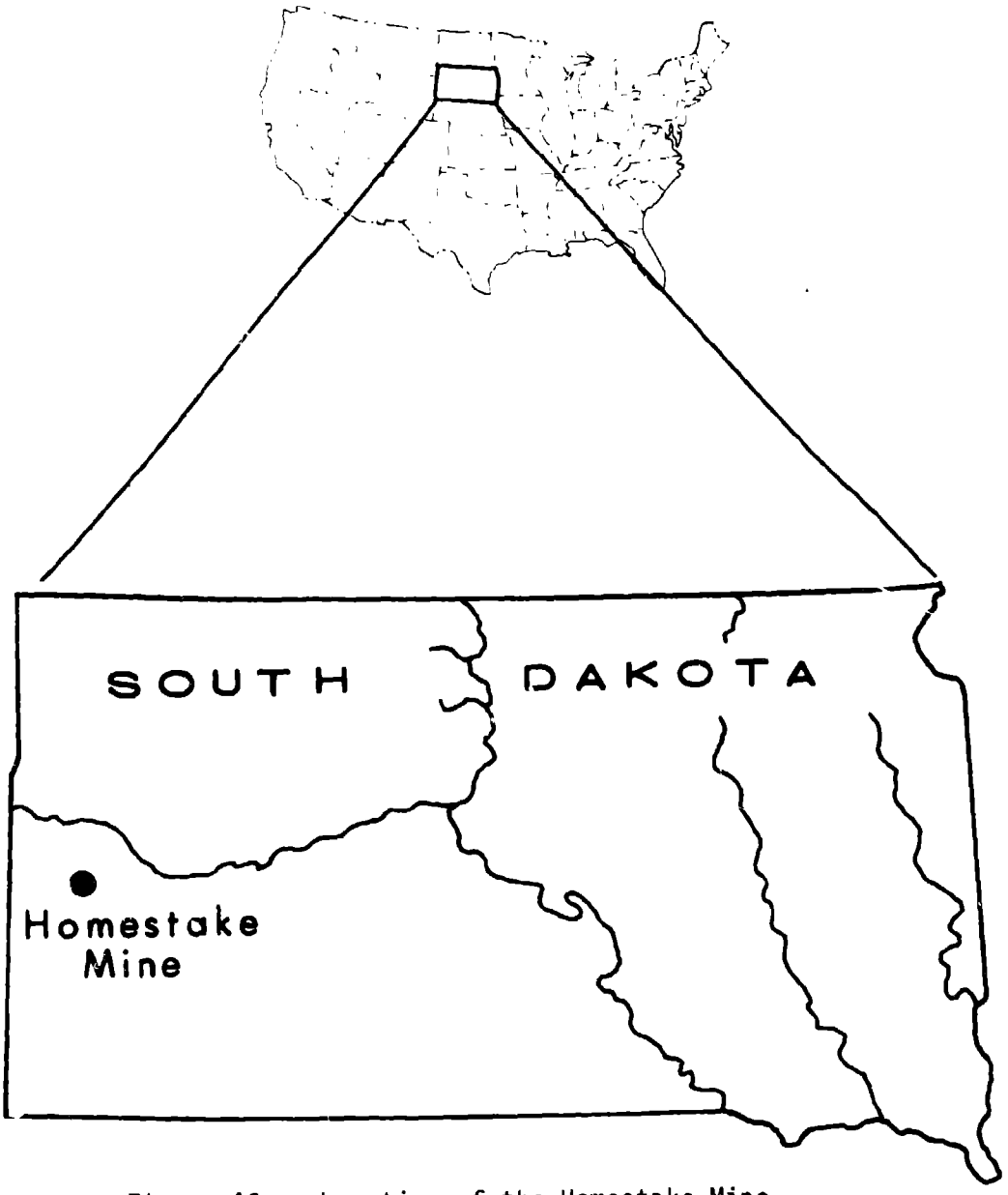

Figure 46. - Location of the Homestake Mine.

FIELD INSTRUMENTATON AND MINE MEASUREMENTS

The objectives of the field instrumentation and mine measurements program were to determine the study stope response to mining. Two types of instrumentation were used for monitoring, rod extensometers and vibrating wire stress change gages. Nineteen instrumentation holes were drilled in the foot and hanging wall areas of the study stope. All holes were percussion machine drill holes. Total footage is approximately 1,200 ft.

Instrumentation Layout

The study stope region involves three panels between the 6950 and 7100 Levels of the mine (Mine designation is 48-51SAB, 21L, 7100). Panels 2 and 3 were instrumented with four extensometers in the immediate hanging wall, one extensometer into the remote hanging wall, one footwall extensometer and one stress gage hole in the wall of the cable bolt drift. Panel 4 is a smaller panel; two less extensometer holes were used in this Panel. The instrumentation of the hanging wall was possible because of a cable bolt drift in the hanging wall. This was quite fortunate for rock mechanics study purposes because ordinarily the hanging wall region, although of great interest, is not readily accessible. Figures 47, 48 and 49 show the instrumentation layout.

Figure 47 is a vertical section perpendicular to the strike of the ore zone taken through the center of the study stope region (which is also the center of Panel 3). Holes 6, 7, 8 and 9 are down holes and contain three-point, grouted anchor extensometers. Hole attitude was specified so as to place the deepest anchor near the hanging wall of the future VCR stope at roughly one-third and two-thirds the distance between levels. The middle anchor and anchor nearest the hole collar were equally spaced also in order to divide the hole length into three equidistant segments. Hole 10 is an uphole and contains a snap ring anchored extensometer located in the remote hanging wall. Hole 15 is also an uphole and contains a snap ring extensometer for monitoring the footwall. Hole 18 is a short eight-foot hole located in the wall of the cable bolt drift. Hole 18 contains a three-gage array of vibrating wire stress gages intended to monitor the stress change in the pillar between top sill and cable bolt drift. All extensometer holes were 3 inches in diameter. Stress gage holes were 2 1/4 in. in diameter. This pattern was essentially repeated in Panels 2 and 4, although two less extensometers were installed in the latter Panel. Hole 14 is short and contains a two-point rather than a three-point extensometer.

Figure 48 shows the top sill or drill level development on the 6950 Level and the instrumentation installed from the cable bolt drift on the same Level. Seventeen of the 19 instrumentation holes were installed here.

Figure 49 shows the bottom sill or extraction level development and location of the two footwall extensometer holes. These extensometers were the snap ring anchor type.

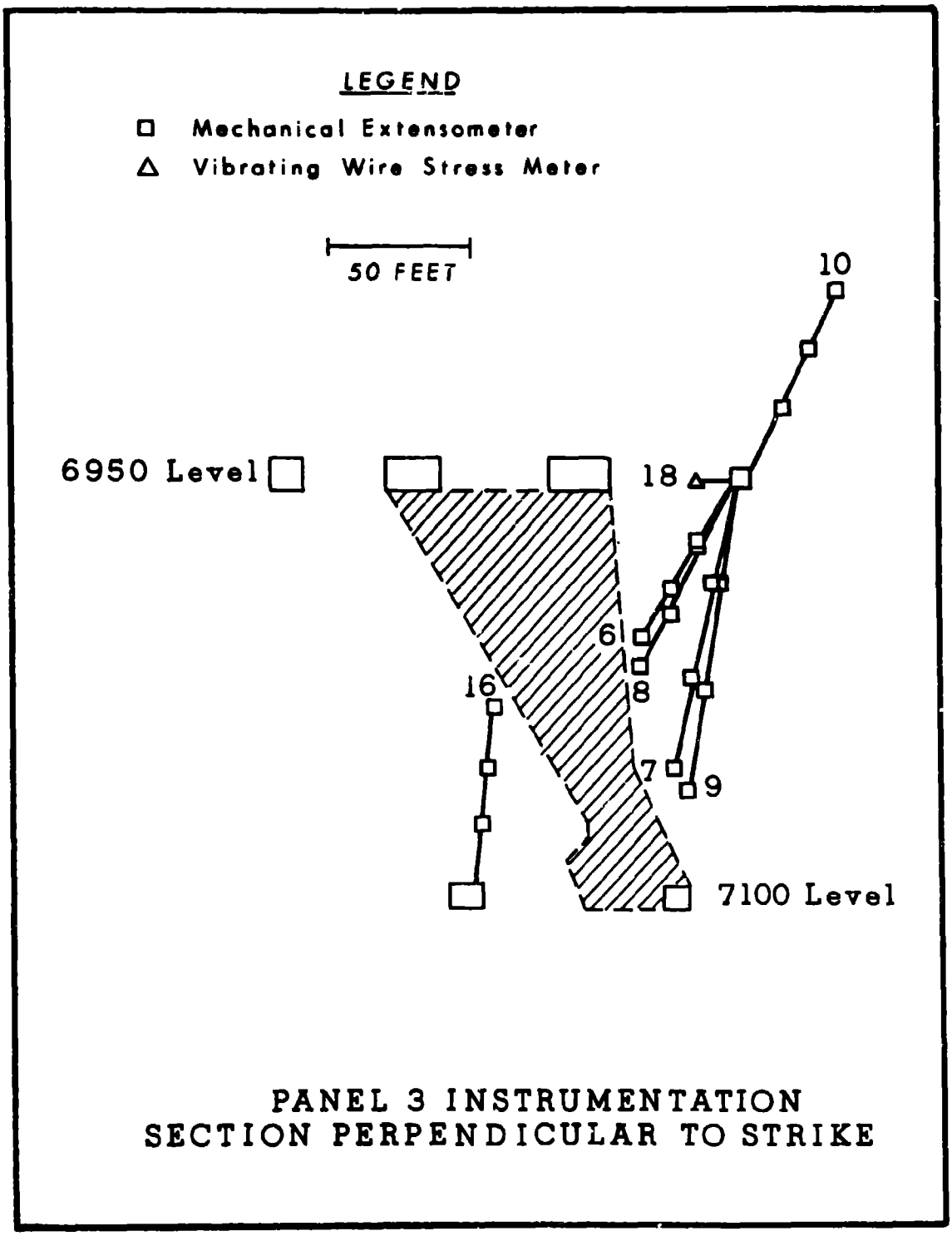

Figure 47. - Vertical section showing instrument layout.

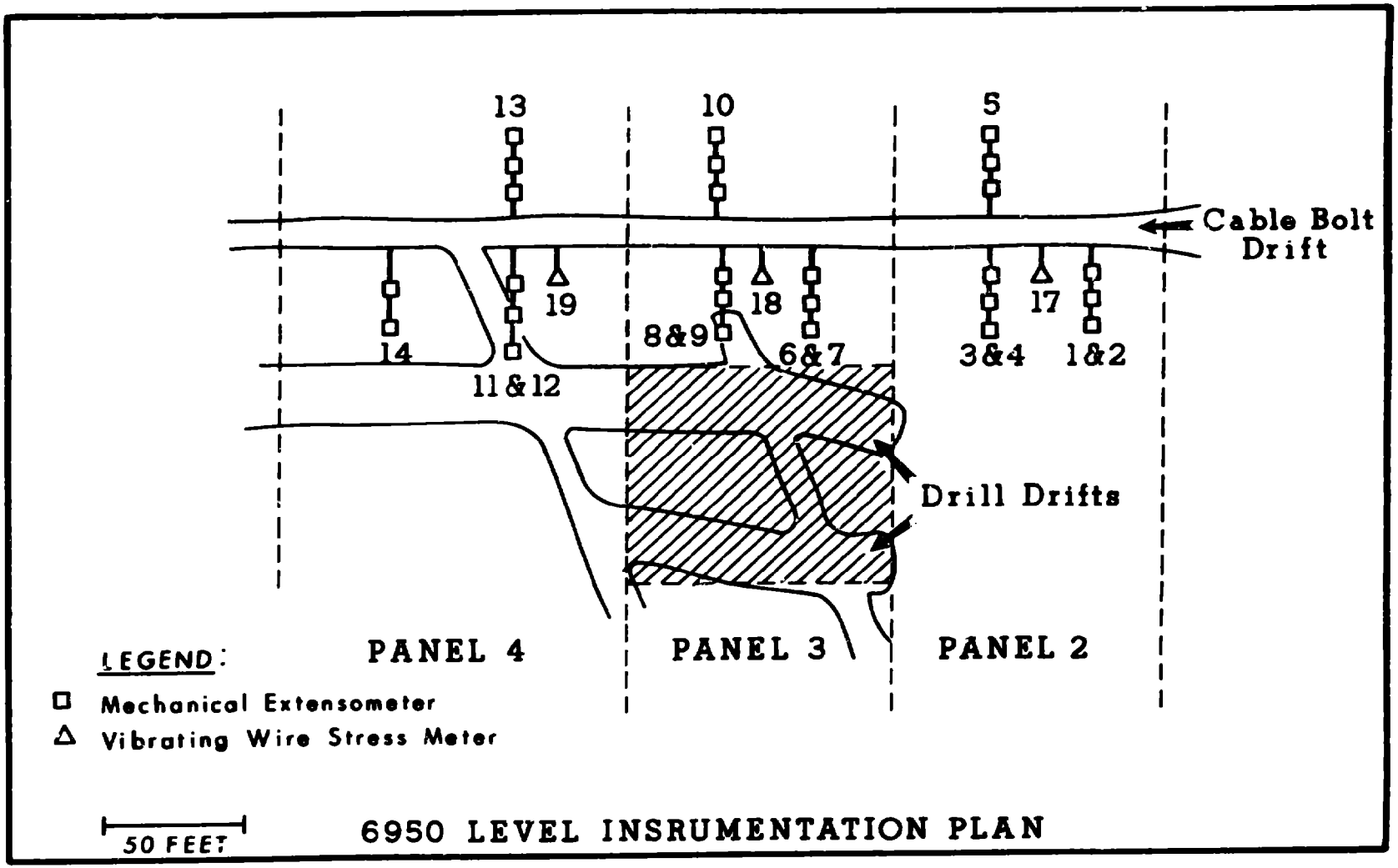

Figure 48. - Plan view of top sill (drill level) instrument layout.

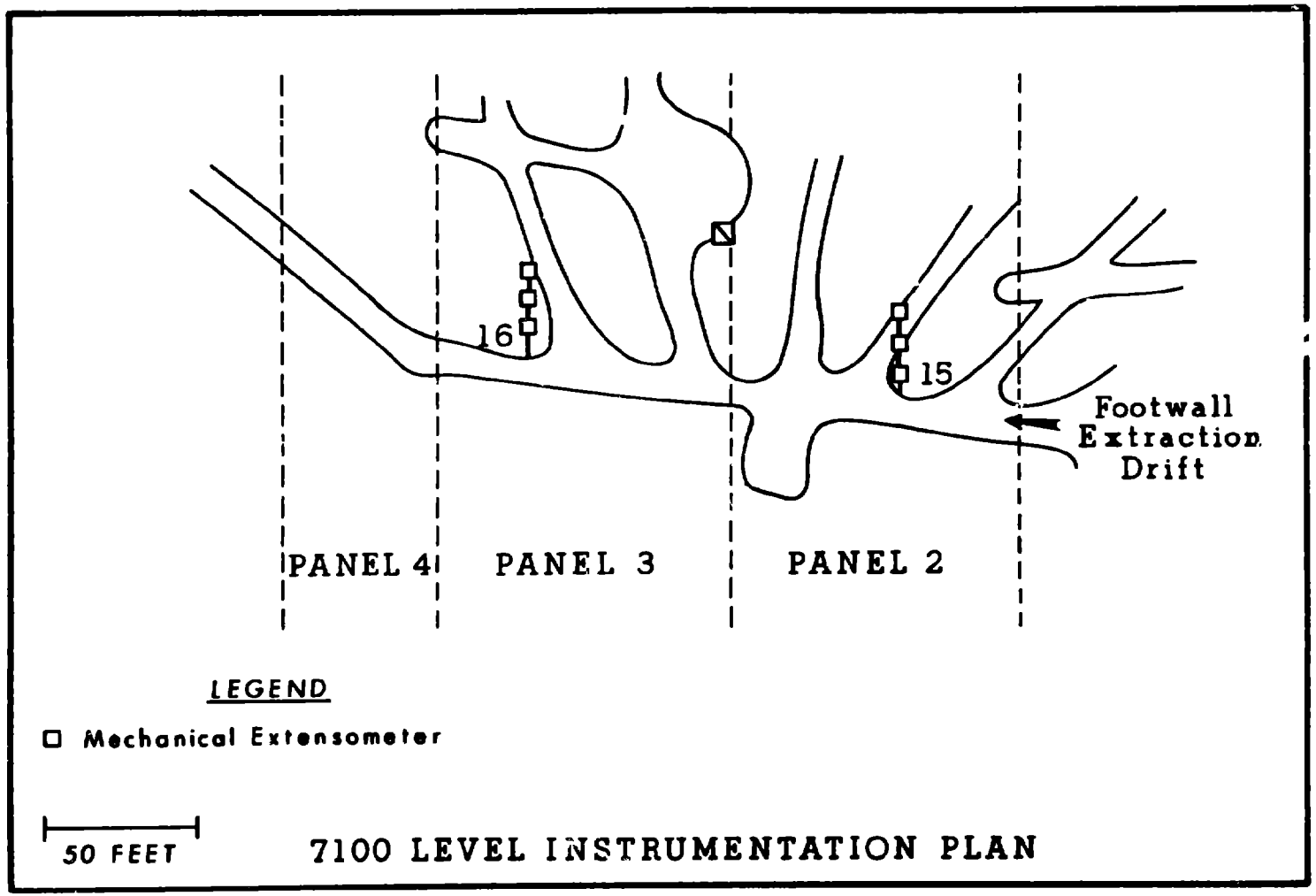

Figure 49. - Plan view of bottom sill instrument layout.

Data Handling

All data were collected manually. Extensometers were read with a dial gage, while the vibrating wire stress gages were read by the meter for these gages. (The reading is essentially the period of vibration of the wire within the gage.) No data loggers or automatic data acquisition system was used. Concentration of 17 of 19 instrumentation heads over a distance of approximately 175 ft within the cable bolt drift made manual reading practical.

All instrumentation was installed well in advance of ring blasting and VCR production blasting. Once installed, the reading schedule varied according to mining activity. Generally readings were obtained immediately before and after blasting and between blasts when time and ventilation permitted.

All readings were entered onto a data sheet with provision for appropriate notes as to size of the blast and so forth. This allowed for an immediate comparison with previous reading and provided a check on the procedure as well as an indication of any increase in hanging wall activity.

Data sheet information was subsequently hard copied and then entered into computer files at the University of Utah in much the same way as Carr Fork Mine data. Plots of displacement versus time and stress change versus time were periodically run from these files. The four hanging wall holes (H-6,7,8,9) between stope hanging wall and cable bolt drift above Panel 3 provided the bulk of the data.

Chronology

Installation of the downhole grouted anchor extensometers began Wednesday, October 26, 1983. Six extensometers were installed in three days by a mixed crew of University of Utah and Homestake Mining Company personnel. The following week, eight additional extensometers were installed. Holes 1-14 were now completed. Installation of the nine vibrating wire stress gages that constitute the three three-gage arrays in Holes 17, 18 and 19 began November 29. These holes and the two footwall extensometer holes were completed December 1, 1983. Ring drilling and blasting for Panel 3 began in March 1984. VCR blasting began in June and was completed in October 1984. The chronology is given in Table 12.

TABLE 12. - Homestake Mine study stope chronology

Activity	Month/Year
Instrumentation	Oct. - Nov. 1983
Ring drilling Panel 3	March 1984
VCR blasting begins	June 1984
Crown pillar (east)	August 1984
Crown pillar (west)	Oct. 1984
Began filling	Jan. 1985

Study Stope Response

The measured response of the study stope at the Homestake Mine is embodied primarily in the hanging wall extensometer readings obtained during mining of Panel 3. Footwall extensometers and vibrating wire stress gages also contribute to the measured stope response but to a much lesser degree.

Panel 2 and Panel 4 are unmined at present. Panel 2 is in fact a pillar formed by mining Panels 1 and 3 on either side. Panel 4 is an end Panel and forms the north rib of mined Panel 3. Panel 2 forms the south rib. All instrumentation was installed well in advance of mining, so that a baseline for each extensometer anchor and stress gage was established prior to ring and VCR blasting in Panel 3.

A complete 500-day history of the remote hanging wall extensometer (H 10) is shown in Figure 50. A positive displacement in Figure 50 indicates an increase in distance between anchor point and the reference plate at the hole collar. The response of the remote hanging wall to VCR mining of Panel 3 is small until the first crown pillar blast (East) when a large increase was observed. After the second crown pillar blast (West), the remote hanging showed very little additional movement. The maximum relative displacement in the remote hanging wall over the entire period of observation is less than 0.18 in.

The immediate hanging wall response to mining Panel 3 is shown in Figures 51, 52, 53, 54. These Figures are the extensometer histories of Holes 6, 7, 8 and 9 from a period just after ring drilling and blasting through VCR production blasting and crown pillar removal. The response of the immediate hanging wall shows a strong association with blasting. Indeed, some anchor loss occurs with mining and slough of the hanging wall. As the stope is enlarged from bottom to top, anchor movement increases significantly, but with continued retreat, subsequent anchor movement diminishes as shown, for example, by Anchor 1 in Hole 7, Figure 52.

Anchor loss does not appear to be associated with a specified amount of displacement as seen, for example, in the history of Hole 6, Figure 51. A displacement failure criterion is thus not justified. The greatest relative displacement in the immediate hanging wall before anchor loss is approximately 0.9 in. One anchor has survived beyond 0.9 in. relative displacement, but a number of anchors were lost at much smaller displacements.

The footwall extensometer for Panel 3 is Hole 15. A three-point snap ring extensometer is installed in this hole. Its response appears unreliable because of erratic readings, the lack of a consistent pattern between anchors and difficulty during installation.

Hole 18 contains a three-gage array of vibrating wire stress gages installed at 0, 45 and 90 degrees to the horizontal in a short hole collared in the cable bolts drift. Figure 55 shows the stress changes calculated from Hole 18 data. Tension is positive in Figure 55; a change of + 1000 psi means, for example, that an original compression of

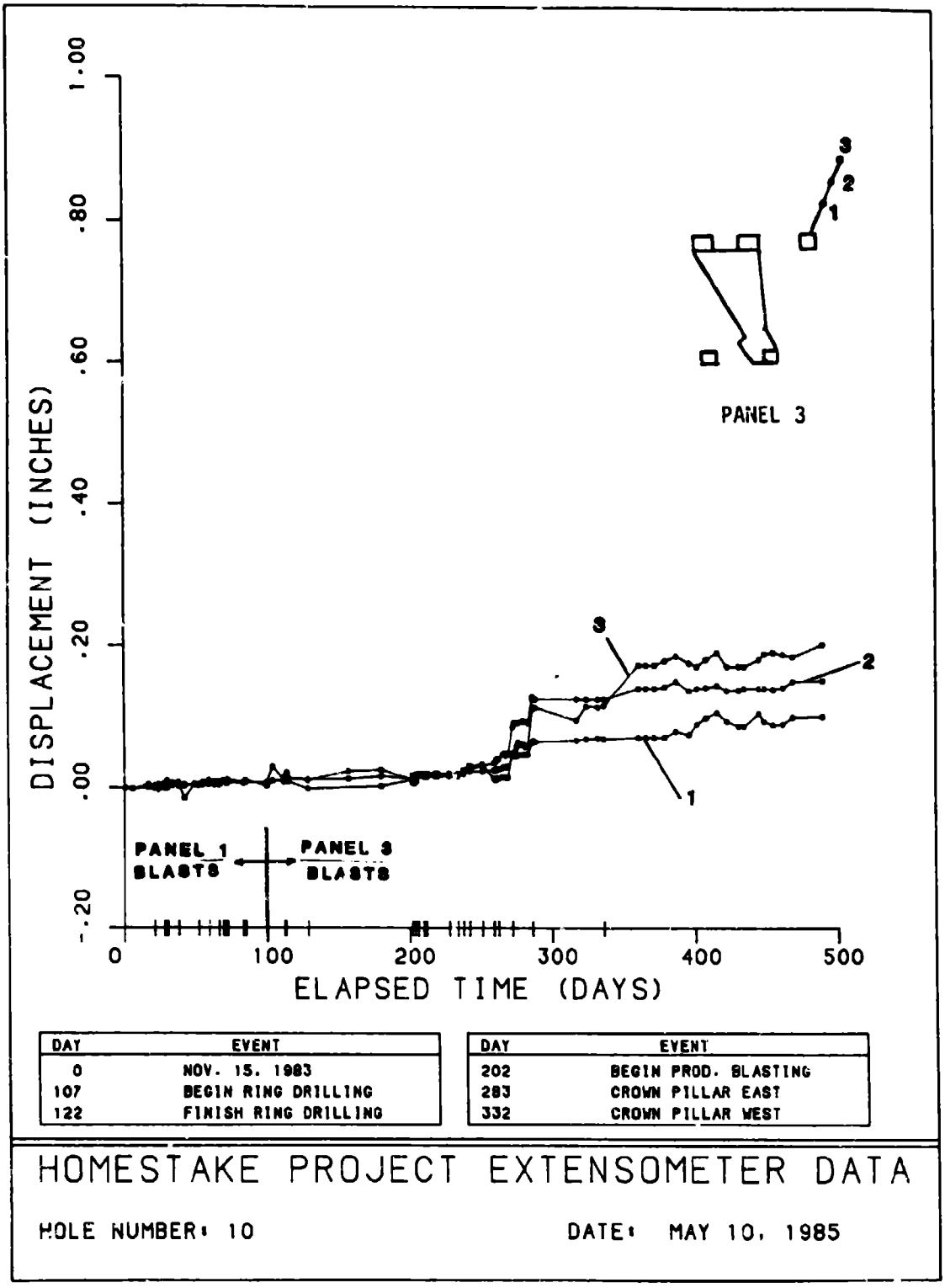

Figure 50. - Remote hanging wall 500-day history.

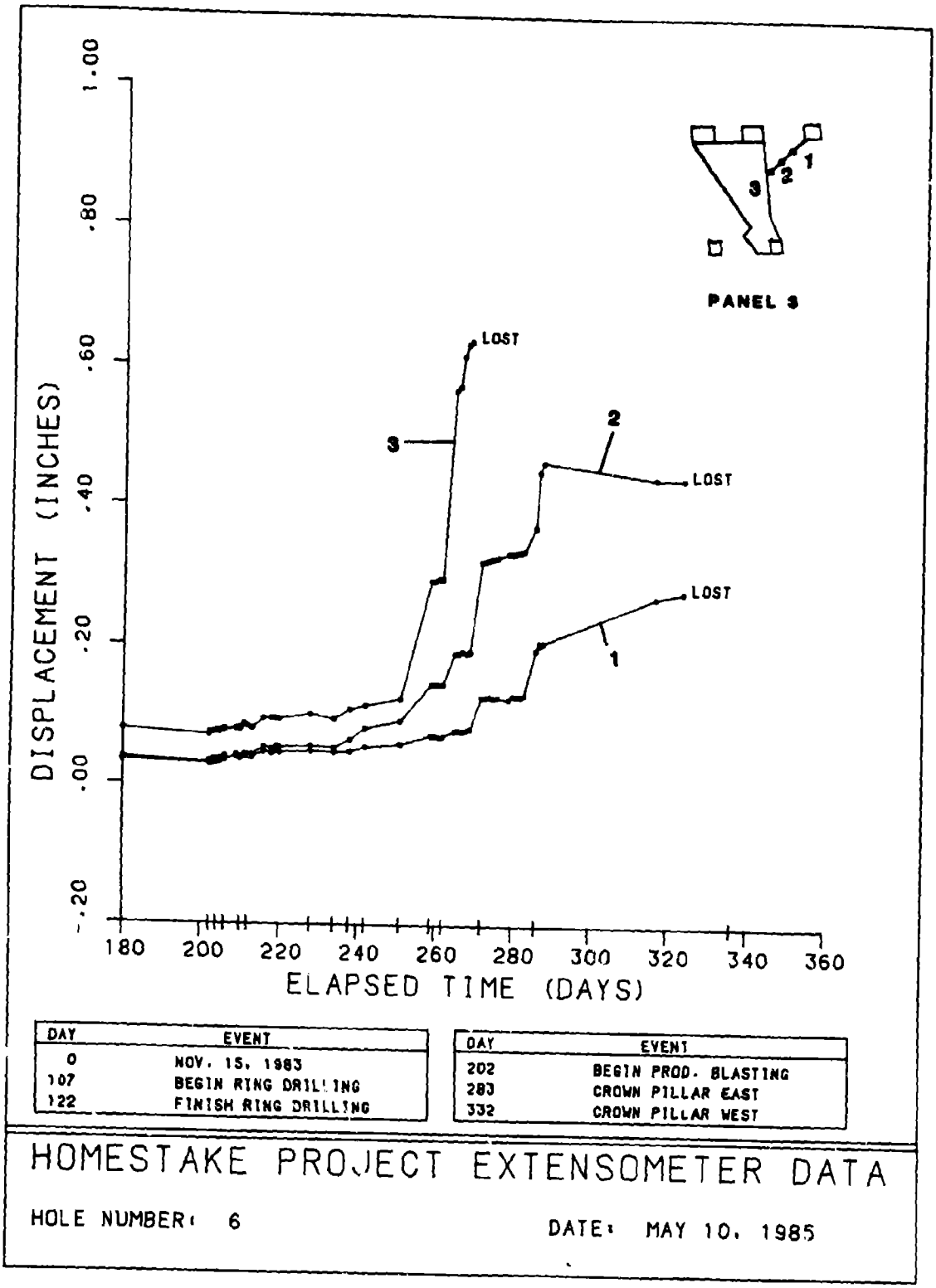

Figure 51. - Hole 6. Panel 3. Immediate hanging wall.

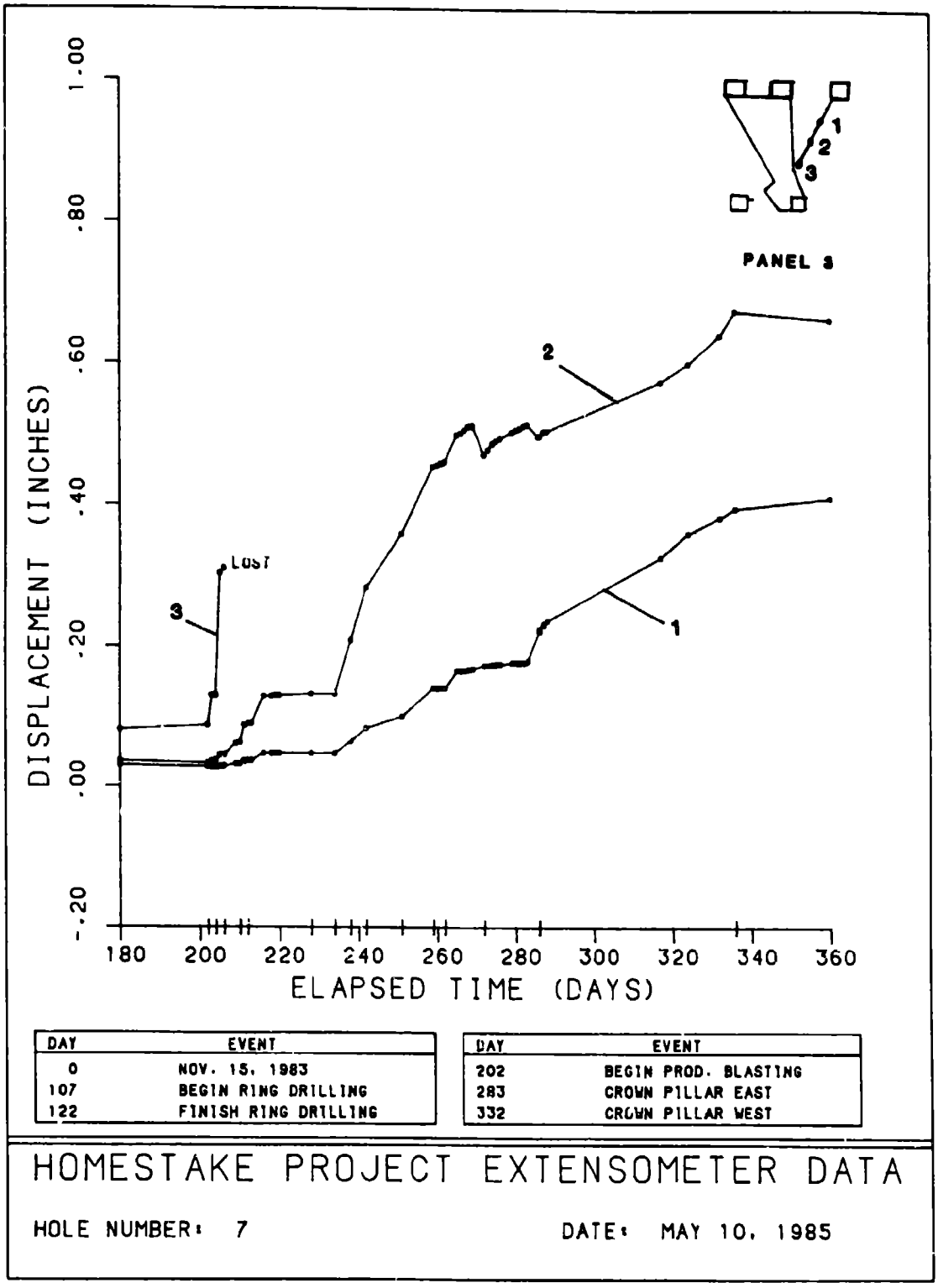

Figure 52. - Hole 7. Panel 3. Immediate hanging wall.

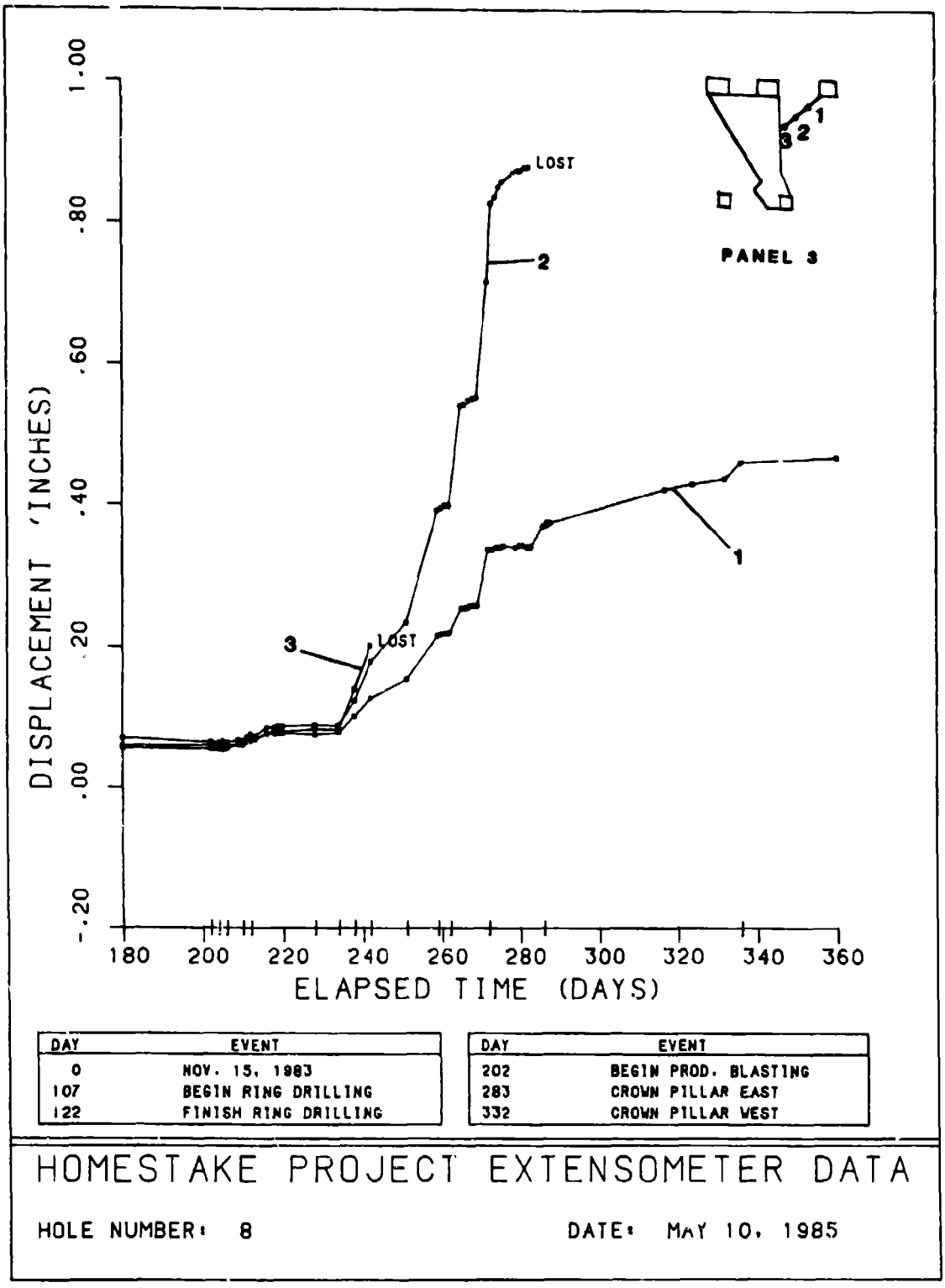

Figure 53. - Hole 8. Panel 3. Immediate Hanging wall.

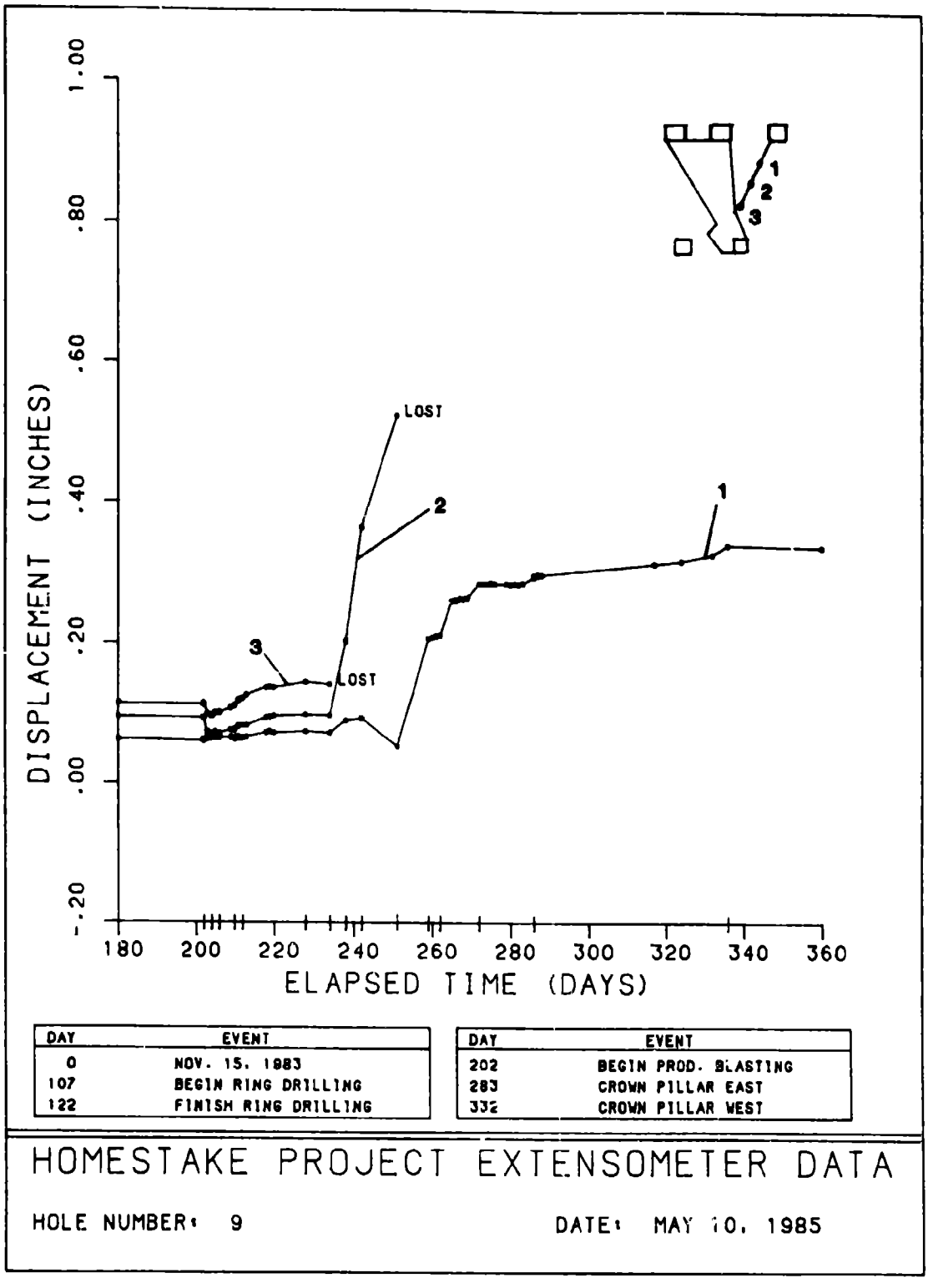

Figure 54. - Hole 9. Panel 3. Immediate hanging wall.

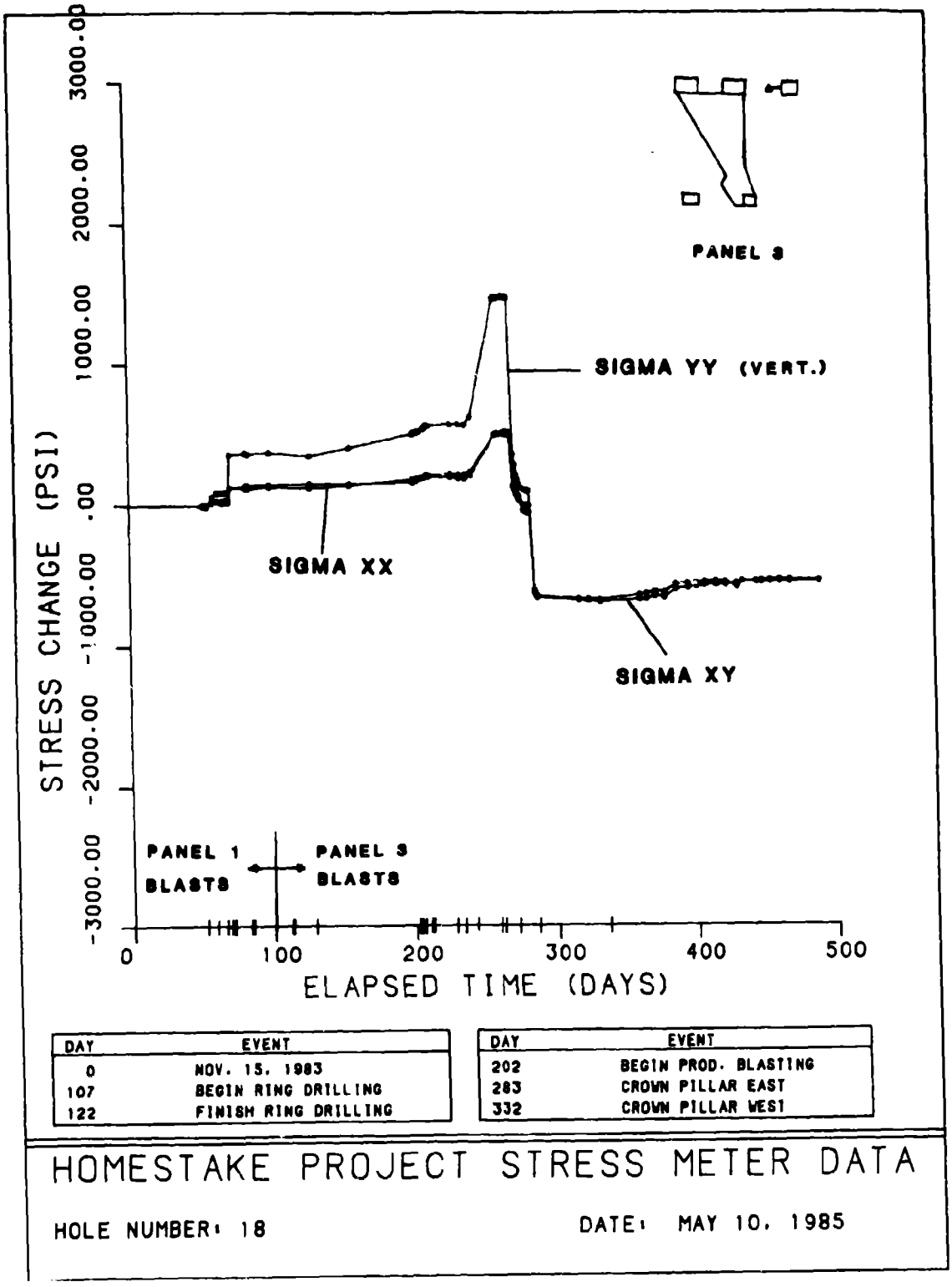

Figure 55. - Hole 18. Vibrating wire stress gage data.

- 9,000 psi is now - 8,000 psi as seen in a plane perpendicular to the hole axis. Figure 55 indicates a decrease in vertical compression in the cable bolt rib (between stope and cable bolt drift) until removal of the crown pillars when a sizeable recompression occurs.

Summary

An instrumentation layout consisting of 19 boreholes containing multi-anchor extensometers and vibrating wire stress gages in the foot- and hanging walls of a three-panel study stope has led to a data base of displacements and stress changes that quantify the study stope response to VCR mining. Installation was completed in late 1983 after preliminary development but well in advance of ring drilling and subsequent production blasting, which began in March and June, 1984, respectively. A reliable baseline was therefore established for each measurement point (extensometer anchor, vibrating wire stress gage). Installation went smoothly and rapidly without unexpected delays. Concentration of much of the layout in the cable bolt drift was quite fortunate in this regard. Cooperation with mine personnel was excellent.

The mined panel (Panel 3) is the central panel of a three-panel region (48-51SAB, 21 Ledge, 7100 Level) and is about approximately 60 ft wide by 90 ft long (on strike) and 150 ft high. At 12 cu ft/ton, Panel 3 would contain about 65,000 tons of ore. These numbers are rough estimates and are only intended to give one a "feel" for the size of the study region. By comparison, the measured tonnage mucked from the Carr Fork Mine test stope is about 30,000 tons.

Inspection of the plots of displacement and stress change versus time show a step-like response that is highly correlated with blasting event and size. Closer examination of the data shows too that proximity of the blast (VCR lift) to an anchor point is also important in determining the step size. There is motion between blasts, and some motion after the last blast. However, the instantaneous motion with blasting and enlargement of the stope accounts for most of the observed changes in instrument readings. Observed relative displacements were generally less than 0.9 inches.

The majority of extensometer anchors in the immediate hanging wall of the mined panel (Panel 3) were lost in the course of mining. Four out of the original 12 survived. All deep anchors (number 3) nearest the stope hanging wall and with one exception all intermediate anchors (number 2) were lost in the immediate hanging wall during mining. Loss of grouted anchors in the immediate hanging wall is indicative of slough or overbreak.

The remote hanging wall extensometer for Panel 3 survives, while the footwall extensometer is a practical loss. The vibrating wire stress gage array in the rib of the cable bolt drift remains readable, but some doubt exists as to its reliability. In this regard, it may be that the wedge anchoring of the stress gages and the snap ring anchored extensometers are not secure enough to survive in a blasting environment. However, the grouted anchor extensometers performed well.

All instrumentation in Panels 2 and 4 is active. Panel 2 instrumentation gives a pillar history formed by mining first Panel 1 on the south side and then Panel 3 on the north side. Panel 4 instrumentation records a partial pillar history formed by mining Panel 3 on the south side.

The data obtained from the instrumentation in Panel 3 is amenable to comparison with finite element analysis of the study stope response to mining. In this regard, although some hanging wall slough is indicated, the study stope region remained stable throughout the period of investigation. Both the quality and the quantity of the mine measurements are adequate for direct comparison with finite element calculations of study stope deformation and slough or yield.

IN SITU STRESS MEASUREMENTS AND ROCK PROPERTIES

The prestope or in situ stresses are in fact the "applied loads" for analysis of stress about the study stope. These data in addition to the rock properties, namely, the elastic moduli and strengths, are essential physical information for the evaluation of safety and stability. Laboratory values of rock properties used in the initial analysis of the study stope response are subsequently scaled to represent rock mass properties. The in situ stress state is determined from consideration of all measurements.

In Situ Stress Measurements

In situ stress measurements at the Homestake Mine have been reported by Bond (1970) on the 6200 Level and by Hooker (1972) on the 3050 and 6200 Levels. Results of in situ stress measurements on the 7400 Level by the Spokane Research Center of the U. S. Bureau of Mines are in rough agreement with values extrapolated from the earlier data as shown in Table 13. The *changes* in stresses with depth according to the former measurements are close to gravity gradients, while the actual horizontal stresses are higher than the gravity components.

The principal stress data presented in Table 13 are in rough agreement with respect to magnitude. However, the recent data from measurements on the 7400 Level differ noticeably from earlier measurements with respect to direction. The early measurements show principal directions aligned with the vertical, parallel to strike and perpendicular to strike. The last set of measurements (7400 Level) show directions that are skewed with respect to the vertical or gravity axis and with respect to local structure.

The difference between the former and last set of measurements is mainly in the presence of vertical shear stresses in the last set of data. Table 13 shows that the magnitudes of the normal stresses relative to coordinate axes parallel and perpendicular to strike, that is, the vein stresses, are comparable. The normal stress parallel to strike is consistently less than the normal stress perpendicular to strike on all levels. On the 7400 Level the normal stresses parallel and perpendicular to strike are 4,200 and 5,500 psi, respectively. The vertical stress from the earlier measurements follows a gravity gradient between 1.0 and 1.3 psi per foot depth. No vertical shear stress is present in these data. However, the last data set (7400 Level) shows sizeable vertical shear stresses. These stresses considerably reduce the vertical normal stress required for equilibrium. Without the vertical shear stresses, the vertical normal stress on the 7400 Level would be 8,226 psi which corresponds to a gravity gradient of about 1.1 psi per foot of depth. This is comparable to the gravity gradients obtained in the earlier measurements.

TABLE 13. - In situ stress measurements

Principal stresses and direction

Source	Stress*	Magnitude	Bearing	Dip**
Bond (1970)	Major	8,000 psi	--	vertical
6200 Level	Intermediate	5,200	N50E	0
	Minor	2,900	N40W	0
Hooker (1972)	Major	3,051	--	vertical
3050 Level	Intermediate	3,687	N43E	0
	Minor	1,845	N47W	0
6200 Level	Major	7,720	--	vertical
	Intermediate	5,349	N30E	0
	Minor	3,624	N60W	0
USBM (1984)**	Major	7,985	N83W	53°
7400 Level	Intermediate	3,411	N08W	71°
	Minor	1,927	N61E	43°

Vein Stresses

Source	Dip Direction		Strike Direction		Vertical	Vertical Shear	Vein Shear
Hooker							
(3050 L)	N43E	3,687 psi	N47W	1,845 psi	3,051 psi	0/0	0
(6200 L)	N30E	5,349	N60W	3,624	7,720	0/0	0
Bond							
(6200 L)	N50E	5,200	N40W	2,900	8,000	0/0	0
USBM							
(7400 L)	N45E	5,496	N45W	4,220	4,237	1925/2064	938

*compression positive
**down positive

The 7400 Level stress measurements involved new equipment and a new three-dimensional stress gage, the CSIRO HI cell. Data from five HI-cell gages were screened for reliability. The screening process included consideration of temperatures that were recorded during overcoring operation. The screened data were subsequently reduced at the Spokane Research Center and independently with a different computer program at the University of Utah. Results are identical, so that the data reduction process appears reliable. The 7400 Level data has the relative advantage of being close to the study stope (6950-7100 Levels). However, the earlier data sets obtained by Bond and Hooker are consistent and provide a check of one set on the other. No check is available for the 7400 Level data.

For these reasons, the vertical shear stresses were ignored. The vertical normal stress was set according to a conservative gravity gradient of 1.25 psi per foot of depth. Thus, the in situ stresses are given by

$$\begin{aligned} \sigma_v &= 1.25\ h && \text{(vertical)} \\ \sigma_{h1} &= 2078 + 0.53\ h && \text{(dip direction)} \\ \sigma_{h2} &= 121 + 0.55\ h && \text{(strike direction)} \end{aligned} \qquad (1)$$

where h = depth in feet and stresses are in psi. The dip and strike directions are azimuths, that is, horizontal directions. At a depth of 7025 ft to the center of the study stope, the stresses are

$$\begin{aligned} \sigma_v &= 8{,}781 \text{ psi} && \text{(vertical)} \\ \sigma_{h1} &= 5{,}801 \text{ psi} && \text{(dip direction)} \\ \sigma_{h2} &= 3{,}985 \text{ psi} && \text{(strike direction)} \end{aligned} \qquad (2)$$

Laboratory Rock Properties

Drill core for laboratory rock properties testing were obtained in three directions from the Poorman, Homestake and Ellison formations. These core were supplied to the Department of Mining Engineering at the South Dakota School of Mines and Technology (SDSMT) for testing. A small sampling of these core were supplied to the Department of Mining Engineering at the University of Utah. The immediate objective of the laboratory test program was to determine Young's modulus, Poisson's ratio, uniaxial compressive strength and tensile strength in three mutually orthogonal directions in each of the three formations. The goal was to determine the elastic and strength properties necessary to define an orthotropic material model of the three formations present in the study stope region. The well developed foliation in the Poorman formation and to a lesser degree in the Ellison and Homestake formations strongly suggested the need for an anisotropic material model. Complex folding suggested that an orthotropic rather than the simpler transversely isotropic model would be needed to account for the directional character of the formations. Drill hole orientations were parallel to

the down dip direction, perpendicular to the foliation and parallel to strike. These three mutually orthogonal directions were intended to follow the principal material axes and are referred to as the 1-, 2- and 3-directions

A compromise in the costs and benefits of laboratory testing was made at the outset. The compromise involved a partial rather than a complete determination of the orthotropic material model. Shear properties would be estimated rather than measured. In the isotropic case, the shear modulus and strength can be estimated from Young's modulus, Poisson's ratio, compressive strength and tensile strength. In the anisotropic case, the shear properties are independent parameters. This is an important point as subsequent results show. However, testing for shear properties using conventional laboratory testing machines would substantially increase costs. Additional laboratory testing and additional drill holes would be needed.

However, a rather involved analysis of some laboratory test data allowed for the estimation of shear properties in the Poorman formation which exhibits the greatest development of schistosity. This analysis provided guidance for estimating the shear properties of the Homestake and Ellison formations. In this regard, the Poorman formation shows the greatest differences in Young's moduli and Poisson's ratios; the largest modulus ratio is about 2. The Homestake formation shows the greatest difference in compressive strengths, while the Ellison formation shows the greatest tensile strength difference. The largest compressive strength ratio is about 2; the largest tensile strength ratio is about 3.

SDSMT Data

Laboratory rock properties tests results obtained at SDSMT (Hladyz and Erickson, 1984) are summarized in Table 14. Values in Table 14 are mean values. The shear properties in Table 14 are estimated from the isotropic-like relations:

$$G_{ij} = E_i/2(1 + \nu_{ij}) \quad (3)$$

and

$$R_i = \sqrt{C_i T_i/3} \quad (4)$$

using the mean values in Table 14. These relations are not unique, but do reduce to the isotropic case with vanishing anisotropy. The shear strengths given by Eqn. 4 follow from the yield condition adopted in subsequent analyses (Pariseau, 1972).

TABLE 14 - Original SDSMT anisotropic rock properties

Property*	Homestake Formation	Poorman Formation	Ellison Formation
E_1	12.7×10^6	13.5×10^6	12.7×10^6
E_2	6.0×10^6	7.2×10^6	9.1×10^6
E_3	9.0×10^6	13.7×10^6	11.0×10^6
ν_{12}	0.18	0.15	0.16
ν_{23}	0.18	0.29	0.17
ν_{31}	0.19	0.22	0.15
G_{12}	5.4×10^6	5.9×10^6	5.5×10^6
G_{23}	2.6×10^6	2.8×10^6	3.9×10^6
G_{31}	3.9×10^6	5.6×10^6	4.8×10^6
C_1	17,100	10,810	12,560
C_2	11,550	8,802	11,340
C_3	14,260	11,400	12,040
T_1	1,378	1,731	1,971
T_2	1,139	994	588
T_3	1,293	2,036	1,699
R_1	2,803	2,497	2,873
R_2	2,094	1,708	1,491
R_3	2,479	2,782	2,611

*The 1- and 3-directions are parallel to the schistosity; the 2-direction is perpendicular to the schistosity. All units are psi (except for Poisson's ratios.

Examination of the SDSMT test data showed large coefficients of variations (standard deviation expressed as a fraction of the mean). In some cases, the scatter suggested bimodal distributions. Removal of outliers in the strength data greatly reduced the scatter and resulted in a modified set of SDSMT rock strength properties. Shear strength properties were again computed from the isotropic relations (Eq. 3a,b). The modified SDSMT laboratories' properties are summarized in Table 15. The modification process is shown in detail in Tables 16, 17, 18 for the Homestake, Poorman and Ellison formations, respectively. The modification process of discarding outliers or extreme values was continued until the coefficient of variation decreased to approximately 30%. In most cases, discarding obviously strange data resulted in an even lower coefficient of variation. An example is seen in Table 17 where discarding two very low values of compressive strength in the 1-direction reduced the coefficient of variation from 58% to 28%. The mean changed from 10,800 to 13,700 psi. The new strength means are viewed as more representative of the sample population. Elastic moduli were not modified at this stage because of the few samples (three) used for each Young's modulus determination.

TABLE 15. - Modified SDSMT rock strength properties

Property*	Homestake Formation	Poorman Formation	Ellison Formation
C_1	20,146	13,674	11,342
C_2	11,547	10,000	11,414
C_3	13,267	12,265	8,155
T_1	1,378	1,731	2,378
T_2	1,139	820	588
T_3	1,293	2,423	1,880
R_1	3,042	2,808	2,998
R_2	2,093	1,653	1,496
R_3	2,391	3,147	2,260

*The 1- and 3-directions are parallel to the schisosity; the 2-direction is perpendicular to the schistosity. All units are psi.

TABLE 16. - Homestake strength modification process

Strength	No.	Dir.	Value	Original $\bar{X}$	Original s_x	Original C.V.%	Modified $\bar{X}$	Modified s_x	Modified C.V.%
			2,418*						
			9,662						
			9,977						
			16,174						
	8	3	17,224	14,257	6,908	48	13,267	3,462	26.1
			22,913*						
			13,297						
			22,388*						
			7,285*						
			22,362						
			8,674*						
			20,034						
C_o	8	1	20,367	17,102	7,394	43	20,146	5,647	28
			23,446						
			9,324						
			25,329						
			7,830						
			11,448						
			12,232						
			8,374						
	9	2	11,681	11,547	3,311	29	11,547	3,311	29
			17,882						
			8,485						
			10,843						
			15,170						
			1,593						
			1,398						
	5	3	1,414	1,293	250	19	1,293	250	19
			949						
			1,385						
			1,282						
			765						
T_o			1,379						
	6	1	1,056	1,378	479	32	1,378	479	32
			1,943						
			1,343						
			1,050						
			911						
	5	2	761	1,139	340	30	1,139	340	30
			1,398						
			1,576						

* = discarded outlier
$\bar{X}$ = mean
s_x = standard deviation
C.V.% = coefficient of variation
C_o = uniaxial compressive strength
T_o = uniaxial tensile strength

TABLE 17. - Poorman strength modification process

Strength	No.	Dir.	Value	Original $\bar{X}$	Original s_x	Original C.V.%	Modified $\bar{X}$	Modified s_x	Modified C.V.%
			14,680						
			8,238*						
			5,336*						
			11,301						
	8	3	11,714	11,402	3,850	34	12,265	3,214	26.2
			9,476						
			12,632						
			17,815						
			1,386*						
			3,022*						
			15,699						
			12,741						
C_o	8	1	8,442	10,807	6,242	58	13,674	3,848	28.1
			13,602						
			19,830						
			11,732						
			11,033						
			9,933						
			7,791*						
			421*						
	8	2	10,733	8,802	3,684	42	10,000	1,565	15.7
			7,929						
			10,748						
			11,833						
			1,631*						
			485*						
	5	3	2,416	2,036	1,109	54	2,423	798	32.9
			3,517						
			2,129						
			2,091						
			2,224						
T_o	5	1	1,656	1,731	478	28	1,731	478	28
			1,681						
			1,000						
			677						
			519*						
			1,877*						
	6	2	1,105	994	478	48	820	226	27.6
			903						
			896						

* = discarded outlier
$\bar{X}$ = mean
s_x = standard deviation
C.V.% = coefficient of variation
C_o = uniaxial compressive strength
T_o = uniaxial tensile strength

TABLE 18. - Ellison strength modification process

Strength	No.	Dir.	Value	Original $\bar{X}$	Original s_x	Original C.V.%	Modified $\bar{X}$	Modified s_x	Modified C.V.%
	8	3	5,854 8,390 8,910 26,263* 6,034 21,146* 8,307 11,433	12,042	7,543	63	8,155	2,058	25
C_o	8	1	10,587 9,407 16,264 10,447 14,175 10,861 10,984 8,014	11,342	2,640	23	11,342	2,640	23
	8	2	10,017 14,235 9,912 12,759 10,879 10,829 11,269 20,545*	12,556	3,537	28	11,414	1,561	13.7
	5	3	1,909 2,249 2,259 973* 1,103	1,699	621	37	1,880	543	28.9
T_o	5	1	1,842 2,070 344* 2,204 3,394	1,971	1,090	55	2,378	694	29.2
	5	2	517 478 611 434 901	588	187	32	588	187	32

* = discarded outlier
$\bar{X}$ = mean
s_x = standard deviation
C.V.% = coefficient of variation
C_o = uniaxial compressive strength
T_o = uniaxial tensile strength

UU Data

Nine laboratory test specimens were prepared for testing in the University of Utah rock mechanics laboratory. Five of the samples were from the Homestake formation; two were from the Ellison formation, and two were from the Poorman formation. All samples had a height to diameter ratio close to two. Four three-strain gage rosettes (0-45-90) were attached to each specimen. Testing was done unconfined and under confining pressures of 1,000, 3,000 and 5,000 psi. An axial load axial displacement curve was recorded during each test. Both axial displacement and confining pressure were under servo-control during a test. Details concerning sample preparation, data acquisition and reduction are contained in a report by Duan (1985).

The objectives of the UU laboratory tests were:

(i) to provide a spot check on SDSMT data,
(ii) to evaluate shear moduli by testing core inclined to the foliation,
(iii) to evaluate shear strength, and
(iv) to obtain first-hand knowledge concerning the mode of failure of the laboratory test specimens.

The most important of these objectives concerned the shear properties, especially shear strength, that up to this stage were being estimated on the basis of isotropic relations which, in fact, are not unique.

The elastic properties tests results showed a linear stress-strain response in all cases for loading to approximately one-half the uniaxial compressive strength. Hysteresis under repeated loading was generally small in the Homestake formation samples as shown in Figure 56, but somewhat more noticeable in the Ellison formation samples as shown in Figure 57. The two Poorman formation samples are at an angle to the foliation and were reserved for shear modulus analysis. The results of the elastic moduli tests are summarized in Table 19.

Table 19. - UU elastic moduli test results

Sample/ Formation	Young's modulus (10^6 psi)			Poisson's ratio					
	E_1	E_2	E_3	ν_{12}	ν_{21}	ν_{23}	ν_{32}	ν_{31}	ν_{13}
1 hf	--	11.19	--	--	0.12	0.11	--	--	--
3 hf	--	9.89	--	--	0.25	0.18	--	--	--
5 hf	12.24	--	--	0.14	--	--	--	--	0.12
6 ef	--	9.55	--	--	0.08	0.14	--	--	--
7 hf	12.8	--	--	0.15	--	--	--	--	0.15
8 ef	--	9.02	--	--	0.19	0.21	--	--	--
9 hf	--	--	12.76	--	--	--	0.21	0.27	--

hf = Homestake formation
ef = Ellison formation
pmf= Poorman formation

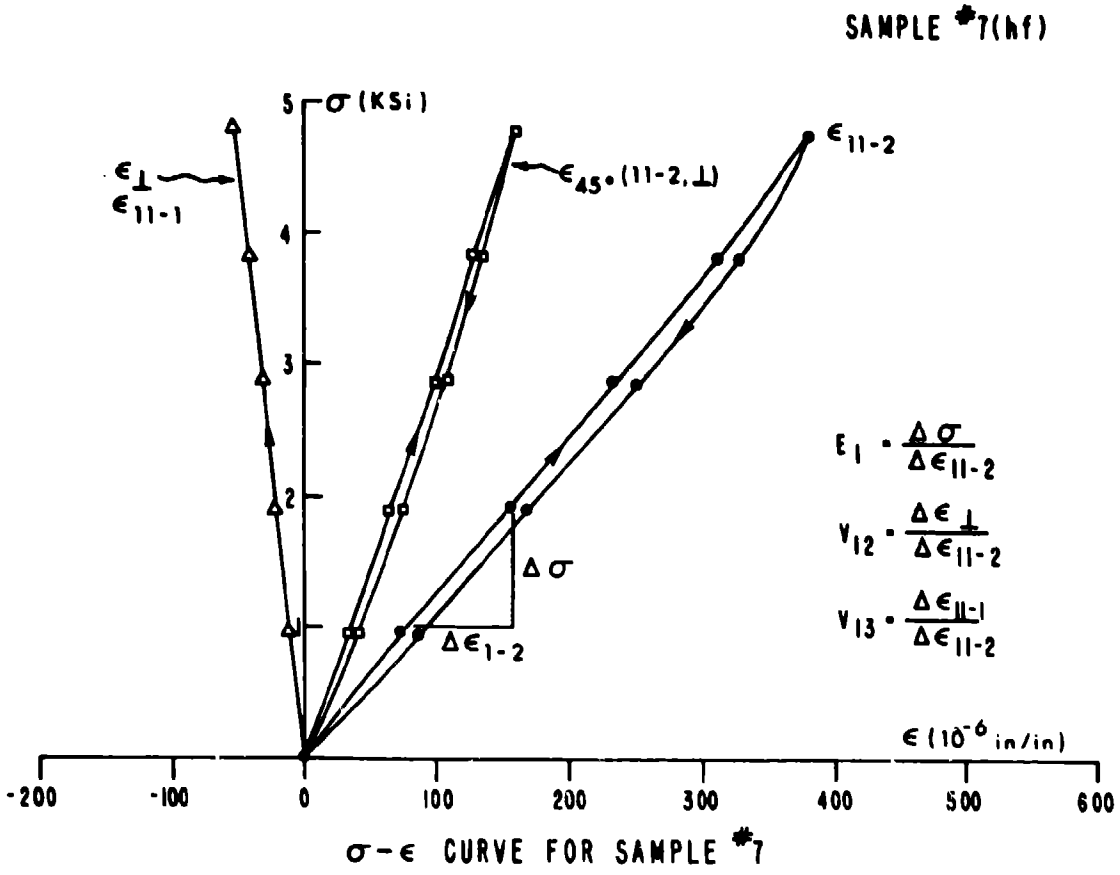

Figure 56. - Homestake formation laboratory stress strain curves.

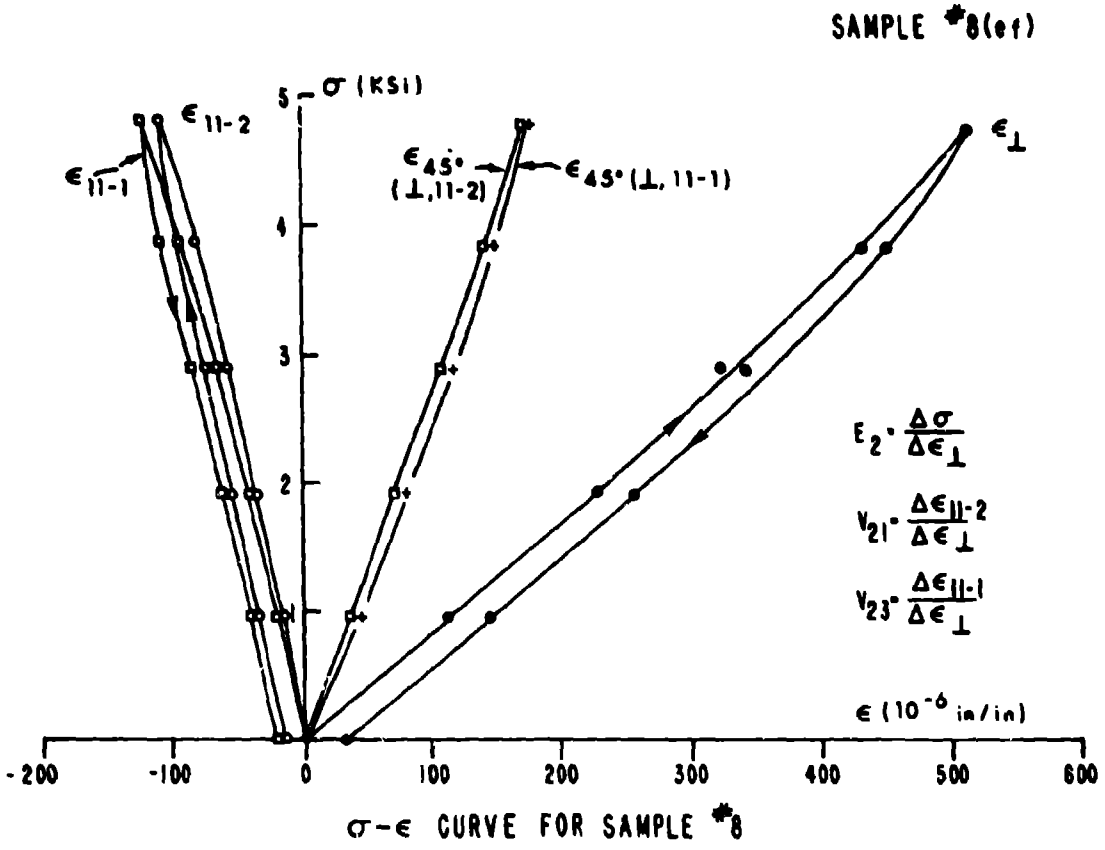

Figure 57. - Ellison formation laboratory stress strain curves.

Although the number of tests are very few, the data in Table 19 provide some check on the SDSMT experimental results. In the case of the Homestake formation, for example in the 1-direction, the UU and SDSMT values for Young's modulus are 12.5 and 12.7 x 10^6 psi, respectively. In the case of the Ellison formation, for example in the 2 direction, the UU and SDSMT Young's modulus values are 9.29 and 9.1x10^6 psi, respectively.

The six Poisson's ratios in Table 19 are not independent because of symmetry and the consequent reciprocity relations:

$$\nu_{ij}/E_i = \nu_{ji}/E_j \qquad (i,j = 1,2,3,\ i \neq j) \qquad (5)$$

These relations provide a check on the data. However, as a practical matter it is difficult to distinguish the 1- and 3-directions in the plane of schistosity. Hence, the check can be expected to be rough at best. In the case of the Homestake formation data, there is enough information for a reciprocity relations test. Table 20 shows the results.

TABLE 20. - Orthotropic reciprocity relations check

Poisson's ratio					
(ν_{21})		(ν_{32})		(ν_{13})	
Experiment	Reciprocity	Experiment	Reciprocity	Experiment	Reciprocity
0.12	0.12	0.21	0.18	0.14	0.26

The first two Poisson's ratios are close, but the third in the plane of schistosity is uncertain, as expected.

The determination of the shear moduli is possible by testing core with axes inclined to the foliation. The two samples prepared from the Poorman formation were inclined 12 and 15 degrees to the foliation. Unfortunately, the first failed prematurely. Application of the orthotropic elastic model to the test configuration shows that $E'\varepsilon = \sigma$ and

$$1/E' = (1/E_1)\cos^4\beta + (1/G_{12} - 2\nu_{12}/E_1)\sin^2\beta\cos^2\beta + (1/E_2)\sin^4\beta \qquad (6)$$

where β is the angle between the foliation and load axis measured in the plane formed by the 1- and 2-directions.

Equation 6 can be solved for G_{12} since all other numbers are known from the test results. Figure 58 is the experimental curve for the Poorman formation sample inclined 15 deg. to the foliation. The final experimental result is

$$G_{12} = 3.81 \times 10^6 \text{ psi (Poorman formation).}$$

In order to estimate the remaining shear moduli G_{23} and G_{31} for the

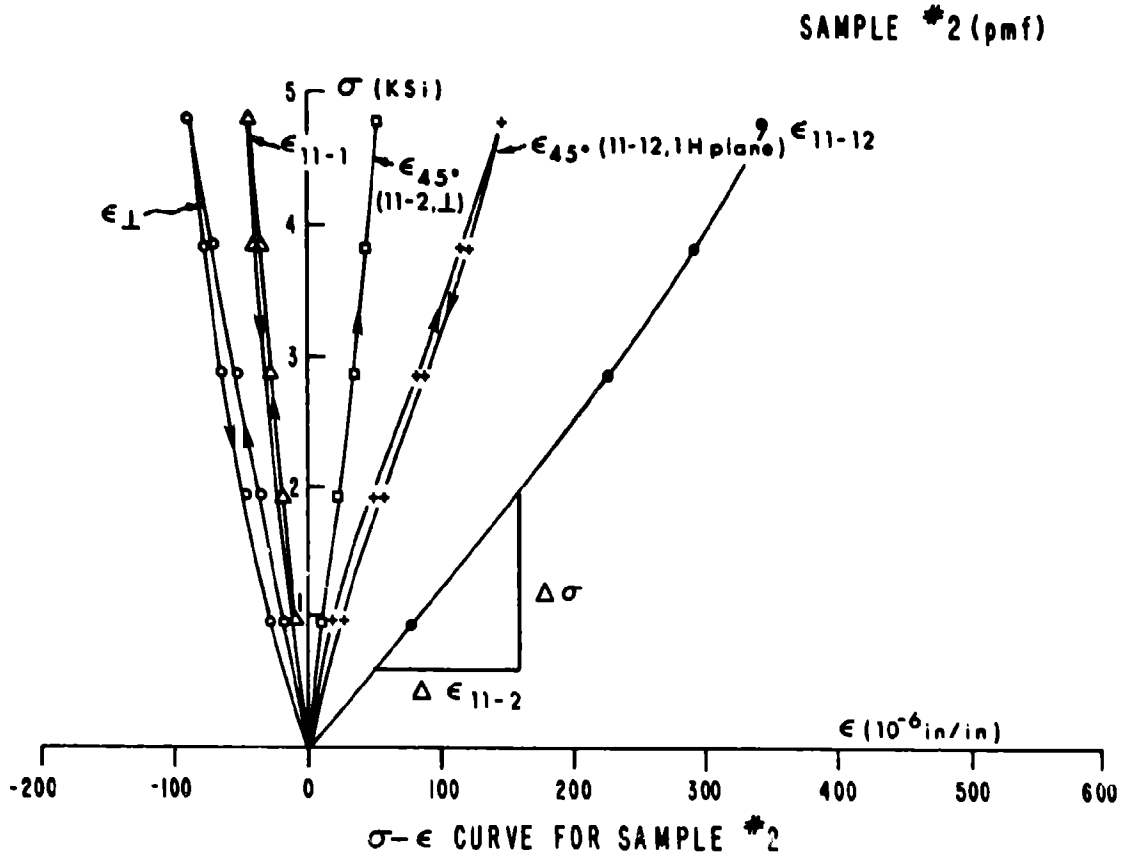

Figure 58. - Poorman formation laboratory stress strain curves.

Poorman formation and G_{12}, G_{23} and G_{31} for the Homestake and Ellison formation, the experimental value of G_{12} obtained for the Poorman was compared with values given by

$$G_{ij} = E_i/2(1 + \nu_{ij})$$
$$G_{ij} = E_j/2(1 + \nu_{ji}) \qquad (i,j=1,2,3)$$
$$G_{ij} = E_i/4(1 + \nu_{ij}) + E_j/4(1 + \nu_{ij}) \qquad (i \neq j) \qquad (7a\text{-}e)$$
$$1/G_{ij} = 2/\sqrt{E_i E_j} + 2\nu_{ij}/E_i$$
$$1/G_{ij} = 1/E_i + 1/E_j + 2\nu_{ij}/E_i$$

The G_{ij} calculated for all formations with experimental E_i and ν_{ij} in Eqs. 7a-e range between a low of 3.214×10^6 psi to a high of 5.918×10^6 psi. In this regard, the Poorman formation shows the greatest calculated range of G_{ij}; the ranges for the Homestake and Ellison are less and nearly the same, respectively. The calculated value of G_{12} nearest to the experimental value of 3.84×10^6 psi is 4.05×10^6 psi and is given by the last of Eqs. 7a-e. Equation 7e was thus used to estimate all other shear moduli.

According to Eqn. 6, Young's modulus E' for core inclined to the foliation is a function of G_{12} as well as E_1, E_2, ν_{12} and β. Hence, a polar plot of E' with G_{12} as a parameter shows graphically the variation and the fit obtained with all the experimental data including the one measurement of G_{12}. Such a plot is shown in Figure 59. The solid curves in Figure 59 represent the results obtained using G_{12} from Eqs. 7a-e in Eqn. 6. The dotted curve is the experimental result (Eqn. 6 only). It shows a good approximation to the result obtained using the empirical relationship Eqn. 7e and further confirms a satisfactory estimation procedure for the remaining shear moduli.

Estimation of the shear strengths follows a procedure that is similar to the procedure used to estimate the shear moduli from tests on core inclined to the foliation. Of course, the procedure for strengths is based on the yield condition (Pariseau, 1972) rather than Hooke's law for anisotropic (orthotropic) elastic solids. The yield condition used is

$$[F(\sigma_y-\sigma_z)^2 + G(\sigma_z-\sigma_x)^2 + H(\sigma_x-\sigma_y)^2$$
$$+ L(\sigma_{yz})^2 + M(\sigma_{zx})^2 + N(\sigma_{xy})^2]^{1/2}$$
$$- (U\sigma_x + V\sigma_y + W\sigma_z) = 1 \qquad (8)$$

where x, y, z are the principal directions of anisotropy. Eqn. 8 is nonlinear in stress. The strength properties F, G, H, L, M, N, U, V, W are related to the uniaxial compressive, tensile and shear strengths relative to the axes of anisotropy (C_1, T_1, R_1, C_2, T_2, R_2, C_3, T_3, R_3). The uniaxial strengths C_i, T_i (i=1,2,3) are known for each formation from tests on core parallel and perpendicular to the foliation.

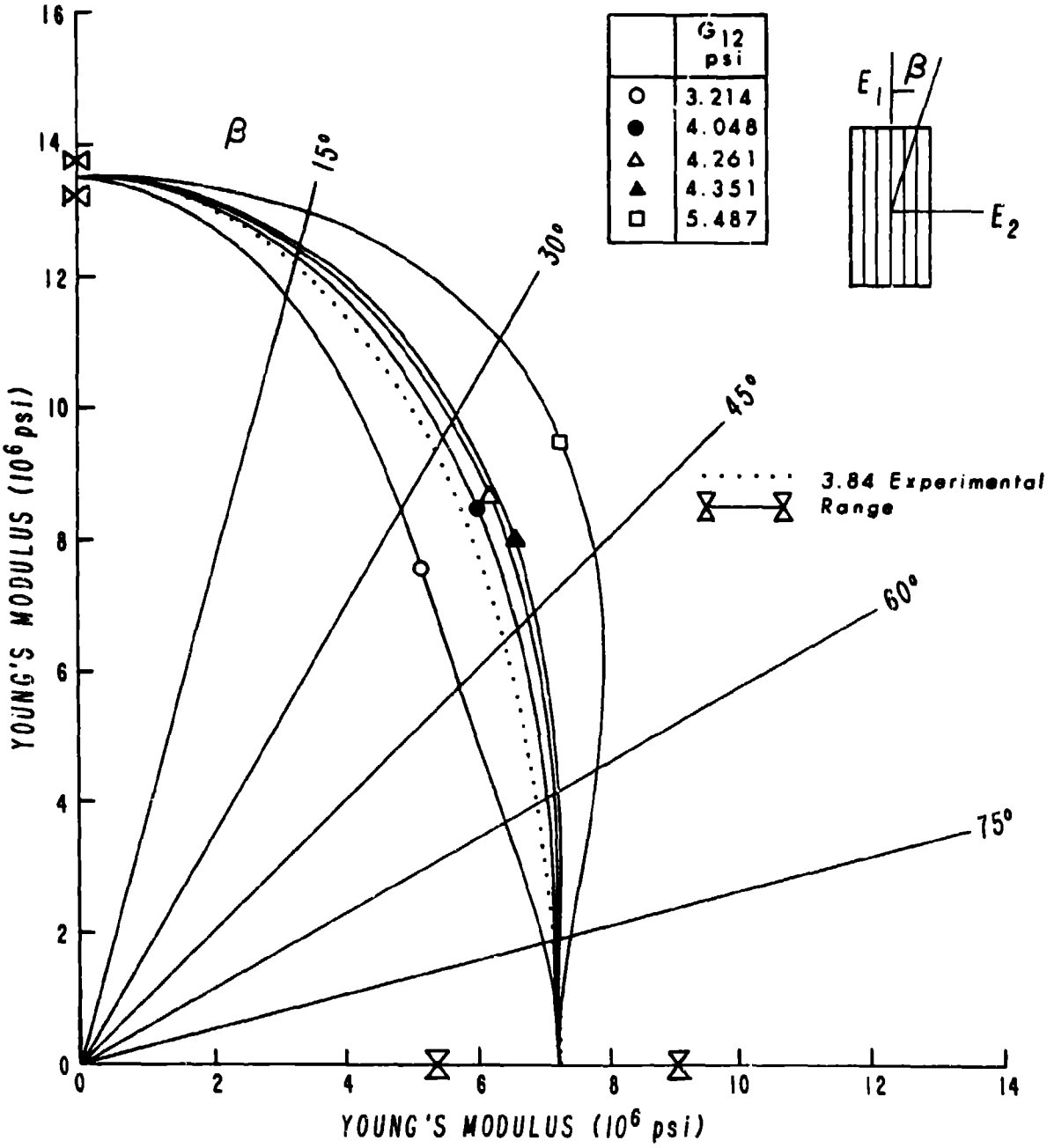

YOUNG'S MODULUS VS. BETA WITH SHEAR MODULUS G_{12} AS PARAMETER FOR POORMAN FORMATION

Figure 59. - Poorman formation modulus versus inclination.

The yield condition for core under uniaxial load σ at an angle to the foliation becomes a complicated function

$$f(\beta,\sigma,n,F,G,H,N,U,V,W) = 1 \qquad (9)$$

that leads to an expression for unconfined strengths at an angle to the foliation that involves R_3 but not R_1 and R_2, for example. A plot of such a function with β as a variable and R_3 as a parameter is shown in Figure 60. The experimental point determined from a test on a core inclined to the foliation 15 degrees indicates a value of about 900 psi for R_3.

Various isotropic strength relations are available, that is, expressions for R_i in terms of C_i and T_i, that reduce to the isotropic case in the instance of vanishing anisotropy. For example, R_2 may be given by a, b, c, d and combinations as given in Eqns. 10:

$$a = \sqrt{C_1 T_1/3}, \quad b = \sqrt{C_3 T_3/3}, \quad c = \sqrt{C_1 T_3/3}, \quad d = \sqrt{C_3 T_1/3} \qquad (10)$$

$$\tfrac{1}{2}(a+b), \ \tfrac{1}{2}(c+d), \ \tfrac{1}{2}(a+c), \ \tfrac{1}{2}(a+d), \ \tfrac{1}{2}(b+d), \ \tfrac{1}{2}(b+c)$$

The dotted lines in Figure 60 correspond to the highest and lowest R values obtained from Eqs. 10. Figure 50 suggests that the lowest result should be used to estimate the shear strengths (R_i) when not determined directly by experiment.

A similar result is obtained testing under confining pressure at an angle to the foliation. This is shown in Figure 61. Again, the lowest R value from Eqs. 10 is nearest the experimental point.

Another set of empirical criteria for estimating shear strengths is the shape of the compressive strength versus inclination curve. Intuitively one expects the plot to be bowl shaped. Very high values of shear strength lead to a dome shape, while very low values lead to a wave shape. Restricting the curve to a bowl shape sets a high and low limit to shear strength. In this regard, only bowl shapes have been reported in the technical literature.

Summary

The results of the in situ stress measurements show that the stress state in the vicinity of the study stope is

$\sigma_v = 1.25\ h$ (vertical)

$\sigma_{h1} = 2078 + 0.53\ h$ (dip direction)

$\sigma_{h2} = 121 + 0.55\ h$ (strike direction)

where the stresses are in psi and the depth h is in feet.

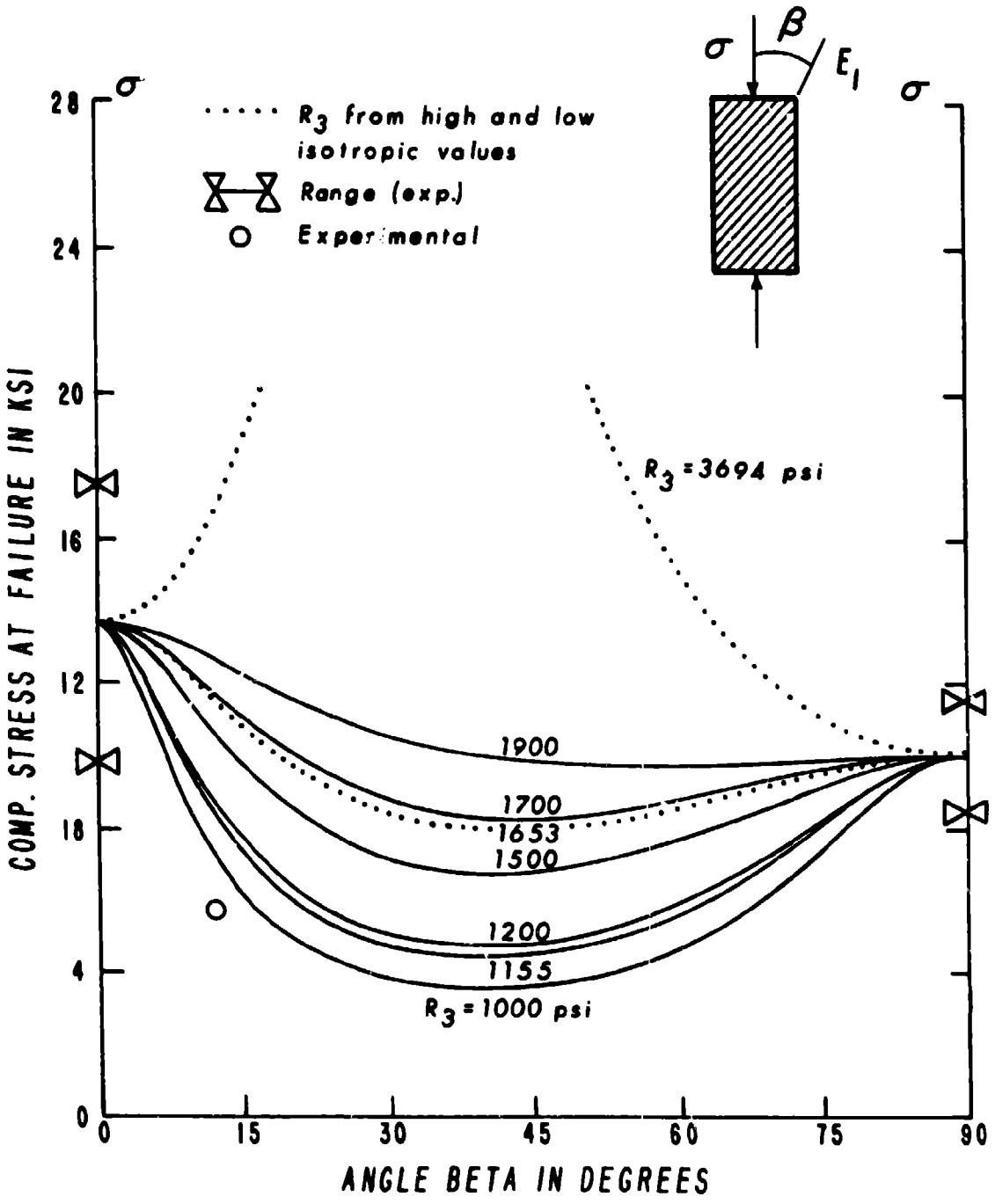

UNCONF. COMP. STRENGTH VS. INCLINATION OF ANISOTROPY FOR POORMAN FORMATION

Figure 60. - Poorman formation strength versus inclination.

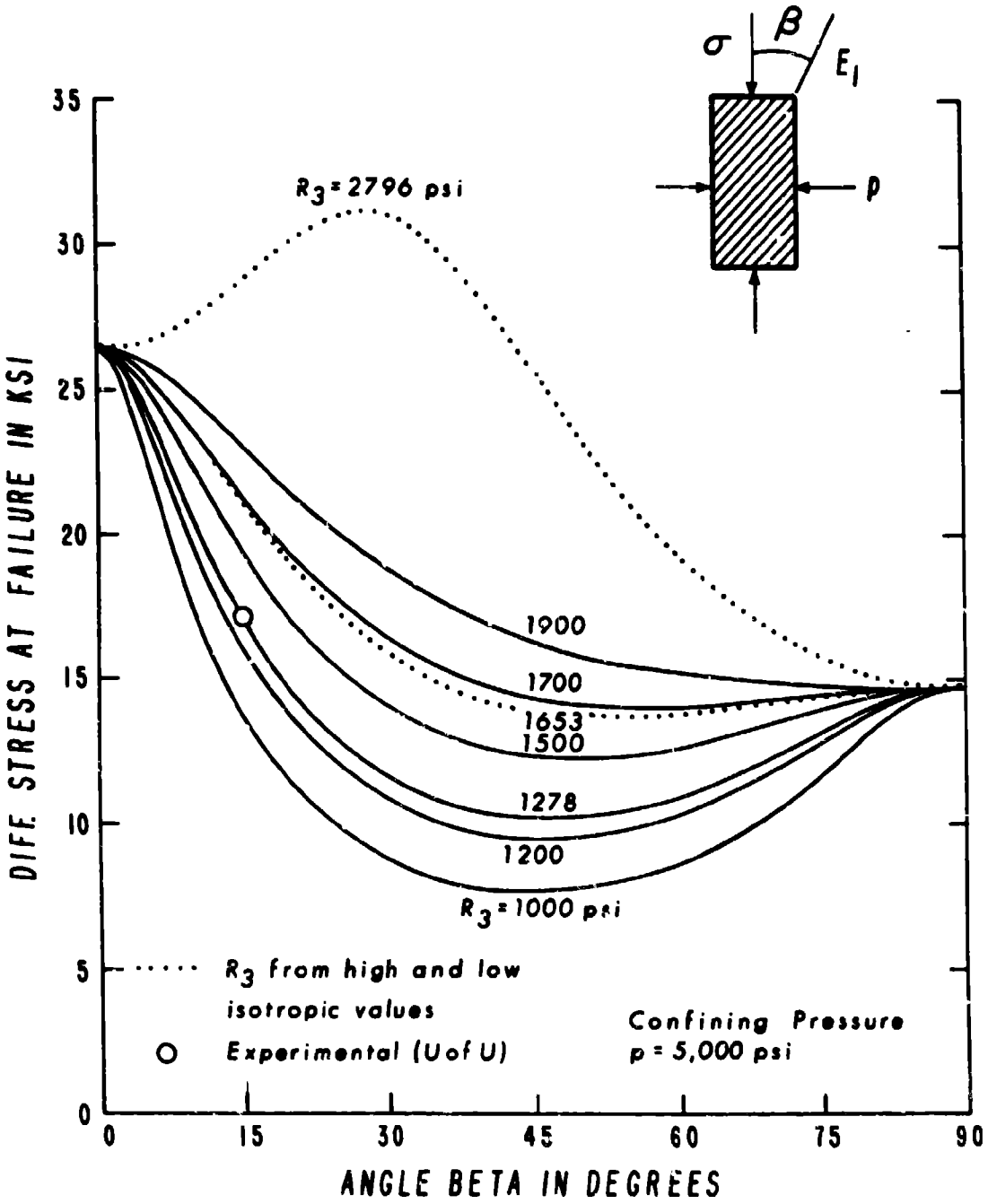

CONF. COMP. STRENGTH VS. INCLINATION OF ANISTROPY FOR POORMAN FORMATION

Figure 61. - Poorman formation strength versus inclination under confining pressure.

The results of merging and modifying the SDSMT and the UU laboratory rock properties data for greatest physical realism are presented in Table 21.

TABLE 21. - Laboratory anisotropic rock properties

Property*	Homestake Formation	Poorman Formation	Ellison Formation
E_1	12.8×10^6	13.5×10^6	13.0×10^6
E_2	9.3×10^6	7.2×10^6	9.2×10^6
E_3	9.0×10^6	13.7×10^6	11.0×10^6
ν_{12}	0.14	0.23	0.20
ν_{23}	0.18	0.15	0.17
ν_{31}	0.19	0.22	0.15
G_{12}	4.8×10^6	3.8×10^6	4.6×10^6
G_{23}	3.9×10^6	3.9×10^6	4.2×10^6
G_{31}	4.3×10^6	5.6×10^6	5.1×10^6
C_1	20,150	13,630	11,340
C_2	11,550	10,000	11,410
C_3	13,270	12,270	8,150
T_1	1,380	2,990	2,350
T_2	1,140	820	590
T_3	1,920	1,910	1,650
R_1	2,050	1,500	1,150
R_2	2,470	2,800	2,120
R_3	2,100	1,280	1,250

*1- and 3-direction are parallel to the schistosity; the 2-direction is perpendicular to the schistosity. All units are psi (except for Poisson's ratios

COMPARISONS BETWEEN FINITE ELEMENT CALCULATIONS AND MINE MEASUREMENTS

Comparisons between theoretical calculations of the study response to mining and the response determined by mine measurements provide a test of the validity of the working hypothesis underlying the theoretical model. The fundamental model used in this study assumes that an element of the Poorman, Homestake or Ellison formation is elastic (orthotropic) under an initial application of load, but with continued loading eventually fractures and flows in a way that depends on the confining pressure of the adjacent rock. In addition to the material law that describes such behavior in equation form, the model also requires satisfaction of the equations of equilibrium and relationships between strain and displacement. This combination of physical and materials laws constitutes the governing system of equations. The finite element approach is used to solve the governing system numerically on the computer but subject to site specific information including study stope geology, geometry, in situ stresses, rock properties and mining sequence. A favorable comparison between the calculated and measured study stope response justifies the use of the model and the method for considering alternate stope and pillar sizes. This, of course, is much cheaper than full-scale mine trials of alternative designs.

Calculated Study Stope Response

A two-dimensional finite element representation of the study stope was developed for vertical section through the center of Panel 3. Input for the analyses consists of:

(i) stope geometry,
(ii) stope geology,
(iii) in situ stress state,
(iv) rock properties,
(v) mining sequence.

The geology and geometry of the region are shown in Figure 62. The outer boundaries of the region in Figure 62 are sufficiently far from the study stope to have negligible influence on results. However, they are not so far as to be wasteful of computer resources. The premining stress state was determined from in situ stress measurements (Eqs. 2). Laboratory rock properties (Table 21) were used initially, but subsequently scaled for the final analyses. The mining sequence corresponds to development and ring excavation and VCR blasting including crown pillar removal. Some lifts in the computer sequence include several VCR lifts. A practical advantage in combining lifts is a reduction in cost of a simulation and a speedup in turn-around time. The main objective of the finite element analysis at this juncture is to obtain initial estimates of displacements and yield zone extent. Comparison with measurements then allows for scaling of laboratory rock properties to field scale or rock mass conditions, provided the initial results are highly correlated. If initially, the correlation between calculated and measured displacements is low, then the input data and

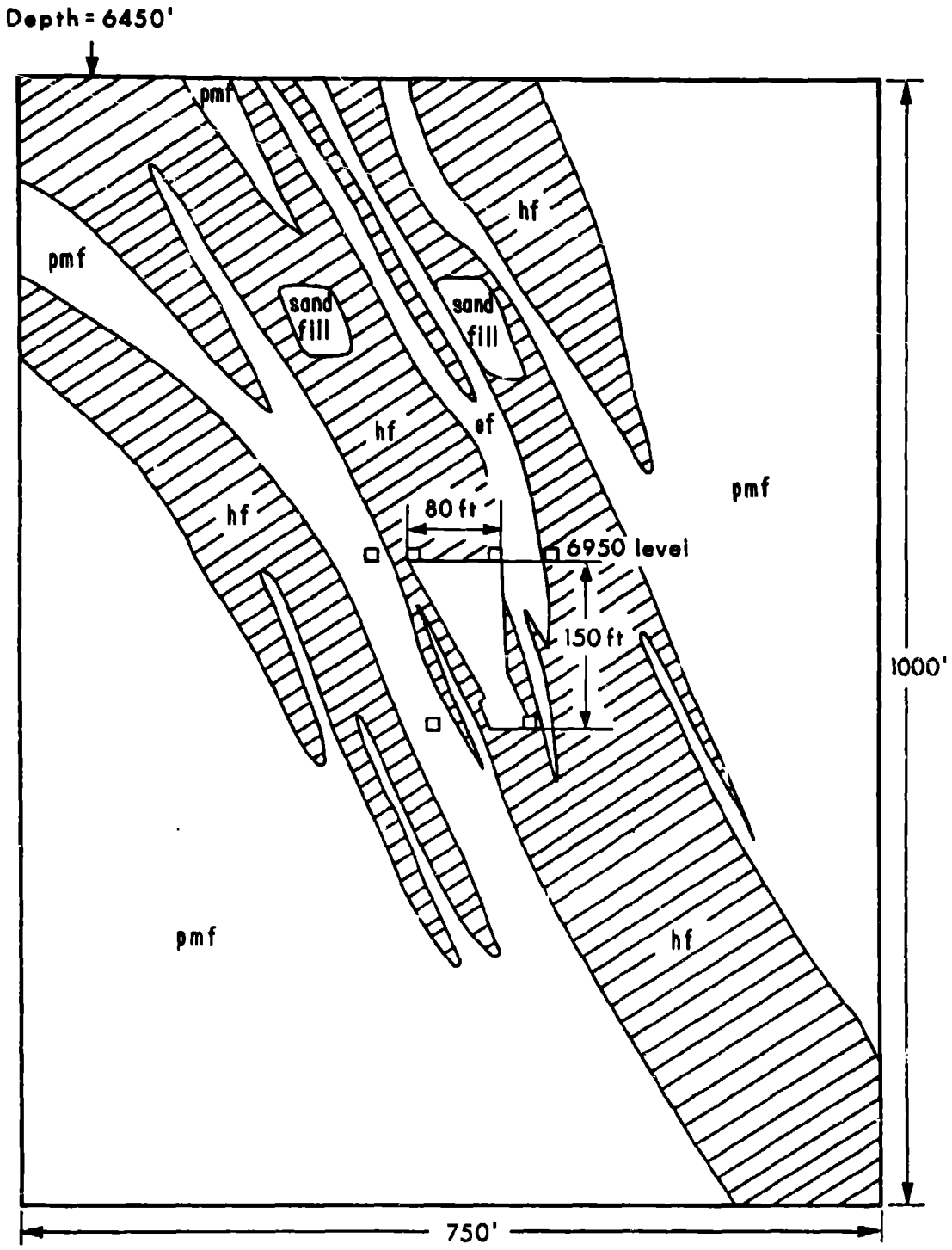

Figure 62. - Homestake Mine study stope region, gemoetry and geology in vertical section looking north.

quite possibly the model itself are suspect. However, if scaling is justified by an initially high correlation, then there is a reasonable expectation that subsequent analyses using scaled rock properties will produce realistic results.

Calculated versus Measured Displacements

Extensometer readings approximate the relative displacement that occurs between anchor point and collar plate from the time of installation to the present. Corresponding calculated displacements are obtained from finite element analyses that simulate the mining sequence. If the finite element model were perfect, the input data exact and the measured displacements flawless, then all the points of a plot of calculated versus measured displacements (relative displacements or extensometer readings) would fall on a straight line passing through the origin with a slope of one. The finite element model is an approximation, of course, and measurements are imperfect in the real world. In the writer's opinion, the current state of the art is such that a reasonable expectation is the achievement of a satisfactory correlation in the elastic range and an adequate degree of agreement between observed and estimated yield zones beyond the purely elastic range of deformation. The meaning of satisfactory and adequate within the present context is not precise, but perhaps at least half the variance between calculated and measured displacements within the elastic range should be accounted for by the model. This means that the correlation coefficient should be greater than 0.71 in the elastic range.

Figure 63 is a plot of calculated versus measured extensometer readings in the elastic range from data obtained from four instrumentation holes (H-6,7,8,9) located in the immediate hanging wall. A regression line is also shown in Figure 63. The correlation coefficient is 0.84. A strong linear relationship between calculated and measured displacements is indicated. Scaling of the laboratory elastic moduli at this point is therefore a potentially successful approach to fixing the rock mass moduli. The scale factor is simply the slope of the regression line (0.31). Multiplication of all laboratory Young's moduli and shear moduli values by 0.31 gives the corresponding rock mass moduli values. Poisson's ratios are unscaled because of their dimensionless character. There are 18 scaled moduli in the finite element model (27 independent elastic properties altogether). Scaling, of course, does not change the correlation coefficient, only the slope of the regression line.

Other regression analyses of calculated on measured displacements are possible. Slightly different scaling factors are then obtained. Instead of taking all measurements together, one could examine the data on a hole by hole basis. One can also subdivide the data further; each hole could be examined anchor by anchor or gage by gage (three per hole). In this regard, the sequential nature of the mining sequence allows for a sequence of regressions, one sequence for each anchor. The first of such a sequence involves only two points, the origin or reading taken at installation time after development headings are cut and the reading taken immediately after the first blast (ring rounds). A

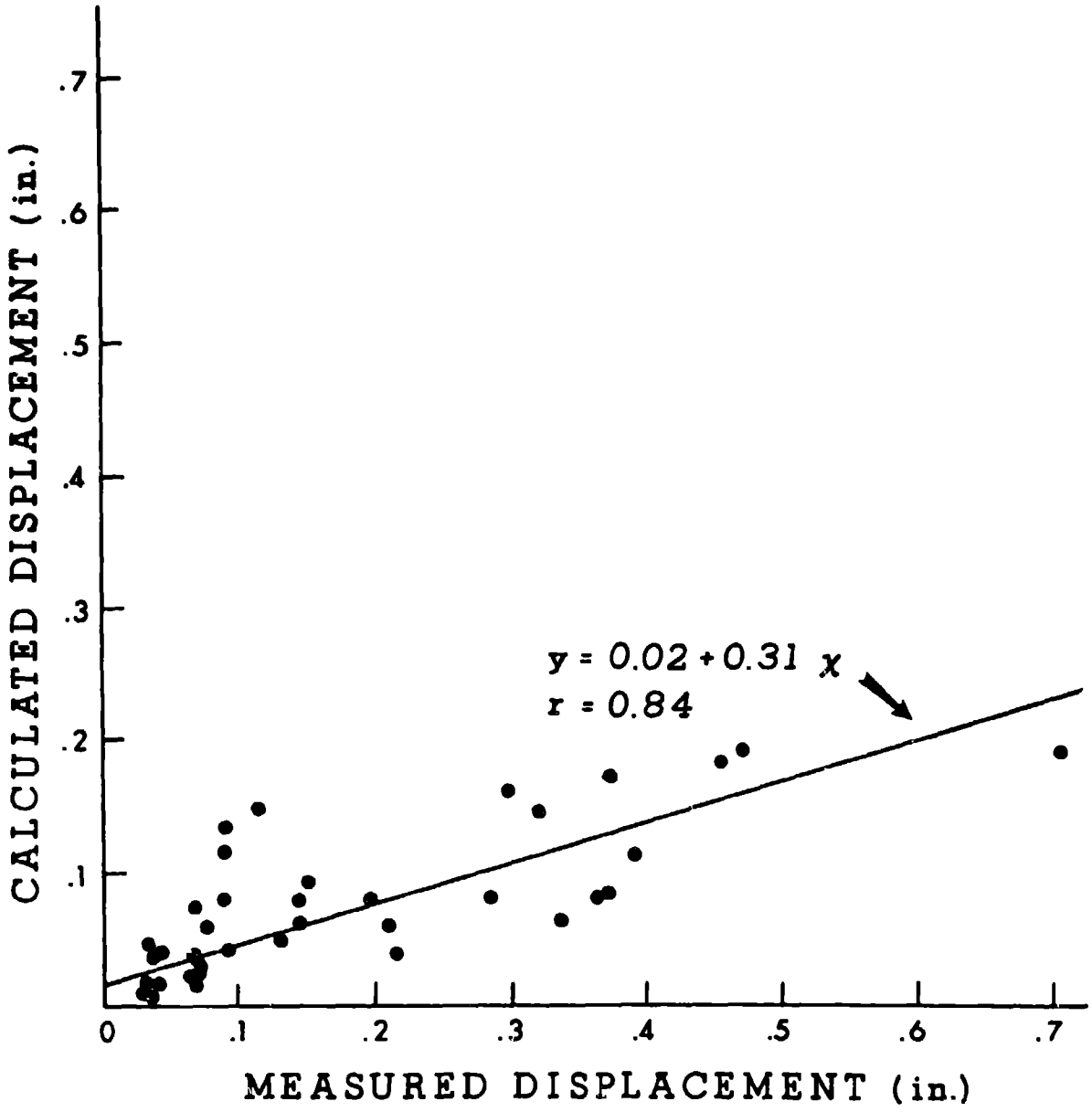

Figure 63. - Calculated versus measured displacements in the immediate hanging wall.

straight line fit to two points automatically yields a correlation coefficient of one, of course. However, as successive blasts are made, additional data for the anchor in question are acquired and the regression analyses become statistically more meaningful.

The Homestake finite element model excavates the study stope (including development headings) in seven cuts, so that there is a maximum of seven points per regression line. Thus the four three-point extensometers located in the immediate hanging wall have the potential for producing 84 computer-generated data points including the origin, but not all anchors survived the entire stoping sequence. In fact, some 8 of 12 remained active after the fifth cut. Table 22 shows the slopes of the regression lines obtained in an anchor by anchor analysis of calculated versus measured displacements for these longer-lived anchors. The average slope is 0.36; the standard deviation is 0.12, and the coefficient of variation is 33%.

TABLE 22. - Anchor regression in the elastic range

Hole	Anchor	Slope	Correlation	Comment
6	1	0.409	0.996	after 6 cuts
6	2	0.440	0.990	after 6 cuts
6	3	0.540	0.963	after 4 cuts
7	1	0.481	0.969	after 5 cuts
7	2	0.303	0.915	after 6 cuts
8	1	0.201	0.984	after 6 cuts
8	2	0.249	0.980	after 5 cuts
9	1	0.271	0.965	after 5 cuts

Average slope	= 0.36
Standard deviation	= 0.12
Coefficient of variation	= 33%

The anchor by anchor correlations in Table 22 are very high and show a strong linear relationship between calculated and measured displacements at each measurement site. The slopes of the regression lines vary, although within about the same range as the laboratory elastic moduli. The average slope of 0.36 was selected for use as a scale factor for elastic moduli (Young's moduli, shear moduli) in subsequent study stope analyses. This is somewhat greater than the 0.31 factor determined in combined regression of all data within the elastic range. The 0.36 scale factor is associated with very high correlation coefficients (all greater than 0.92), while the 0.31 is associated with a somewhat lower correlation (0.84). The differences are not of great practical significance, however. Multiplication of the average laboratory values of Young's and shear moduli by 0.36 gives rock mass moduli values that lead to reasonable estimates of displacement within the elastic range as measured in the mine.

Calculated versus Observed Yield Zones

Estimates of rock mass strengths from laboratory rock properties are beyond current theory and of necessity must be done after the fact of mine observations. The procedure is similar to the estimation of rock mass moduli, but requires more judgment in determing the extent of the yield zone. Anchor loss associated with caving of the hanging wall is certainly beyond the elastic limit, but the elastic limit may be exceeded prior to final loss through progressive fracturing and flow. Both fracture and flow lead to displacements considerably larger than those associated with a purely elastic response. One indication of inelasticity and yield is therefore a measured displacement substantially greater than the calculated elastic displacement. Unfortunately, the situation is complicated by the fact that some yield zone development occurs in the finite element analysis even with laboratory strengths. Figure 64 shows the calculated extent of yielding using laboratory rock properties and a single cut mining sequence. Figure 64 shows that no yield zone encloses any anchor point in the immediate hanging wall. Scaling the elastic moduli does not change this result.

In fact, all the deep anchors and three out of four of the intermediate anchors were lost after the final crown pillar blast. The yield zone must therefore be more extensive than that indicated in the laboratory rock properties based analysis. This was expected, but the question remains as to what scale factor might be used to obtain adequate agreement with the yield zone observed through anchor loss.

A very simple initial estimate of the strength scale factor was made on the basis of a uniaxial strain energy criterion. The criterion is $(C_o)^2/E$ = constant where C_o = uniaxial compressive strength and E = Young's modulus. According to this criterion, strengths scale as the square root of the ratio of field to laboratory moduli. The scale factor for elastic moduli is 0.36; the initial strength scale factor was thus 0.6.

A strength scale factor of 0.6 leads to extensive yielding as shown in Figure 65. The yield zone in Figure 65 is close to the cable bolt drift and if manifested as caving would lead to loss of the drift. This was not observed, so that 0.6 is too drastic a strength scale factor.

The yield zone shown in Figure 66 results from an intermediate strength scale factor of 0.8. Hanging wall yield occurs in Figure 66 but does not threaten the cable bolt drift and holds the potential for not encompassing the surviving extensometer anchors in the immediate hanging wall. A strength scale factor of 0.8 was therefore decided upon for subsequent analysis.

The single cut analyses provide a relatively inexpensive first look at the effects of scaling. However, the actual mining sequence becomes important when yield zones develop. Figures 67a-f show the evolution of the yield zones during a seven cut computer mining sequence using scaled elastic and strength properties. The hanging wall yield zone in Figure 67f is similar to the single cut result in Figure 66. However, the footwall yield zone that evolves during sequential mining is noticeably

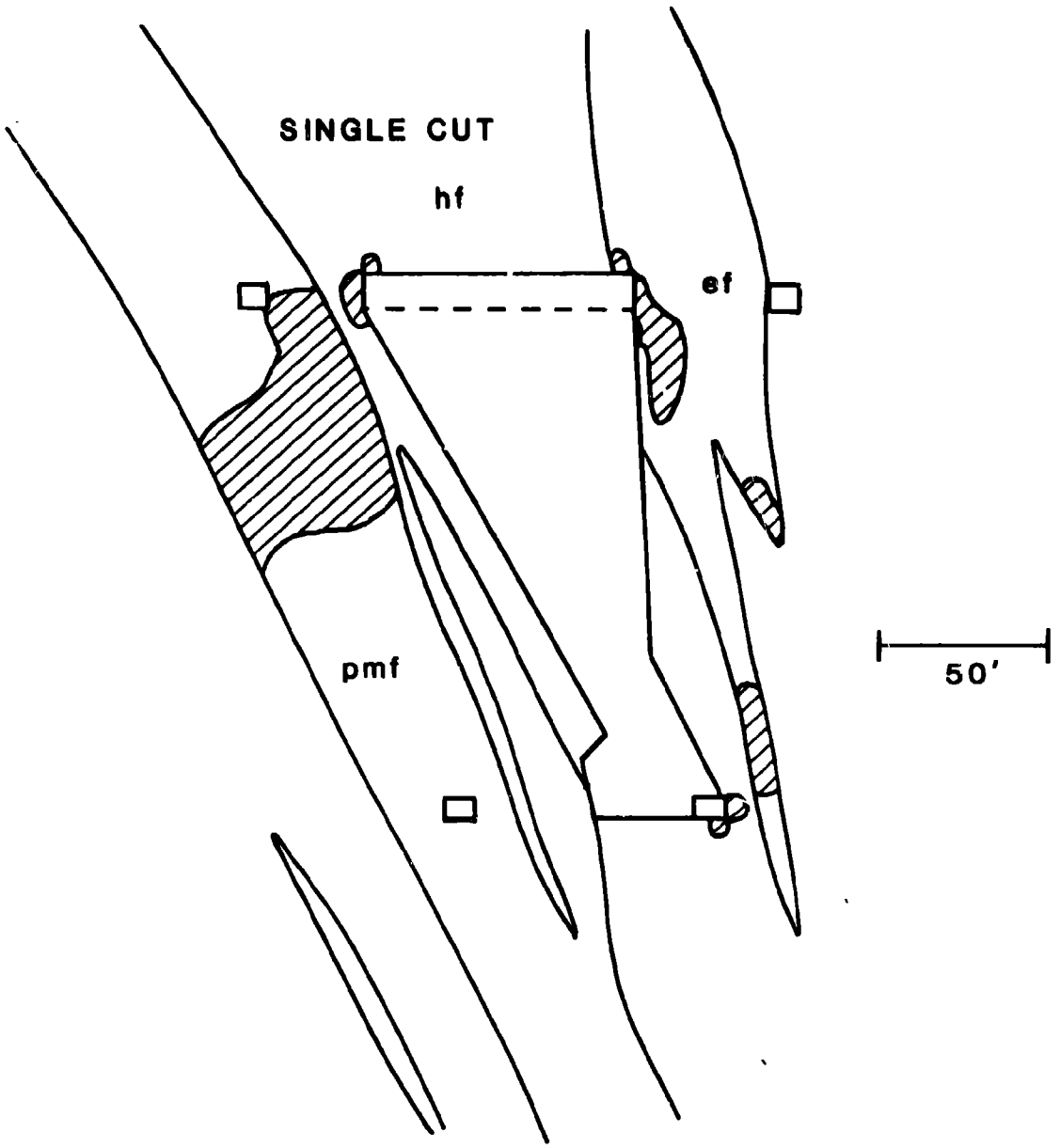

Figure 64. - Yield zone extent from scaled elastic moduli and full strength laboratory rock properties. One cut mineout.

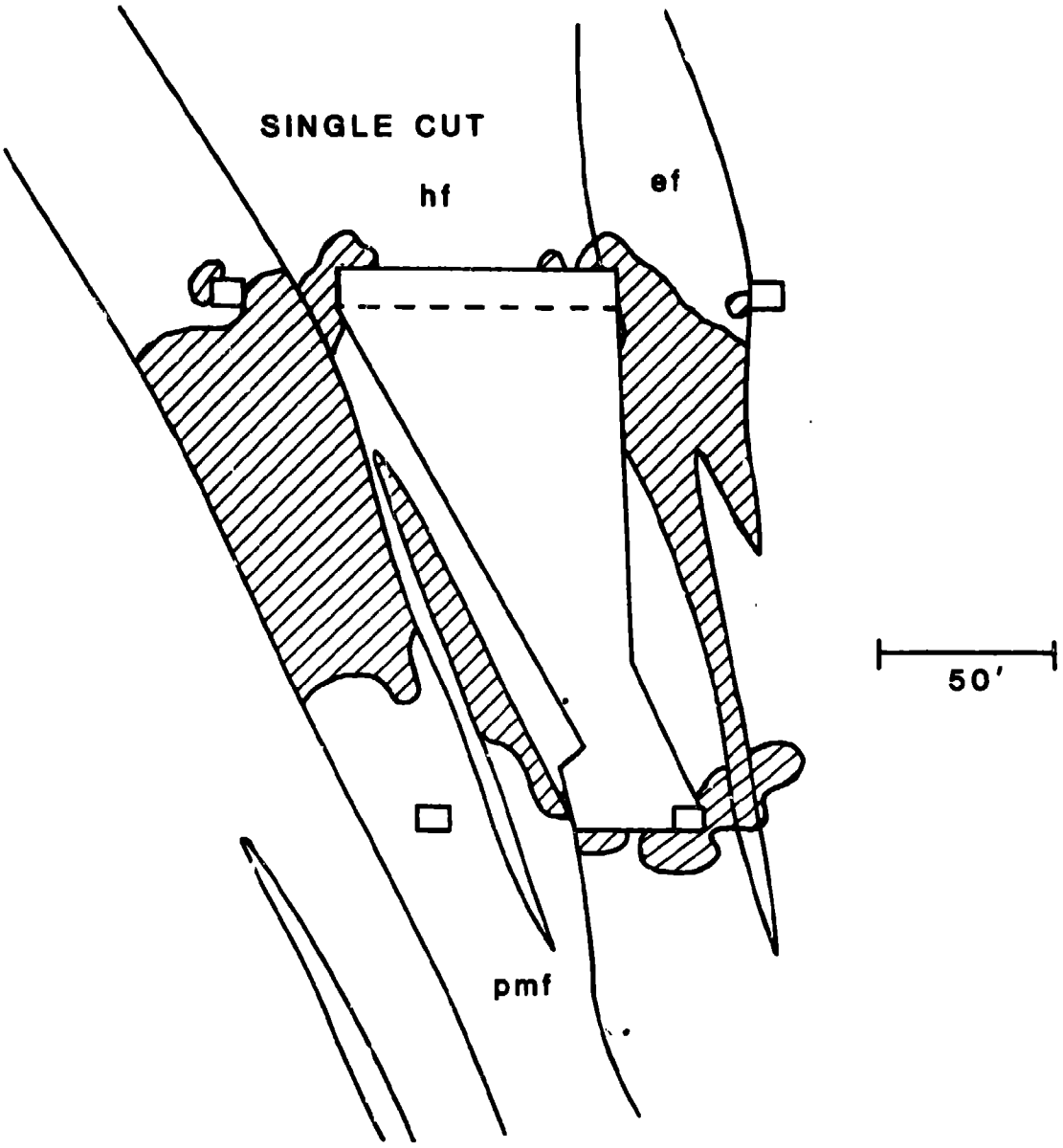

Figure 65. - Yield zone extent from scaled elastic moduli and 0.6 strengths. One cut mineout.

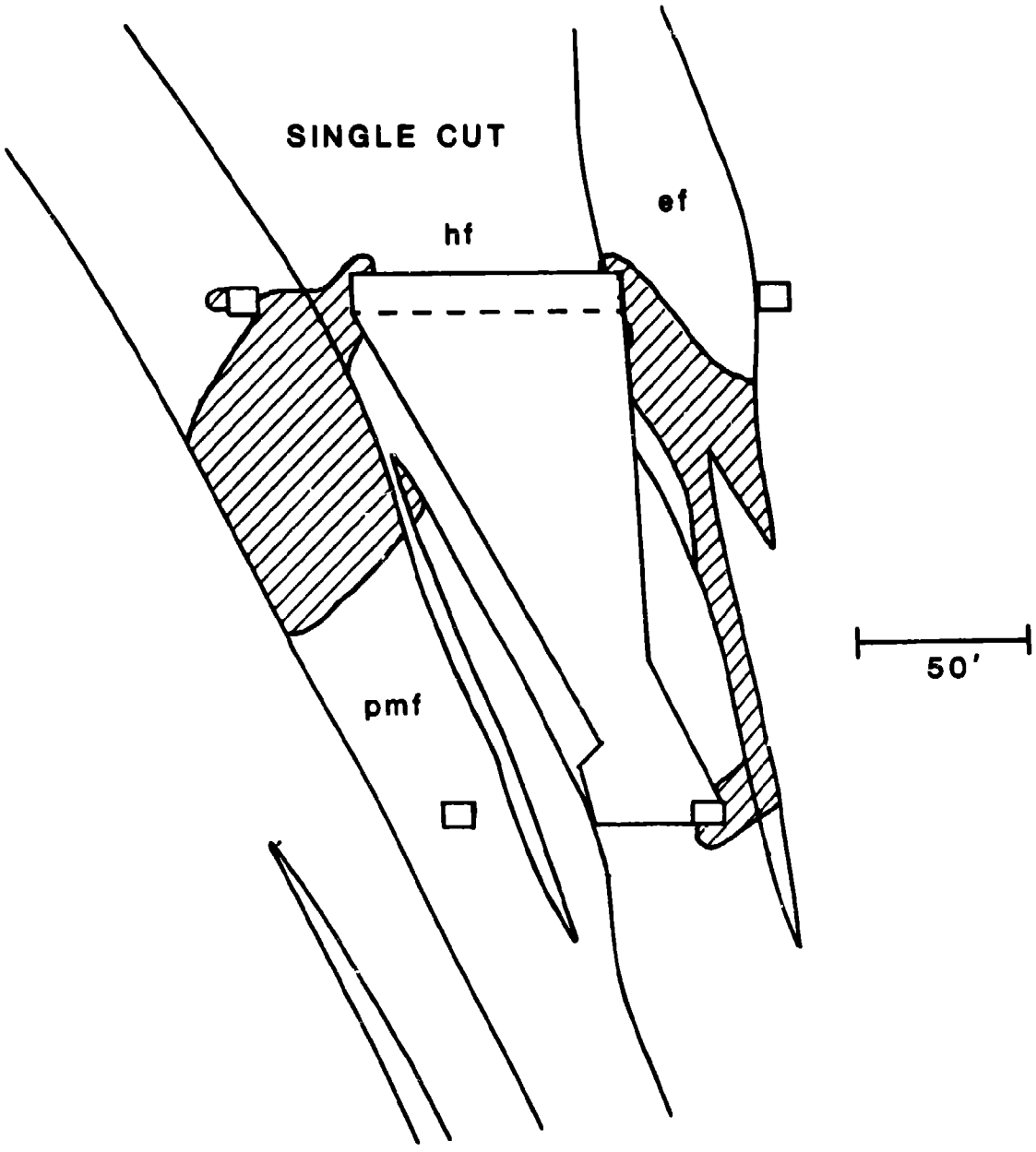

Figure 66. - Yield zone extent from scaled elastic moduli and 0.8 strengths. One cut mineout.

different and more extensive than the single cut estimate. The single cut estimate shows no yielding in the vicinity of the footwall extensometer (Hole 15). In fact difficulty with the footwall extensometer was experienced at the outset. The anchors are the snapring type and may have slipped because of blasting, but erosion of the footwall during draw of the swell could also occur as well as yielding caused by overstressing. The latter effect is aggravated by the sharp corner that is formed at the footwall and bottom of the crown remaining. A high stress concentration forms at this corner and is carried upwards with retreat towards the topsill. This effect is absent in the single cut analysis which is therefore less realistic than the multiple cut sequence that simulates more closely the actual VCR mining sequence. This is an excellent example of the practical importance of path dependency encountered in theoretical treatments of plasticity theory for geologic media. The mining sequence is indeed an important consideration where yield zones are observed.

The seven cut mining sequence using scaled elastic and strength properties (shown in Figures 67a-f) leads to a different correlation than the original estimate. The reason is that while the elastic moduli do not strongly influence extent of the yield zones, the reverse is not true. The strength properties have a noticeable affect on the displacements because of the extent of yielding. The effect is to decrease the correlation within the elastic range to 0.80 from 0.84, a decrease of about 5%.

In this regard, it is of interest to note that even if the elastic range is ignored and all data obtained up to anchor loss is used in a regression of calculated on measured displacements, the correlation coefficient is still 0.68. This means that despite the highly simplified fundamental model of elastic perfectly plastic rock mass inelasticity that was used in the analysis, it has some validity, although there is certainly room for improvement. The specification of the 27 independent elastic properties and the 27 independent strength properties for the rock mass model is non-unique but certainly not fortuitous. In the writer's opinion, the correlation of 0.8 in the elastic range is satisfactory. The agreement between calculated and observed yield zones is adequate, so that the model is reliably calibrated with a scale factor of 0.36 for elastic moduli and 0.8 for strengths.

Stope and Pillar Size Analyses

A finite element model calibrated against mine measurements allows one to consider alternative designs and the influence of such parameters as formation dip and stope width to height ratio. Productivity favors larger stopes and small pillars, while stability may favor small openings and larger pillars. However, large and small are not absolute. From a stress analysis view, a square opening 100 x 100 ft is as stable as a square opening 10 x 10 ft. What is important is shape of an opening characterized, say, by the ratio of opening length to width. From a structural geology viewpoint, size of an opening may be important because of the greater chance of encountering a fault or similar feature as the size of an opening is increased. Consideration of opening sizes

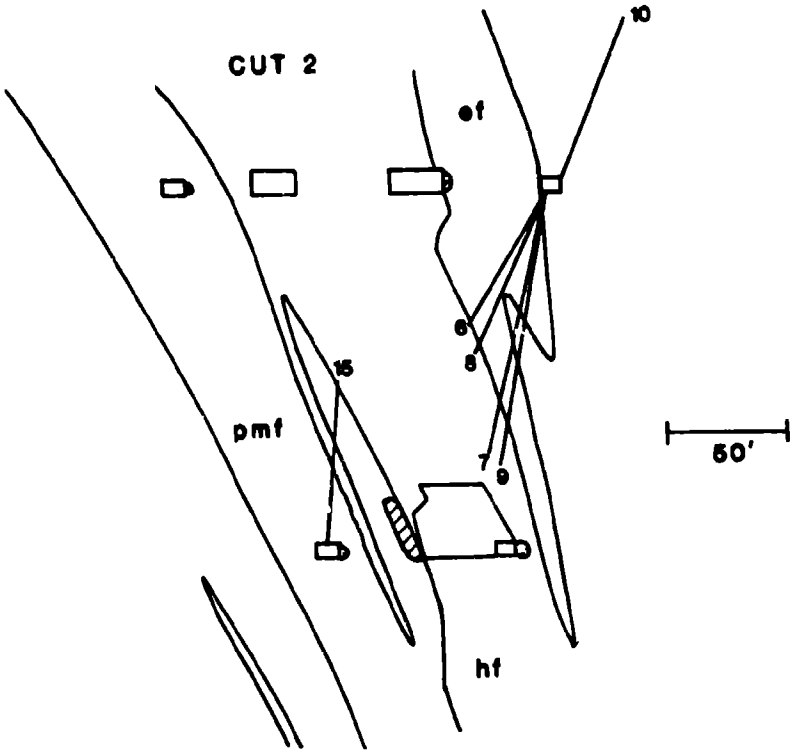

Figure 67. - (a) Yield zone from scaled properties. Cut 2.

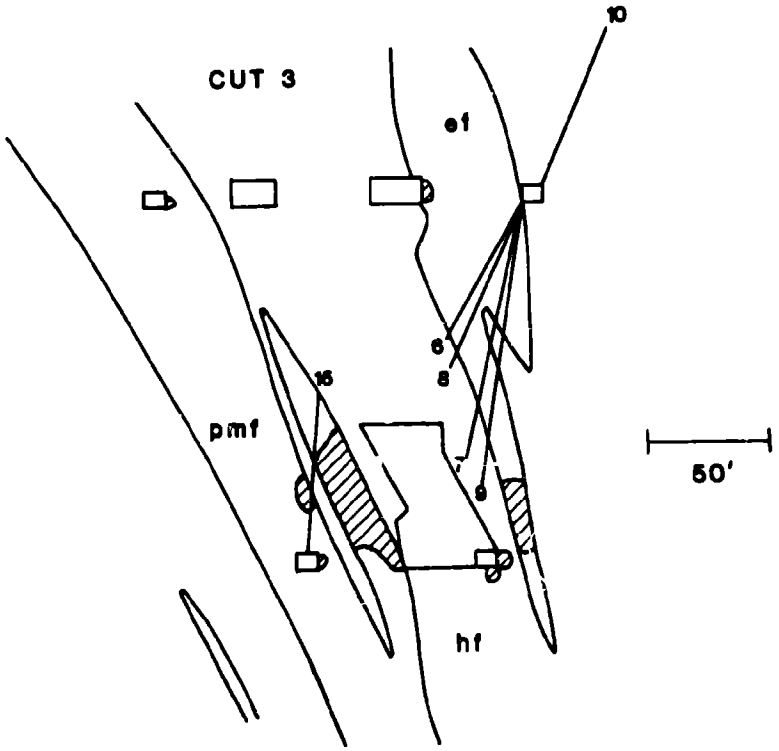

Figure 67. - (b) Yield zone from scaled properties. Cut 3.

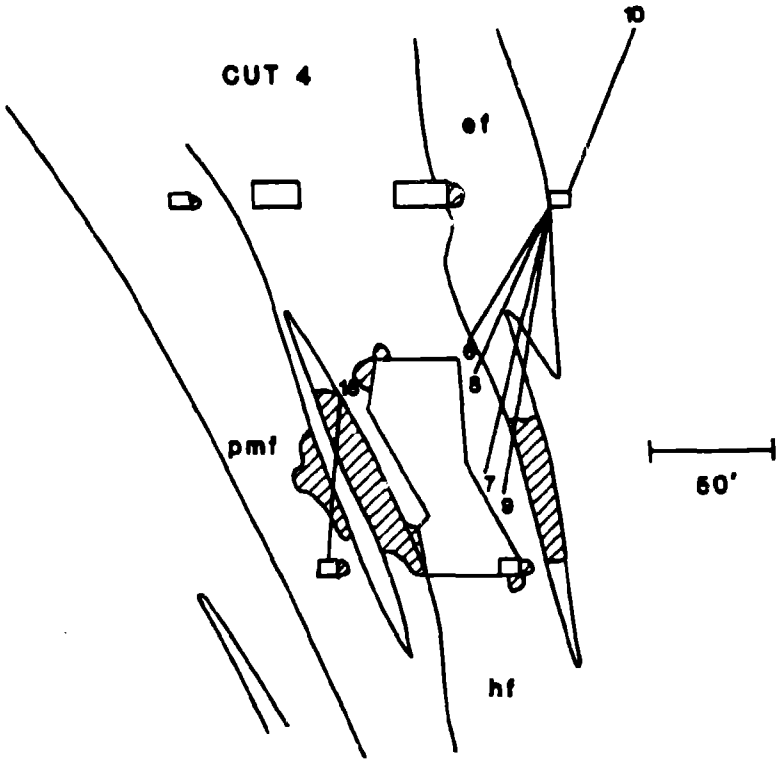

Figure 67. - (c) Yield zone from scaled properties. Cut 4.

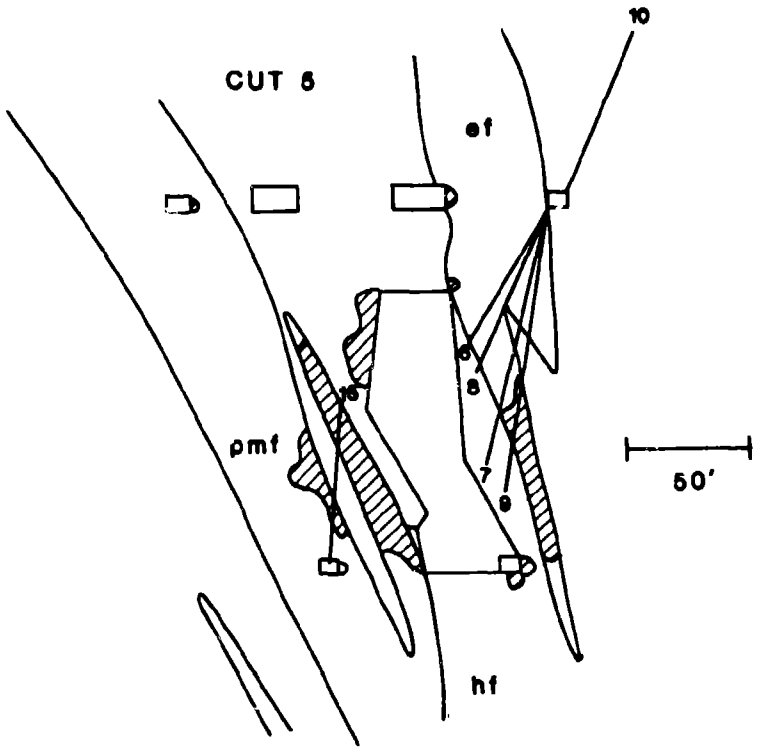

Figure 67. - (d) Yield zone from scaled properties. Cut 5.

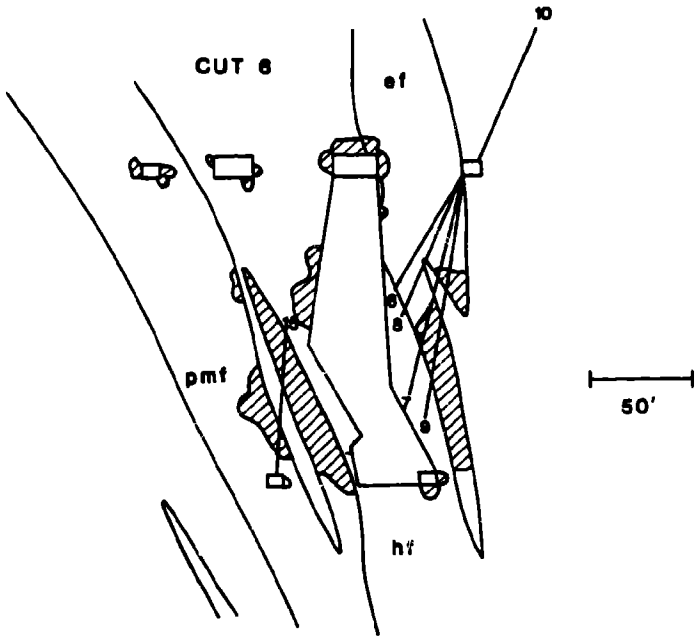

Figure 67. - (e) Yield zone from scaled properties. Cut 6.

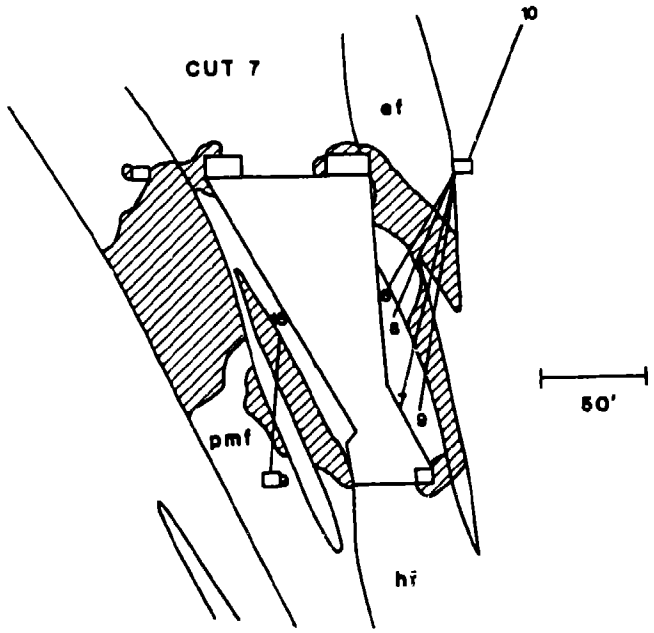

Figure 67. - (f) Yield zone from scaled properties. Cut 7.

that are of the same order of magnitude as the study stope used to calibrate the model helps to overcome the geologic question. This is the utility of rock mass properties and a calibrated model for parameter studies of alternate stope and pillar sizes.

Influence of Dip

The complex folding of the Homestake formation leads to ore bodies of varying dip. Other factors being equal, it is of interest to examine the influence of dip on the stability of a typical stope over the range of 50° to 90° (vertical). A typical stope as seen in vertical section perpendicular to strike is 50 ft wide; level interval is 150 ft. The footwall is Poorman formation, the ore zone is in the Homestake formation and the hanging wall is Ellison formation. Dips of 50, 60, 75 and 90 degrees were considered in two series of runs. In the first series stope width is equal to the width of the Homestake formation. In the second series, 20 ft of Homestake formation are left in the immediate hanging wall. The study stope geology suggested these two series. Rock mass properties and in situ stresses are the same as in the final study stope analysis. Figure 68 shows four stope geometries considered. The finite element mesh for the 60 degree case is shown in Figure 69. Figures 70 and 71 show the mesh refinement and geology for the two series (60 degree case).

The results of the second series are shown in Figure 72 in the form of contours of local safety factor and yield zone extent. Figure 72 shows the effect of the relatively strong Homestake formation on the hanging wall where much of the yield zone is in the Ellison formation above the Homestake formation. The Poorman formation also yields but on the footwall side. Both footwall and hanging wall yield zones are associated with high stress concentrations at the acute corners of the dipping stopes. Generally, the greater the inclination of the stope from the vertical, the sharper these corners and the greater is the stress concentration. In the yield zone, the elastic limit is exceeded and the response becomes elastic-plastic. Figure 72 also shows a stress concentration about the footwall haulage drift. The cable bolt drift was omitted in these generic analyses.

The results of the first series of analyses for dip effect are similar to the results shown in Figure 72 except that the Ellison formation forms the immediate hanging wall without intervening Homestake formation.. As the dip decreases from 90 to 50 degrees, stress concentration in the acute corners increases and the yield zones spread. The footwall yield zone may not be a serious practical problem. However, the hanging wall yield zone may be the source of an eventual cave. The potential for a cave is less when the stronger Homestake formation forms the immediate hanging wall.

Stope Width to Height Ratio

A 60 degree dipping stope of varying width but of fixed height (level interval) was analyzed in order to assess the influence of width

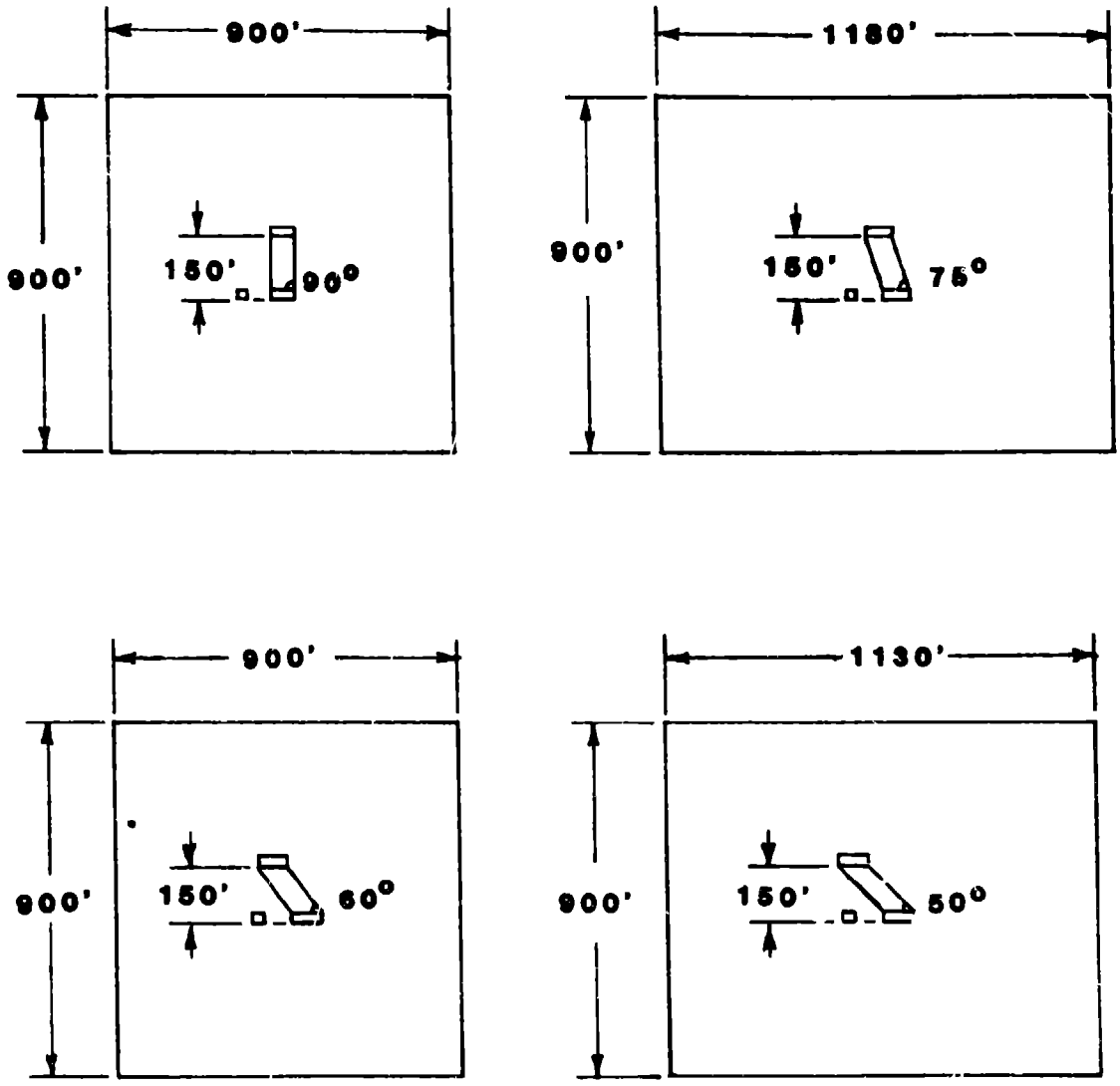

Figure 68. - Stope geometries used for analysis of dip effect.

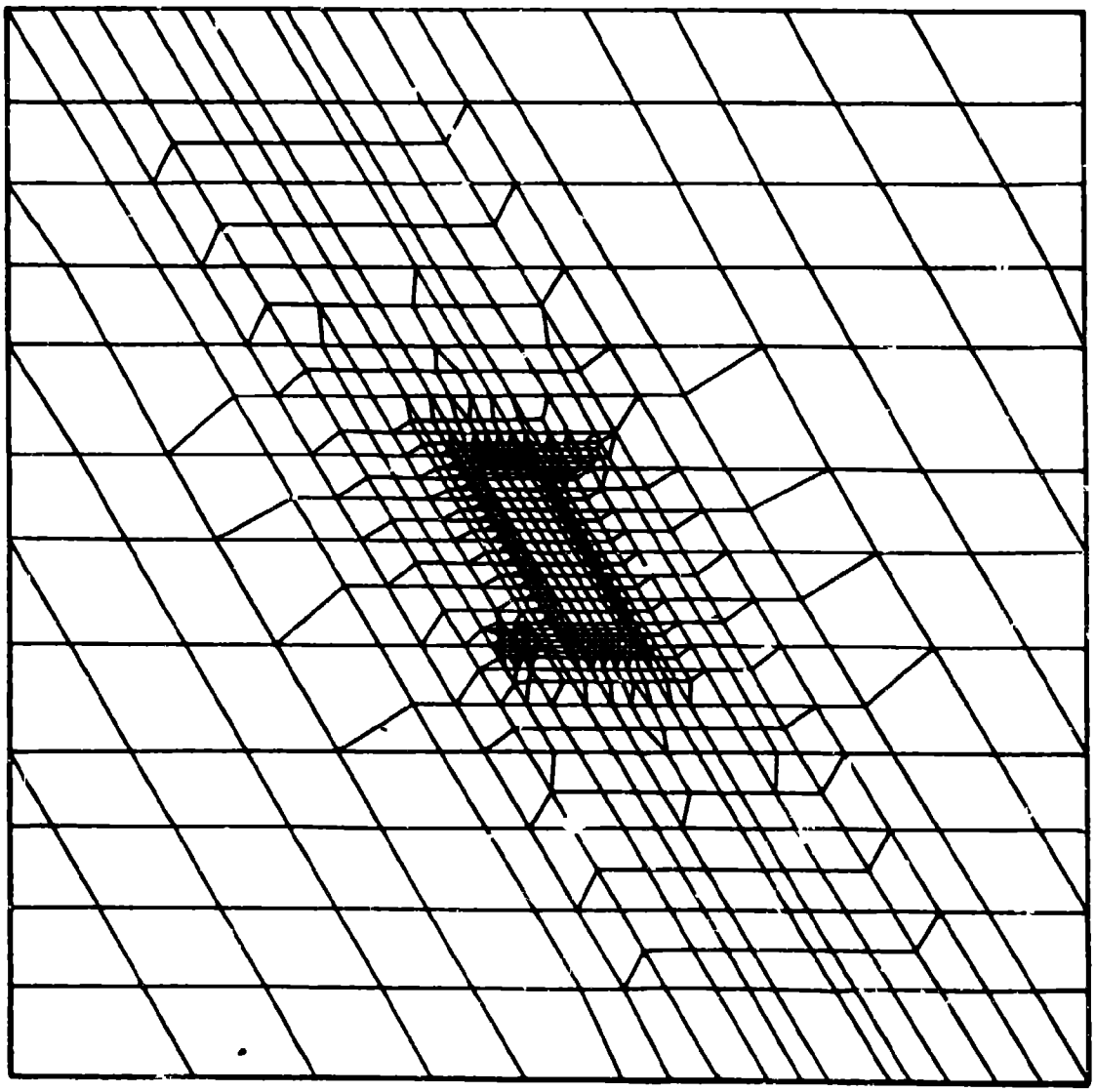

Figure 69. - Finite element mesh for 60^{o} dip.

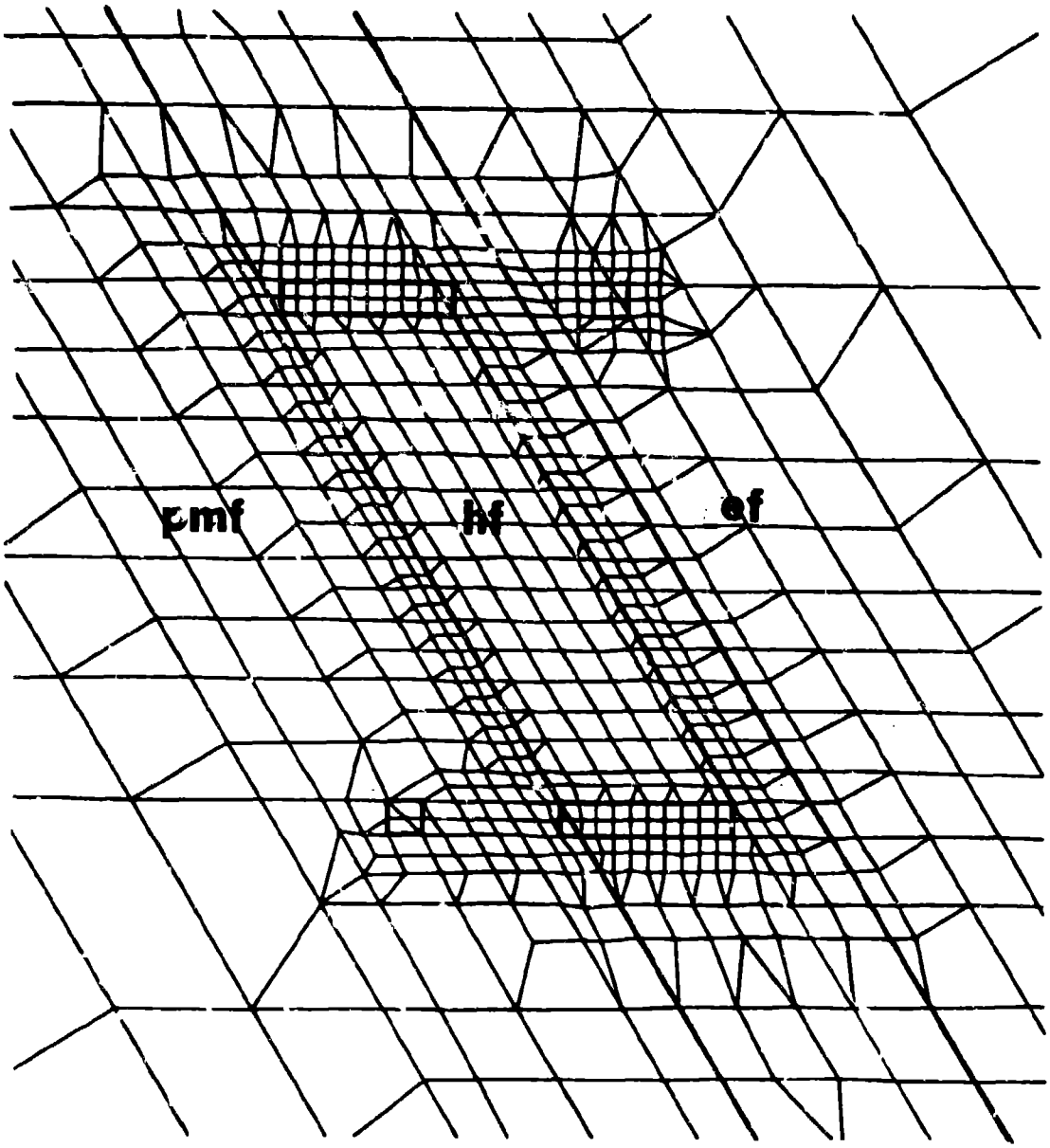

Figure 70. - Mesh refinement for Ellison hanging wall.

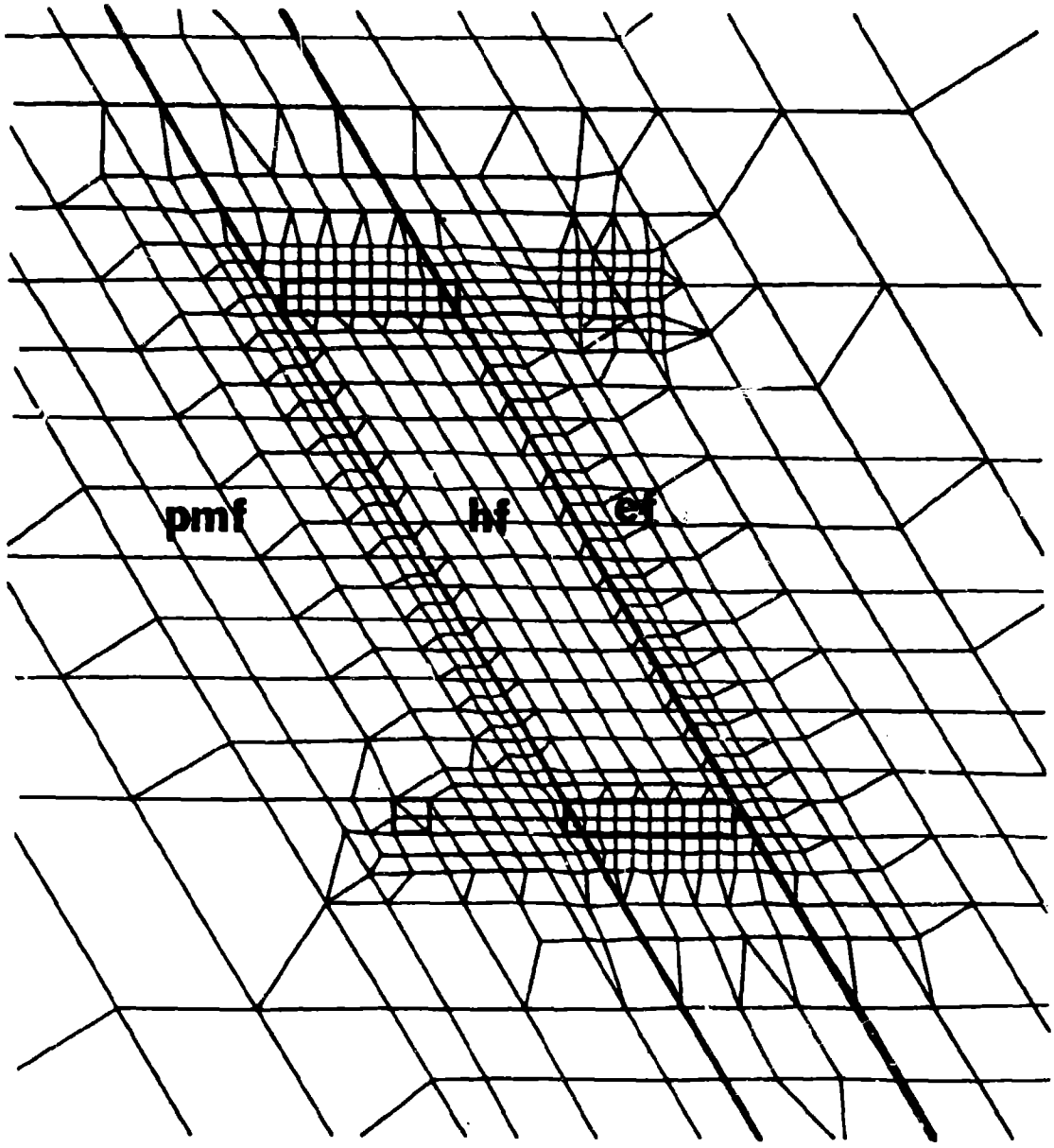

Figure 71. - Mesh refinement for Homestake hanging wall.

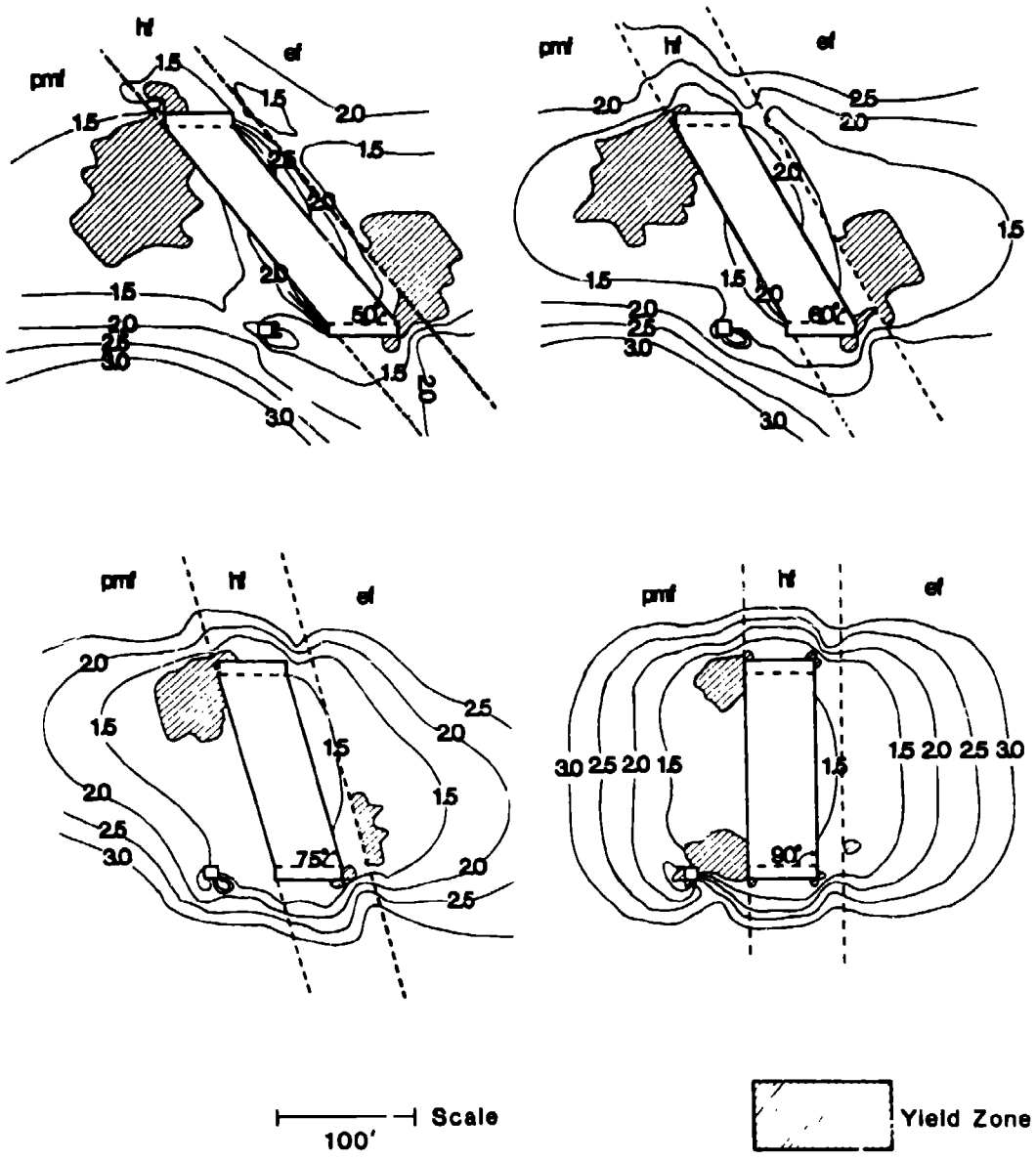

Figure 72. - Yield zone extent and safety factor contours as a function of dip for a Homestake formation hanging wall.

on stability. Four widths were considered, 25, 50, 75 and 100 ft, as shown in Figure 73. Rock mass properties and in situ stresses are the same as in the final study stope analysis. The results are summarized in Figure 74 in the form of yield zone extents in the footwall and hanging wall. The immediate hanging wall is Homestake formation. A second series with Ellison formation on the immediate hanging wall is much the same. Both show an insensitivity of yield zone extent to change in the stope width (perpendicular to strike). The yield grows slowly with increase in stope width. This is perhaps not too surprising because the sharpness of the acute corners does not change with width. The peak stress concentration is therefore insensitive to width increase over the range studied (25 to 100 ft).

Stope Length

A plan view analysis offers the potential for assessing the influence of stope length (measured on strike) on stability. A longitudinal view offers the same possibility. Both views also offer the possibility of assessing the influence of pillar length (along strike) on stability. Unfortunately, the dip of the formations precludes the use of a two-dimensional computer program for such analyses. Both problems are truly three-dimensional. A compromise that provides some guidance for stope and pillar lengths is to assume vertical beds (dip 90°). The results should be reasonable for near vertical as well as vertical stopes. A plan view shows all three formations; a longitudinal section would be entirely in ore. The plan view was selected for analysis. Rock mass properties and in situ stresses are the same as used in the final study stope analysis. In plan view, the applied stresses are horizontal. The stress acting perpendicular to the vein is a compression of 5,780 psi; the stress acting parallel to the strike direction is a compression of 4,090 psi. These are the horizontal principal stresses at stope mid-height; their ratio is 0.71.

Figure 75 shows the yield zone extent in plan view for stopes 50 ft wide and of varying strike length: 25, 50, 100, 200 and 400 ft. The analysis is symmetric about the stope centerline, so only one-half the stope is shown. Figure 75 also shows the mesh refinement used. A distinction needs to be made between the case where stope length is less than stope width and the case where stope length is greater than stope width.

For lengths greater than the width, the peak compression stress concentration in the corner and the relative displacement across the vein on the stope centerline are proportional to the length-to-width ratio. This is reflected in the spread of the yield zones at lengths greater than the width (50, 100, 200 and 400 ft strike length, 50 ft width). At 50 ft and 100 ft, the yield zones are limited in extent. However, at 200 ft the yield zone in the hanging wall (Ellison formation) bridges the opening. At 400 ft, yield zones in the Poorman and Ellison formation bridge both the footwall and hanging wall.

In the one case examined where the strike length is less than the stope width (50 ft x 25 ft), a zone of high compression causes yielding

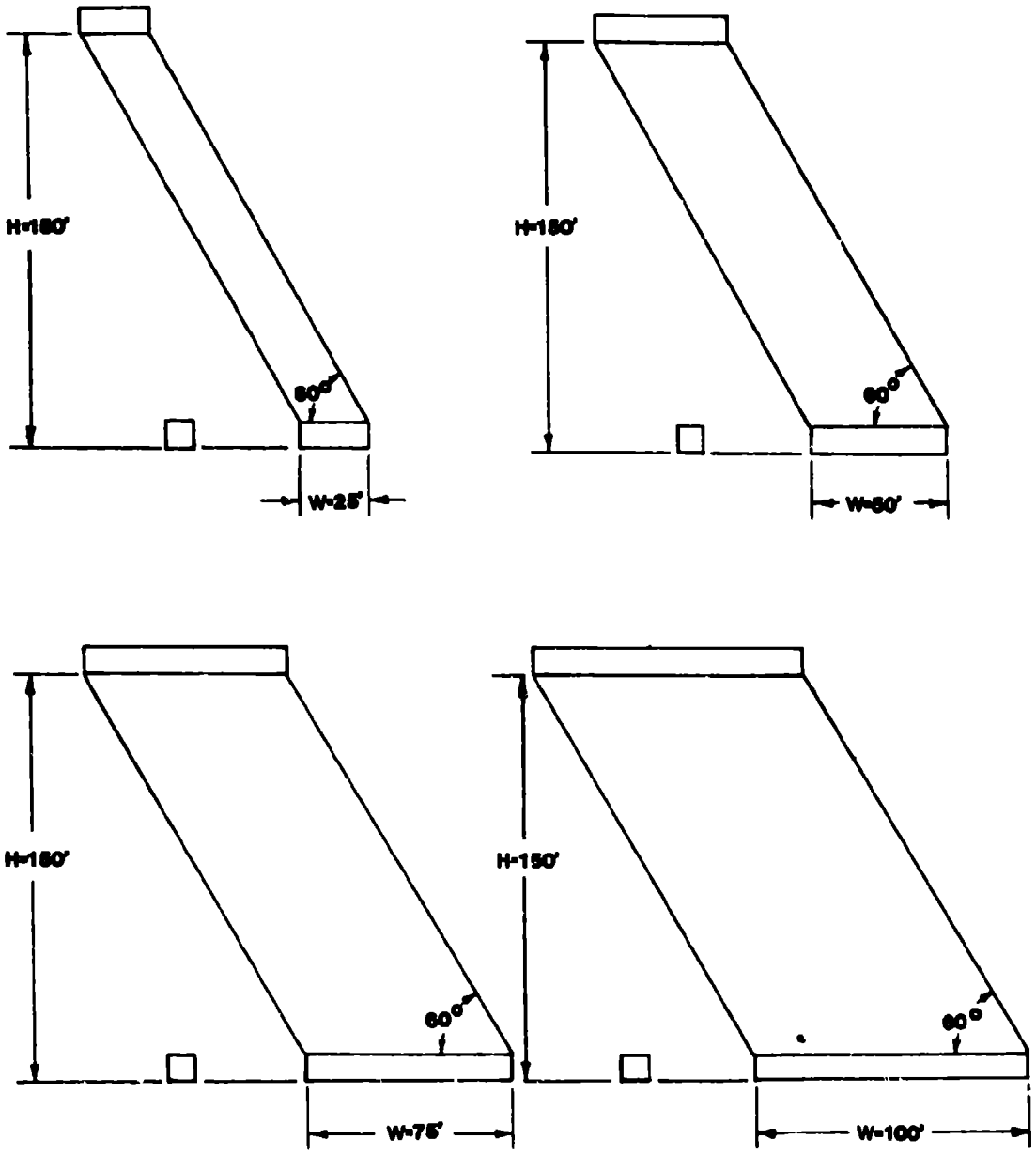

Figure 73. - Stope widths used in the 60^{o} width to height ratio study.

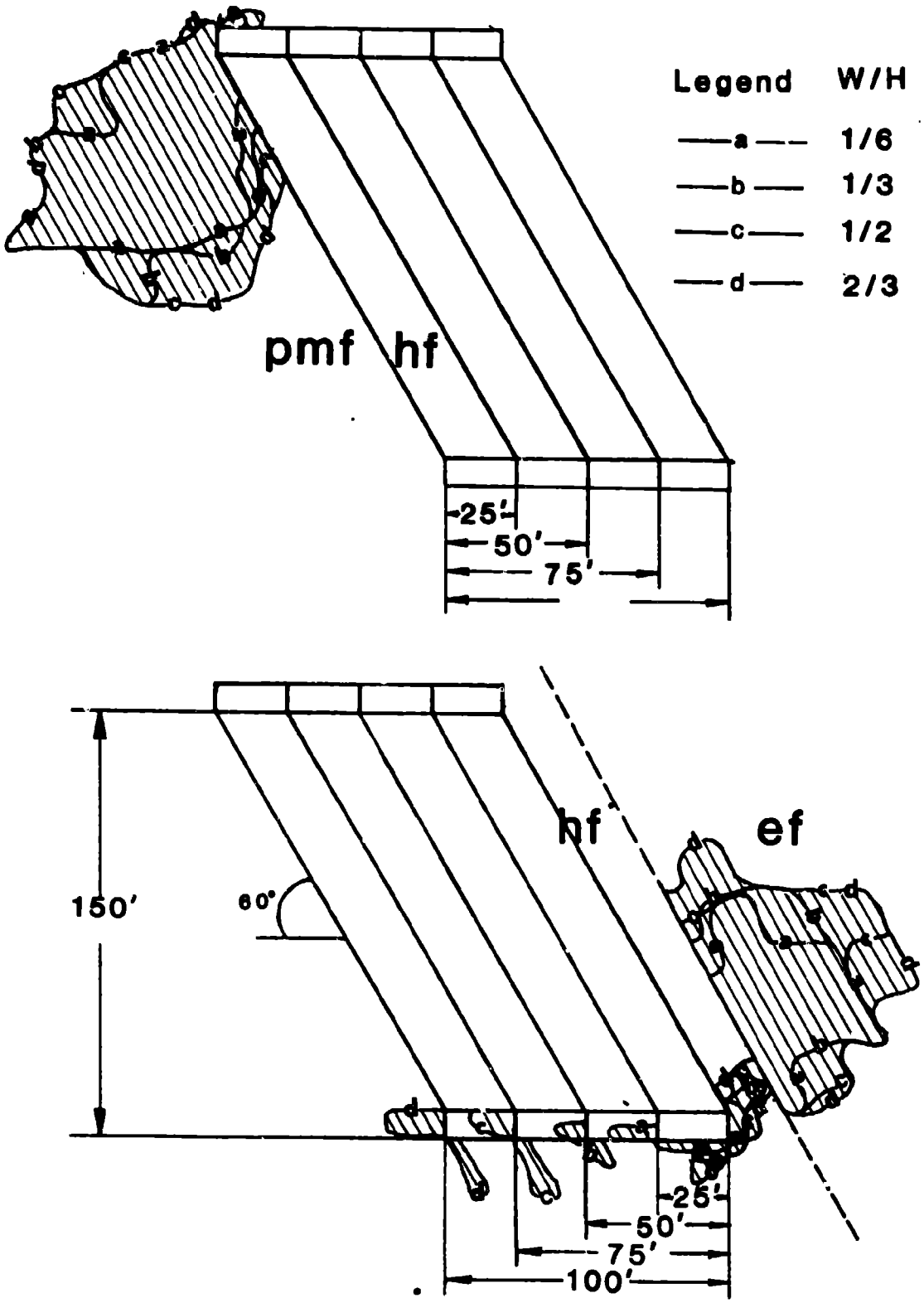

Figure 74. - Footwall and hanging wall yield zones as a function of width for a Homestake hanging wall and 60° dip.

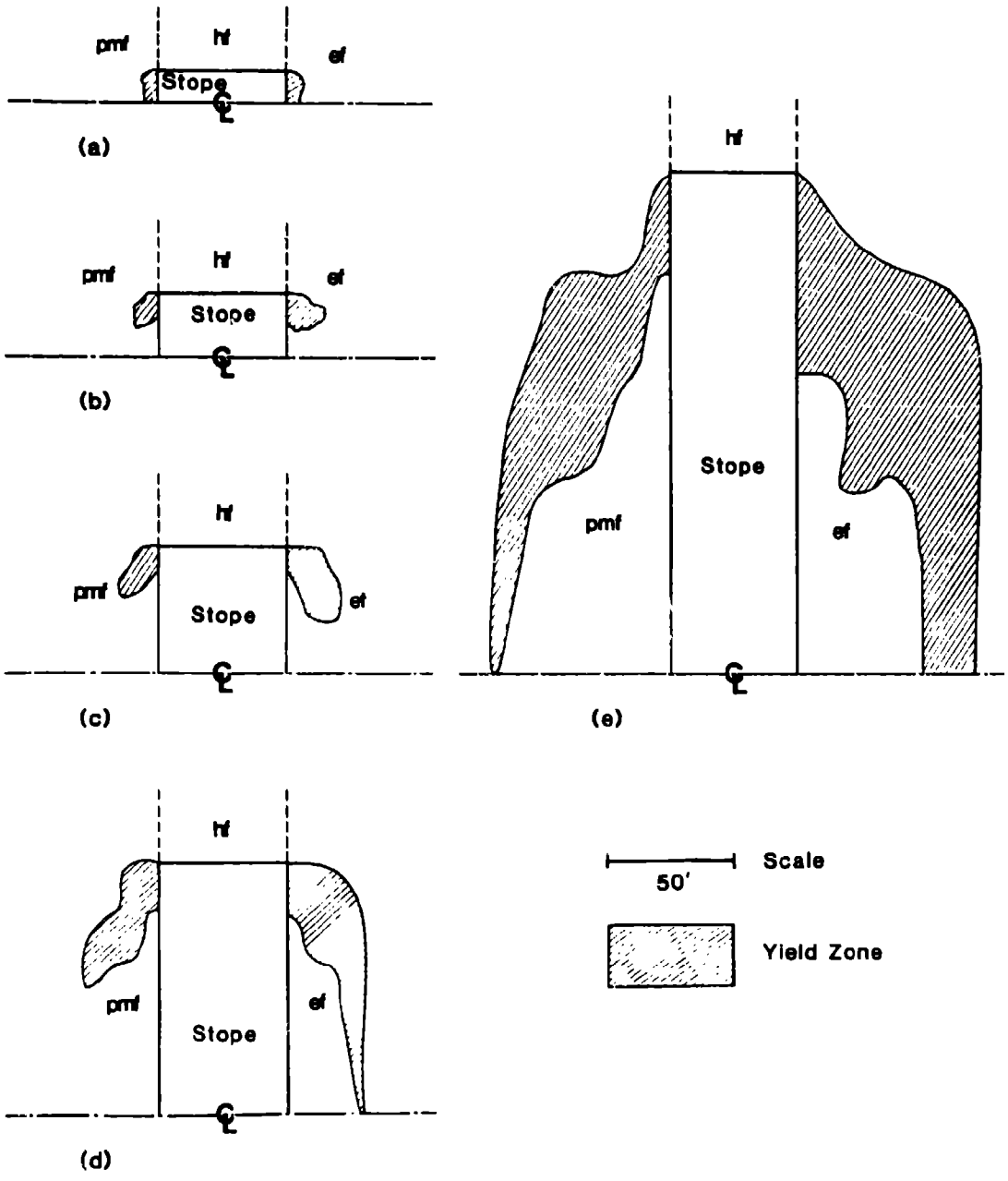

Figure 75. - Plan view yield zones as a function of stope length at fixed width (a) 50 x 25 ft, (b) 50 x 50 ft, (c) 50 x 100 ft, (d) 50 x 200 ft, (e) 50 x 400 ft.

to bridge both footwall and hanging wall. This suggests that transverse stopes may be at a disadvantage relative to longitudinal stopes.

Figure 76 shows the stress concentration about the plan view stopes from a purely elastic view. The high stress concentrations at the corners are evident; their exact value is difficult to determine but this is of less importance than the fact that yielding does occur when strengths are incorporated into the analyses. Figure 76 also shows that the narrow stope (50 ft x 25 ft) has the highest compressive stresses along the footwall and hanging wall. A slight tension occurs in the footwall (Poorman formation) at a stope 50 ft x 100 ft. Tension increases at greater stope lengths and appears in the hanging wall (Ellison) also.

Figure 77 shows closure across the vein as a function of the length-to-width ratio in the purely elastic case. The linearity of closure with respect to length-to-width ratio is substantiated by the results shown in Figure 77.

The spread of the yield zone across the hanging wall from stope end to end (bridging) indicates a potential cave of the hanging wall. At strike lengths between two and four times the stope width, yielding in an Ellison hanging wall is extensive enough to suggest caving. The critical length-to-width ratio for an isolated stope is probably closer to four than to two.

Pillar Length

Stopes separated by pillars may interact if sufficiently close. In this regard, stope spacing, stope length, pillar length and extraction percentage as seen in plan view are related and only two can be independently specified. A rough rule of thumb states that the zone of influence of a single opening is proportional to opening size. Hence, stope interaction is small when pillar length exceeds stope length. A second consideration is the pillar width to length ratio (as seen in plan view). Stubby pillars are usually stronger on average than tall, slender pillars of the same rock type. Confining pressure of adjacent rock across and along the vein is also important to pillar stability.

In order examine the question of pillar stability, the plan view mesh was modified to represent a row of stopes and pillars along strike. Symmetry of the problem requires consideration of only one-half of an adjacent stope. Stope width across the vein was then held constant at 50 ft in a series of runs at 50% extraction and 75% extraction as seen in plan view. (Extraction here is the ratio of mined area to mined area plus pillar area). In each of the series, stope lengths along strike were 50, 100 and 200 ft.

At 50 percent extraction pillar length is equal to stope length. The extent of yielding associated with a series of stopes and pillars at 50% extraction is shown in Figure 78. The results are quite similar to those obtained for isolated stopes of the same size. Hence, the rule of thumb for the extent of the zone of influence of a stope is substanti-

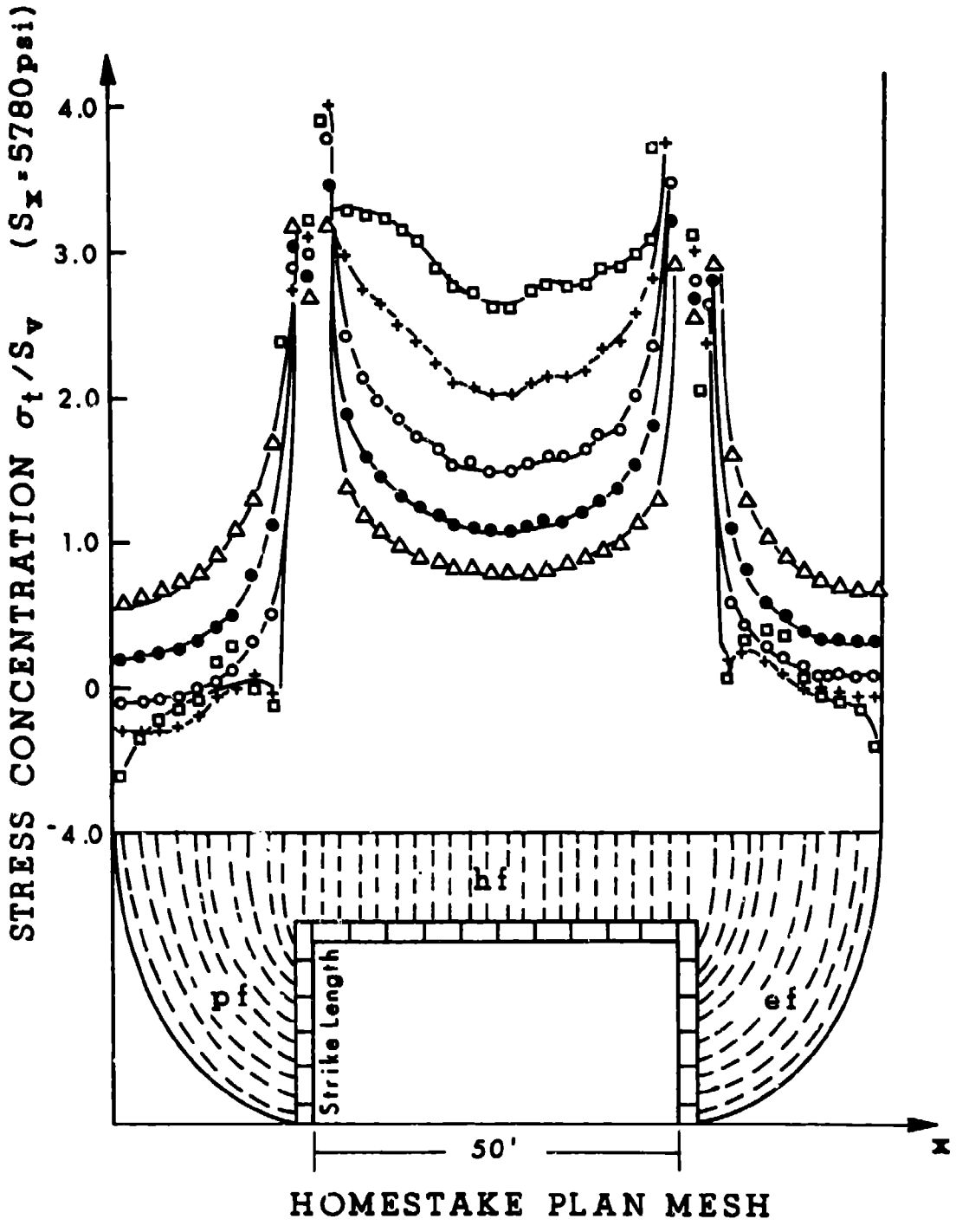

Figure 76. - Stress concentration in plan view at various stope lengths and fixed width.

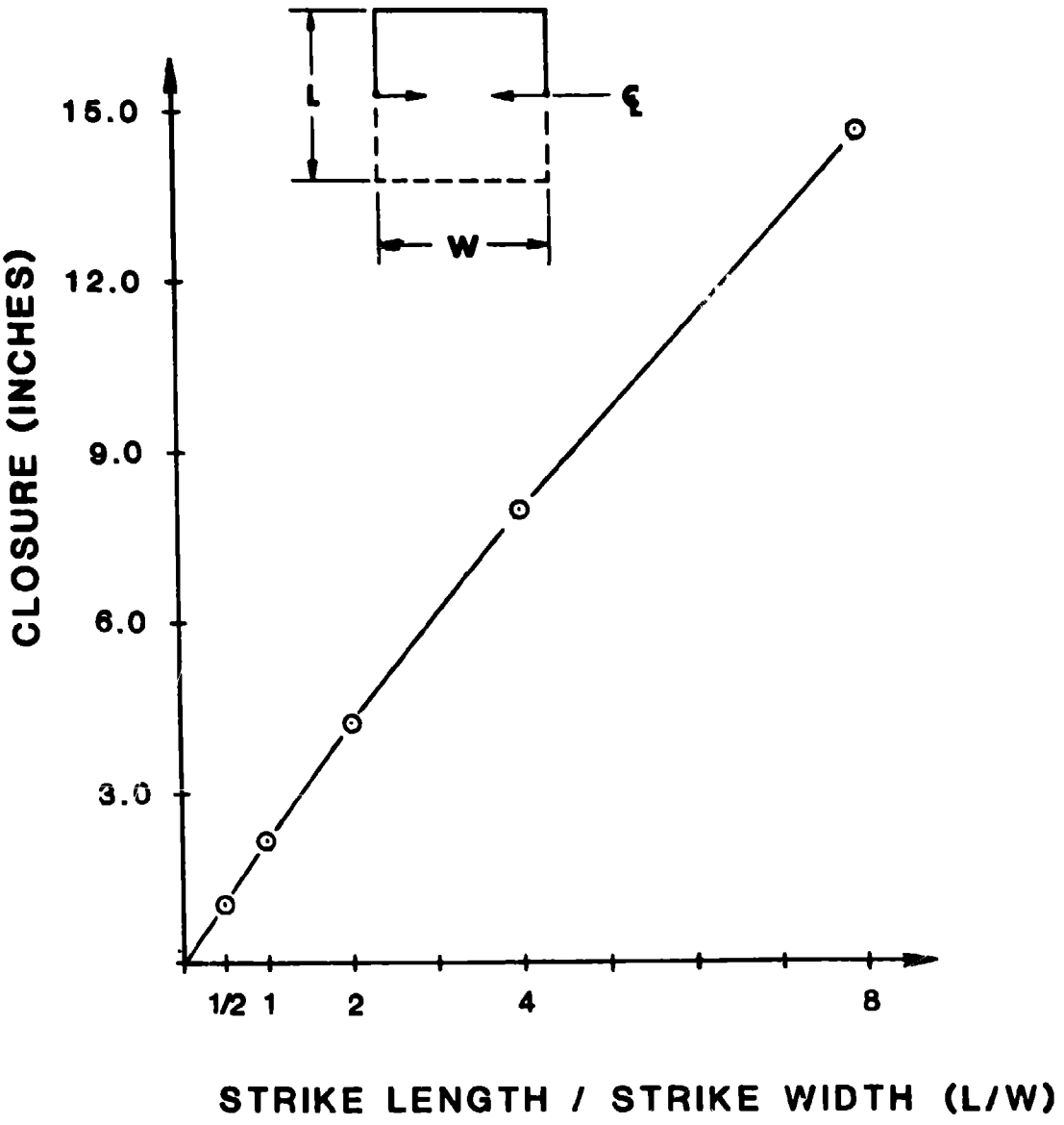

Figure 77. - Stope closure in plan view as a function of length to width ratio.

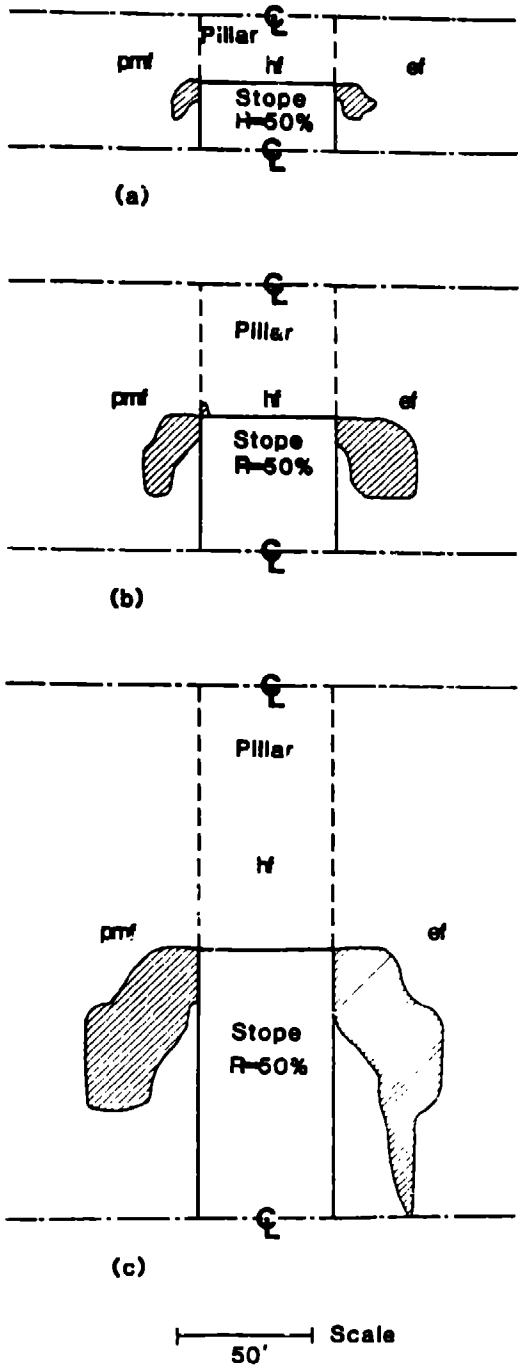

Figure 78. - Yielding at 50% extraction (plan view) for stope and pillar length of (a) 50 ft, (b) 100 ft and (c) 200 ft. Stope width is 50 ft.

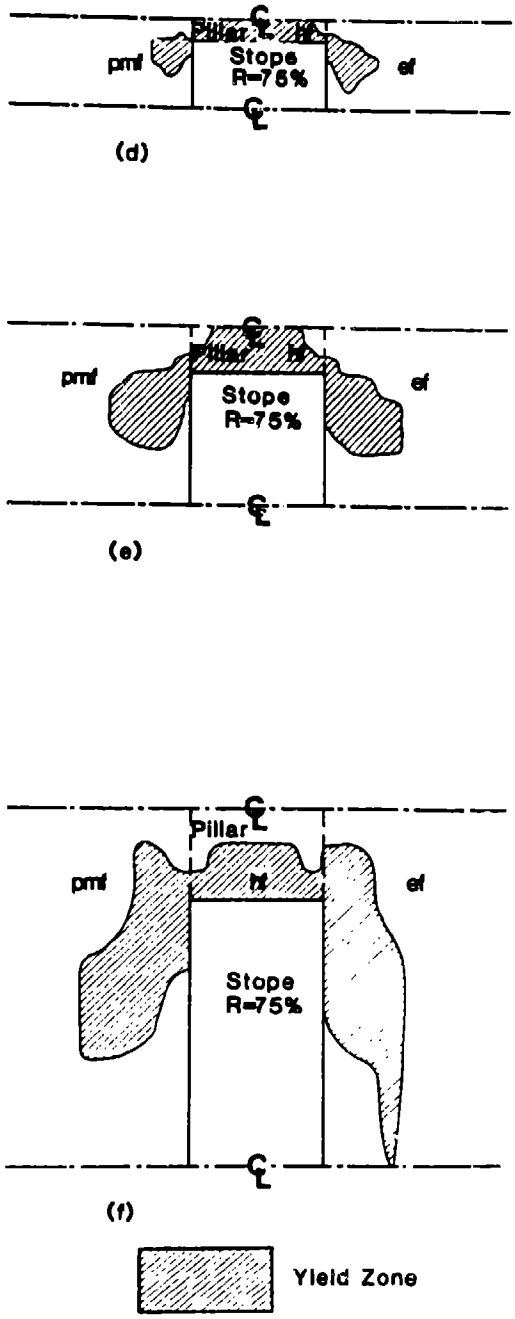

Figure 79. - Yielding at 75% extraction (plan view) for stope and pillar lengths of (a) 50 ft/17 ft, (b) 100 ft/33 ft and (c) 200 ft/67 ft. Stope width is 50 ft.

ated in this case. Yielding of the pillars in the Homestake formation was not observed, nor was failure at the stope ends in the case of the isolated stope. However, the safety factor in the skin of the pillar is generally less than two, and near the corners it drops close to one.

The results of the stope and pillar size analysis series at 75% extraction are shown in Figure 79. The stope sizes of 50 x 50 ft, 50 x 100 ft and 50 x 200 ft are the same as in the 50% extraction and isolated stope series. Pillars between the 50 x 50 ft and 50 x 100 ft stopes are 17 ft and 33 ft along strike. Both show extensive yielding indicative of collapse. However, the pillars between the 50 x 200 ft stopes do not show yield zones that encompass the entire pillar cross section. Yielding is extensive, but the yield zones do not extend entirely through the core of a pillar. Although the extraction is the same at 75%, and therefore the average pillar stress across the vein is the same for each of the three stope and pillar size combinations, the length to width ratio is different (17/50, 33/50, 67/50) in each case. The distribution of stress is different, and as a consequence the extent of yielding is different. Unfortunately, the larger stope and pillar combination (50 x 100 ft stope, 50 x 67 ft pillar) also shows more extensive hanging wall and footwall yielding than the smaller stope and pillar combinations.

At fixed stope width (across the vein) and fixed extraction percentage, increasing the stope length tends to destabilize the hanging wall and the footwall. The companion increase in pillar length has the opposite effect on the pillar; it tends to increase pillar stability. Hanging wall and footwall stability are governed largely by stope length to width ratio; extraction percentage mainly influences pillar stability. However, pillar length to width ratio also influences pillar stability.

CONCLUSION

The background, objectives and approach to a second geomechanics case study have been presented. The study was a cooperative effort by the Homestake Mining Company, the U. S. Bureau of Mines and the University of Utah. During the course of the study a full scale stope was mined to completion and backfilled. The mining method used large diameter blastholes in true vertical crater retreat fashion in contrast to the first study at the Carr Fork Mine where the method was large diameter blasthole stoping with post-fill. The main geomechanics objective was the same, however, and that was to establish a procedure for optimizing stope and pillar dimensions. The approach was also the same and involved a combination of mine measurements, laboratory testing and finite element calculations.

Some 19 instrumented drill holes, some over 100 ft long, were used to monitor the response of the center panel, one of three in the study stope region, as mining progressed from the development phase through ring drilling and blasting on the extraction level to removal of the crown pillars and backfilling. Although the study stope is relatively deep (between the 6950 and 7100 levels) bursting is not a problem. The primary concern is slough and caving of the hanging wall. In this regard, the presence of a cable bolt drift in the hanging wall provided a unique opportunity for a geomechanics study because of the access it provided to the hanging wall region which is ordinarily inaccessible and thus difficult to instrument and monitor. Relative displacement measurements from multi-anchor rod extensometers that were grouted in the hole provided the bulk of the useful data. A few snap ring extensometer anchors in the immediate hanging wall were lost in the course of mining. Anchors nearest the hole collars in the cable bolt drift were not lost. All the instrumentation in the two panels adjacent to the mined panel is intact and operative (May, 1985). With very few exceptions, extensometer readings were less than 0.9 inches. However, there was no correlation between reading and anchor loss. Some anchors survived large displacements; some were lost at 0.3 inches of displacements. Jumps in readings generally coincided with blasting. The larger crown pillar blasts were especially noticeable. Generally, the mine measurements phase of the study went according to plan. All instrumentation was installed on schedule well in advance of mining so that base line data were obtained for all measurement sites. Instrument survivability was excellent and the data obtained sufficient for rock mechanics analyses.

A vertical section through the center of the steeply dipping mined panel was selected for finite element analysis. This section is perpendicular to strike and is the section most amenable to a detailed two dimensional analysis. Plan and longitudinal sections would be valid only for vertical stopes. The finite element analyses provide a set of theoretical model displacements associated with a simulated mining sequence that can be compared with actual or measured displacements. The model includes the cross section geology and the three major formations (Poorman, Homestake, Ellison) present. These formations were viewed as orthotropic elastic-plastic materials because of the well-developed foliation present, especially in the Poorman formation. Rock properties needed to define the anisotropic elastic and strength moduli

were determined from laboratory tests on core samples from a set of approximately orthogonal drill holes in the study stope region. The yield criterion is nonlinear and anisotropic, while the plasticity is based on associated flow rules. The in situ stress state was evaluated from earlier in situ stress measurements obtained from doorstopper and borehole deformation gage data and from recent (1984) hollow inclusion cell data. The UTAH-II finite element program was used for all analyses.

Three sets of finite element analyses were obtained from the Homestake Mine study in much the same way as for the Carr Fork Mine study. The first set of calculations provides data for determining whether the initial finite element representation of the study stope is close to reality and, if so, data for estimating scale factors that allow for the extrapolation of laboratory rock properties to rock mass values. Upon completion of the first set of calculations, a second detailed simulation of the mining sequence using the initial estimates of the elastic and strength properties scale factors is undertaken. This provides a check on the initial evaluation and a final calibration of the finite element model. The third set of calculations consists of exercising the calibrated finite element model by considering alternative stope and pillar sizes, in order to demonstrate the potential for design optimization.

A regression analysis of calculated on measured extensometer readings (incremental relative displacements) in the immediate hanging wall using laboratory rock properties gave a correlation coefficient of 0.84. The correlation coefficient is independent of the actual values of elastic moduli, so that the slope of the regression line at this high correlation becomes the scale factor for the elastic moduli and allows specification of the 18 dimensional elastic moduli for rock mass behavior. A proportional reduction in laboratory strengths and a reanalysis of the study stope section then allows for fixing the strength scale factor by a reasonable match between calculated yield zone extent and that inferred from extensometer anchor loss. Scale factors of 0.36 and 0.8 for dimensional elastic and strength properties were determined. A second regression analysis of calculated on measured displacements using rock mass properties scaled from laboratory values gave a correlation coefficient of 0.80. This was deemed adequate for parameter studies of alternative stope layouts. Fine tuning could improve the correlation, but as a practical matter the additional costs apeared to outweigh the additional benefits since the correlation was already high.

The validated and calibrated finite element model was used to examine the influence of dip and stope width on stability as seen in section and the influence of stope length and pillar length as seen in plan view. As the dip is decreased from the vertical, footwall stability is decreased in VCR stopes; hanging wall stability is influenced to a lesser degree. Increasing the width of a stope measured across the vein has little influence on stability provided the stope length along strike remains greater than width (longitudinal stope) and width is less than level interval (stope height). A Homestake formation hanging wall is more stable than an Ellison formation hanging wall. Increasing the stope strike length in plan view gradually decreases footwall and hang-

ing wall stability of an isolated stope. Caving is definitely indicated at a length that is eight times width. Stability is marginal at about four times width. Transverse stopes in which strike length is less than width show yield zones bridging the footwall and hanging wall. Pillars that are as long as the stopes (in plan view) effectively isolate the stopes (longitudinal). Thus at 50% extraction as seen in plan view stope stability is governed by the stope length to width ratio (four or less). Pillar stability is influenced by the pillar length to width ratio also, even though average pillar stress across the vein is constant at constant extraction ratio. A greater pillar length to width ratio favors stability. Pillars are stable at 50% extraction, however, at 75% extraction pillars are definitely unstable. These results are guidelines only, but are indicative of the alternatives that can be considered on the computer at much less cost than full scale mine trials.

In conclusion, the high correlation achieved between calculated and measured displacements and yield zones substantiates the underlying rock mechanics model and finite element representation of the study stope geology, geometry, mining sequence, and in situ stress state. Parametric studies for optimizing stope and pillar sizes using the field calibrated and validated finite element model are therefore justified. The main geomechanics objective of the study stope project was thus achieved. The basic approach that was successful at the Carr Fork Mine has proved successful at the Homestake Mine.

REFERENCES

Bond, P. H., 1970, "The Directions and Magnitudes of the Principal Stresses at the 6200 Foot Level of the Homestake Mine, Lead, South Dakota," M. S. Thesis, South Dakota School of Mines and Technology.

Duan, F., 1985, "Report on Rock Properties for the Homestake Mine," Department of Mining Engineering, University of Utah.

Hooker, V., Personal Communication.

Hladyz, Z. and D. J. Erickson, 1984, "Mechanical Properties of Rocks from the Homestake Mine," Department of Mining Engineering, SDSMT, Final Report prepared for the Homestake Mining Company.

Mitchell, S. T., 1980, "Vertical Crater Retreat Stoping Proves Successful at Homestake Mine," Mining Engineering, Vol. 32, pp. 1581-1586.

Orr, S. A., 1983, "Refinement of Vertical Crater Retreat Stoping at the Homestake Mine," Homestake Mining Company Report.

Pariseau, W. G., 1972, "Plasticity Theory for Anisotropic Rocks and Soils," Proc. 10th U. S. Symp. Rock Mech., pp. 267-295.

Slaughter, S. L., 1968, "The Homestake Mine," Ore Deposits of the United States, 1933-1967, ed. J. D. Ridge, Vol. 2, AIME, N.Y., pp. 1436-1459.

Waterland, J. K. and Connolly, T., 1966, "Cut-and-Fill Stoping," Mining Congress Journal, Vol. 52, pp. 29-36.

APPENDIX

IMPORTANCE OF ANISOTROPY

Schistosity imparts a directional character to rock, of course, and thus raises a question concerning anisotropy. All rocks probably show some degree of anisotropy when tested with sufficiently sensitive apparatus (see e.g. Thill, and others, 1969). Strengths as well as elastic properties may vary with direction. However, the question here concerns not the presence but the importance of anisotropy to engineering design.

Anisotropic elastic analysis is a specialty area, while consideration of strength anisotropy is rare indeed. This is somewhat surprising in view of the enormous tonnages of rock mined from sedimentary and metasedimentary formations throughout the world. In this regard, the additional computational cost of including anisotropy in a finite element analysis of stress and stability is negligible. In situ stress measurement costs are also about the same as in the isotropic case. Rock properties testing costs may be more because of the additional number of samples needed to define anisotropic rock behavior. However, if the total number is kept the same, then testing costs will be about the same. These costs are miniscule compared with the cost of judging a stope design safe when in fact stability is doubtful. The difficulty with anisotropy is thus not so much one of input data gathering and computational costs, but is rather a conceptual one arising from a lack of familiarity with the implications of anisotropy for ground control.

The general lack of experience with anisotropy in geomechanics problems makes intuition unreliable. A systematic, step-by-step approach to the question concerning the importance of anisotropy to ground control thus seemed prudent. Accordingly, a sequence of analyses was developed that gradually approached conditions at the Homestake Mine in the vicinity of the study stope between the 6950 and 7100 Levels. The sequence begins with rechecks of the finite element program, UTAH-II, used for the calculations and ends with a comparative isotropic anisotropic analysis of the study stope area. The latter comparison approaches the mine measurements and finite element calculations from the isotropic viewpoint as though anisotropy was never considered. Some of these results have been reported earlier (Pariseau, Duan and Schmuck 1984).

Program Check

In order to establish a measure of confidence in subsequent finite element analysis, computer program results are compared with several known analytic and numerical solutions of relatively simple problems. The series begins with several problems run previously. Next are a number of analyses of stress about circular openings in isotropic and anisotropic elastic media. Stress concentration factors for rectangular openings are then calculated in a parametric study within the purely elastic domain involving anisotropy, applied loads, and width to height ratio. The consequences of strength anisotropy for rectangular openings are then examined within a framework of plasticity theory.

Elastic Isotropy

The hollow cylinder under internal or external pressure offers the opportunity to obtain a point-by-point comparison between finite element (FE) and analytic or exact results. Computation of the relative numerical error indicates the best that can generally be expected for the mesh refinement and element size used. Mesh refinement is an important consideration in every finite element analysis. In addition, a check is provided on the user's calculations of input external forces equivalent to the uniform pressure applied to the cylinder walls. The adequacy of the overall size of the mesh relative to opening size can also be examined.

Figure 80 shows two comparisons of analytic (exact) with numerical (FE) results. The mesh refinement is characterized by the use of 18 roughly square elements over one-fourth of the opening boundary. The ratio of boundary element size to opening size (hole radius) is approximately 0.1. In this problem, the size of the mesh, that is, the wall thickness of the cylinder, is taken into account by the analytic solution. The relative error in circumferential stress and radial displacement which usually are of greatest interest is less than 0.1%. Agreement between analytic and numerical results is thus excellent.

A circular opening in a plane of infinite extent subject to an initially hydrostatic stress state is similar to the thick-walled cylinder under a uniform external pressure. In fact, as the thickness of the cylinder increases, the two solutions become identical. This feature allows one to assess the adequacy of the mesh size relative to the opening size. The mesh used and the results of the analysis are shown in Figure 81a and 81b. The mesh refinement near the opening is the same as before, but the outer boundary is square instead of circular. Calculation of the applied forces is somewhat easier when the boundaries are parallel to the coordinate axes. The results in the isotropic case are again within 0.1%. As a rule of thumb, the distance between the opening wall and the outer mesh boundary should be roughly five times the opening radius in order to achieve acceptable results in the vicinity of the opening. This rule is certainly verified in this problem.

Elastic-Plastic Isotropy

A recheck of the isotropic elastic-plastic segments of UTAH-II is presented in Figure 82 Figure 82 compares results with those obtained earlier by Reyes (1966) who used a finite element program based on the same analytic formulation of elastic-plastic behavior but programmed in a different manner. The agreement between the numerical results shown in Figure 82 is quite good. This is not always the case with finite element programs as even very elaborate code comparisons sometimes show (Morgan and others, 1981). It is of interest to note that the z-direction stress is not always the intermediate principal stress even in the elastic domain as Figure 82c shows. This fact complicates the use of the Mohr-Coulomb yield condition, but presents no difficulty for the UTAH-II program which uses Drucker-Prager type yield conditions.

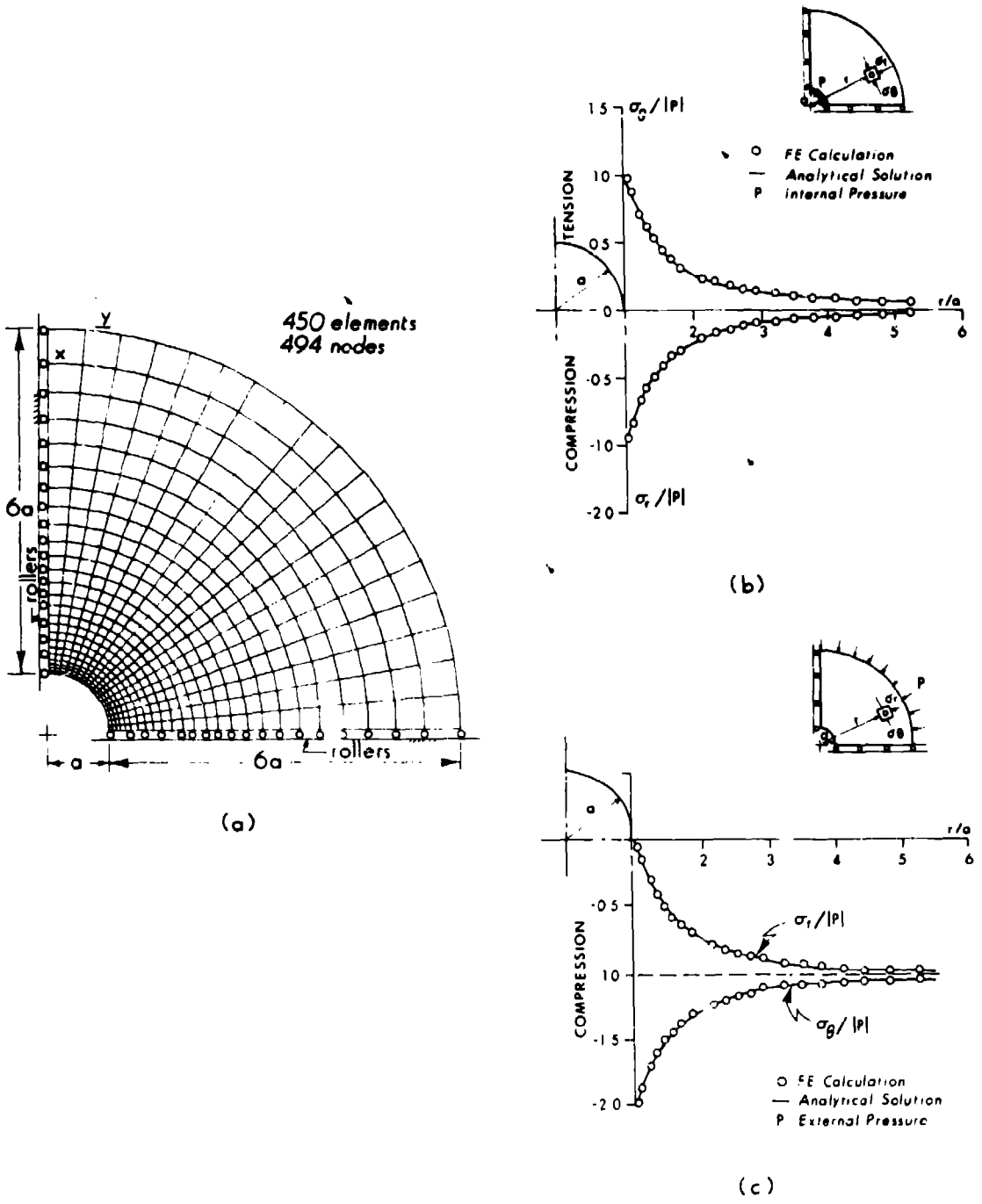

Figure 80. - Isotropic elastic hollow cylinder problem for program recheck.

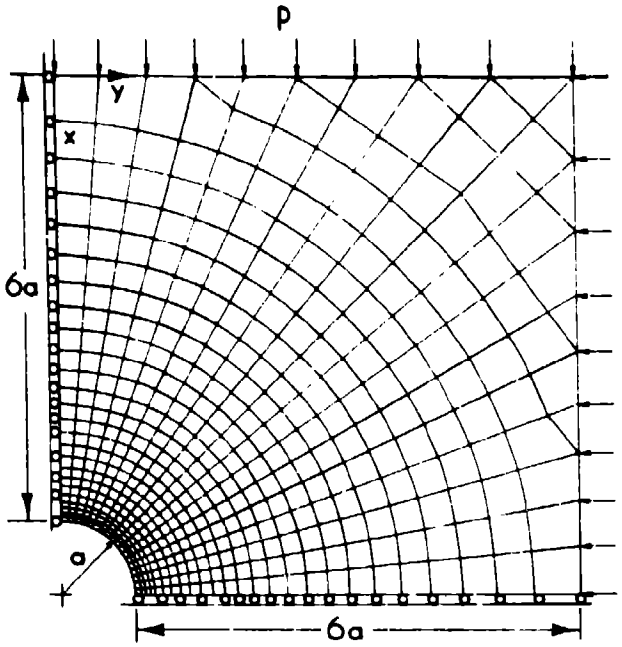

(a)

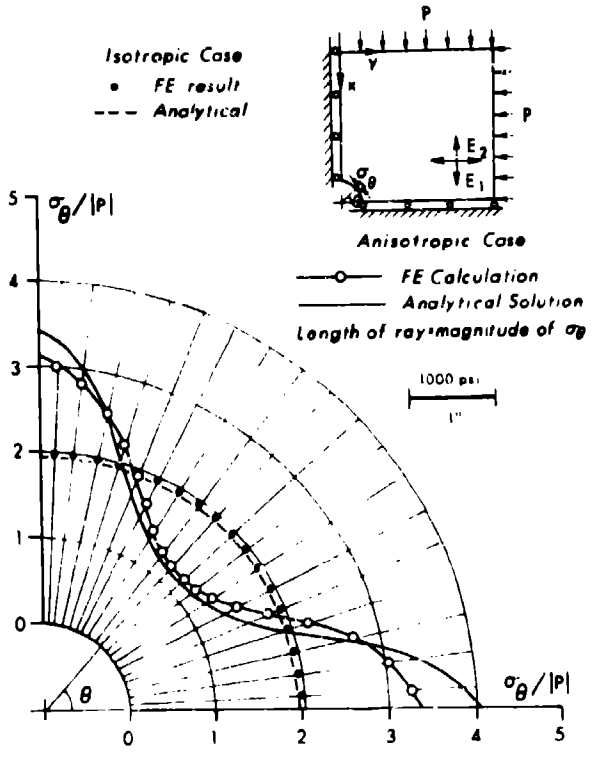

(b)

Figure 81. - Circular hole in an infinite isotropic elastic plate problem for mesh refinement check.

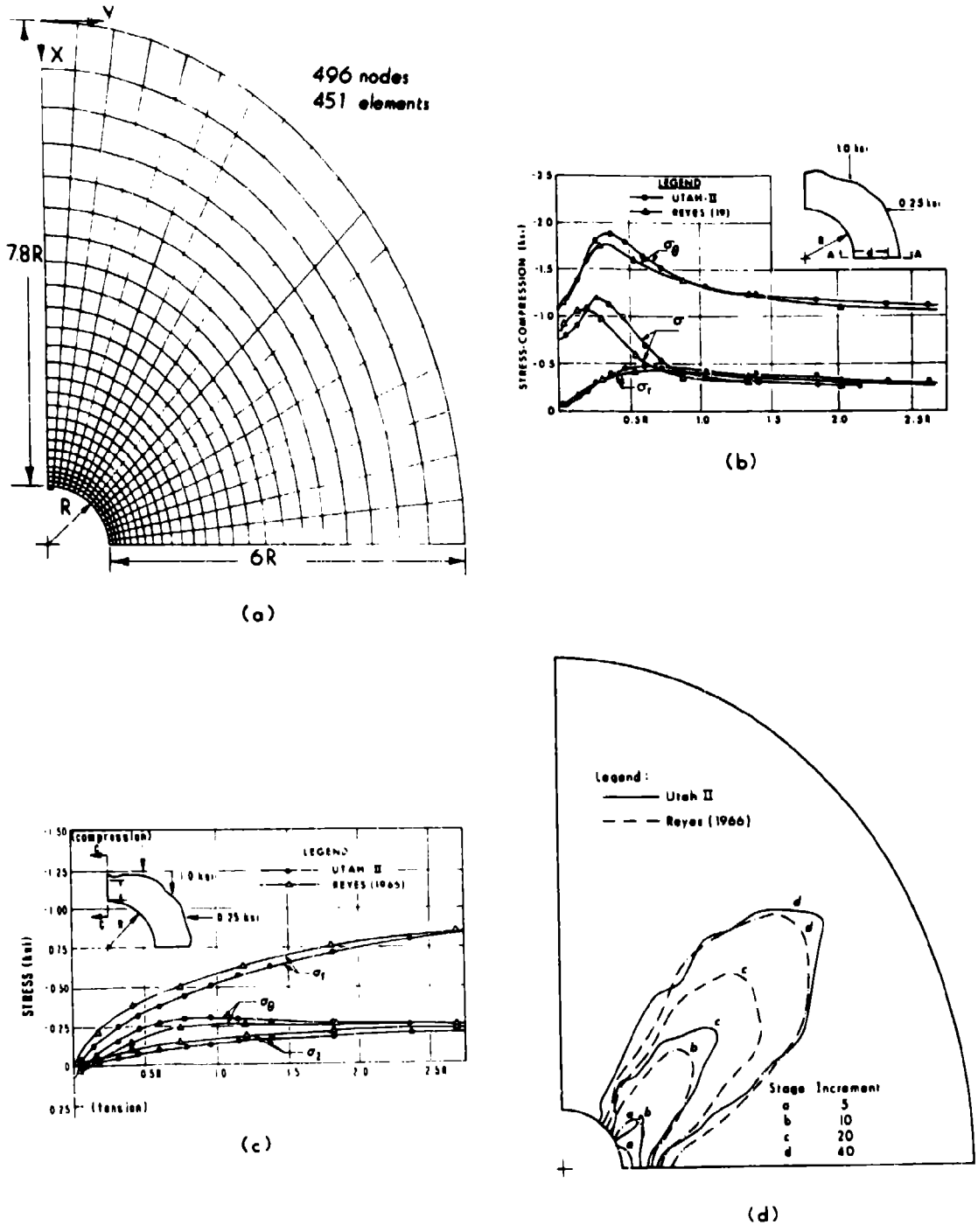

Figure 82. - Isotropic elastic-plastic program recheck.

Elastic Anisotropy

The results of an anisotropic analysis for stress concentration at the wall of a circular opening are also shown in Figure 81b. Agreement in the anisotropic case does not appear as accurate as in the isotropic case, although the differences are not large from the rock mechanics view (about 10%). This deserves some comment, however. The analytic (exact) result is taken from Lekhnitskii (1963) and applies at the opening boundary, while the finite element results are extrapolated to the opening boundary from stresses at the element centroids that are a small distance away from the opening. The stress state changes quite rapidly near the opening, especially so with the degree of anisotropy used in this problem. As a consequence, the extrapolation process involves some judgment as illustrated in Figure 83. Better agreement between the analytic and finite element results could be obtained by simply revising the extrapolation to fit the exact values, but clearly there is no point in doing so when one has the exact results. These results do indicate that with the mesh refinement used, careful extrapolation produces accurate results. Without extrapolation, the difference between boundary stress concentration and stress concentration at the centroid of an element adjacent to the boundary grows with element size. Even with the relatively small elements used in this example, the difference ranges between 2% and 20% depending on the location of the boundary point considered. Again, mesh refinement is an important consideration.

Stress concentration about rectangular openings in isotropic media has been determined experimentally by Obert and Duvall (1967) and analytically by Heller and others (1958). A square opening in an anisotropic elastic medium is discussed by Lekhnitskii (1968). Under a uniaxial compressive load, the peak tensile stress concentration occurs at right angles to the load on the centerline of the opening. The peak compressive stress concentration occurs near the corner of a rectangular opening and is senstive to the radius of curvature of the corner. A sharp corner causes a high stress concentration. This feature complicates comparisons with finite element results whether isotropic or anisotropic because of the impracticality of refining a mesh to the degree needed to accurately represent corner geometry. A brief study of this question suggests that the element dimension at the corner is roughly comparable to the radius of corner curvature in the analytic problem. With this rough equivalence, the peak stress concentrations obtained by the FE method compare favorably with experimental and analytic results in the isotropic case as shown in Figure 84. The observed difference of about 10% in Figure 84 is not numerical error but arises from the fact that the FE results are taken at the element centroids while the analytic results are at the opening boundary.

A comparison between analytic and FE results in the case of a square opening in *anisotropic* elastic rock is shown in Figure 85. Only one quadrant is necessary because of the symmetry of the problem. The mesh and boundary conditions are shown in Figure 85a. The degree of anisotropy in Figure 85 is characterized by the ratio of Young's modulus in the horizontal x-direction to the vertical y-direction Young's modulus (E1/E2). The anisotropy is that of an orthotropic material

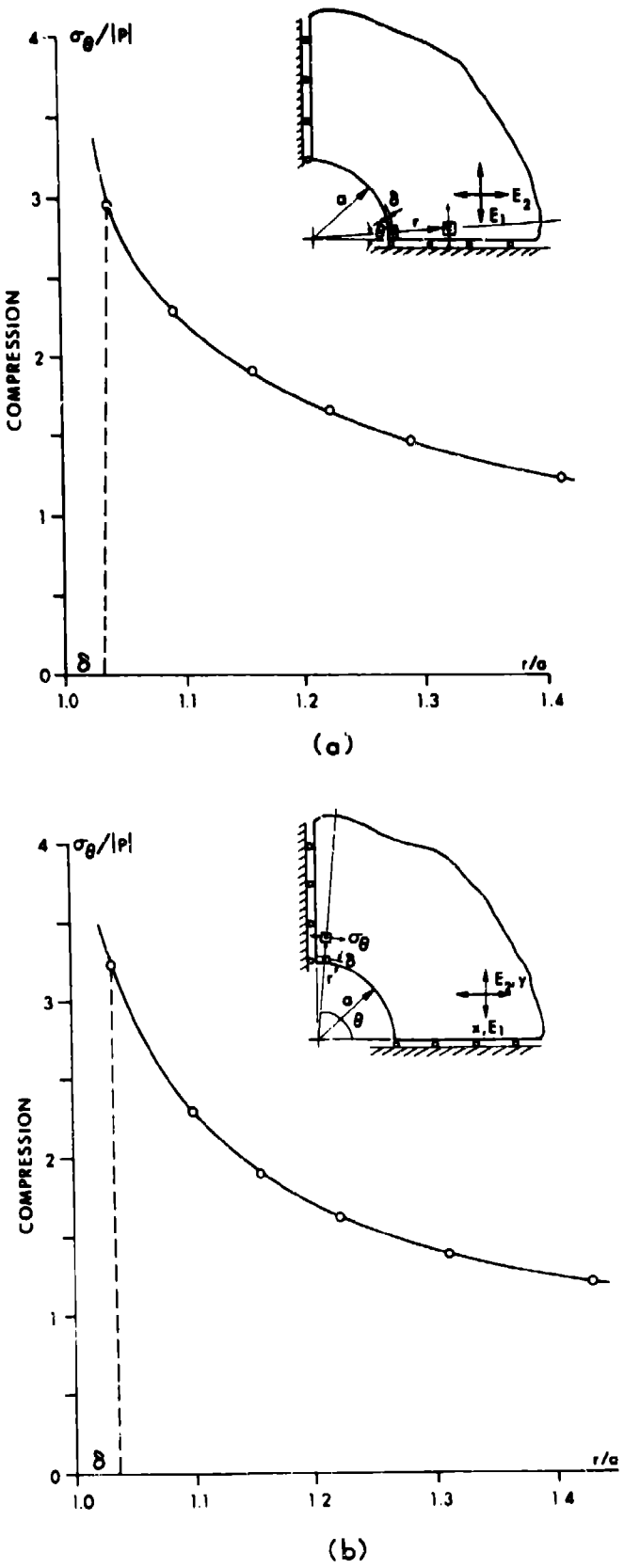

Figure 83. - Extrapolation from element centroids to hole boundary for accurate stress concentration estimates.

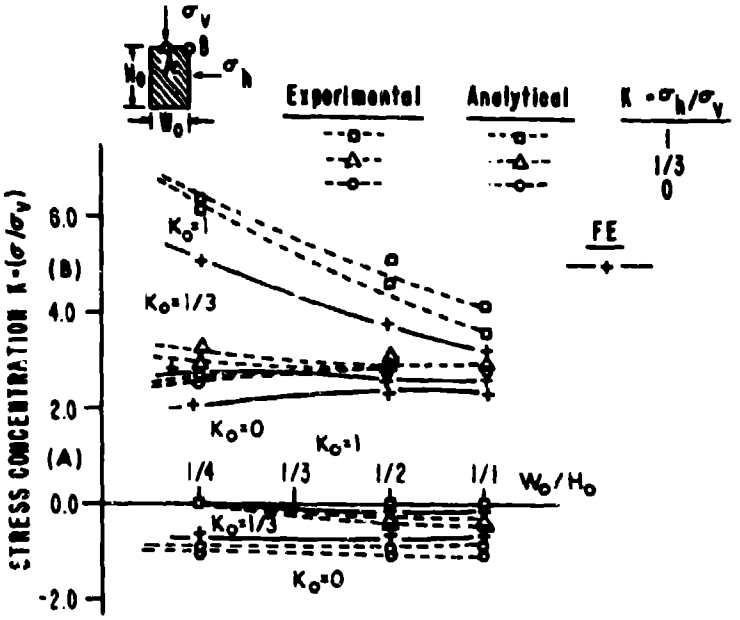

(a)

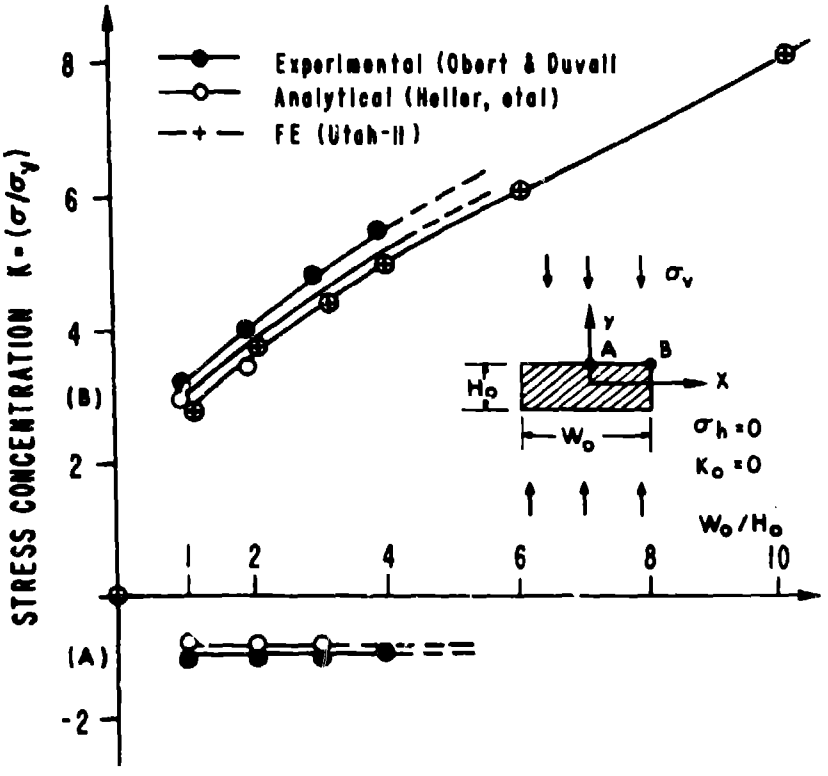

(b)

Figure 84. - Isotropic elastic rectangular opening stresses as function of the width to height ratio.

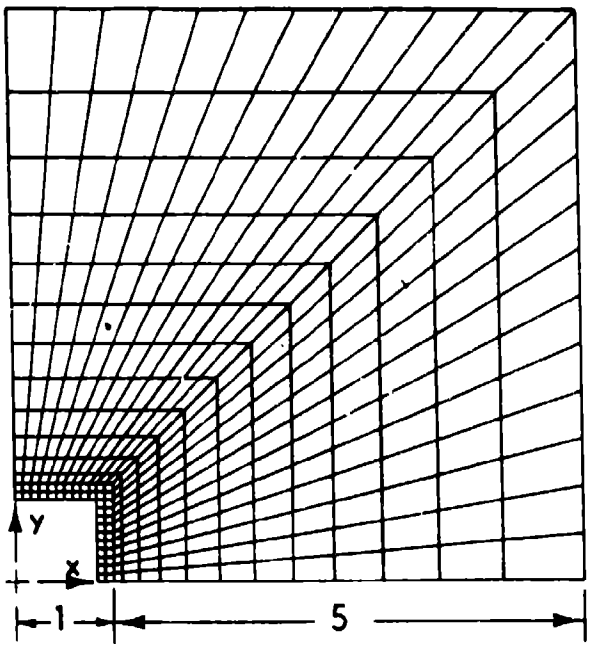

(a)

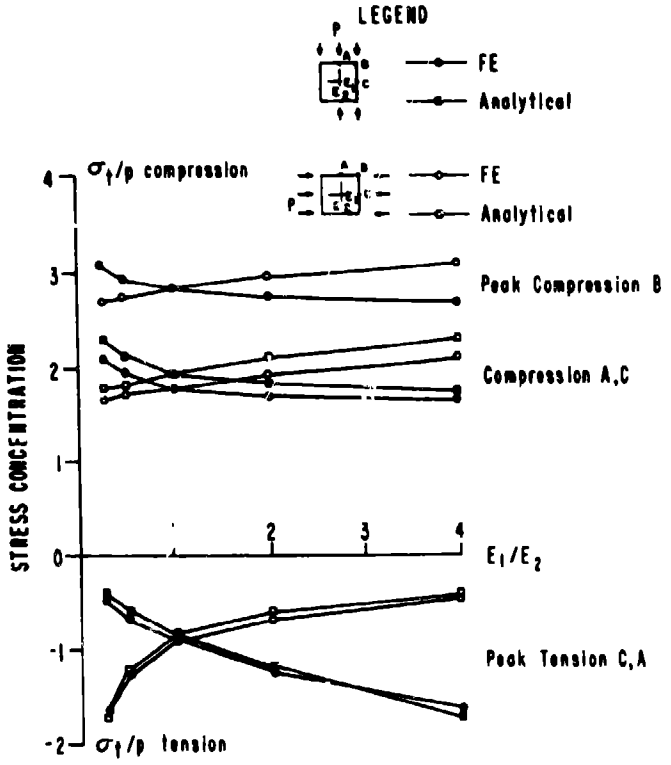

(b)

Figure 85. - Anisotropic elastic square opening program check.

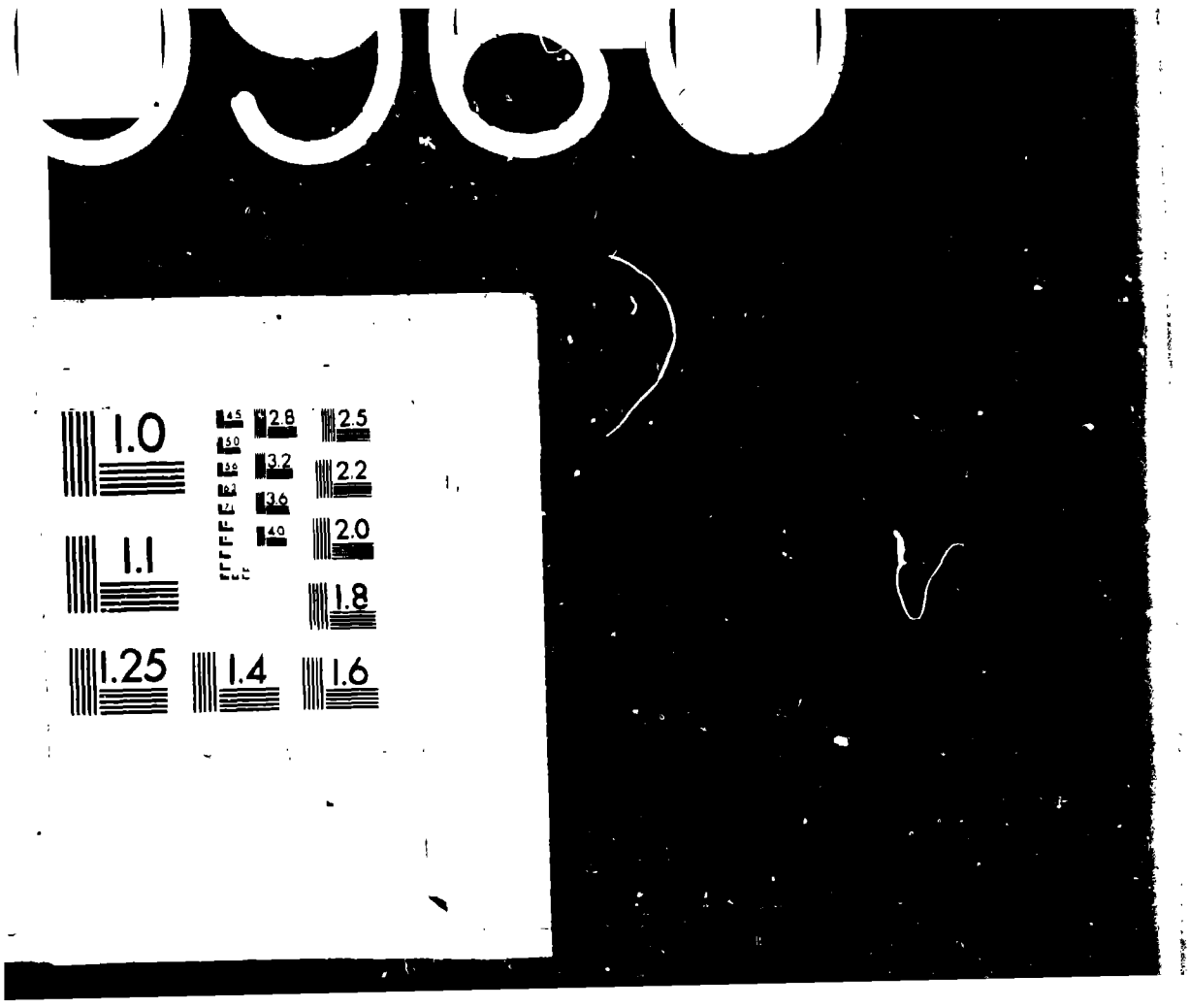

σ_A =

σ_B =

where

Again
bound
ment

defor
the
open

the
is u
bein
show
rela
conc
for

perp

requiring nine elastic constants, three Young's moduli, three Poisson's ratios, and three shear moduli. However, in order to simplify interpretation of results the effects of Poisson's ratios are neglected as suggested by Kawamoto (1964). The shear moduli are given by $1/G12 = 1/E1 + 1/E2$, $1/G23 = 1/E2 + 1/E3$, $1/G31 = 1/E3 + 1/E1$. The three direction moduli are not needed, however E3 was assigned the same value as E1. (Figure 10a shows the uniaxial stress strain curves.)

The analyses are plane strain and the loading is uniaxial first in the vertical y-direction and thus parallel to E2 and then in the horizontal x-direction parallel to E1. In Figure 85b, the ratio E1/E2 is increased by increasing E1 at fixed E2. The alternative of decreasing E2 at fixed E1 has no effect because the stresses depend on the ratio of moduli rather than their absolute values. This was verified by direct FE calculation at ratios of 1/4 to 4 obtained by decreasing E2 at fixed E1. If the hole were circular, then the analytic solution shows that the stresses at points A and B are

$$\sigma_A = \sigma_h \left(2 + \sqrt{E_1/E_2}\right) - \sigma_v \sqrt{E_1/E_2} \qquad (11a,b)$$

$$\sigma_B = -\sigma_h \sqrt{E_2/E_1} + \sigma_v\left(2 + \sqrt{E_2/E_1}\right)$$

where σ_h = horizontal applied stress,
σ_v = vertical applied stress,
E_1 = horizotal Young's modulus,
E_2 = vertical Young's modulus.

Again, if allowance is made for the difference in stress at the opening boundary and at the element centroids near the boundary, then the agreement of the FE results with the analytic solution is acceptable.

Even under uniaxial loading within the purely elastic range of deformations, two additional complications can be considered, changing the width relative to the height and changing the orientation of the opening relative to the load direction.

Stress concentration about rectangular openings as a function of the width to height ratio is presented in Figure 86. The applied load is uniaxial and compressive. A modulus ratio of two was selected as being representative of rock anisotropy. The results shown in Figure 86 show little difference between the isotropic and anisotropic cases relative to the compressive stress concentration. The tensile stress concentration also follows the trend noted in the square opening case for which an analytical comparison was available.

Elastic-Plastic Anisotropy

Intuitively, strength differences between directions parallel and perpendicular to a well developed plane of schistosity, especially tensile strength differences, would seem important to the analysis of hanging wall stability. Indeed, strength considerations are essential to safety and stability analyses. Nine independent strength parameters are needed to define orthotropic strength (three compressive, three

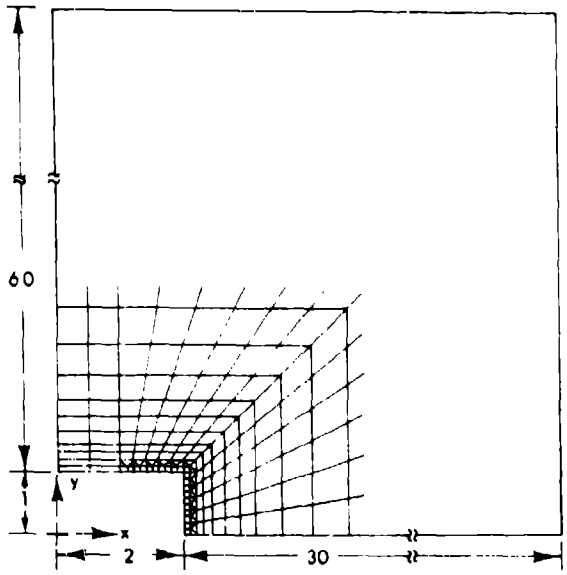

(a)

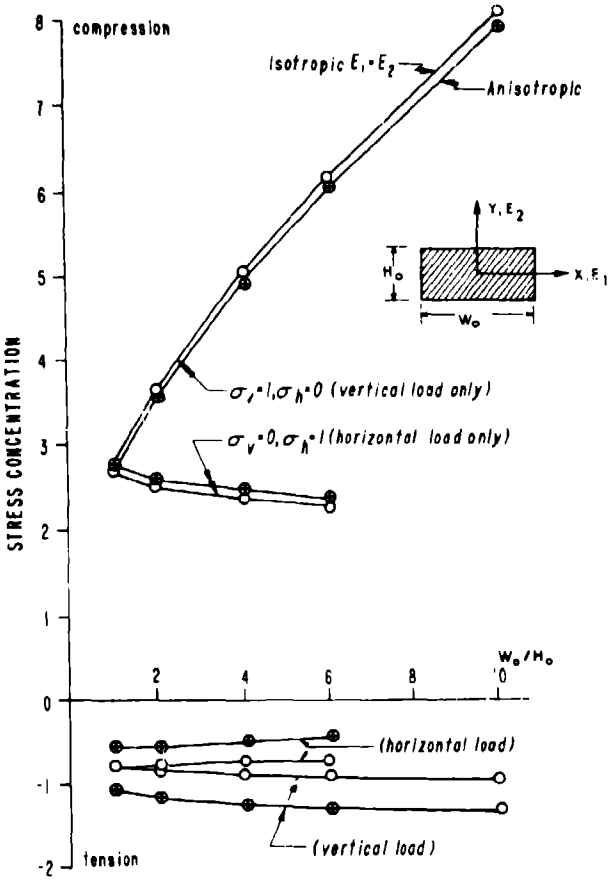

(b)

Figure 86. - Anisotropic elastic rectangular opening stresses as a function of width to height ratio at a modulus of two.

tensile and three shear strengths). Eighteen material constants, nine elastic moduli and nine strengths are thus needed to define the expected anisotropy (orthotropy) of an elastic-plastic material.

With so many material parameters, it is not immediately clear how one should evaluate the results of an elastic-plastic calculation. In the elastic case, the degree of anisotropy is conveniently characterized by the ratio E1/E2 in plane analyses that neglect Poisson's ratios. The results are then viewed in terms of stress concentration factors that are compared with the isotropic case. The main practical consequence of elastic anisotropy is a change in the displacement field relative to the isotropic case. However, as long as the displacements are elastic, the actual pattern is of no great importance to stope design.

Strength, of course, limits the range of a purely elastic response. In this regard, stress concentration factors used in elastic design indicate whether the entire periphery of an opening is safe with respect to strength, but purely elastic design of stopes may be inefficient. A more economical approach may allow for some inelastic or plastic zone development provided they are limited in extent either naturally or by rock reinforcement and support. In this design approach, the extent of the plastic zone becomes an important consideration. A practical way of viewing the consequences of strength anisotropy is therefore to compare the extent of the plastic zone with the corresponding isotropic case.

Although it would be a great convenience to be able to define plastic zone development in the course of mining by purely elastic stress field calculations, there is no evidence and no reason to suppose that such is the case. A genuine elastic-plastic calculation based on an elastic-plastic stress-strain law is required. The UTAH-II finite element program has the necessary elastic-plastic analysis capability. The plasticity is based on a yield condition for anisotropic geologic media and associated flow rules (Pariseau, 1972).

In order to gain some insight into the effects of strength anisotropy, a series of elastic-plastic finite element stress analyses were done at different width to height ratios under different initial states of stress. The elastic anisotropy used previously is retained; the ratio of Young's moduli in the horizontal x-direction to the vertical y-direction is two (E1/E2 = 2). The shear modulus G12 is again computed from the approximate relationship obtained with neglect of Poisson's ratio $1/G12 = 1/E1 + 1/E2$. This has the advantage of recovering the isotropic case when E1 = E2, otherwise equality of Young's does not necessarily imply isotropy. Young's modulus in the third direction perpendicular to the plane of analysis is equal to the horizontal Young's modulus, thus in these analyses E3 = E1. Also G23 = G12. In effect, the material is elastically transversely isotropic, a less complex form of anisotropy than the orthotropic case. The uniaxial stress strain curves are shown in Figure 87a.

The strength anisotropy is based on an elastic limit of 0.1% strain and ratios of compressive to tensile strength of 10. These are reasonable values for rock. The yield envelope, that is, the yield function, is nonlinear (quadratic). As a consequence, the ratio of compressive

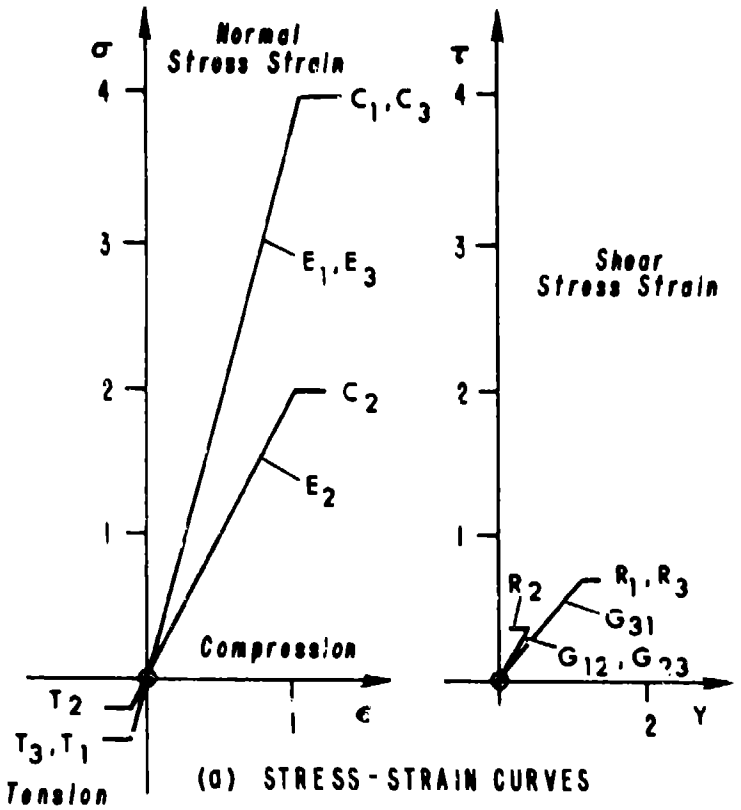

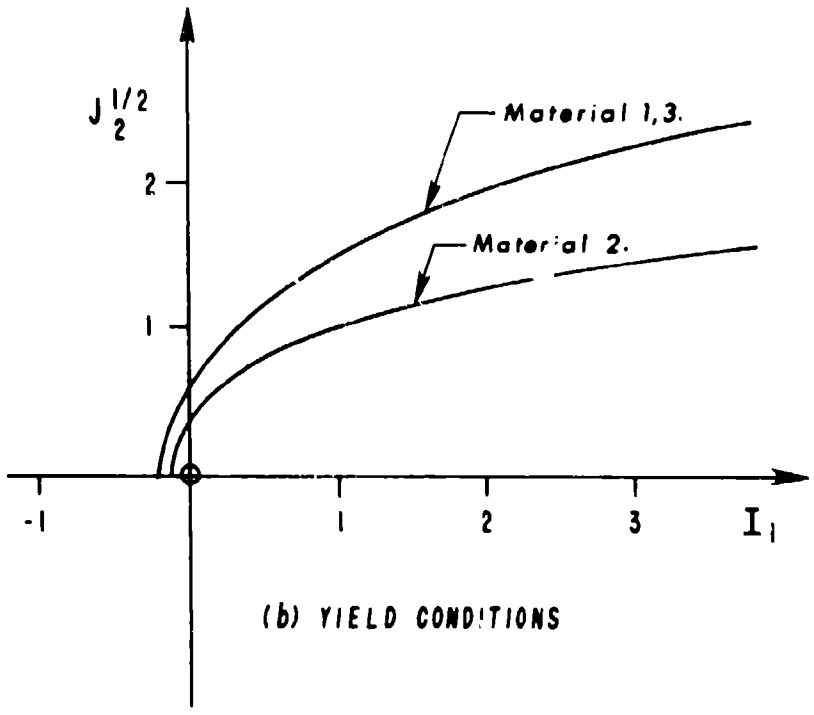

Figure 87. - Anisotropic elastic-plastic response. (a) elastic stress-strain relation. (b) yield conditions.

strengths C1/C2 is two, and likewise the tensile strength ratio T1/T2 = 2. Also, C3 = C1 and T3 = T1. A high correlation between strength and modulus is implied by these relationships, a feature often observed in rock properties data. The shear strengths R1, R2 and R3 are calculated from the *anisotropic* relationship $R = \sqrt{(CT/3)}$. Thus, the material is also transversely isotropic with respect to strength. The strength character of the material becomes isotropic whenever the elastic properties indicate isotropy, that is, when E1/E2 = 1. Yield envelopes are shown in Figure 87b.

Figure 88 shows the extent and type of yield about rectangular openings for various width to height ratios and loading conditions in the isotropic and anisotropic cases. The width to height ratio effect depends on the applied loads. Under vertical load, increasing the width to height ratio from a width greater than height tends to increase the extent of yielding. However, the extent of the yield zone under horizontal load varies little with width to height ratio at widths greater than height.

Although the ratio E1/E2 = 2 and hence the strength ratios C1/C2 = 2 and T1/T2 = 2 can be achieved in an infinite variety of ways, two natural choices are: (i) to fix E2 at the isotropic value and increase E1, (ii) to fix E1 at the isotropic value and reduce E2. Once a modulus is fixed, then so are the strengths at 0.1% strain to the elastic limit.

The results of these two anisotropic alternatives relative to the isotropic case are quite different under the same uniaxial compressive load applied parallel to E2 (vertical y-direction) as shown in Figures 81a,b. In the first case (Figure 88a), the isotropic yield zone is greater than the anisotropic zone; in the second case (Figure 88b), the anisotropic yield zone is much greater in extent than the isotropic yield zone.

Under uniaxial compressive load applied parallel to E1 (horizontal x-direction), there is little difference in the extent of the yield zones between the isotropic and the two anisotropic cases shown in Figures 89a,b.

Under combined (hydrostatic) loading, the yield zone extent is small in the isotropic case and in the anisotropic case obtained by increasing E1 at fixed E2 as shown in Figure 90a. However, at fixed E1 with a reduction in E2 to obtain E1/E2 = 2, the yield zone extends over the full height of the opening, but is about the same size at all width to height ratios. This suggests that for stress states near hydrostatic, the small dimension of the opening could be increased to a width to height ratio of one without sacrifice of stability.

These results seem reasonable after considerable reflection but would surely be difficult to anticipate in advance, especially the development of the large yield zone shown in Figure 88b. In this regard, the anisotropy assumed for this brief parameter study, although reasonable for rock, is highly simplified. In particular, the shear strengths are computed from the *isotropic* relationships. The consequences of this assumption are unknown. These results thus indicate

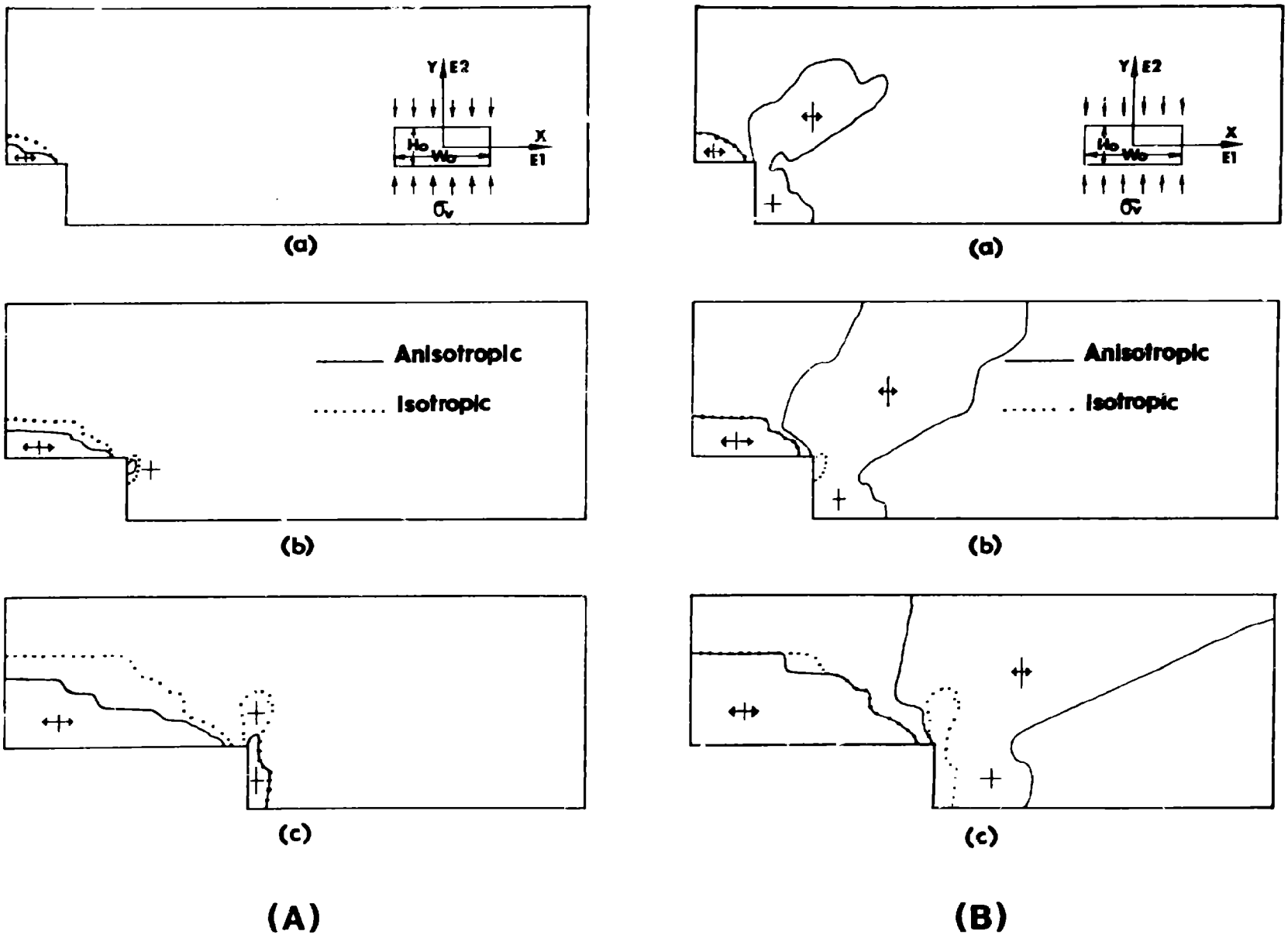

Figure 88. - Anisotropic and isotropic elastic-plastic response under vertical loading with (a) E2 fixed and E1 increased, (b) E1 fixed and E2 decreased.

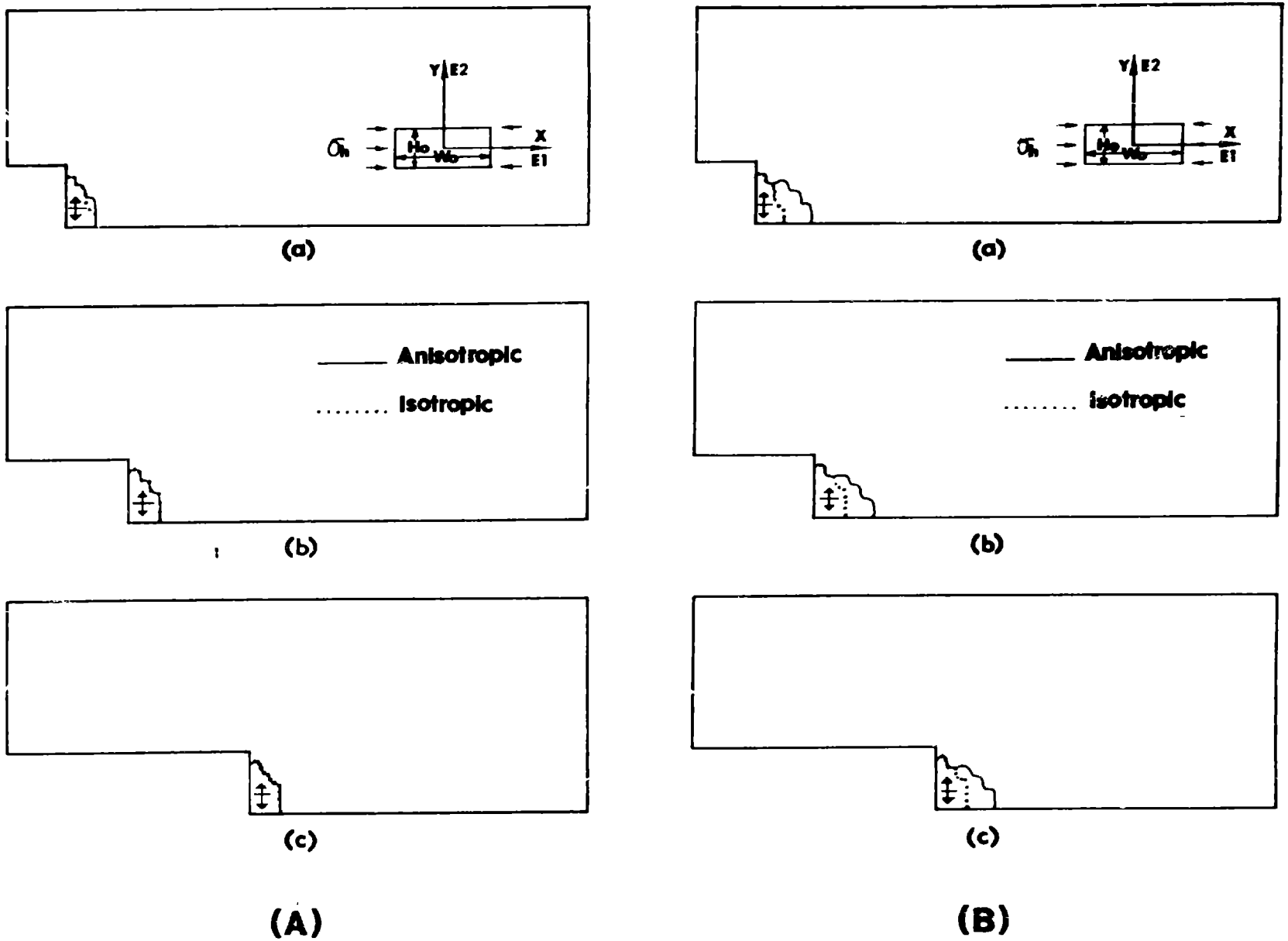

Figure 89. - Anisotropic and isotropic elastic-plastic response under horizontal loading with (a) E2 fixed and E1 increased, (b) E1 fixed and E2 decreased.

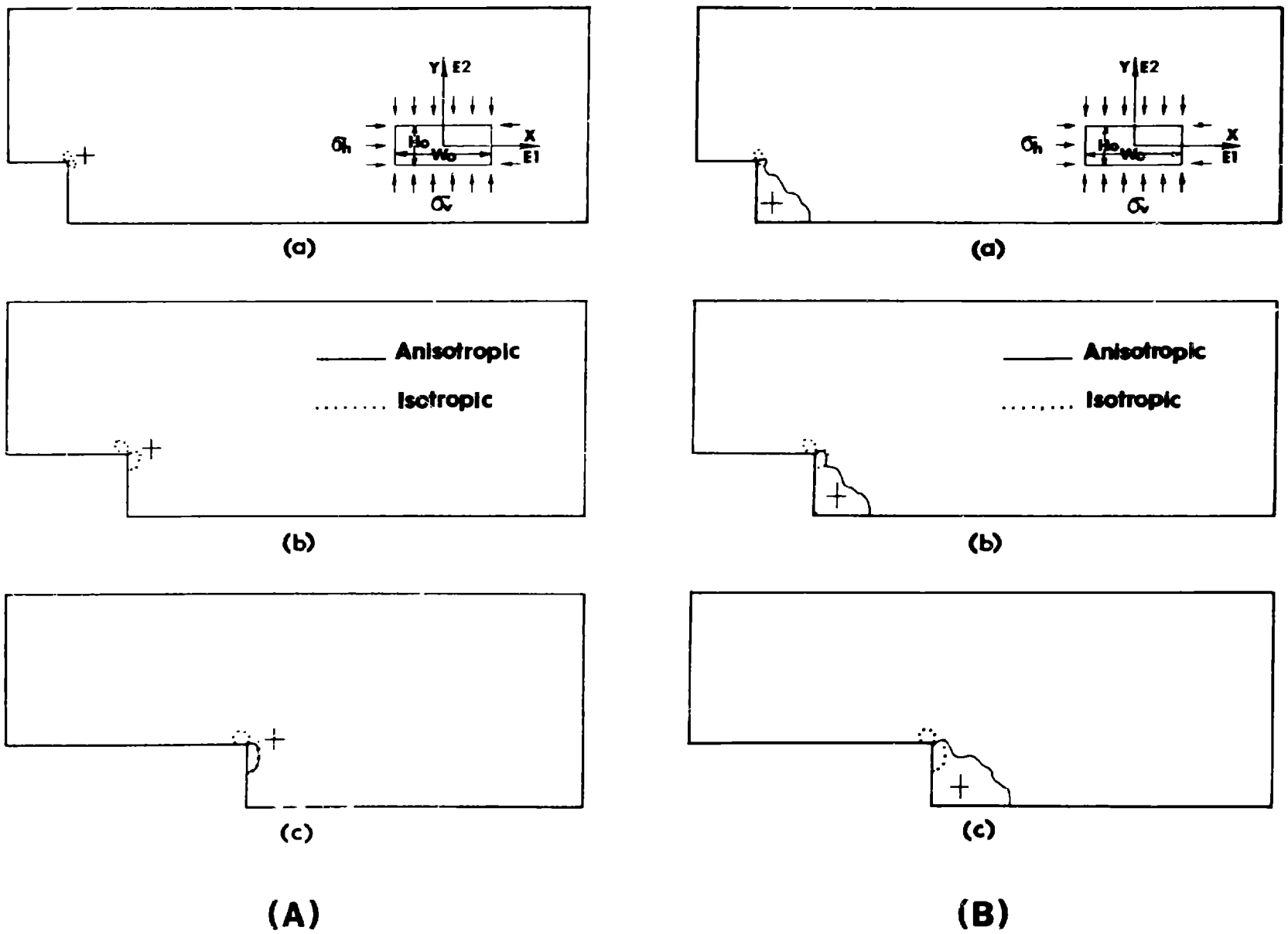

Figure 90. - Anisotropic and isotropic elastic-plastic response under hydrostatic loading with (a) E2 fixed and E1 increased (b) E1 fixed and E2 decreased.

that the importance of strength anisotropy to the analysis of stability depends on a combination of circumstances including the applied loads and opening geometry as well as the rock properties. At this juncture, with the exception of the guidance contained in Eqns. 11, there appear to be no simple rules of thumb for deciding the issue in advance.

Isotropic Study Stope Response

The importance of anisotropy for ground control at the Homestake Mine can be examined comparing purely isotropic analyses with the previous anisotropic results. If one were to avoid any consideration of anisotropy at the outset, then laboratory test data would be averaged without regard to sample drill hole orientation, although the Poorman, Homestake and Ellison formations would still be distinguished. Stope geometry and geology, in situ stresses and the mining sequence remain the same for an isotropic analysis of the study stope response.

The process of determining the scale factors for the elastic moduli and strengths is also the same. First a single cut finite element analysis is done using unscaled or laboratory rock properties. Calculated displacements are then correlated with measured displacements for an initial estimate of the scale factor for elastic moduli. Strength is scaled initially in proportion to the square root of the elastic moduli scale factor. The yield zone extent using scaled properties is then compared with the observed extent in the mine. A final scale factor for strengths is then determined. Next, the study stope is mined out sequentially using the original elastic moduli and the final strength scale factors in order to check both for accuracy. The check is a regression analysis of calculated on measured displacements and a comparison of yield zone extent. This final check is necessary because of the interaction effect of elastic and strength properties on displacement. Interactions between scaled elastic and strength properties can also be examined in combinations between isotropic and anisotropic elastic and strength properties.

Displacements and Elastic Moduli

The initial comparison between measured and calculated displacements using isotropic elastic properties produced correlations on an anchor by anchor basis of 0.9 or greater in the immediate hanging wall (Holes 6, 7, 8 and 9) of the study stope Panel 3. The average slope of the regression lines was 0.31. The rock mass Young's moduli were then obtained by multiplying the isotropic laboratory values by 0.31. The average rock mass Poisson's ratios, one for each formation, are equal to the laboratory isotropic value which is just the average of the anisotropic laboratory values. The shear moduli for the isotropic analyses are obtained from Young's moduli and Poisson's ratios.

The isotropic elastic results are close to the anisotropic results. This is not too surprising because the anisotropic Young's moduli, for example, are within 33% of the computed isotropic Young's moduli and are thus within a range of scatter in laboratory test data defined by the

coefficient of variation.

Yield Zones and Strengths

Some scaling of strengths is necessary as shown by the results in Figure 91a. Figure 91a shows almost no yielding when laboratory isotropic rock properties are used. In fact, loss of extensometer anchors in the hanging wall shows significant yielding and caving. Scaling isotropic strengths by the square root of the elastic scale factor results in the yield zone shown in Figure 91b. The extent of the zones of yielding are noticeably less than inferred from mine observation, so that a lower rock mass strength was indicated. Figure 91c shows the yield zones obtained with a 0.40 instead of a 0.56 scale factor.

The yielding in Figure 91c is more extensive than that inferred in the mine, so that an isotropic strength scale factor somewhat greater than 4.0 is indicated.

A sequential seven cut stoping sequence using scaled elastic and strength properties is shown in Figure 91d. As in the anisotropic case, the results are different from the one cut case in that the footwall yields more when sequentially mined than when mined in one cut. The reason is the same; the acute corner on the footwall side is carried up with the retreating sill when sequentially mined. This results in a traveling zone of high stress concentration on the footwall. In a single cut, the corner is stationary and forms a highly stressed zone in only one locality, the topsill footwall corner.

The isotropic approach appears to achieve the same objective as the anisotropic approach. Both produce comparable elastic moduli scale factors and give high correlations between measured and calculated displacements. Yield zone extents are roughly the same. The isotropic strength scale factor is one-half the anisotropic strength scale factor and consequently the isotropic rock mass strengths are approximately one-half the anisotropic compressive and tensile strengths. However, the shear strengths are comparable because the anisotropic shear strength is much less than the value given by any isotropic relationship between compressive, tensile and shear strengths.

The relatively low anisotropic shear strength has a physical explanation in the presence of a well-defined foliation, especially in the Poorman formation. The field observations enforce this shear strength, so that when approached from the isotropic view the low shear strength required automatically produces low compressive and tensile strengths. The physical presence of foliation also allows for a shear failure mode that is distinct from compression failure unlike the isotropic case. Shear failure along foliation planes is observed in the field as well as in the laboratory. A more realistic approach is therefore obtained in the anisotropic case that allows for three distinct failure modes and the independent specification of tensile, compressive and shear strengths.

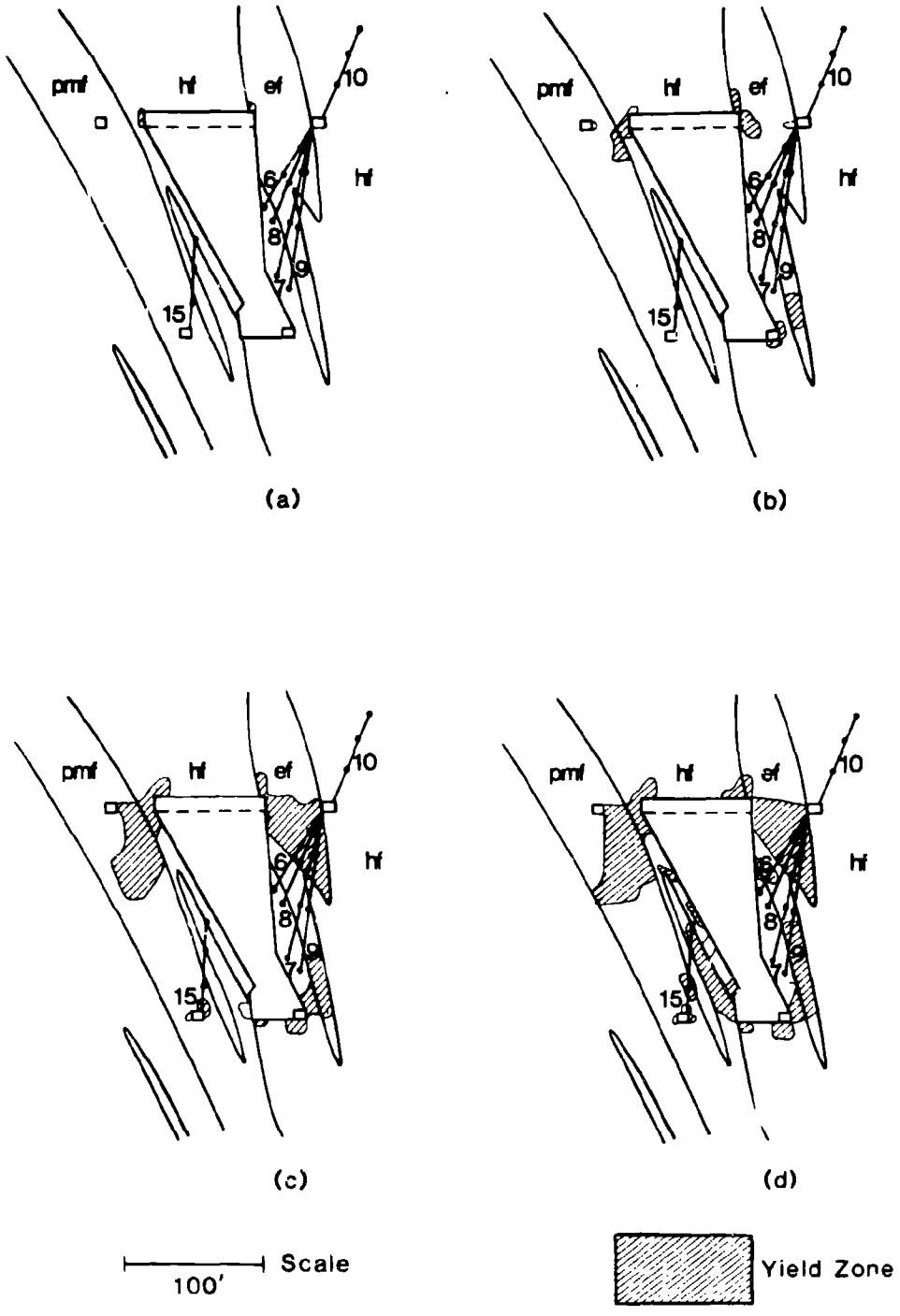

Figure 91. - Isotropic analyses and yield zones. (a-c) one cut sequence, (d) seven cut sequence.

Isotropic-Anisotropic or Mixed Response

Four combinations of plastic and strength properties are possible:

(a) isotropic elasticity - isotropic strength,
(b) isotropic elasticity - anisotropic strength,
(c) anisotropic elasticity - isotropic strength,
(d) anisotropic elasticity - anisotropic strength.

Figure 92 shows the extent of yielding for each combination cut when the stope is mined in a single cut. Figure 92 shows the dominance of strength in determining extent of yielding. Changes in elastic properties have little effect on yielding but changes in strength have a noticeable effect on displacements. The coupling between strengths and moduli is therefore mainly one-way.

Summary

Although the simpler isotropic approach to obtaining scaling factors that calibrate the finite element model appears at first glance to work as well as the more elaborate anisotropic approach, the physical reality of well-developed foliation indicates that the anisotropic approach is preferred. Differences in displacement predictions within the elastic range of response are small, but differences due to strengths are significant. In this regard, shear strength plays a critical role. In order to obtain a rough match between calculated and inferred yield zone extent, the same magnitude of shear strength was needed regardless of approach. In the anisotropic approach, shear strength can be specified independently of compressive and tensile strengths. Greater flexibility and a closer approach to physical reality therefore favor the anisotropic approach to scale factor determination and finite element model calibration at the Homestake Mine.

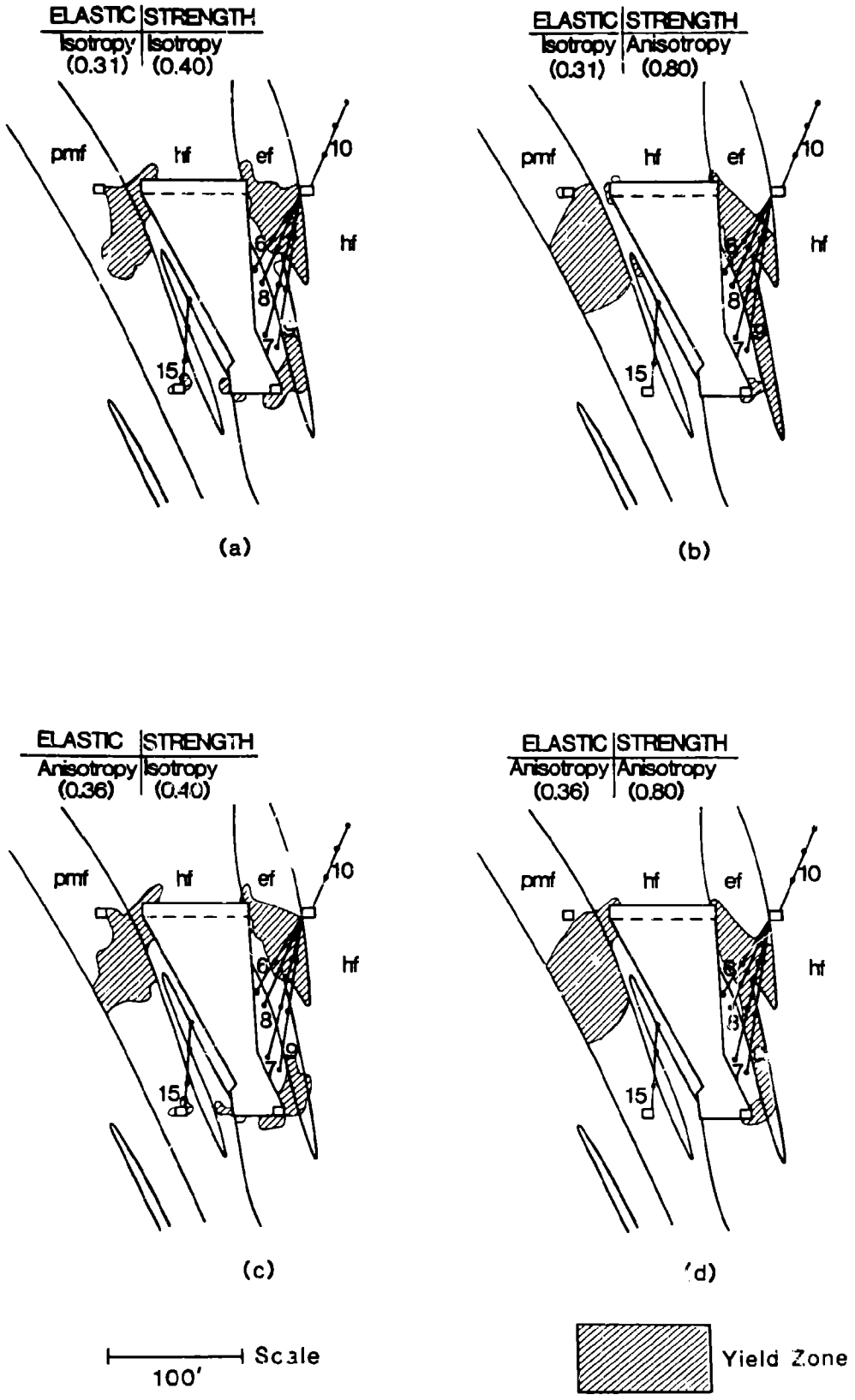

Figure 92. - Mixed isotropic-anisotropic analyses and yields (all one cut sequence).

FINITE ELEMENT MODELING OF CABLE BOLTS

This section is concerned with the development of a practical finite element approach to the design of cable bolting systems in underground hardrock mines. Control of the hanging wall with cable bolt systems in vertical crater retreat (VCR) stopes is of particular concern. The finite element method offers a quantitative design approach to cable bolting. However, the range of scales from bolt holes a few inches in diameter containing cables of even small diameter to stopes well over one hundred feet in height poses a modeling requirement that spans four orders of magnitude and makes it impractical to represent system details in a direct manner even in a two dimensional analysis. A mesh of adequate size would require an inordinate amount of computer storage that even if available would be time consuming to prepare and enormously expensive to run. A practical finite element approach, indeed any numerical approach, must therefore sacrifice some detail in order to be cost effective. How this objective might be achieved in a numerically acceptable and physically meaningful way is the question examined here.

In this regard, the stiffness of artificial support is known to be small relative to the surrounding rock mass and thus to have little effect on the outcome of elastic and elastic-plastic analyses. The expectation is that inclusion of support elements in analyses of hanging wall stability, for example, will not modify the results obtained without artificial support (cable bolts) to an extent that would reverse or significantly change an evaluation of stability. This implies that up to the point of slab formation and caving, hardrock support systems have little influence on displacements. This does not mean that cable bolts, for example, are ineffective in actual practice; experience points to the contrary. What it does mean is that the mechanics of artificial support including cable bolt systems are not properly accounted for in current state of the art computer programs. Mechanically speaking, cable bolt systems become most effective just when the numerical analysis becomes the least effective.

Despite the expectation that the inclusion or omission of cable bolts from the finite element representations of the two test stopes studied would not influence the results, an attempt was made to incorporate cable bolt effects into the Homestake Mine study stope mesh (Donovan, Pariseau and Capak, 1984). Motivation for the attempt was found in the research of others concerning the use of slender elements for interfaces, joints and thin clay seams. These early results indicated that it appeared practical to use slender elements for cable bolts in large scale finite element meshes contrary to original expectations. Small but noticeable differences were observed with the use of slender elements as rock and then as bolt material. The differences seemed physically plausible in that specification of bolt properties for the slender elements led to an increase in tension in the now stiffer bolt elements and a decrease in stress in adjacent rock elements near the hanging wall. The background research and the physically plausible initial results thus pointed to the conclusion that slender elements represented a viable approach to the study of cable bolt effects on hanging wall stability. However, a subsequent discovery opened a line

of numerical investigation that casts some doubt on the generality of this conclusion.

Bolt Element Study

Analysis of a cable bolted region by the finite element method requires careful consideration of several numerical features. Without special attention, the slenderness of a bolt in comparison to the supported structure leads to numerical difficulties and erroneous results. The representation of a bolt in two dimensions also requires special attention for the results to be physically and numerically accurate.

There are two alternatives to modeling bolts in a practical way. One is to introduce a special element for bolt representation. The other is to use standard elements with bolt-like properties. In either approach, much of the detail of bolt geometry, grout annulus, breather tube, steel strands and so forth are not explicitly duplicated numerically, but rather are averaged in some sense to obtain a representation of the mechanical behavior of the bolt hole assemblage. Usually, the special bolt element representation is a truss element, a one dimensional structural member. However, standard elements are two dimensional in plane problems and three dimensional in three dimensional problems. The purported advantage of special bolt, joint and interface elements is better numerical behavior. However, this is not necessarily the case as experience with standard elements for joint and interface modeling shows (Pande and Sharma, 1981, Morgan and others, 1982, Desai and others, 1984, Fossum, 1985). Desai refers to standard elements as "slender" elements when used for joint and interface modeling because the length of such elements is usually much greater than their width. The use of standard elements has the obvious advantage of not requiring the additional programming and added cost of specialized bolt elements.

A set of computer runs was designed to look at two problems with slender elements: (i) the slenderness or aspect ratio, and (ii) the two dimensional representation of a bolt in a three dimensional supported rock mass.

The computer codes used were Utah-II (Pariseau, 1978) and Utah-III. Implementation of these codes was on a UNIVAC 1100/60 mainframe computer. Utah-II was written for rock mechanics analyses in two dimensions. Elastic, elastic-plastic and elastic-brittle analyses are available; analyses can be plane strain, plane stress or axially symmetric. Quadrilateral elements composed of four constant strain triangles are the primary elements, however, constant strain triangles can be used as well. A Drucker-Prager yield criterion and associated flow rules are used for elastic-plastic analysis. The stiffness equations are solved using a Gauss-Seidel line iteration with successive over-relaxation. Consequently, the band-width problem is not present. This greatly facilitates mesh design and preparation. A compact scheme for storing the global stiffness matrix is used; only non-zero stiffnesses are stored. Utah-III is a three dimensional program analogous to Utah-II.

Single Element Aspect Ratio Study

One rule of thumb for avoiding numerical difficulty is that elements should have an aspect ratio (the length of the element to its height) of less than 7 for accurate displacements and less than 3 for accurate stresses (Cook, 1974). There is some evidence in the literature, however, that higher aspect ratios can be used. (Pande and Sharma, 1979) reported successful use of aspect ratios over 100,000. (Fossum, 1985) also reports success with very high aspect ratios for four and eight node isoparametric quadrilateral elements. Desai and others (1984) used a slender element to represent a soil-structure interface that was well behaved to aspect ratios of 100. However, such results are problem specific. No theorems have been reported. Different circumstances thus require independent evaluation.

A series of computer runs was therefore undertaken to determine the acceptable slenderness of the 4CST quadrilateral elements used in Utah-II. A five element column, shown in Figure 93, was subjected to a uniform uniaxial compression. The height of the center element (number 3) was varied to produce different aspect ratios. The stress distribution in the slender element and the vertical displacements over the height of the column were compared to the exact (analytic) stress and displacement distributions to determine at what aspect ratio numerical problems were severe enough to invalidate the results. Slender element aspect ratios of 10, 25, 50 and 100 were thus analyzed. The results from each of these tests were printed after 50, 75, 100, 150 and 200 iterations of the equation solver to trace the convergence of the solution to the known theoretical solution. These analyses were done elastic-plastically, but the compressive strength was intentionally set high, so no failure occured and the solution was elastic. Table 23 shows the material properties used.

TABLE 23. - Material properties for aspect ratio study

Property	Value
Young's modulus, E	2.4×10^6 psi
Poisson's ratio, ν	0.20
Shear modulus, G	1.0×10^6 psi
Uniaxial compressive strength, Co	10,000 psi
Uniaxial tensile strength, To	1,000 psi
Shear strength, R	1,826 psi

Figure 94 shows the convergence of the vertical stress component σ_x to the known result. The values of σ_x are normalized by dividing by the applied x-direction stress p. At an aspect ratio of 10, convergence is rapid. At 25, there is some indication of numerical difficulty, but accurate results were achieved with 100 or more iterations. Elements with aspect ratios of 50 and 100 showed severe instability and did not give reliable results; the error was greater than 5% at 200 iterations. Previous experience has shown that solutions should converge reasonably

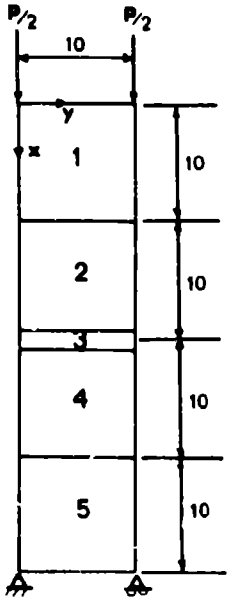

Figure 93. - Finite element mesh for aspect ratio study.

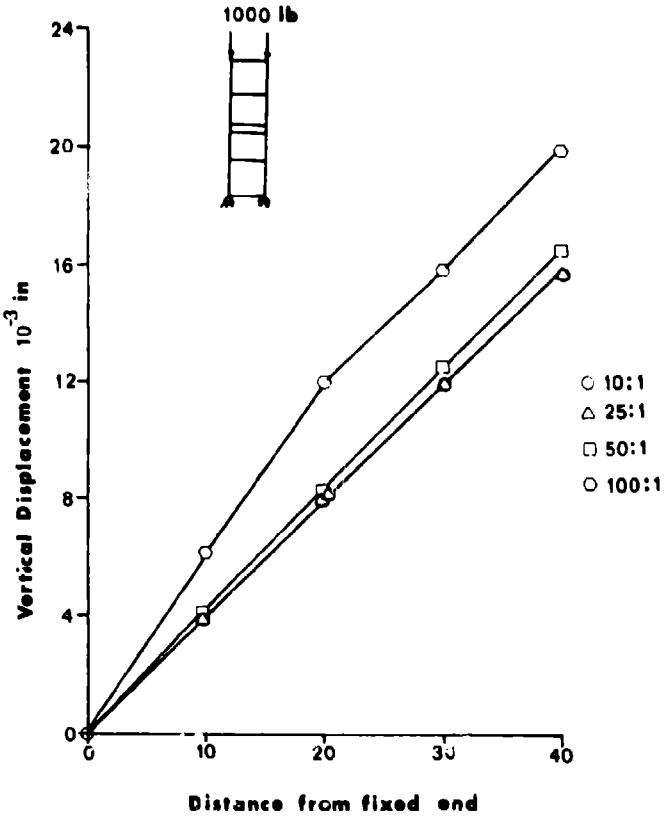

Figure 95. - Vertical displacement as a function of aspect ratio.

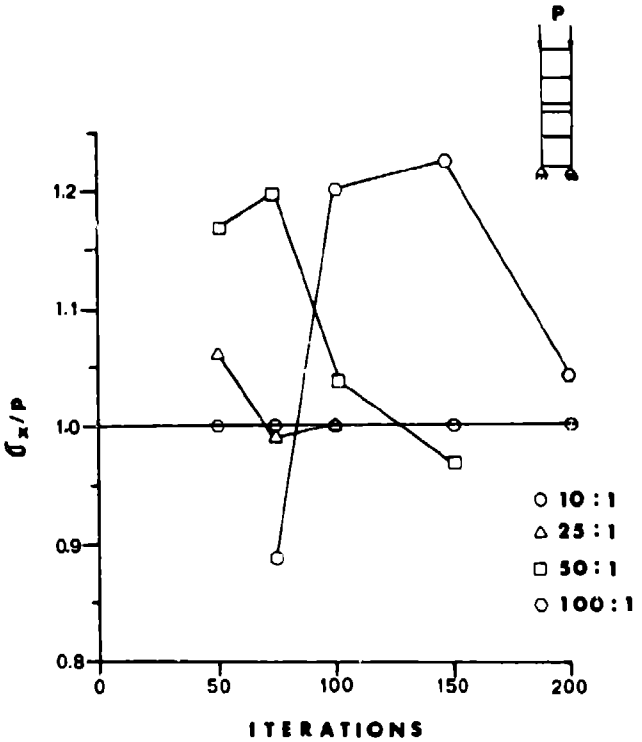

Figure 94. - Convergence of stress as a function of aspect ratio.

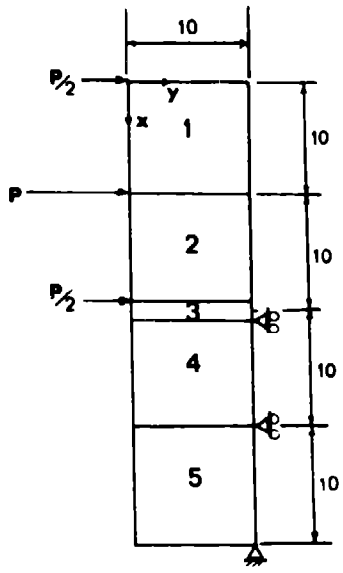

Figure 96. - Five element mesh for shear loading effect.

well between 100 and 200 iterations. A greater number of iterations can make run time prohibitive and in many cases does not significantly improve the results.

Nodal displacements show similar poor behavior for very slender elements. Figure 95 shows the vertical displacement profile along the left hand edge of the column as a function of the distance from the fixed end. The displacements shown are taken after 100 iterations. The elements with aspect ratios of 10 and 25 show no effect on the accuracy of the displacement solution. The columns containing elements with aspect ratios of 50 and 100 show noticeably erroneous results and cannot be considered accurate.

In a finite element formulation, material properties may also influence numerical behavior. The column model of Figure 93 was loaded uniaxially as before. The elastic and shear moduli of the slender element were scaled, first by a factor of 10, then by a factor of 1/10. The vertical component of stress for slender elements of various aspect ratios are listed in Table 24. The applied uniaxial stress is -83.3 psi (compression is negative). It is clear that the low modulus elements caused little difficulty even at aspect ratios of 50 and 100. The high modulus element, however, caused poor results for all aspect ratios tested. A bolt element may be considerably stiffer than the adjacent rock elements and may thus produce instability if an aspect ratio limitation, say, of 10 is not enforced.

TABLE 24. - Vertical stress component for thin elements with high and low moduli relative to surrounding elements

Aspect Ratio	Modulus Scale Factor	Stress (psi)
10	10	-102.7
20	10	-18.4
50	10	-47.2
100	10	-50.6
10	1/10	-83.3
20	1/10	-83.3
50	1/10	-83.3
100	1/10	-83.3

The effect of loading of the column was tested by applying a shear loading, as shown in Figure 96, to the five element column. It is felt that since the applied forces are included in the equilibrium equations, some loading arrangements may result in faster convergence than others. The shear loading resulted in a somewhat slower convergence, but it did not alter the conclusion that aspect ratios of above 10 are generally undesirable.

Although the potential for numerical difficulty with slender elements is demonstrated by these numerical experiments, some fundamental

questions regarding the reason for the poor behavior still exist. It is unclear why an element with an aspect ratio of 10 should give good results, but not one with an aspect ratio of 50. For this reason, it was decided to study the ill-conditioning question on a more basic level and look at stiffness matrix terms for a one element system. Diagonal dominance and positive definiteness are sufficient conditions to guarantee convergence of the solution, although they may not be necessary. Testing for diagonal dominance in a single element system involves printing out the element stiffness matrix and applying certain simple norms to the matrix. The test should be done on the global stiffness matrix; however, for a single element model, the global and element stiffnesses are identical. For a quadrilateral element, the stiffness matrix is 8 by 8 corresponding to 2 degrees of freedom per node.

A matrix [K] is said to be diagonally dominant if for all $i \leq n$,

$$|K_{ii}| > \sum_{\substack{j=1 \\ j \neq i}}^{n} |K_{ij}| \qquad (12)$$

where n is the dimension of the matrix. Stiffness matrices of elements having aspect ratios of 1, 2, 4, 10, 50 and 100 were tested for diagonal dominance according to Eqn. 12. In no case was this criterion satisfied. Again, this does not mean that the system is divergent, only that this particular criterion is not satisfied.

A more liberal criterion for diagonal dominance is that the largest term of a particular row must be on the diagonal, thus:

$$\frac{|K_{ij}|}{|K_{ii}|} < 1 \qquad \text{(for all } i \leq n,\ i \neq j\text{)} \qquad (13)$$

All of the slender element stiffness matrices satisfied this condition in a strict sense. However, elements having aspect ratios greater than 10 showed an off-diagonal term nearly equal to the diagonal term. It can be shown, in fact that the ratio approaches unity by expressing the terms of [K] explicitly in terms of the width/height ratio. Figure 97 shows the relationship between aspect ratio and the value of $|K_{ij}|/|K_{ii}|$. The rapid rate at which the function approaches one could be a clue as to the source of numerical ill-conditioning when such occurs.

After establishing the rapid approach of the maximum off-diagonal term to the diagonal term in the single element system as an indicator of potential ill conditioning, it was decided to look into the possibility of improving the numerical behavior of a slender element by the introduction of compensating elements with slenderness in the opposite direction. A mesh, shown in Figure 98, was constructed and subjected to a uniform uniaxial compression. The global stiffnesses associated with nodes a, b, c and d are now dependent not only on the stiffness of slender element A, but also on the stiffnesses of each of the surrounding elements.

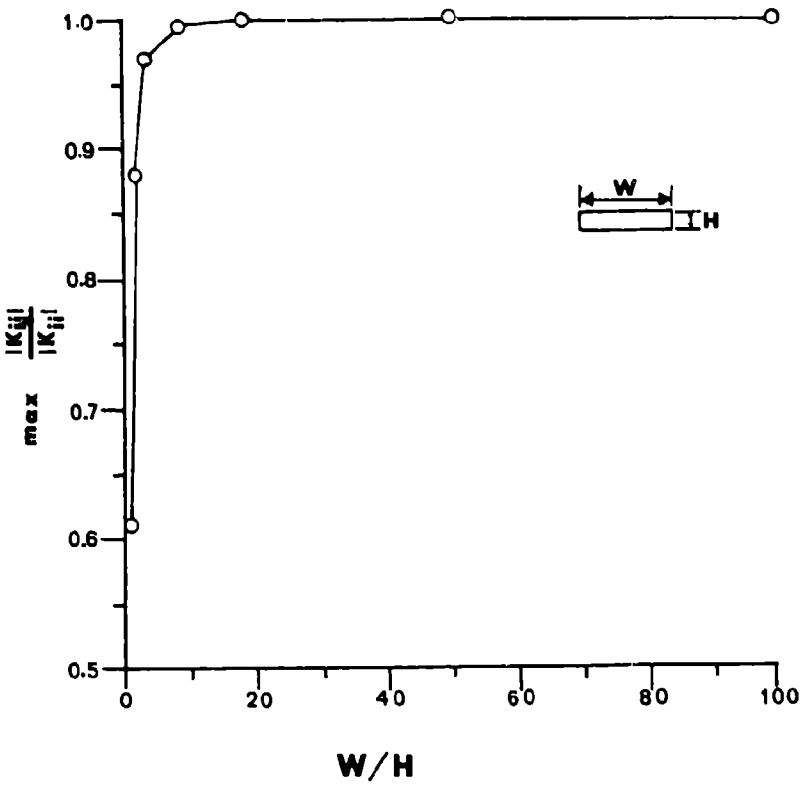

Figure 97. - Diagonal dominance as a function of aspect ratio.

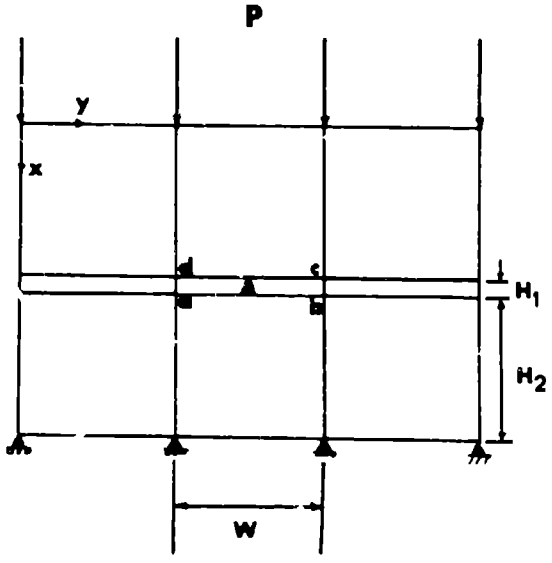

Figure 98. - Nine element mesh for global stiffness study.

A set of runs was developed to test the effect of the adjacent elements on the overall numerical stability of the system. This was done by fixing H_1 and W while varying H_2. The ratio of H_1 to W was set at 10 and W/H_2 was varied from 1 to 10. The global stiffnesses associated with nodes a, b, c and d were examined to see if any improvement over the single element system could be seen. Table 25 gives the maximum K_{ij}/K_{jj} found in the global stiffness matrix terms influenced by the slender element A. It appears that there is some benefit from a numerical standpoint to adding elongated elements adjacent to a slender element. This has a drawback, however, in that the mesh refinement in the vicinity of the slender elements would be sacrificed.

TABLE 25.- Diagonal dominance and aspect ratio with compensating element.

W/H_1 (1)	H_2/W (2)	Max $\frac{\lvert K_{ij}\rvert}{\lvert K_{ii}\rvert}$ Element (1)	Element (2)	Global Stiffness
10	1	.995	.610	.882
	2	.995	.880	.889
	5	.995	.980	.826
	10	.995	.995	.719

Element A = Element 1

The slender element study indicates that the use of elements with aspect ratios greater than 10 may lead to numerical difficulty and should be avoided. This restriction is especially crucial when the slender element is considerably stiffer than the surrounding elements, as is the case in bolting. The requirement may be relaxed somewhat if a soft layer, such as clay, is being modeled with slender elements. The addition of elongated "compensating" elements to a slender element is somewhat beneficial, but the mesh refinement tradeoff should be considered.

2D - 3D Equivalence

Two dimensional (2D) finite element analyses are used much more frequently than three dimensional (3D) analyses because of restrictions of cost and computer storage requirements. Thus, as a practical matter, it is desirable to have a method of representing a bolt in a two dimensional finite element mesh.

Consider a tunnel with a single row of regularly spaced bolts as shown in Figure 99. The planes containing the bolts are planes of symmetry, so only the material between two such planes needs to be considered. The reduction of this three dimensional problem to two dimensions involves averaging the bolt effect in 3D over the distance between bolts. Once the discrete bolt reactions are replaced by a distributed average, all cross sections are similar and amenable to a 2D analysis. The longitudinal plane containing the bolts is shown in Figure 100.

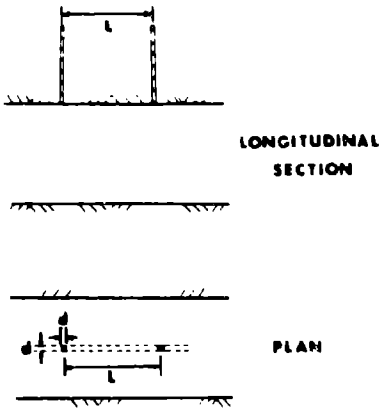

Figure 99. - Tunnel with a row of regularly spaced bolts in the back.

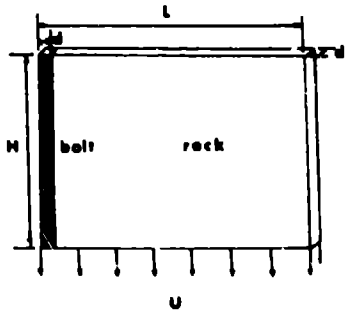

Figure 100. - Longitudinal section containing a bolt subject to a uniform downward displacement.

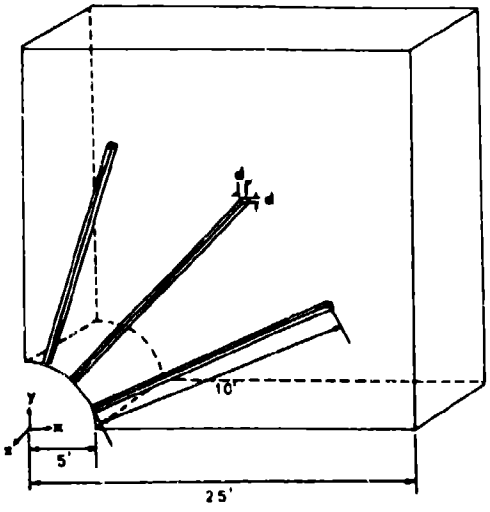

Figure 101. - Circular tunnel with reinforcement.

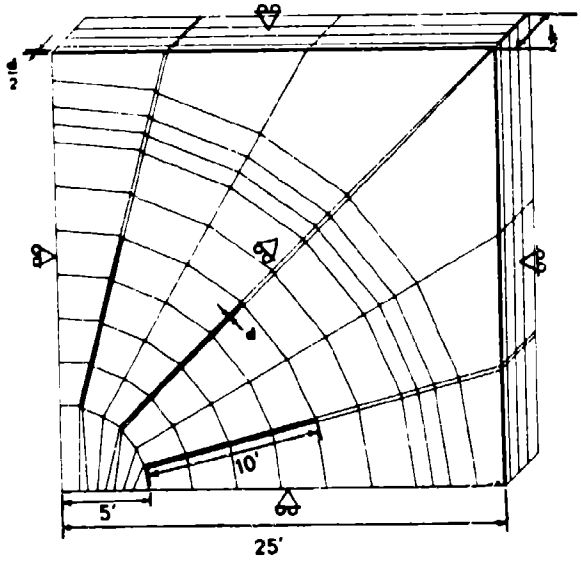

Figure 102. - Mesh used for 2D-3D circular tunnel comparisons.

Under the action of a prescribed displacement, the total reaction force is:

$$F_T = F_R + F_B \tag{14}$$

where F_R = Force in the rock
F_B = Force in the bolt.

In view of the stiffness relations,

$$[K]'\{u\}' = [K_R]\{u_R\} + [K_B]\{u_B\} \tag{15}$$

A uniform displacement means that the equivalent system stiffness is simply the sum of the individual member stiffnesses, thus:

$$[K]' = [K_R] + [K_B] \tag{16}$$

In the one dimensional case,

$$\frac{A'E'}{H'} = \frac{A_R E_R}{H_R} + \frac{A_B E_B}{H_B} \tag{17}$$

where E', E_R and E_B are the elastic moduli
H', H_R and H_B are the lengths of the members
A', A_R and A_B are the cross sectional areas.

For the sheet shown in Figure 100, $H' = H_R = H_B$. The cross sectional areas are:

$$A' = Ld \tag{18}$$

$$A_R = (L-d)(d)$$

$$A_B = d^2$$

Substituting these expressions into Eqn. 14 gives

$$E' = \left(\frac{d}{L}\right)E_B + \left(1 - \frac{d}{L}\right)E_R \tag{19}$$

Thus, a linear scaling of the elastic moduli will result in a two dimensional element that is equivalent to the three dimensional element subjected to a uniform uniaxial displacement. The linear scaling gives an equivalent modulus equal to the bolt modulus E_B when L=d, that is when the bolts are skin to skin. When the spacing is large compared to the bolt diameter, the effective modulus is E_R, the rock modulus.

It is of interest to know the peak stress level that would be developed in a bolt in order to judge whether or not bolt breakage is indicated. The stress in the equivalent two dimensional element is given by:

$$\sigma_B' = E' \varepsilon_B \tag{20}$$

The true bolt stress is

$$\sigma_B = E_B \varepsilon_B \tag{21}$$

Solving for the true bolt stress, the following is found:

$$\sigma_B = \sigma_B' \left(\frac{E_B}{E}\right) f \tag{22}$$

The factor f is the ratio of peak to average strain in the bolt and can be evaluated numerically.

A three dimensional analysis of a circular tunnel with a fan of three bolts in the back using Utah-III was made to determine f. A conceptual view of the three dimensional mesh is shown in Figure 101. The actual mesh was constructed by stacking identical pages of elements behind one another. The resultant mesh is shown in Figure 102. The front and back faces of the mesh are planes of symmetry, so only the half-span between two bolts is modeled. A hydrostatic initial stress was imposed, except in the bolt elements, which were initially stress free, corresponding to bolt holes. A list of the material properties used in the 3D analysis is given in Table 26. Steel properties were assigned to the bolt elements. A companion set of runs was made using a two dimensional mesh identical to one slab of elements from the 3D mesh. The rock elements were assigned the same material properties as in the 3D runs. The elastic properties of the bolt were scaled by the procedure described previously.

TABLE 26. - Material properties used in 3D analysis

Property	Rock	Bolts
Young's modulus, E	2.4×10^6 psi	30.0×10^6 psi
Poisson's ratio, ν	0.20	0.33
Shear modulus, G	1.0×10^6 psi	11.25×10^6 psi
Compressive strength, C_o	10,000 psi	80,000 psi
Tensile strength, T_o	667 psi	80,000 psi
Shear strength, R	1,491 psi	46,188 psi

The ratio of peak strain in the 3D mesh to the indicated strain in the 2D model was calculated for bolt spacings of 1, 2, 4, 6, 8 and 10 feet. The results of the calculations are shown in Figure 103. This figure shows that as the bolt spacing increases, the ratio of true strain to indicated strain increases. With an increase in spacing down the tunnel, the peak bolt strain increases due to the added mass of rock loading the bolt. The strain in the bolt should never exceed the strain which would be indicated if no bolts were included. Figure 103 shows

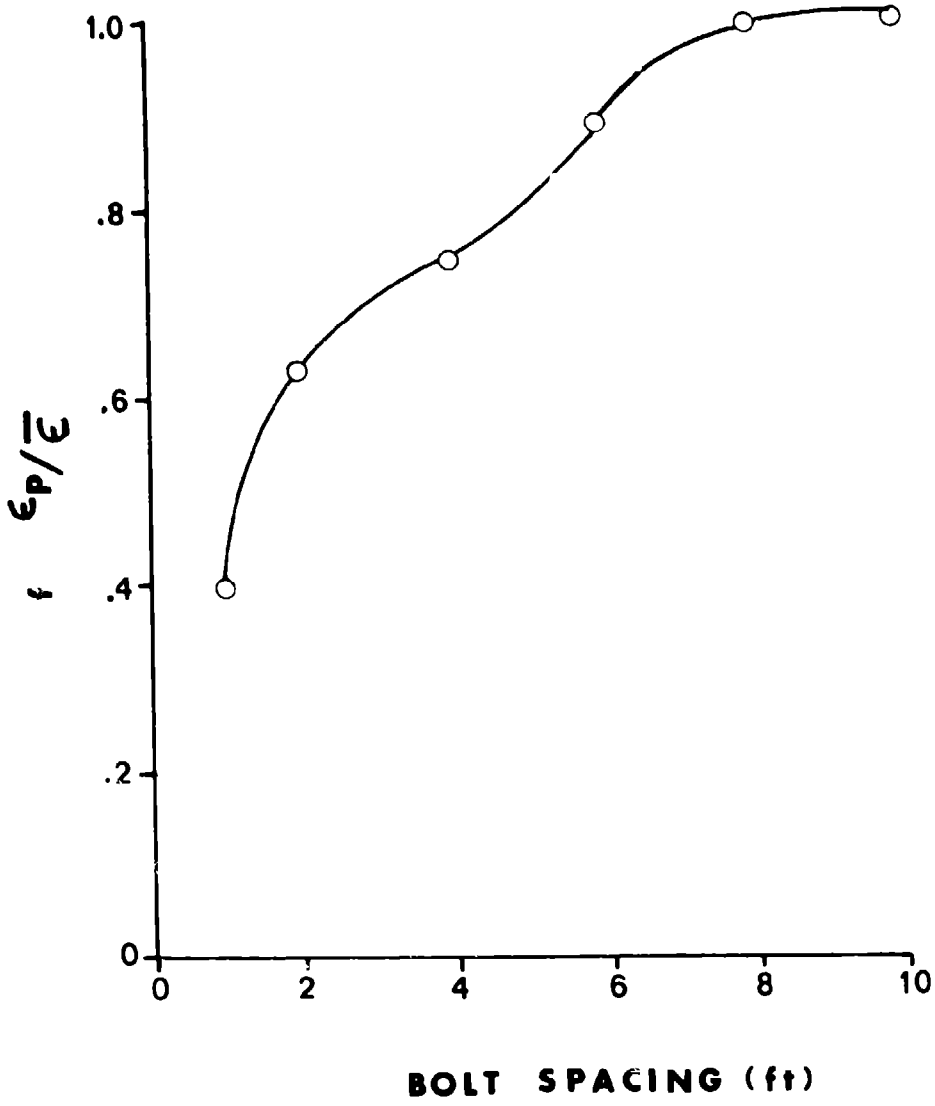

Figure 103. - Ratio of peak to average strain in bolts at various spacings.

this to be the case. At a spacing of about 8 feet, the peak bolt strain approaches the indicated strain. In this case, the true bolt stress is simply the indicated stress times the ratio of the true bolt modulus to the scaled modulus.

Linear scaling of material properties is a simple and convenient way of distributing the discrete effect of a bolt over the distance between bolt fans in a regularly spaced bolting pattern. Other scaling possibilities include prescribing a uniform force along the tunnel, or varying the geometry of the element, so that the area terms of the stiffness formulation are changed. These techniques are not as convenient as material property scaling which can be done on input with no additional programming.

Single Bolt Study

The mechanical response of a single bolt passively loaded during excavation is not well known. Analyses of single bolts subjected to such loading would help to explain the nature of a passively reinforced system and give some idea of what to expect when modeling actual bolting systems in VCR stopes. To avoid questions associated with modeling a bolt in two dimensions, an axially symmetric analysis was used. This seems to be a reasonable approach because of the large bolt spacing in comparison with the bolt diameter. The effect of the bolt should die out relatively rapidly, so that there is negligible interaction between adjacent bolts.

Finite element runs were thus developed to study the behavior of a bolt-rock-grout system under passive loading. The loading of the bolt occured as a result of the excavation of a portion of the rock mass below the bolt. Because of the axial symmetry, the excavation appears as a "pill box" shaped room rather than a tunnel, but the effect of passive loading on the bolt, grout and surrounding rock mass can still be investigated. Figure 104 shows the dimensions of the mesh used in this analysis. The actual mesh is shown in Figure 105. The outer dimensions of the mesh should be such that an isolated excavation is being modeled, that is, the stress induced by the excavation is negligible at the boundaries. Material properties used for the grout, rock and steel are listed in Table 27. Perfect bonding between steel and grout is implied by the use of compatible elements. The analyses are elastic-plastic.

One run was made in which the span was unsupported and one in which the span was supported by a single bolt in the center of the roof. The elements were assigned an initial gravity stress field. For the bolted span, a hole for the bolt and grout was first excavated in a gravity stress field. The bolt was then placed in the hole and the room excavated. In practice, a portion of the room would be excavated before bolt placement, so that actual loads would be somewhat less than the computer results.

A comparison of stresses in the rock with and without the bolt is shown in Figure 106. The stress components are plotted against radial

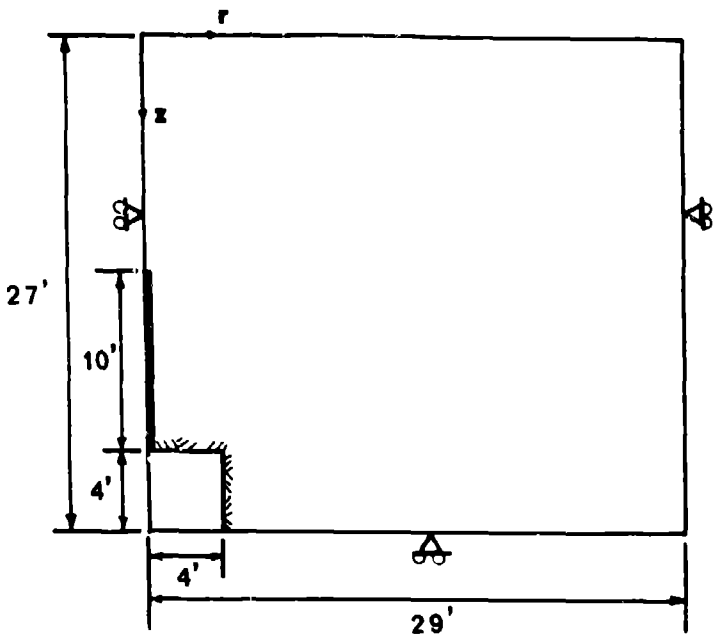

Figure 104. - Conceptual model of axisymmetric excavation.

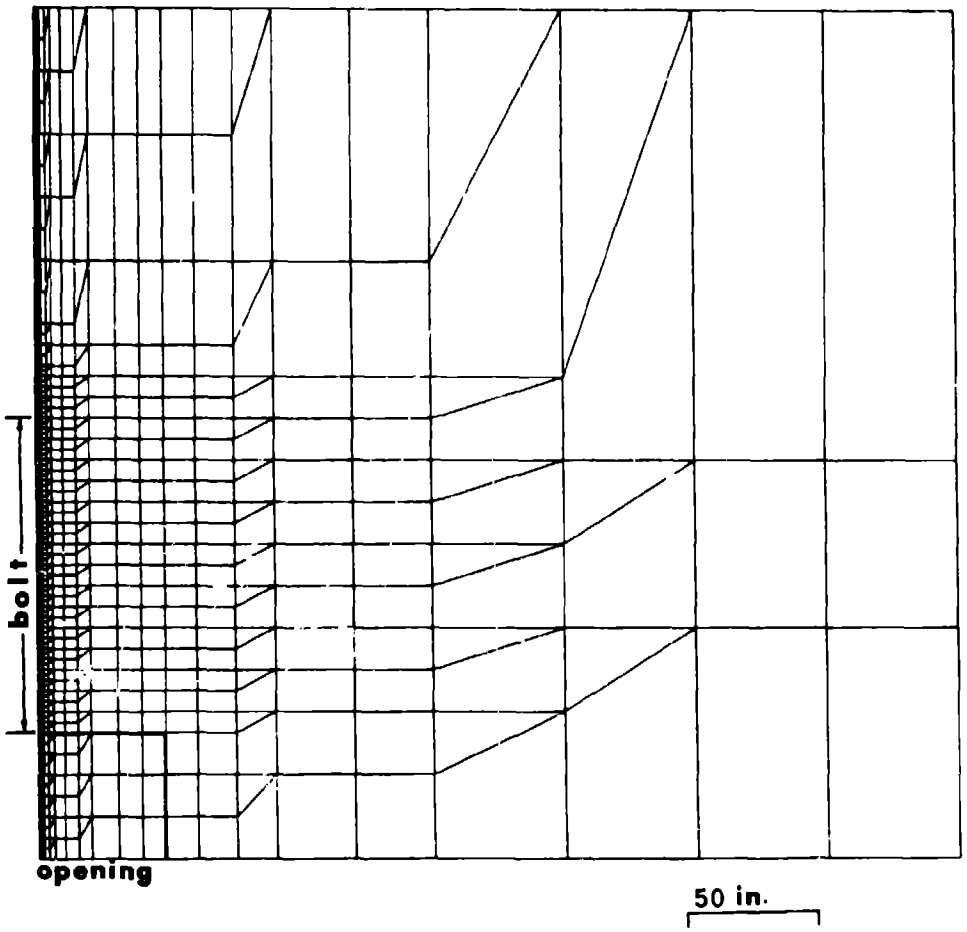

Figure 105. - Axisymmetric mesh used in single bolt study.

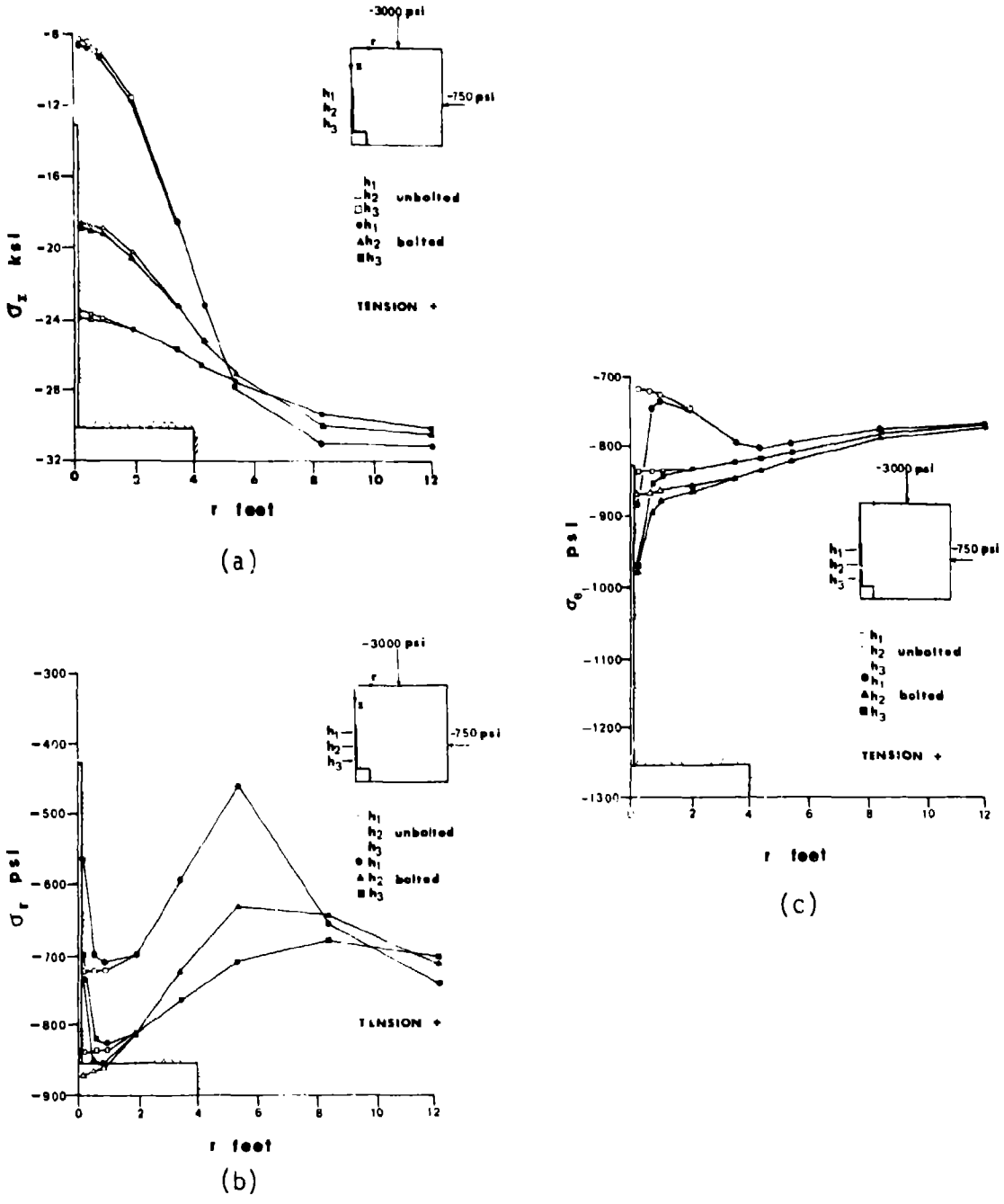

Figure 106. - Stress versus distance from bolt center (a) vertical stress, (b) radial stress, (c) circumferential stress.

distance, r, from the mesh centerline. Figures 106 show a very rapid approach of the stress components in the bolted mesh to the components in the unbolted mesh. Roughly 10 bolt hole diameters from the span centerline, there was negligible difference in the stress fields of the two meshes. The influence of a 2 in. grouted bolt hole on the elastic stresses would thus be limited to approximately 20 in. from the hole center.

TABLE 27. - Material properties for axisymmeric analyses

Property	Rock	Grout	Steel(bolt)
Young's modulus E (10^6 psi)	2.4	5.0	30.0
Poisson's ratio ν	0.20	0.20	0.33
Shear modulus G (10^6 psi)	1.0	2.08	11.25
Compressive strength C_o (psi)	10,000	3,500	80,000
Tensile strength T_o (psi)	1,000	233	80,000
Shear strength R (psi)	1,826	521	46,188

In addition to the effect of the bolt on the surrounding rock mass, the tension in the bolt and radial stress at the interfaces are of interest. A radial tension at the interface between the bolt and grout or the grout and rock could indicate debonding, while a large axial tension in the bolt could lead to bolt breakage. Figure 107 shows the axial tension in the bolt as a function of height above the opening. This figure clearly shows that the peak tension developed in the bolt occurs near the opening where the rock displacements are presumably the greatest. Figure 108 shows a radial tension at the interfaces near the hole collar. Debonding may occur near the collar if the magnitude of this tension exceeds the bond strength of the interfaces.

The single bolt study brings out several important points concerning bolting. First, the effect of a single fully grouted bolt is very localized. This indicates that a bolt does not add much stiffness to the system in the elastic domain. It is felt that the real utility of a fully grouted cable bolt is in the post-failure support of slabs. Unfortunately, finite element modeling of slab formation and support is beyond the state of the art. A second important result is the development of the maximum bolt tension close to the opening. If a bolt broke,

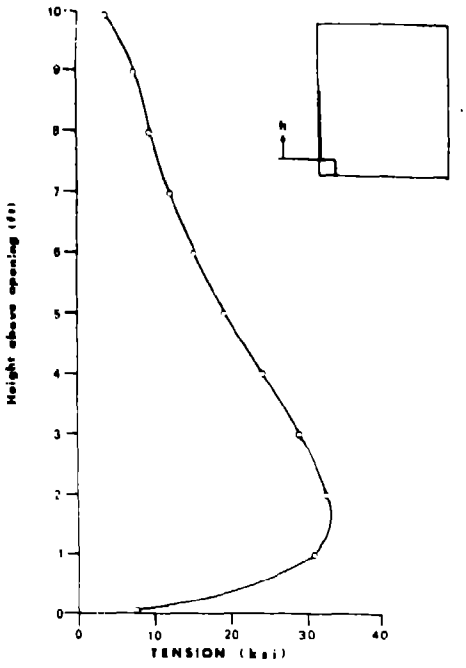

Figure 107. - Axial tension in bolt over axisymmetric excavation.

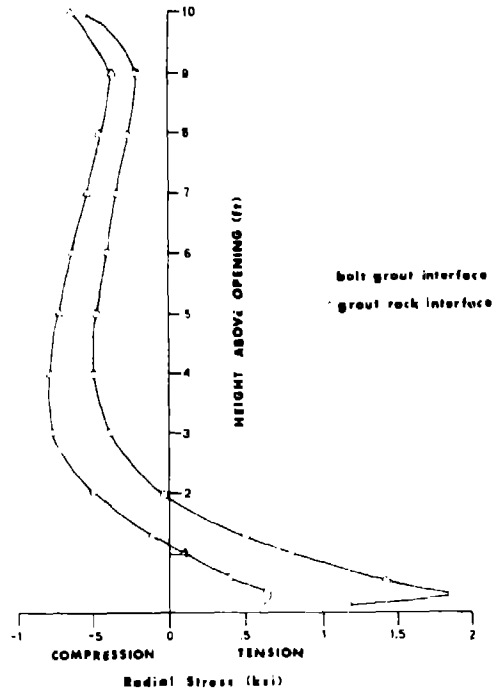

Figure 108. - Radial stress at the bolt-grout and grout-rock interfaces.

relatively thin slabs could be left unsupported. Finally, there is the radial tension which is present at the interfaces. This could result in debonding near the opening, where support should be maximum. A more in-depth look at debonding is necessary to fully understand the implications of the radial tension near the opening.

Slender Element Restudy

During a check on the width to height ratio of a slender element needed for accurate results, (rule of thumb: use an aspect ratio of 10 or less) aspect ratios of 1, 10, 100 and 1000 were tried; ratios up to and including 100 gave quite accurate results! This surprising event was quite favorable towards the use of slender elements for cable bolt representation in large scale meshes and promised considerable economy. However, it also raised a question concerning the variation from the initial aspect ratio investigation. Figure 109a shows the simple three element mesh that was used and the results obtained during the check run. Figure 109b shows a mesh corresponding to the original analyses. The geometry, material properties, boundary conditions and all run parameters are identical in the two analyses. The single difference between the two is in the mesh node numbering. Nodes 3 and 4 are interchanged. The difference in results is enormous. The numbering in Figure 109a (good) gives about exact analytic results, while use of the mesh in Figure 109b (bad) gives errors greater than 20%. The bad numbering scheme in Figure 109b is also the natural numbering scheme within the context of numerical analysis as such. In this regard, the bandwidth is the same in both cases, although an iterative equation solver is used in the UTAH-II program so the question of bandwidth does not arise. Node numbering is a matter of choice, of course, and there are many different patterns possible. The discovery that results using slender elements could be highly sensitive to node numbering was surprising. Very little information on the subject was found in the literature. It thus appeared to be a new phenomenon that called for immediate investigation because if node number sensitivity carried into large scale meshes, the consequences would be devastating, especially if such sensitivity remained at aspect ratios less than, say, 10. This was thought not to be the case, but evidence was needed to decide the issue on an objective basis. Additional small and medium scale meshes containing slender element combinations were investigated.

Small Scale Slender Element Behavior

In addition to the three element mesh containing a single element, a five element column containing a single element was investigated. The five element column removes the boundary conditions from the nodes immediately adjacent to the slender element nodes in the center of the mesh. The results were the same in the five element column. The five element column was used in the original aspect ratio study; these results were reproduced when the bad node number sequence in Figure 109b was used. Accurate results were achieved when the good numbering scheme

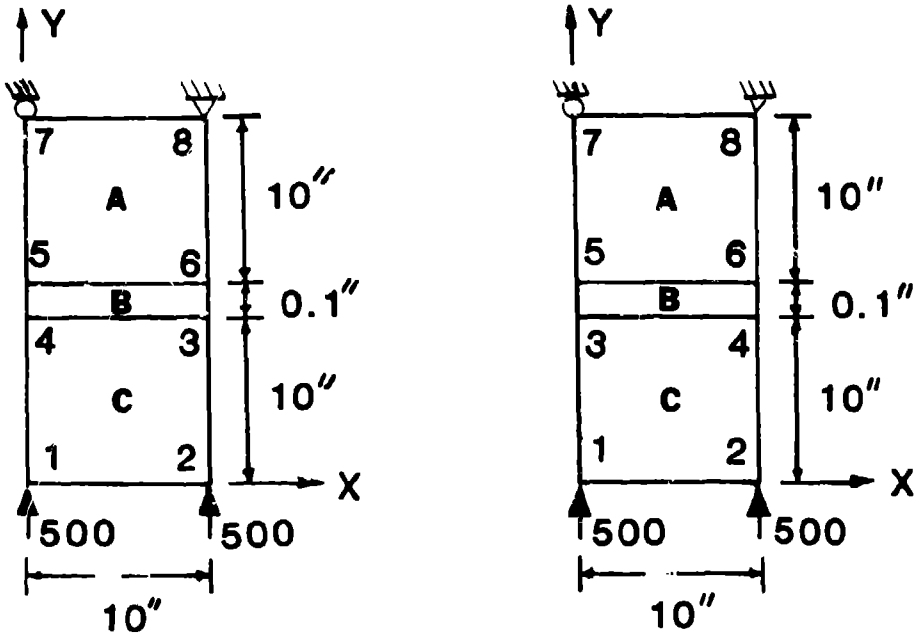

	σ_x	σ_y	T_{xy}	σ_x	σ_y	T_{xy}
A	0.00	-100.00	0.00	0.22	-92.09	-0.78
B	0.00	-99.98	-0.02	-7.51	-121.36	-2.86
C	0.00	-100.00	0.00	-0.33	-100.25	-0.10

(a) GOOD (b) BAD

Figure 109. - Three element mesh for slender element studies.

in Figure 109a was used. these results showed that the boundary conditions were not the source of the difference in results and also explained the difference between the original results and the check results. Both were associated with the node numbering sequence. Several rules were then formulated for distinguishing good and bad numbering schemes. It should be noted that the relative degree of diagonal dominance (ratio of absolute value of off-diagonal to diagonal node stiffness) is the same regardless of the numbering scheme. The distinction between the two schemes is therefore one of some subtlety.

The next step in complexity was to examine several small meshes including a six element mesh containing two slender elements and a nine element, three column mesh containing three slender elements in the central row. The variety of numbering schemes is much greater, but the trend inferred from the three element mesh study was also present in these small meshes. The good numbering schemes gave results to within 0.1% of the exact solution, while the bad numbering schemes often gave errors ranging from 8% to more than 34% at a slender element aspect ratio of 100. The distinction between the good and bad numbering schemes is not immediately evident as the patterns in Figure 110 show. The one rule that gave consistently good results at the 100 to 1 aspect ratio required numbering the nodes of the slender element in sequence. The order was immaterial.

These small scale homogeneous mesh studies have two special features in that the slender element is the same material as the surrounding elements and is oriented parallel or perpendicular to the load axis. In a large mesh, the slender element would have bolt properties and would except in unusual cases be inclined to the loading. These features were present in the original large scale mesh using slender elements, so that small scale mesh studies using an inclined slender element and using a modulus different from the surrounding medium were undertaken.

The inclination effect is not purely geometric even in a homogeneous mesh. A shear load exists relative to local axes parallel and perpendicular to the long and short dimensions of the slender element shown in the three element mesh in Figure 111. Inclination, that is, shear, appears to have a substantial effect on results. Table 28 shows the error as a function of inclination at a fixed aspect ratio of 100. The 45° case at an aspect ratio of 10 is included in Table 28 for comparison.

The results in Table 28 indicate that even with a good node numbering scheme, high aspect ratio elements should be avoided if loaded in shear.

An analytic derivation of the 4CST element stiffness confirms the effect of inclination and moreover shows that it is the product of shear modulus and aspect ratio that is important. This is why very high aspect ratios can be used in conjunction with a very low shear modulus to represent the shear behavior of lubricated or low friction

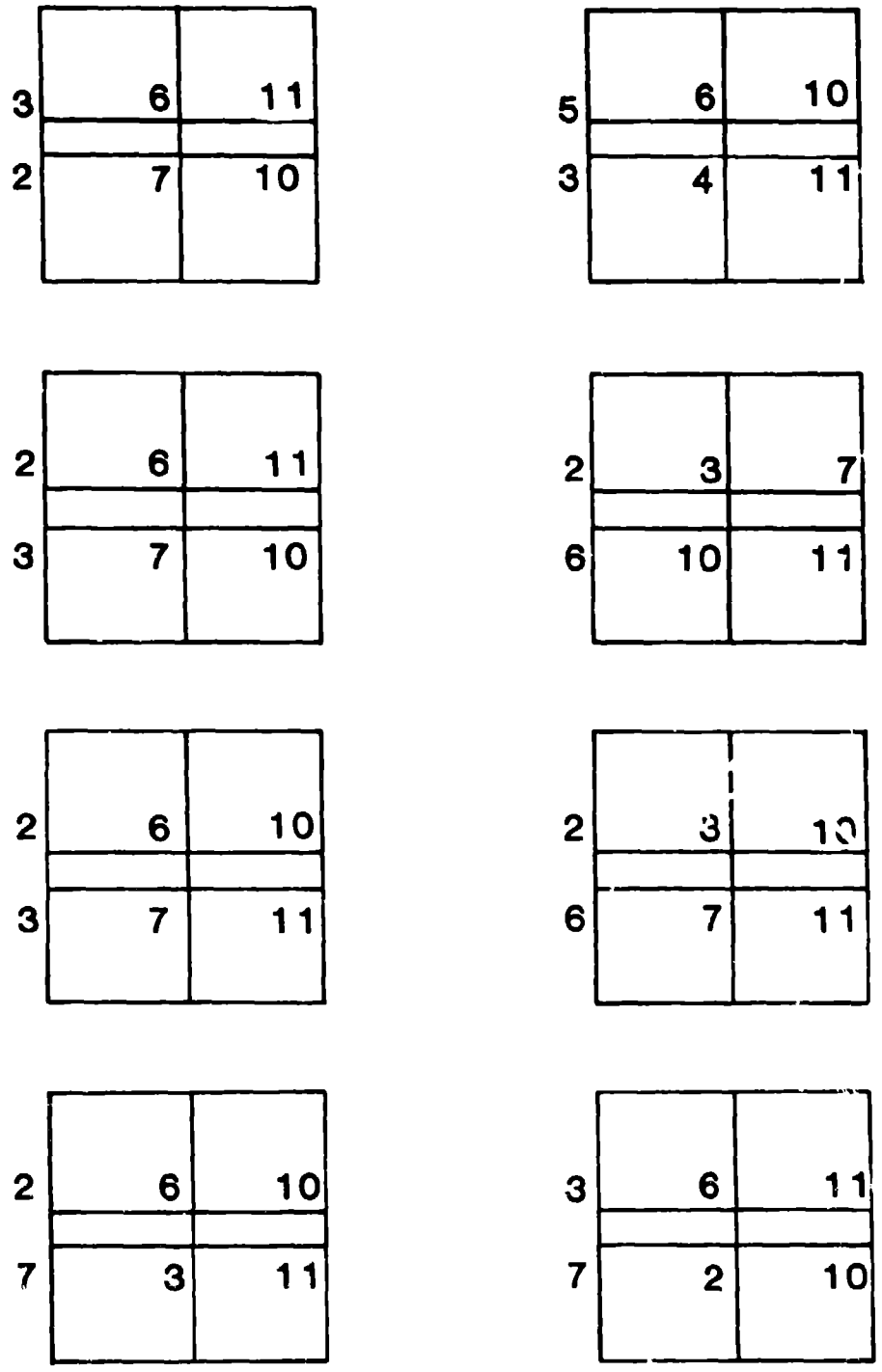

Figure 110. - Good and bad node numbering patterns with slender element meshes.

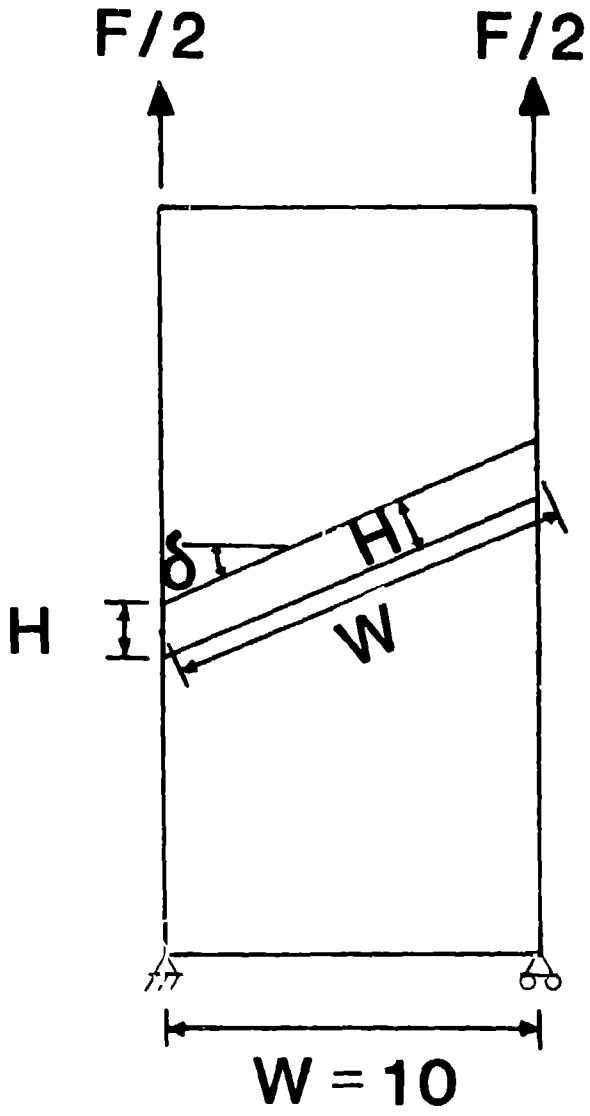

Figure 111. - Mesh used for slender element inclination effect study.

TABLE 28.- Error and inclination in a unaxial loaded three element mesh.

Inclination	Aspect Ratio	Max Error
0°	100	0%
10°	100	2%
30°	100	26%
45°	100	20%
45°	10	0%

interfaces. The normal load behavior of such slide lines may also be acceptable if parallel of perpendicular to the load.

A contrast in modulus between slender and adjacent elements will also induce shear loading. The shear will be greatest when loaded parallel to the long axis of the slender element and least when loaded perpendicular. Table 29 shows the results obtained in the three element uniaxially loaded mesh at an aspect ratio of 100.

TABLE 29. - Modulus contrast study in a three element mesh.

Modulus Ratio* (E)	(G)	Max. Stress Error	Max. Displ Error
0.1	0.1	0%	0%
10.0	10.0	27%	5%
10.0	1.0	26%	3%

*(Slender element modulus)/(adjacent element modulus)

The results in Table 29 point out the need to distinguish between two categories of slender element use: (i) low modulus slender elements typically used for interfaces and (ii) high modulus slender elements that may be used to represent reinforcement (rebar, cable bolts, tendons, rods). In this regard, the introduction of a second modulus changes the diagonal dominance measure. The low modulus slender element improves diagonal dominance and thus aids convergence, while the high modulus slender element decreases diagonal dominance and thus impedes convergence.

Medium Scale Slender Element Behavior

Although the use of high aspect ratio slender elements for bolt analysis requires caution, in all cases, the use of elements with an aspect ratio of 10 or less appeared to be safe in the sense that accurate results were obtained with a reasonable computational effort. Nevertheless, an intermediate step using a medium scale mesh was taken

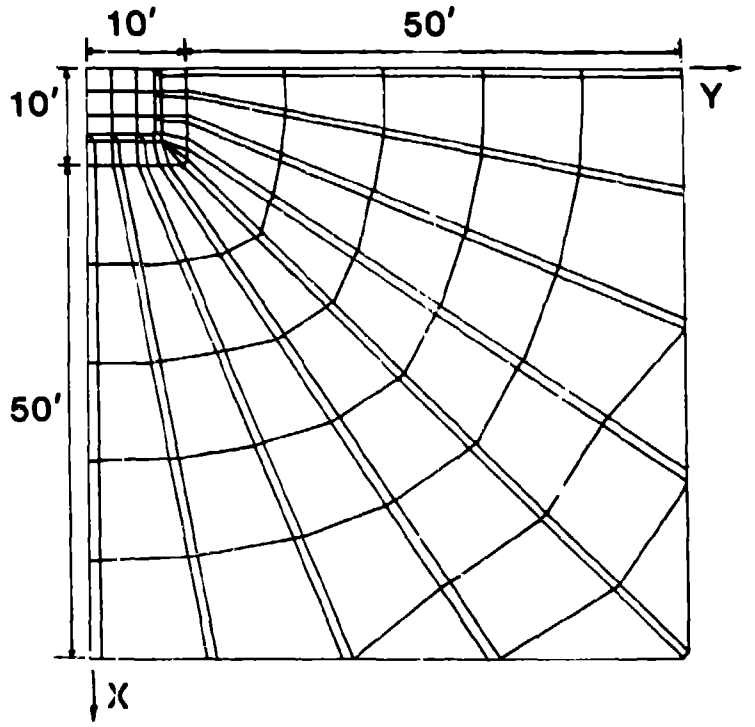

(a) FIXED LENGTH

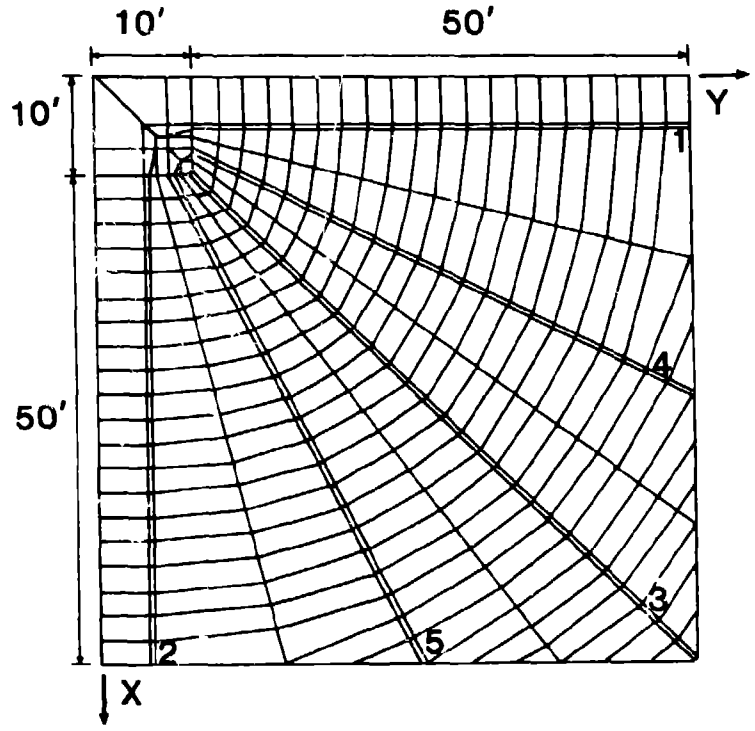

(b) FIXED HEIGHT

Figure 112. - Meshes used in medium scale meshes containing slender elements.

before final evaluation of the original large scale mesh results. Two medium meshes were used, one in which the width to height ratio was varied by changing element height at a fixed width, the other in which the height was fixed and the width varied. Width is the long dimension of a slender element, height is the short dimension. Figure 112 shows the two medium scale meshes used. The geometry of the meshes simulates a fan of cable bolts such as installed from the cable bolt drift in the study stope area of the Homestake Mine. The meshes allowed investigation of a single bolt in any position and combinations of bolts of various aspect ratios, loading conditions and material properties.

In fact, the analyses were done using a homogeneous mesh; bolt elements were assigned the same properties as the adjacent rock elements. The reason for this is that at realistic spacing of bolt fans, the 2D-3D scaling of bolt modulus results in a modulus nearly equal to the rock modulus. Also, analyses at modulus ratios of 1.25, 1.50 and 2.00 which correspond to much closer fan spacings showed negligible effects on accuracy, unlike the case with a modulus contrast of 10.

The results obtained in the medium scale mesh studies using slender elements confirms and adds to the inferences drawn from the results of the small scale mesh studies.

(i) Inclination of slender elements to the global axis has a strong, adverse effect on accuracy obtained at a given computational effort.

Arrays of parallel rows of slender elements loaded parallel and perpendicular to the long axes of the slender elements show excellent accuracy (maximum stress error less than 0.5%) with an aspect ratio of 20.

(ii) Loading conditions also have some effect; biaxial loading (results not given in table 30) decreases accuracy somewhat relative to uniaxial loading either parallel or perpendicular to the long dimension of the slender elements.

(iii) The more slender elements present, the less accurate are the results at a fixed computational effort. This is generally the case even without slender elements; large meshes usually converge more slowly than small scale meshes which contain relatively few elements and nodes, a large percentage of which are boundary nodes that are skipped in the iteration.

Summary

In all cases studied, the question was essentially one of accuracy obtained at a fixed number of iterations. Convergence although slow and sometimes oscillatory was also always the case. The question is thus a practical one that relates to the rate of convergence. In this regard, the diagonal dominance criterion is a valid but sensitive nonlinear index that is probably influenced by machine word length. The closer the ratio of absolute values of off-diagonal to diagonal terms in any

row is to one, the slower is the convergence rate. The rate of

TABLE 30. - Intermediate scale aspect ratio study results, uniaxial load.

Bolt Pattern	Aspect Ratio	Max. Stress Error %	
		Fixed Length	Fixed Height
unbolted	(basic mesh)	0	--
1 vertical	40:1	0	--
1 horizontal	40:1	0	--
1 45°	40:1	25	--
1 45°	20:1	5	20
1 45°	10:1	0	1
1 45°	5:1	0	--
3*	40:1	13	--
3	20:1	2	8
3	10:1	--	9
5*	40:1	37	--
5	20:1	8	40
5	10:1	1	30
9*	40:1	60	
9	20:1	40	
9	10:1	15	

* 3 bolts at 0°, 45°, 90°
5 bolts at 0°, 22°, 45°, 67°, 90°
9 bolts at 0°, 11°, 22°, 34°, 45°, 56°, 67°, 79°, 90°

convergence is also slowed by the number of slender elements in a mesh, that is, by the number of nodes that lessen diagonal dominance by virtue of high ratios of off-diagonal to diagonal terms. Node numbering alternatives do not change diagonal dominance, but nevertheless influence the rate of convergence.

Sequential numbering of slender element nodes, indeed all element nodes is best. The starting number and the order (ascending or descending) is immaterial.

Slender elements with a relatively low modulus speed convergence; high modulus slender elements retard convergence. In this regard, the product of shear modulus and aspect ratio needs to be considered. Very high aspect ratios can be used with a very low shear modulus in slender elements parallel or perpendicular to the global reference axes. Inclined elements will require a greater computational effort to achieve a given accuracy.

These inferences are limited to an iterative equation solver. An elimination equation solver may give different results. In this regard, the positive definiteness of the global stiffness matrix was examined for several single element meshes at aspect ratios of 10, 20, 50 and 100. All showed at least one very small but negative eigenvalue. A single element system would therefore not be positive definite. However, a positive definite system may still result when slender elements are mixed with elements of ordinary aspect ratios. The efficacy of an elimination equation solver as an alternative to a slowly converging iterative equation solver is an interesting possibility for cable bolt design studies but its investigation is beyond the scope of the project.

The net result is that slender elements, those of aspect ratio greater than 10 should be used with great caution. An aspect ratio of 5 or less is preferable. A 2 1/2 in. diameter cable hole would thus need to be represented by a slender element 2 1/2 in. high and no longer than 25 in. A large scale two dimensional mesh such as the one used to represent the Homestake Mine study stope would require several thousand elements and would contain a large number of nodes with very low diagonal dominance. The very low convergence rate and the possibility of a false convergence limited by word length would make the mesh impractical to run, or if run, would very likely give results of uncertain reliability.

The use of a slender element to model bolt hole geometry is not recommended. Since some loss of geometric detail occurs from modeling the bolt grout assemblage in a cable bolt hole in the beginning and the constitutive behavior is modified accordingly, the inclusion of the effects of a cable bolt grout assemblage within a modified rock element of ordinary aspect ratio represents a reasonable, consistent and effective alternative. In fact, since the modulus of cable bolt grout assemblages in a fan of bolts is reduced in any event to account for fan spacing, the modulus for elements traversed by a cable bolt hole (and thus representing a rock-grout-cable bolt assemblage) will differ very little from the modulus for rock elements as such.

The quantitative results obtained in the study of slender element usage for cable bolt design substantiates (i) the oiriginal expectation that artificial support cannot noticeably influence ground motion until slab formation and detachment from the parent rock mass occurs, (ii) although the extent of yielding can be anticipated in an elastic-plastic analysis, the mechanics of artificial support in the post-rupture range is beyond current modeling capabilities.

REFERENCES

Cook, R. D., 1981, Concepts and Applications of Finite Element Analysis, John Wiley and Sons, New York.

Desai, C. S., M. M. Zaman, J. G. Lightner and H. J. Siriwaradane, 1984, "Thin Layer Element for Interfaces and Joints," Int. J. for Num. Meth. in Geomech., v. 8.

Donovan, K., W. G. Pariseau and M. Cepak, 1984, "Finite Element Approach to Cable Bolting in Steeply Dipping VCR Stopes," Geomechanics Applications in Underground Hardrock Mining, SME-AIME, N.Y., pp. 65-90.

Fossum, A. F., 1985, "A Simple Perfect Slip, Finite Element Slideplane," RE/SPEC Inc. Publ. No. 85-01.

Heller, S. R., Jr., Brock, J. S. and Bart, R., 1958, "The Stresses Around a Rectangular Opening with Rounded Corners in a Uniformly Loaded Plate," Trans. Third U. S. Congress on Applied Mechanics, pp. 357-368.

Kawamoto, T., 1964, "On the State of Stress and Deformation around Tunnel in Orthotropic Elastic Ground," Memoirs of the Faculty of Engineering, Vol. 10, Kumamoto University, Japan, pp 1-30.

Lekhnitskii, S. G., 1963, Theory of Elasticity of an Anisotropic Elastic Body, (P. Fern, translator), Holden-Day, N.Y., p. 163.

Lekhnitskii, S. G., 1968, Anisotropic Plates, (S. W. Tsai and T. Cheron, translators), Gordon and Breach, N.Y., p. 266

Morgan, H. S., Krieg, R. D., and Matalucci, R. V., 1981, "Comparative Analysis of Mine Structural Codes Used in the Second WIPP Benchmark Problem," Sandia Report SAND81-1389, p. 167.

Obert, L., and Duvall, W. I., 1967, Rock Mechanics and the Design of Structures in Rock, Wiley, N.Y., p. 650.

Pande, G. N., and K. G. Sharma, 1979, "On Joint/Interface Elements and Associated Problems of Numerical Ill-Conditioning," Int. J. Num. Anal. Meth. Geomech., Vol. 3, pp. 293-300.

Pariseau, W. G., 1972, "Plasticity Theory for Anisotropic Rocks and Soils," Proc. 10th U. S. Symp. Rock Mech., pp. 267-295.

Pariseau, W. G., 1978, "Interpretation of Rock Mechanics Data," USBM Final Report, Contract No. H0220077 (two volumes).

Pariseau, W. G., F. Duan and C. H. Schmuck, 1984, "Numerical Assessment of the Influence of Anisotropy on Steeply Dipping VCR Stopes," Geomechanics Applications in Underground Hardrock Mining, SME-AIME, N.Y., pp. 39-63.

Reyes, S. F., 1966, "Elastic-plastic Analysis of Underground Openings by the Finite Element Method," Ph.D. Thesis, University of Illinois, Univ. Microfilms, Ann Arbor, p. 116.

Thill, R. E., Willard, R. J., and Bur, T. R., 1969, "Correlation of Longitudinal Velocity Variations with Rock Fabric," J. Geophys Res., Vol. 74, pp. 4897-4909.